UNIVERSITY OF OKLAHOMA

GRADUATE COLLEGE

ADMICELLAR-POLYMERIZED THIN ELASTOMERIC COATINGS FOR ENGINEERED INTERFACES FOR ENHANCED COMPOSITE PERFORMANCE

A Dissertation

SUBMITTED TO THE GRADUATE FACULTY

In partial fulfillment of the requirements for the degree of

Doctor of Philosophy

By

Harry J. Barraza
Norman, Oklahoma
2003

Downloaded from SHAREOK. Persistent Handle URL: https://hdl.handle.net/11244/635

UMI Number: 3102431

UMI®

UMI Microform 3102431

Copyright 2003 by ProQuest Information and Learning Company.

All rights reserved. This microform edition is protected against unauthorized copying under Title 17, United States Code.

ProQuest Information and Learning Company
300 North Zeeb Road
P.O. Box 1346
Ann Arbor, MI 48106-1346

© Copyright by Harry J. Barraza 2003
All rights reserved.

ADMICELLAR-POLYMERIZED THIN ELASTOMERIC COATINGS FOR ENGINEERED INTERFACES FOR ENHANCED COMPOSITE PERFORMANCE

A Dissertation APPROVED FOR THE
SCHOOL OF CHEMICAL ENGINEERING AND MATERIALS SCIENCE

By,

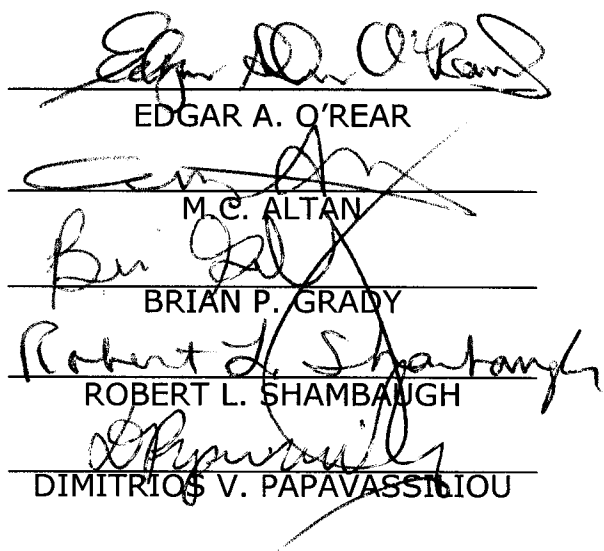

EDGAR A. O'REAR

M.C. ALTAN

BRIAN P. GRADY

ROBERT L. SHAMBAUGH

DIMITRIOS V. PAPAVASSILIOU

ACKNOWLEDGMENTS

It is a great pleasure to have the opportunity to express deserved recognition to the members of my defense committee and all professors at OU-CEMS. Each of them, in one way or another, encouraged me to explore the joy of doing research and have sown the seed of sharing knowledge with others as a most noble goal in life. In special, to Dr. Edgar A. O'Rear, my deepest feelings of gratitude and admiration for his trust and continued support in each of my research endeavors. I consider myself very fortunate in having met, and learned from, such a fine and sharp mind!

To Dr. M.C. Altan, in the School of Aerospace and Mechanical Engineering, my sentiments of appreciation and admiration. This work is in great part the result of your persistence in helping me, and others, realize that one can always give more than 100%! Thanks for all your trust and enthusiasm. Also, in the AME school, a word of

gratitude goes to my very good friends: Youssef K. Hamidi and Levent Aktas. Please, keep up the good work!

Personal friends and colleagues that helped me grow during this educational experience are also gratefully acknowledged: Wei-Li Yuan, with whom I spent countless hours learning the AFM basics; Francisco Pompeo; Olga Matarredona; Napaporn Komesvarakul, 'Cheng'; Duc Le; Kristian Olivero; and others not mentioned here, to whom I ask to please accept my unwritten thanks.

This work is also an expression of the love, patience and unselfish support of my beloved wife, Maria Leonor. May the paths of our lives be always filled with the never-ending desire of re-creating ourselves. To my daughter, Karen Sofía; my mom and dad, Myriam and Cesar; and my brothers: Henry, Harold and Cesar Jr.

"Non enim dedit nobis Deus spiritum timoris sed virtutis et dilectionis et sobrietatis".

II Ti: 1-7

CONTENTS

ABSTRACT xii

1. INTRODUCTION 1

2. THEORETICAL BACKGROUND 16

2.1 Fiber wetting and adhesion 16
2.2 Overview of admicellar polymerization 21
2.3 Elastomeric interlayers in glass-fiber reinforced polymers 27

3. EXPERIMENTAL METHODS 38

3.1 Dynamic contact angles on admicellar-coated fibers 38
3.2 Procedure for RTM composites fabrication 40
3.3 Mechanical testing 47
3.3.1 Interfacial adhesion in fibrous composites 47
3.3.2 Tensile testing 49
3.4 Voids characterization 51

4. WETTING BEHAVIOR OF ELASTOMER-MODIFIED GLASS FIBERS 57

4.1 Introduction 57
4.2 Experimental section 61
4.2.1 Characterization of glass fibers 61
4.2.2 Modification of glass fibers by admicellar polymerization 73
4.2.3 Contact angle measurements 76
4.3 Results and discussion 78
4.4 Conclusions 89

5. ELASTOMERIC SIZINGS FOR GLASS FIBERS AND THEIR ROLE IN FIBER WETTING AND ADHESION IN RESIN TRANSFER MOLDED COMPOSITES 95

5.1 Introduction 95
5.2 Experimental 103
5.2.1 Matrix characterization 103
5.2.2 Preform characteristics and sizing types 105
5.2.3 Molding setup and filling procedure 107
5.2.4 Specimen preparation and mechanical testing 112
5.2.5 Void content quantification by image analysis 114
5.3 Results and discussion 115

5.3.1 Matrix uniformity 115
5.3.2 Effect of molding speed 119
5.3.3 Effect of fiber architecture 130
5.3.4 Effect of sizing type 136
5.4 Conclusions 147

6. MOISTURE ABSORPTION AND WET-ADHESION PROPERTIES OF RESIN TRANSFER MOLDED COMPOSITES CONTAINING ELASTOMER-COATED GLASS FIBERS 155

6.1 Introduction 155
6.2 Experimental studies 161
6.2.1 Modification of fibers by admicellar polymerization 161
6.2.2 Molding setup and composites fabrication procedure 162
6.2.3 Specimen preparation, mechanical testing and moisture diffusion studies 164
6.2.4 Fractography studies 170
6.3 Results and discussion 171
6.3.1 Moisture saturation levels and diffusion rate behavior 171
6.3.2 Effect of sizing type on wet-adhesion 183
6.3.3 Microscopic analysis of failed surfaces 192
6.4 Conclusions 197

7. PERFORMANCE OF GLASS WOVEN FABRIC COMPOSITES WITH ADMICELLAR-COATED THIN ELASTOMERIC INTERPHASE 203

7.1 Introduction 203
7.2 Experimental studies 210
7.2.1 Preform characteristics and laminae configuration 210
7.2.2 Modification of fibers by admicellar polymerization 213
7.2.3 Molding setup and composites fabrication procedure 216
7.2.4 Specimen preparation and mechanical testing 217
7.2.5 Chemical and surface analysis of coated fibers 219
7.2.6 Atomic Force Microscopy (AFM) analysis 221
7.3 Results and discussion 222
7.3.1 Performance of WF composites with elastomeric coatings 222
7.3.2 Chemical characterization and surface distribution of admicellar coatings on woven fabrics 232
7.3.3 Admicellar films wetting and topological properties 243
7.3.4 Thickness distribution of admicellar sizings 256
7.4 Conclusions 259

OVERALL CONCLUSIONS AND FUTURE WORK 267

LIST OF TABLES

4.1	Classification of samples by origin and specifications	62
4.2	Surface atomic concentration for desized (F1) and commercial (F4, C4) fibers	64
4.3	Surface tension (dyne/cm) for different substrates at 25 °C	78
4.4	Contact angles in water measured at 25 °C for different fiber treatments and reference substrates	79
4.5	Contact angles in glycerol measured at 25 °C for different fiber treatments and reference substrates	79
4.6	Contact angles in EPON 815C measured at 25 °C for different fiber treatments and reference substrates	80
5.1	Preform architectures and sizing types	111
5.2	Important thermo-mechanical parameters measured by DMA	118
5.3	Void volume fraction for composites fabricated with different fiber treatments and molding velocities	121
5.4	Mechanical properties of layered composites	124
6.1	Experimental conditions for RTM-composites fabrication and related properties	164
6.2	Effective diffusivity constants for different molded parts evaluated by the ASTM D2344 standard (ASTM) and the Crank's [32] complete series-solution (SERIES)	182
7.1	Sizing types and tensile properties of RTM-parts	225
7.2	XPS atomic concentration ratios for various glass surface treatments	242

LIST OF FIGURES

1.1	Commercial fiber drawing and coating processes	2
1.2	Typical Resin Transfer Molding (RTM) operation sequence	6
1.3	Lead-lag behavior resulting from the imbalance in the intertow/intratow microflow during RTM	8
2.1	Coordinate system for the numerical profile solution of an equilibrium droplet on a single fiber	18
2.2	Experimental setup for filament wetting experiment	21
2.3	Sequential steps in surface modification of inorganic substrates by admicellar polymerization	23
2.4	Adsorption isotherms of (a) anionic (SDS); and (b) cationic (CTAB) surfactants on desized glass fibers	25
2.5	Model of crack interaction in a simple composite with strong interface adhesion	31
2.6	Crack progression and arrest in a model composite due to a debonding or Cook-Gordon mechanism	33
3.1	Typical tensiogram and its major components	40
3.2	RTM molding setup and data acquisition system	42
3.3	Ram-plate connector accessory and plungers of the molding press	43
3.4	Positive displacement system (plunger/cylinder) for liquid prepolymer injection	44
3.5	Impregnating flow front progression for the RTM fabrication of random-mat composites	46
3.6	Three-point bending configuration for the short beam shear strength test according to ASTM D2344/D2344M-00	48
3.7	Setup used for tensile testing according to ASTM D3039/ D3039M-00	50
3.8	Typical tensile stress-strain curves	51
3.9	Examples of circular (a), Ellipsoidal (b) and Irregular (c) voids found in RTM composites	54
4.1	Average surface roughness (R_a) of 13.0 μm diameter fibers with various surface treatments	68
4.2	Topographical features of desized fibers (F1) by AFM	70

4.3	Topographical features of admicellar-coated fiber (F3) by AFM	71
4.4	Topographical features of commercial sized fibers: (a) AFM micrograph of fiber F4; (b) SEM micrograph of fiber C4; (c) SEM micrograph of fiber F4	72
4.5	Tensiogram of desized fiber (F1) in water	81
4.6	Tensiograms of an elastomer-coated fiber (F3) in water	84
4.7	Tensiogram of a commercial sized fiber (F4) in water	85
4.8	Tensiogram of an elastomer-coated fiber (F3) in Epon 815C	87
4.9	Tensiogram of a commercial sized fiber (F4) in Epon 815C	88
5.1	High-speed filling RTM fixture	109
5.2	Relative spatial positions of test specimens in a molded disk	113
5.3	Elastic modulus (E') response of neat resin and desized fiber composite at two different curing conditions	117
5.4	Cross-section micrographs of composites molded at different velocities	122
5.5	Impregnation qualities of composites with desized reinforcement (Type II)	128
5.6	Cross-section micrographs of composites having a random nonlayered structure	131
5.7	Mechanical properties of composites with random nonlayered structure	134
5.8	Tensiogram for water advancing over polystyrene coated fiber	140
6.1	Representative micrographs of two different reinforcement architectures	172
6.2	Percent moisture gain with time for big samples of neat resin parts (N)	175
6.3	Percent moisture gain with time for big samples of commercial sized composites (Im)	175
6.4	Percent moisture gain with time for big samples of desized (control) composites (IIm)	176
6.5	Percent moisture gain with time for big samples of polystyrene-coated composites (III)	176
6.6	Percent moisture gain with time for big samples of poly (styrene-co-isoprene) coated composites (IV)	177
6.7	Percent moisture gain with time for small samples of commercial sized composites (Im)	180
6.8	Percent moisture gain with time for small samples of desized (control) composites (IIm)	180
6.9	Percent moisture gain with time for small samples of poly (styrene-co-isoprene) coated composites (IV)	181

6.10 Ultimate tensile strength of RTM-parts after moisture saturation 185
6.11 Stiffness of RTM-parts after moisture saturation 185
6.12 Interlaminar shear strength (ILSS) of RTM-parts after moisture saturation 186
6.13 Effectiveness in mechanical properties retention (UTS: Ultimate Tensile Strength; E: Stiffness; and SBS: Short Beam Shear Strength) of investigated sizings 191
6.14 SEM micrographs at low (L) and high (H) magnifications of failed surfaces 193

7.1 (a) Micrograph of FibreGlast Plast # 245 plain weave fabric; and (b) Laminae configuration in RTM composites 212
7.2 Stress-strain behaviors of composites with different surface treatments 223
7.3 Interlaminar Shear Strength (ILSS) properties of RTM-parts 229
7.4 UV/Vis analysis of THF-extracts from admicellar-coated fibers at three different surfactant/monomer ratios 233
7.5 XPS survey spectra and atomic compositions of glass fibers With three different surface treatments 236
7.6 XPS oxygen/silicon versus carbon/silicon ratios for different fiber surface treatments 239
7.7 Hydrophobicity assessment by the drop test 244
7.8 Hydrophobicity testing sequence at the yarn scale 246
7.9 Topmost surface morphology of desized fibers by AFM 248
7.10 Dimensional and topographical features of admicellar-treated fibers type SI1 by AFM 249
7.11 Dimensional and topographical features of admicellar-treated fibers type SI10 by AFM 255
7.12 Surface height histograms from bearing analysis of fibers with different surface treatments 258

ABSTRACT

A surface-polymerization technique known as admicellar polymerization has been evaluated as an alternative method to tailor the interfacial properties of glass/epoxy composite parts molded by resin transfer molding (RTM). Initially, small-scale polymerization reactions were carried out to investigate the feasibility of covering glass fibers with a thin elastomeric film that would render them fairly hydrophobic. After the treatment, the admicellar-modified fibers not only exhibited a chemically heterogeneous surface with high contact angles with water (θ_a = 72 ± 8); but also had statistically identical wetting characteristics to fibers coated with commercial sizings when probed with an epoxy resin (Epon 815C). In subsequent experiments, random-mat glass fibers modified with the same technique described above were used as the reinforcement for RTM-parts molded in a high-speed setup. These disk-shaped parts were mechanically tested, both under dry and wet conditions, to study the enhancement in structural integrity achieved with the insertion of controlled-thickness elastomeric interphases. In the dry-condition testing, the admicellar poly (styrene-co-isoprene) sizing performed significantly better than the uncoated control samples in the tensile and flexural tests. For the same sizing type, the interlaminar shear strength was more than 30%

higher than the desized composites and compared statistically to the adhesion levels provided by commercially sized reinforcements. Greater data scatter and poorer adhesion performance was observed for those composites containing fibers with a polystyrene coat. We inferred that beneficial effects of a nanometer-thick elastomer interlayer are more evident when cooperative segmental motions take place, that is, when the surface glass transition temperature of the sizing is far below the room temperature. Other factors, such as chain structure, as well as the presence of unsaturated moieties in the isoprene block branches, may also contribute to augment the interactions between poly (styrene-co-isoprene) and the epoxy functional groups. It is worth noting that RTM composites containing woven fabrics coated with poly (styrene-co-isoprene), at different coverage levels, gave a similar dry-adhesion performance trend as the random-mat reinforcement. Firstly, tensile properties augmented in more than 50% for all cases; whereas, the interlaminar shear strength (ILSS) increased proportionally with the amount of elastomeric film present. The maximum increase in interlaminar adhesion registered, with respect to the desized composites, was more than 37 % and corresponded to fibers treated in a polymerization reaction with a surfactant/monomer ratio of 1:10. For this particular admicellar sizing the ILSS level was only 9% lower than that observed with a silane-

based commercial sizing, which signals the potential of admicellar sizings as alternative coatings for glass fiber reinforcements with comparatively similar performance as the proprietary organosilane treatments.

Wet-adhesion properties of random-mat glass fibers with admicellar sizings were investigated by transient water sorption measurements carried out at constant temperature (45 °C). These experiments showed that lower effective diffusivity values correlated with improved overall mechanical performance in relation to the control unsized samples; and revealed the importance of changing the surface energy characteristics of glass fibers by using distinctively hydrophobic pure polymers. Admicellar polystyrene and poly (styrene-co-isoprene) coatings appear to create an interface with much higher resistance to moisture attack than the organosilane/matrix interface in composites with commercial sizing. This fact was corroborated by comparing their effectiveness in property retention, which showed the mechanical property (e.g., ultimate tensile strength, stiffness and interlaminar shear strength) increased with respect to the uncoated composites in the dry state as well as after water saturation. Poor wet-adhesion properties of commercial sizings were attributed to higher contents of inert material present in these coatings. Fractography

analysis was consistent with previous observations regarding catastrophic failure in composites without coating. In all, the results described herein have implications for composite manufacture applications because they show the possibility of creating tailored interfaces from pure polymers with relatively low market prices.

1. Introduction

In recent years there has been a rapid integration of fiber-reinforced composites into key technological areas (e.g., transportation and infrastructure) demanding materials with lower weight/strength ratios, longer lifetimes and lower cost. Improved mechanical performance of fiber reinforced polymeric composites has been linked to the establishment of a stronger interphase between the matrix and fiber surfaces, as well as on the relative stability of the interfacial region against aggressive environments. The concepts of 'interphase engineering' and 'tailored interphases' have been incorporated in the literature to describe the systematic approach aimed at controlling the interphase structure to ultimately enhance the physical and mechanical properties of a composite [1, 2]. For glass fibers, modification of the surface by means of organosilane coupling agents is the standard commercial approach to minimize the interfacial free energy, provide for better wetting, and ensure increased adhesion of glass reinforcements to a number of thermoplastic and thermoset polymer matrices, including epoxies [3]. Sizings currently utilized in

the glass-reinforcement market are proprietary formulations containing up to 10% of active silane coupling agents, while the remaining 90% is a mixture of low molecular weight epoxies, lubricants, surfactants, anti-stats and other polymeric film formers [4, 5]. Figure 1.1 illustrates a typical glass fiber manufacturing and sizing application process. The molten glass passes through fiber-forming dies at a temperature of over 1000 °C, and then the fibers are rapidly cooled by the aqueous sizing solution to a deposition temperature of less than 100 °C. In addition to the high speeds at which the process takes place (e.g., greater than 1000 m/min), the fact that the sizing precursor consists of highly diluted organic compounds in water limits the kind of coatings that can be applied and the coating homogeneity [6].

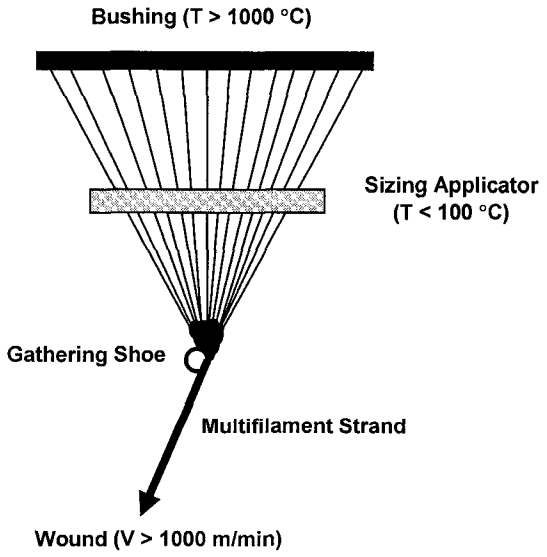

Figure 1.1 Commercial fiber drawing and coating processes. Adapted from Thomason and Dwight [5].

The multifunctional nature of commercial sizings, combined with the complexity of their chemistry, makes it very difficult to optimize their final composition and deposition rate on the fibers. Even basic knowledge such as the percent of fiber sizing coverage is still difficult to account for during manufacturing, and only time-consuming off-line techniques such as X-ray photoelectron spectroscopy are available nowadays in order to interrogate the sizing distribution. Recent investigations, on the other hand, have demonstrated that excessive non-reactive components (e.g., binding agent) present in the commercial sizings tend to remain in high concentrations within the interphase, weakening the resin network crosslink density [7], reducing the fiber/matrix interfacial adhesion [8] and increasing the potential for water ingress [9].

Deficiencies in the composites performance related to excessive non-reactive components in commercial sizings have led researchers to focus their attention on creating monomolecular, reactive surface layers which may strongly interact with both the organic and inorganic constituents present at the interphase [10]. A first attempt by Fagerholm's group was based on the idea of readily adsorbing long chain alcohols and/or polyelectrolytes on alumina-silicate sites to change the wetting characteristics of glass filaments [11-14]. Later on,

DiBenedetto [15] pointed out that monolayer and submonolayer coatings could improve interfacial bond strength when one end of the molecule was tethered to the surface of the reinforcement and the functional groups or polymeric chains on the other end reacted with and/or interpenetrated the matrix phase. Examples of such an approach include the attachment of tethered polysulfone [16], as well as polystyrene chains [17] to the surface of E-glass fibers. In the case of polystyrene, it was confirmed that a low attachment density was required to provide optimum mixing with the matrix free chains and, thus, higher interfacial bond strength.

Grafting of high- and low-molecular weight polymers as a technological alternative to induce stronger bonds at the composites interphase has been also carried out either via direct polymerization from chemical initiators attached to the glass surface [18, 19], or by plasma polymerization of gaseous monomers onto the fibers surface [20-23]. Plasma-deposited films are believed to be more uniform in coverage, distribution and thickness than commercial sizings. However, the equipment required for producing the low-temperature plasma is expensive and no experience has been reported in the open literature for operations up to industrial scale.

The need for substantial improvements in glass fiber coating technologies is not only driven by the necessity of maintaining fiber strength but also of controlling the size chemistry to form a stronger interphase. Sizings also play a direct role during the physical interaction of the polymeric matrix with the reinforcement. For instance, the wetting characteristics of sized fibers when impregnated with a liquid resin can override other process variables during composite fabrication, and lead to defects such as voids and un-impregnated areas (e.g., dry spots) that largely compromise the ultimate performance of molded parts. One example of a composite fabrication process where the influence of sizing wettability is particularly significant is in resin transfer molding (RTM).

RTM was introduced almost 50 years ago as an alternate scheme to producing high-performance composites for aerospace applications [24]. However, RTM has been rapidly adopted to manufacture structural components in the automotive industry, and together with other liquid molding processes (e.g., vacuum assisted resin transfer molding, resin infusion), are thought to be the mainstream technological routes for high-performance composites fabrication in the next decade [25, 26]. In the RTM process, an uncured liquid resin is mechanically injected into a mold containing an inorganic porous or

fibrous reinforcement. The resin is expected to displace the air inside the mold, quickly filling up all empty spaces within the preform as shown schematically in Figure 1.2.

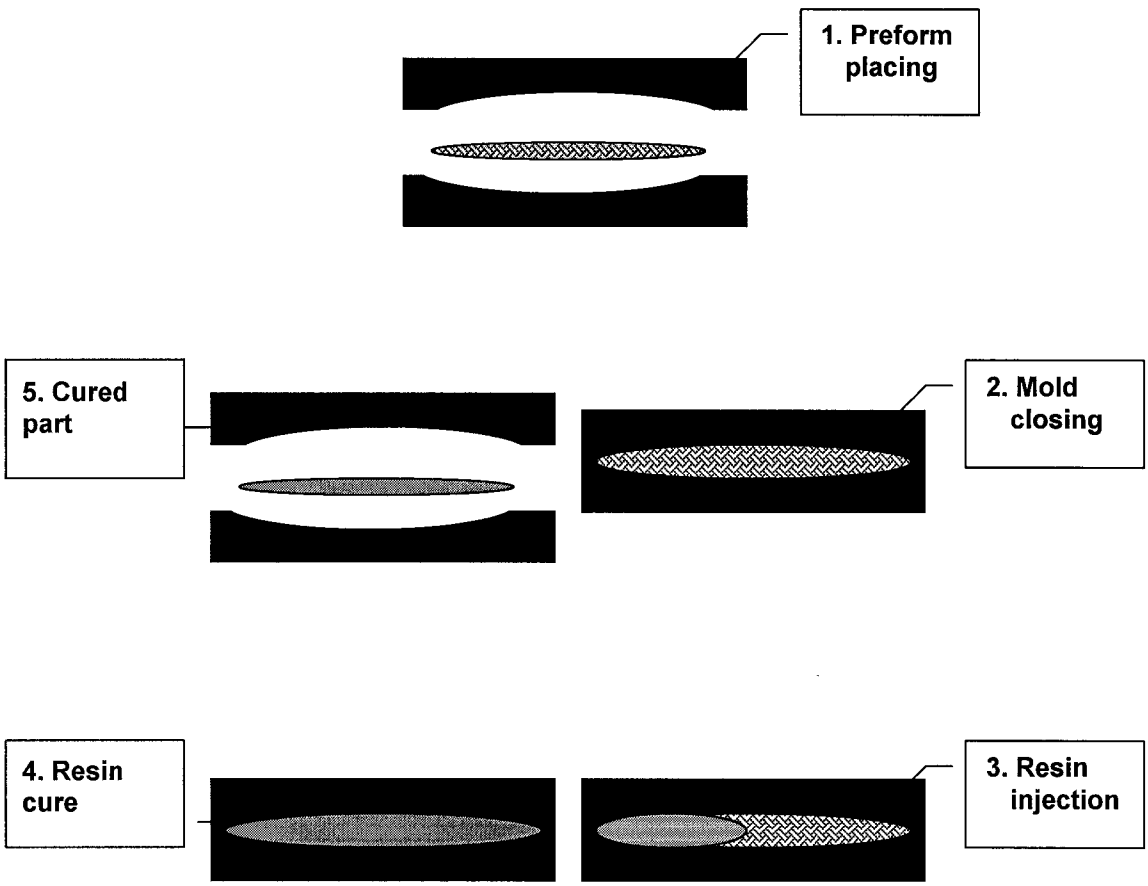

Figure 1.2 Typical resin transfer molding (RTM) operation sequence. Adapted from Dugan [27].

In the case of fibrous reinforcements, the network of channels for the resin flow is not uniform and contains a wide distribution of intertow and intratow channel spacings, as well as a broad range of channel orientations (e.g., random-fiber preforms). Such heterogeneous microstructure forms high and low permeability zones within the reinforcement; and at the same time creates an imbalance between viscous and surface forces during the flow of the polymeric mixture. Permeability variations at the flow front, coupled with non-isothermal effects coming from the curing kinetics, are responsible for transient phenomena that decrease impregnation quality and ease of spreading of the resin through the inorganic preform. In particular, the formation of processing defects such as voids during RTM have been shown to depend primarily on the capillary number, advancing contact angle and orientation of fibers relative to the flow direction [28]. Patel and Lee [29] put forward a simple unidirectional model that predicts void formation as the result of the extensive fingering at the flow front (i.e., lead-lag behavior). According to these authors, the lead-lag appears when either the intertow or primary flow predominates over the flow between fiber interstices (i.e., capillary flow), and *vice versa*. The manifestation of flow front lead-lag is directly related to the impregnation rates as depicted in Figure 1.3. For instance, at low filling velocity, the flow inside the fiber tows or intratow flow is

dominant. High capillary pressures cause the microflow within the narrow channels formed by two parallel fibers inside a tow to move ahead of the macroflow, which takes place in the intertow spacing. At high flow velocity the situation is reversed: the macroflow moves ahead of the microflow. In this latter case, the capillary effect is very small compared to the externally applied pressure, and therefore the viscous forces dominate the filling pattern [30].

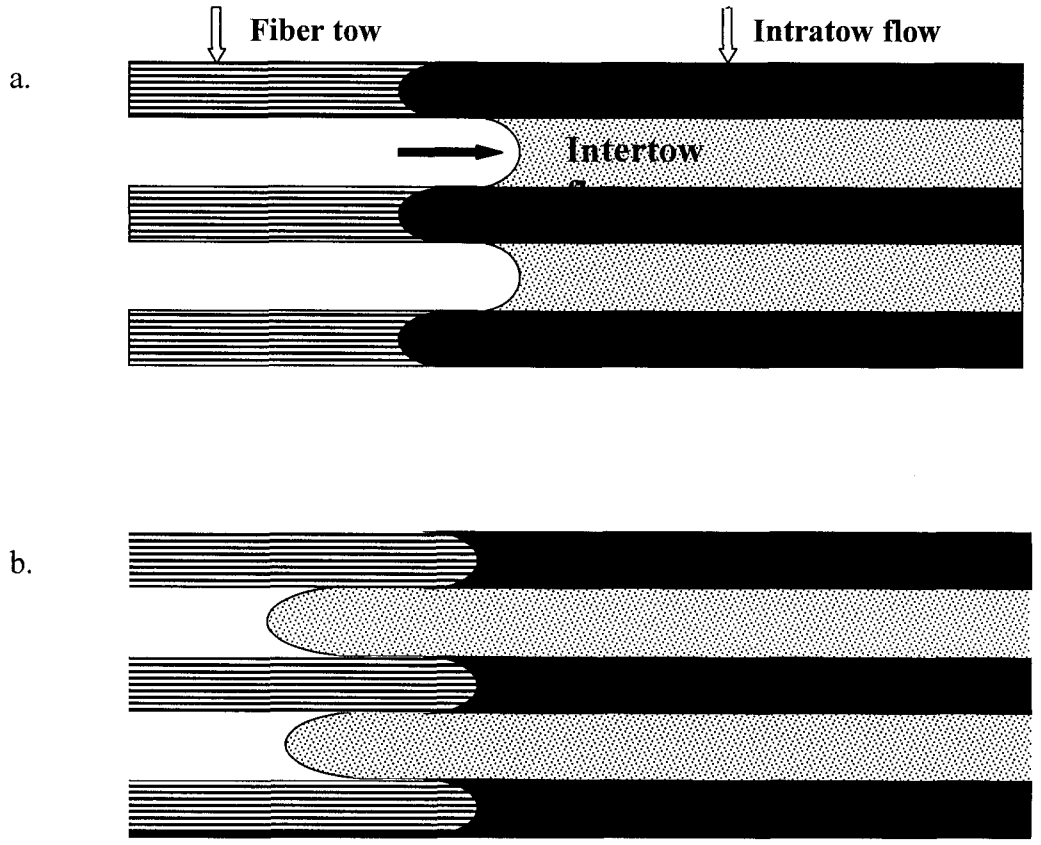

Figure 1.3 Lead-lag behavior resulting from the imbalance in the intertow/intratow microflow during RTM. (a) Low impregnation velocity (high capillary pressure). (b) High impregnation velocity. Adapted from [30].

Clearly, there is still considerable room for improvement with regard to the development of new sizing concepts to provide a strong bonding between the fiber and polymer matrix; and at the same time modify the wetting characteristics of the reinforcement to reduce the chances of defects formation during polymer impregnation. The current research addresses the central question of whether applying a thin elastomeric coating to glass fibrous reinforcements changes appreciably their interfacial characteristics to the extent that enhanced wetting and spreading of low-viscosity epoxy/amine systems – commonly used in RTM – could be attained. Together with the wetting behavior, this research aims to demonstrate that by incorporating thinner sizings containing less inactive 'building' agents it is possible to create an almost one-dimensional interphase region, sufficiently thin, such that no drastic changes in the matrix network structure would probably take place. This new elastomeric sizings would not only be advantageous as a result of their reduced thickness, but also because they constitute a 'soft interphase'. It is generally accepted [31-33] that a soft interphase changes the stress distribution and decreases stress concentration, consequently increasing the fracture toughness properties of the composite. To fulfill these objectives, we applied a surfactant-mediated technique known as admicellar polymerization, which is a relative new and versatile way of modifying the wetting

characteristics of inorganic substrates. Although initially conceived and tested for modifying highly porous materials such as alumina [34-36] and silica [37, 38], its applications have also been extended to the formation of conducting thin films (2-10 nm thick) over atomically flat substrates such as mica [39]; as well as to the production of improved fillers for conducting polymer composites and modification of other low surface area substrates, including glass fibers [40, 41]. The study of the wetting behavior modification of different types of glass fibers by the introduction of a thin poly (styrene-co-isoprene) sizing is the main topic covered in **Chapter 4**.

After achieving the desired surface modification, the thrust of the investigation changed to the fabrication and mechanical testing of RTM parts to assess the degree of structural integrity enhancement achieved by the use of admicellar-polymerized thin flexible coatings. Important parameters such as a void content, strength, stiffness and the interlaminar shear strength (ILSS) were measured and correlated to the type of sizing applied in composites containing random glass fiber preforms. In **Chapter 5**, the dry-state mechanical properties of parts with elastomeric coatings are compared to those properties of parts molded with unsized fibers and with commercially sized fibers. Subsequently, in **Chapter 6**, we assessed the effectiveness of

admicellar-coated elastomeric sizings in preventing adverse consequences of moisture absorption to the strength, stiffness and interlaminar shear strength of molded glass fiber/epoxy resin parts after immersion in water at 45 °C until saturation. Finally, in **Chapter 7**, the effect of using different surfactant/monomer ratios during the admicellar polymerization was correlated to the amount of coating deposited on the glass surfaces (i.e., coverage). Varying the elastomeric sizing coverage showed to be influential in the composites mechanical properties, especially in the resistance of the interphase to delamination as suggested by three-point bending results (i.e., interlaminar shear strength, ILSS).

References

1. H. Ishida, in: The Interfacial Interactions in Polymeric Composites, G. Akovali (Ed). Kluwer Academic Publishers, Dordrecth, The Netherlands, pp. 169-199 (1993)
2. J.F. Gerard and B. Chabert, *Macromol. Symp.* **108**, 137 (1996)
3. B. Larson and L. Drzal, *Composites* **25**, 711 (1994)
4. K. Bezarti, L. Cangemi and F. Dal Maso, *Composites Part A* **32**, 197 (2001)
5. J.L. Thomason and L.J. Adzima, *Composites Part A* **32**, 313 (2001)
6. J.L. Thomason and D.W. Dwight, *Composites Part A* **30**, 1401 (1999)
7. J.K. Kim, M.L. Sham and J. Wu, *Composites Part A* **32**, 607 (2001)
8. A. Nakai, T. Osada, H. Hamada and N. Takeda, *Composites Part A* **32**, 487 (2001)
9. R.J. Gorowara, W.E. Kosik, S.H. McKnight and R.L. McCullough, *Composites Part A* **32**, 323 (2001)
10. H. Ishida and T. Chaisuwan, *Polym. Mater. Sci. Eng.* **85**, 534 (2001)
11. A.C. Lassas, H. Fagerholm, B. Stenlund, J. Näsman, *Polym. Compos.* **14**, 1 (1993)
12. H. Fagerholm, C. Lindsjö, J. Rosenholm, K. Rökman, *Colloids. Surf.* **69**, 79 (1992)

13. H. Fagerholm, C. Lindsjö, J. Rosenholm, *J. Mater. Sci.* **30**, 2420 (1995)
14. H. Fagerholm, J. Rosenholm, T. Horr, R. Smart, *Colloids Surf. A* **110**, 11 (1996)
15. A.T. DiBenedetto, *Mater. Sci. Eng.* ***A302***, 74 (2001).
16. A.T. DiBenedetto, S.J. Huang, D. Birch, J. Gomez and W.C. Lee, *Composite Structures* **27**, 73 (1994).
17. R. Lin, R.P. Quirk, J. Kuang and L.S. Penn, *J. Adhes. Sci. Technol.* **10**, 341 (1996)
18. K. Fujiki, *Recent Res. Develop. Polym. Sci.* **3(Pt. 2)**, 439 (1999)
19. S. Shalaby, D. Clupper and T. Taylor, US Patent 5874509, p6 (1999)
20. S. Chou, SH. Chen, *Polym. & Polym. Compos.* **8**, 267 (2000)
21. S. Chou, SH. *Chen, Polym. & Polym. Compos.* **8**, 477 (2000)
22. D. Marks, F. Jones, *Composites Part A* **33**, 1293 (2002)
23. V. Cech, R. Prikryl, R. Balkova, A. Grycova and J. Vanek, *Composites Part A* **33**, 1367 (2002)
24. K.D. Potter, *Composites Part A* **30**, 619 (1999)
25. N.J. Johnston, *Book of Abstracts, Composites 2000: An International Symposium on Composite Materials*, University of Delaware (2000)

26. L. Fong and S. Advani, *Resin Transfer Molding – Technical Report CCM 95-09*. University of Delaware Center for Composite Materials, Newark (1995)
27. F.D. Dugan, PhD Thesis, University of Michigan, Ann Arbor (2000)
28. N. Patel, V. Rohatgi and J.L. Lee, *Poiym. Eng. Sci.* **35**, 837 (1995)
29. N. Patel and J.L. Lee, *Polym. Compos.* **17**, 104 (1996)
30. W.B. Young, *J. Compos. Mater.* **30**, 1191 (1996)
31. L.J. Broutman and B.D. Agarwal, *Polym. Eng. Sci.* **15**, 757 (1974)
32. M. Labronici and H. Ishida, *Compos. Interfaces* **2**, 199 (1994)
33. G. Vörös and B. Pukánszky, *Composites Part A* **32**, 343 (2001)
34. G. Funkhouser, M. Arevalo, D. Glatzhofer and E.A. O'Rear, *Langmuir* **11**, 1443 (1995)
35. D. Glatzhofer, G. Cho, C. Lai, E.A. O'Rear and B. Fung, *Langmuir* **9**, 2949 (1993)
36. C. Lai, E.A. O'Rear, J. Harwell and M. Hwa, *Langmuir* **13**, 4267 (1997)
37. B. Kitinayan, J. O'Haver, J. Harwell and S. Osuwan, *Langmuir* **12**, 2162 (1996)
38. J. O'Haver, J. Reynolds, J. Harwell, B. Grady, L. Evans and W. Waddell, *Book of Abstracts, 219th ACS National Meeting, San Francisco, 2000*; American Chemical Society: Washington, DC (2000)

39. W.-L. Yuan, E.A. O'Rear, G. Cho, G. Funkhouser and D. Glatzhofer, *Thin Solid Films* **385**, 96 (2001)

40. S. Sakhalkar and D. Hirt, *Langmuir* **11**, 3369 (1995)

41. B. Grady, E.A. O'Rear, L. Penn and A. Pedicini, *Polym. Compos.* **19**, 579 (1998)

2. Theoretical Background

2.1 Fiber wetting and adhesion in composite materials

Many authors in the science and technology literature have often used, indiscriminately, the term 'adhesion' to refer to multiply related phenomena that usually encompass either physical or chemical interactions between two solid phases at the interface. As stated recently by Sharpe [1], the two common approaches to the definition of adhesion (i.e., physical chemistry and technology) relate to clearly different processes. In physical chemistry, the adhesive contact or so-called adhesive force is defined by the work of adhesion, W_a, which corresponds to 'the free energy change, or reversible work done, to separate unit areas of two media from contact to infinity in vacuum' [2]. This equilibrium thermodynamic definition specifically accounts for atomic or molecular attractions as the fundamental explanation to why materials brought into contact may resist separation, 'without saying anything about the goodness of poorness of the resistance' [1]. On the

other hand, the 'practical adhesion', as used in the technology field, is a synonym of mechanical resistance to separation of joint materials or adhering systems. Unlike the work of adhesion, the practical adhesion is a nonequilibrium property that depends on the failure mechanisms of the solid-solid system, testing geometry and rate, testing environment, etc.

In fiber/polymer composites processing, the surface and interfacial energies determine how individual macroscopic liquid matrix droplets will deform when they adhere to the reinforcement surface. The same relationships derived by Young and Dupré for liquid droplets on flat surfaces – exposed to a vapor phase – can also be applied to account for the wetting behavior in the case of fibers [3], although, the equilibrium shape configuration of the thin wetting liquid film on a fiber is different from that in a planar surface. Young's equation expressed as,

$$\cos\theta = \frac{\gamma_{SV} + \gamma_{SL}}{\gamma_{LV}}, \qquad (2.1)$$

defines the degree of 'attraction' of the liquid for the substrate in terms of the equilibrium contact angle (θ). If the contact angle is 0°, then a 'spreading' condition is predicted for the liquid on the substrate.

If the contact angle is less than 90°, the liquid is said to 'wet' the substrate; and if it is greater than or equal to 90° the liquid-solid interaction is termed to be 'non-wetting'. Thermodynamic 'spreading' or 'wetting' as described above is a necessary condition for acceptable processability as well as attainment of acceptable mechanical properties in any composite system. It assists in displacement of the gas phase from the fiber surface by the matrix resin [4]. Figure 2.1 depicts a cross section of a liquid droplet at equilibrium on a single filament, with coordinate system and shape parameters according to the numerical solution for drop profile by Yamaki and Katayama [5].

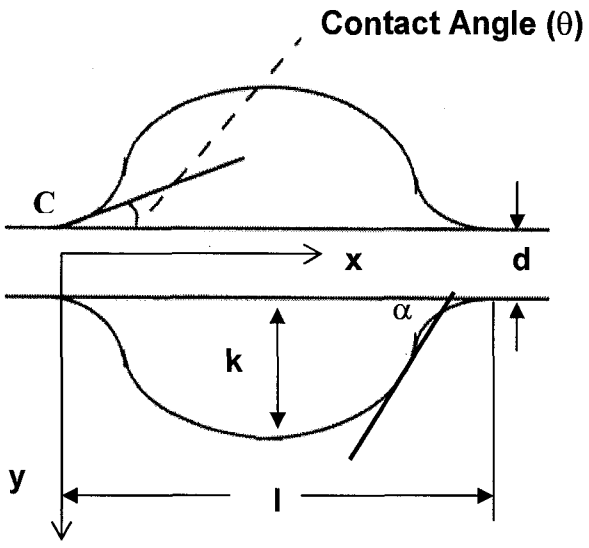

Figure 2.1 Coordinate system for the numerical profile solution of an equilibrium droplet on a single fiber. Adapted from [5].

The numerical solution followed by the authors in reference [5] has boundary conditions y_0 and x_0 at the fixed point C, and d =

filament diameter. The contact angle (θ) is given in terms of the drop length parameter (L = 2l/d), the maximum diameter parameter (K= 2k/d) and α, the contact angle where the liquid surface becomes linear. A numerical solution of this form is commonly used in conjunction with visual techniques [6, 7] to estimate the equilibrium contact angle and, in this way, assess changes in wettability of fibrous materials resulting from surface modifications carried out by either physical or chemical procedures.

During composite fabrication moving liquid fronts cause the contact angle to deviate from the static or equilibrium contact angle. Therefore, a static contact angle value measured by the visual technique described above would be a mere approximation of the actual transient wetting behavior occurring at the intertow and intratow scales. Some authors [8] have proposed that in liquid molding operations wherein the capillary numbers are small, that is, on the order of 10^{-4}, the static contact angle provides an excellent approximation to the true dynamic contact angle. However, in industrial practice impregnation of the preform must be performed as quickly as possible to shorten cycle times, which precludes the attainment of such low capillary numbers. In addition, it is well known that there is a critical capillary number for void mobilization (ca. 1 –

2.2 x 10^{-3}) below which extensive void entrapment would occur [9, 10].

Measurement of dynamic contact angles is difficult, especially at the fluid front velocities typically encountered in liquid composite molding (e.g. 0.01 – 4 cm/s). An alternative procedure is to measure the force exerted by a test liquid when advancing or receding over a solid probe at a constant front displacement velocity. Wilhelmy [11] first introduced the gravimetric method of measuring contact angles, which later on was adapted by Miller and Young [12] for evaluating the surface free energy of glass monofilaments. A schematic drawing of a typical experimental setup for fiber contact angle measurements is shown in Figure 2.2. In the latter approach the force, *F*, acting on an advancing (or receding) fiber, which is partially immersed in a liquid, is analyzed and can be expressed as

$$F = W + P\gamma_{LV}Cos\theta - B \quad , \tag{2.2}$$

where *W* and *P* are the weight and wetted perimeter, respectively, of the solid fiber tested, γ_{LV} corresponds to the surface tension of the liquid, and B is the buoyancy force. This latter parameter is usually neglected if the solid is slightly immersed and dimensionally uniform

and, in the particular case of fibers, if the diameter is less than 50 μm. The Wilhelmy technique is especially suitable for measuring contact angles smaller than 15°, where most optical methods fail [12, 13].

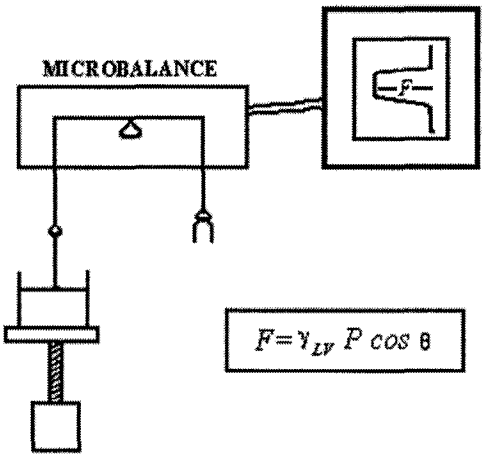

Figure 2.2 Experimental setup for filament wetting experiment. Adapted from [12].

2.2 Overview of admicellar polymerization

The development of alternative treatments to modify the interfacial characteristics of glass fibers is a subject of continuous research, and several techniques have been recently devised and patented [14-18]. Among these alternative treatments, admicellar polymerization stands as a relatively new and versatile technique that was initially conceived and tested for modifying highly porous materials such as alumina [19-21] and silica [22, 23].

Notwithstanding, its applications have been also extended to the formation of conducting thin films (2-5 nm thick) over atomically flat substrates like mica [24], as well as to the production of improved fillers for conducting polymer composites [25]. Another successful example of the application of admicellar polymerization is the formation of thin films with co-monomers (e.g., styrene and isoprene) over inorganic oxides of low surface area, including glass fibers, using low-cost materials like surfactants and redox and/or AIBN-type initiators [26, 27]. O'Haver et al. [28] presented an excellent review accounting for current and potential applications of this surfactant-aided polymerization technique.

The first step in the admicellar polymerization involves the adsorption of surfactant molecules on the mineral oxide surface as seen in Figure 2.3. The thermodynamical models describing the interaction of ionic surfactants on oppositely charged surfaces are based on the premise of electrostatic attractive forces as being the major driving force for ionic surfactant head groups to adsorb on the solid surface. Other types of interactions are expected to be present (e.g., lateral chain-chain hydrophobic attraction), but their contribution is thought to be much lower than the electrostatic forces [29, 30]. To measure the amount of adsorbed surfactants over a particular

inorganic substrate it is necessary to construct adsorption isotherms following the well-known surfactant depletion methods.

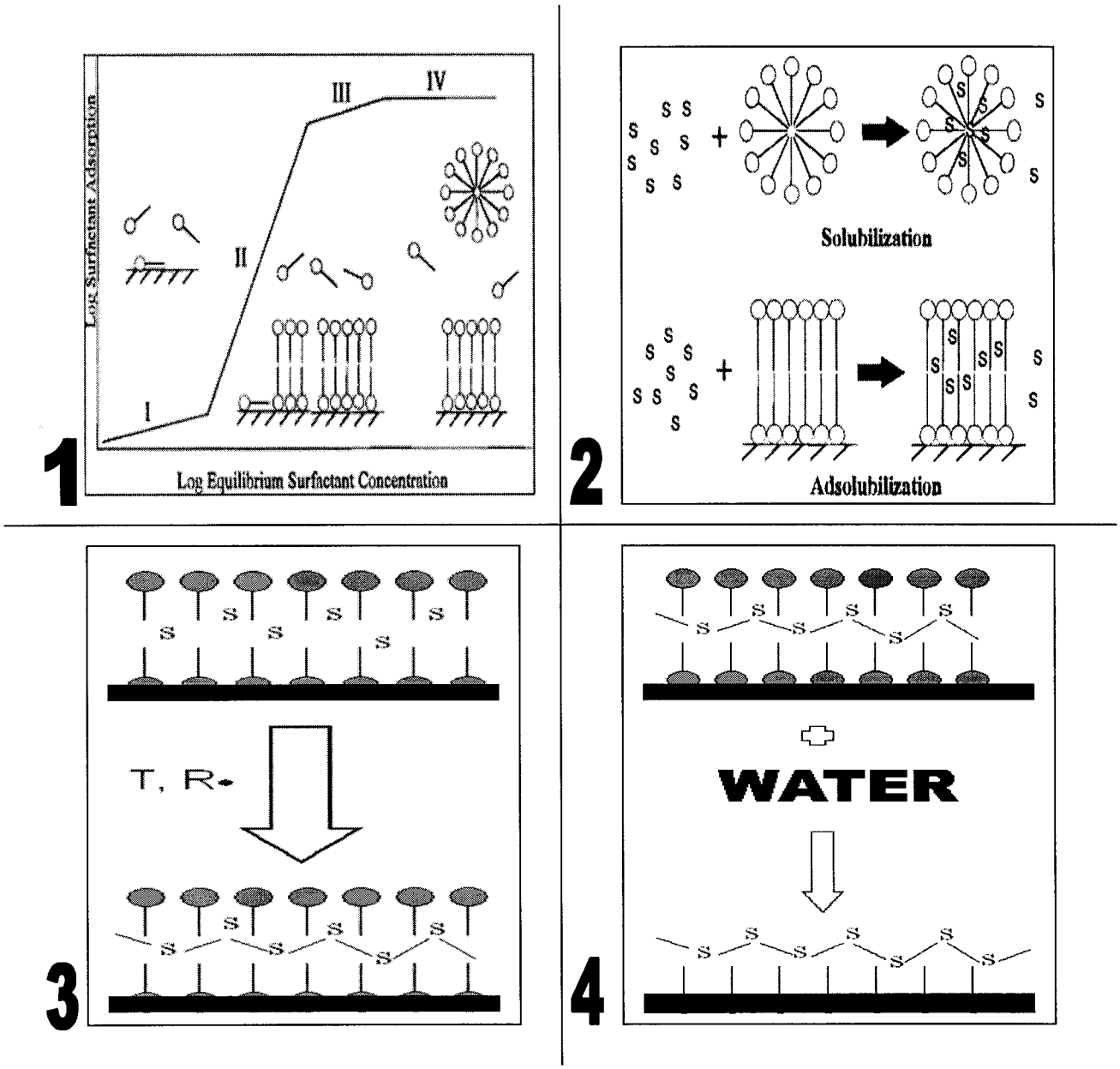

Figure 2.3 Sequential steps in surface modification of inorganic substrates by admicellar polymerization: 1. Surfactant adsorption. 2. Monomer adsolubilization. 3. Polymerization. 4. Film exposure.

Figure 2.4 depicts two adsorption isotherms constructed by exposing a measured weight of desized glass fibers (i.e., bare glass surface) to surfactant solutions of known initial concentration. The surfactants used herein were sodium dodecyl sulfate (SDS), with a CMC of ~8000 μM; and cetyltrimethylammonium bromide (CTAB), with CMC of ~920 μM. The shapes of both isotherms are very different, suggesting completely different adsorption kinetics. This behavior perhaps originates from the effect of heterogeneous adsorption sites both in number and energy level distribution. In the case of SDS, a highly negative charged molecule, a rapid adsorption is expected to take place over multivalent cationic sites such as the aluminum and calcium oxides in the glass fiber surface. Later, the DS^- ions will neutralize those silanol groups that have been protonated to $(SiOH_2)^+$ under the acidic conditions used in the experiments. This isotherm, having an S shape, is characteristic of a cooperative adsorption mechanism; and the saturation level attained close to the Critical Micelle Concentration (CMC), signals the adsorption of SDS beyond monolayer coverage. On the other hand, the ascension to the plateau observed in the CTAB isotherm is faster and takes place at lower bulk concentrations (Figure 2.4b). One reason for this is that glass tends to have a negative surface charge in aqueous solutions at pH values over 3.6, thus cationic surfactants will adsorb rapidly. Moreover, surfactants

with longer hydrocarbon chains have a much greater driving force for aggregation (i.e., lower CMC) and stronger tail-tail interactions.

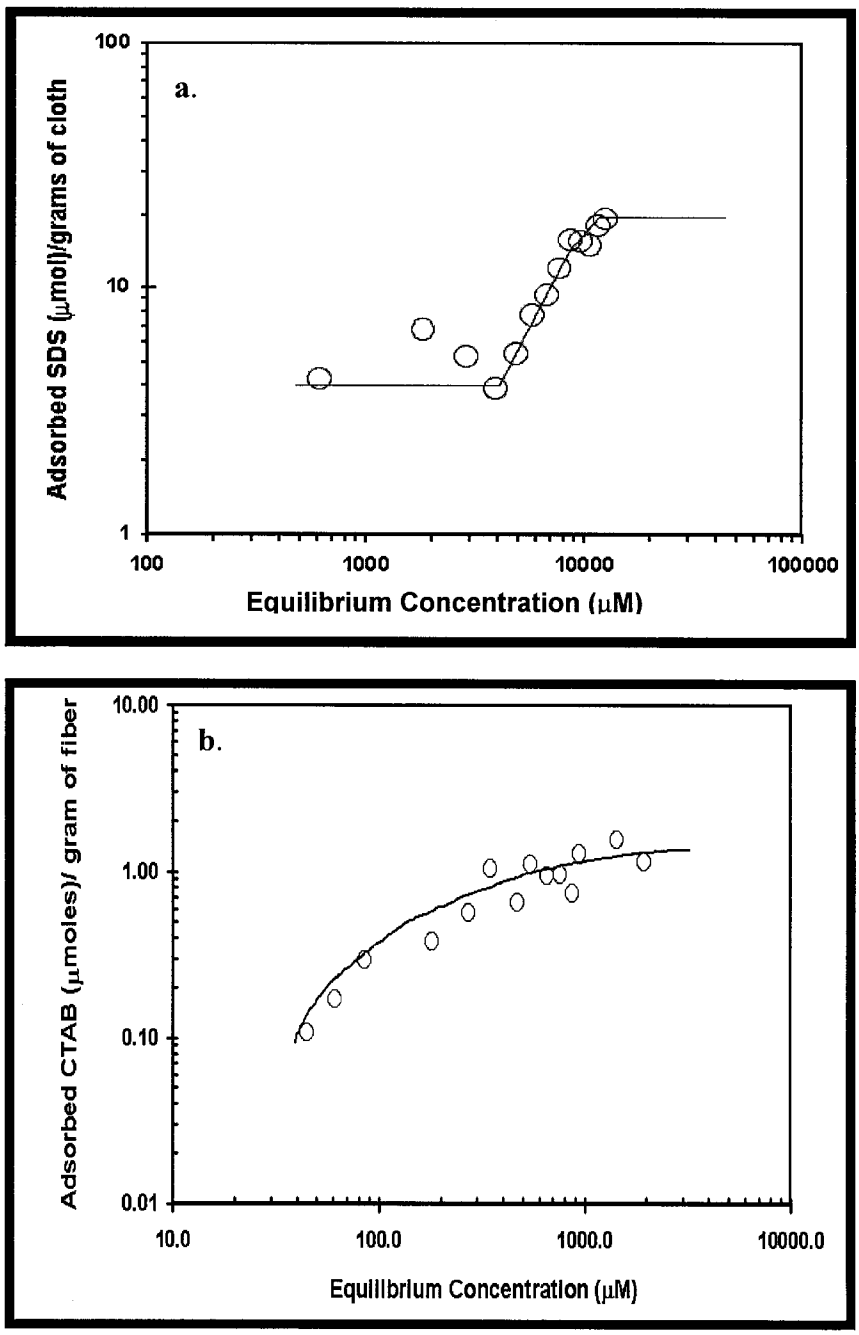

Figure 2.4 Adsorption isotherms of (a): anionic (SDS), and (b): cationic (CTAB) surfactants on desized glass fibers.

Surface aggregates formed by adsorbed surfactant molecules at surfactant concentrations below the CMC, usually called admicelles, hemimicelles or solloids, can be used to solubilize organic molecules in the same manner as bulk micelles do. Similar to solubilization, adsolubilization is driven by the preferential partitioning of the hydrophobic components to the interior of the admicelle as sketched in Figure 2.3, step 2. Monomer such as styrene and isoprene easily adsolubilize when brought in contact with aqueous surfactant solutions; and even some nonionic long-chain and aromatic alcohols, which are more hydrophilic, have also been shown to follow the same partitioning behavior [31-33]. Recent studies have demonstrated the versatility of the adsolubilization process by adsorbing metal ions and aromatic compounds simultaneously in the admicelles [34]. Once monomer molecules are located inside admicelles, the subsequent process (step 3 in Figure 2.3) is to initiate the polymerization by means of a suitable free-radical producing compound such as a soluble inorganic salt (e.g., potassium persulfate) or an inorganic azo-initiator (e.g., AIBN). The so-formed thin polymeric film will be completely exposed after thoroughly rinsing off surfactant with water. The latter procedure, followed by vacuum drying of the solid to drive-off water and unreacted monomer, constitutes the conclusion of the admicellar surface modification technique (step 4). Further details on reactant

quantities and reaction conditions used for admicellar-coating of glass fibers with elastomeric thin films will be presented in the coming chapters.

2.3 Elastomeric interlayers in glass-fiber reinforced polymers

Among the many reasons for the extended use of glass-fiber reinforced polymer composites as load-bearing components are their easy processing and low specific gravity. However, this particular combination of brittle fiber/brittle matrix composites is not free from intrinsic limitations that hamper their extended-life usage without catastrophic failures. On one hand, polymeric matrixes are regarded as relatively weak, low in modulus and high in thermal expansion. They also shrink greatly upon solidification, imbibe water and other liquids to a substantial degree, and cannot perform well at moderately elevated temperatures. These properties lead to internal cracking, difficulty in maintaining good adhesion, and chemical and thermal degradations in service [35]. On the other hand, failure of glass also occurs with a known dependence on time [36]. For instance, at a constant applied stress the time-to-failure is inversely proportional to the applied stress (i.e., static fatigue). Also, the stress-to-failure varies directly with changes in the strain rate (i.e., dynamic fatigue). These latter phenomena are closely related to surface flaws or defects

present in the glass surface that induce different crack initiation mechanisms and propagation rates when the material is loaded or strained.

In practical circumstances, the structural integrity and reliability of composite parts are dictated not only by the relative strength of their individual components while subjected to tensile loads (i.e., simple rule of mixture of individual properties), but by their capacity to absorb potential energy coming from other mechanical stress conditions: bending, torsion, compression as well as concentrated loads. Thus, a necessary element for the structural composites design is to obtain the maximum efficiency in stress transfer between the fiber and matrix across the interface. To control the interface and/or interlaminar properties in composites, a viable approach is to coat the fibers with appropriate polymers so that a new interphase/interlayer region will be formed. Kim and Mai [37], for instance, recently defined five key variables for the interlayer that may be tailored in order to optimize the mechanical performance of fiber-reinforced composites: a. type and nature of the interlayer; b. modulus, CTE (coefficient of thermal expansion) and glass transition temperature; c. thickness; d. modulus of matrix relative to interlayer; and e. interaction at the interface region.

Studies relating fiber coating to composite stiffness and toughness are abundant. For example, the theoretical work by Matonis and Small [38] is the first one indicating the introduction of a soft interlayer of finite thickness. Their simulation considered a hypothetical three-phase ordered composite represented by a spherical insert encapsulated by a number of concentric layers embedded in an infinite polymeric matrix. They considered a soft rubber interlayer between a styrene-acrylonitrile (SAN) matrix and glass inserts. In all calculations, the glass reinforcement was assumed to be loaded at volume fractions in the order of 15% to 20%. The major finding in this study was that in order to obtain adequate stress transfer, only a very thin layer of rubber is admissible: $R_0/R_1 \approx 0.999$; where $R_0/R_1 = 1$ represents the limiting case when the rubber interlayer thickness diminishes to zero. The use of slightly thicker layers of rubber ($R_0/R_1 \approx 0.96$) was shown to lower the modulus considerably, leading to an overall improved toughness but reduced strength. Jao and McGarry [39] later on developed a more refined finite-element analysis incorporating the multiaxial stress state of the continuum, and found that local stress concentrations occur in fiber-reinforced polymer composites, whether the structure is subjected to mechanical loads or temperature variations. Furthermore, they showed that the incorporation of a thin rubber coating, in the order of a 1% of

the fiber diameter, significantly mitigates the stress intensity, especially at the fiber-end corner. Other theoretical works have reached similar conclusions in that the interphase region between fibers and matrix in a composite can significantly affect the load transfer characteristics, even when the interphase is very thin [40].

Experimental evidence of the benefits of soft interlayers began with the pioneering work of Lavengood and Michno [41], followed by the work of Tryson and Kardos [42], who showed that solution-cast thick ductile innerlayers are effective in preventing filament abrasion as well as in enhancing crack-arrest mechanisms during composite fracture. Today it is generally accepted that a soft interphase is advantageous because it changes the stress distribution and decreases stress concentration, consequently increasing the fracture toughness. Labronici and Ishida [43] published a comprehensive review of the methods used by various investigators, and as a general trend they observed that fracture toughness of reinforced composites typically increased by 0 to 100% while the strength and modulus values decreased by 0 to 50% with the use of rubbery coatings.

Toughening mechanisms operating as a result of the introduction of an interlayer of elastomeric nature are very diverse, but it can be

assumed that they all converge towards the necessary condition of interface debonding during the micro-failure event. In those cases where the adhesion between the fiber and the matrix is very strong, the crack propagation rate can be very high and thus lead to brittle fracture of both matrix and fibers (i.e., fracture toughness of the composite is low), as represented schematically in Figure 2.5.

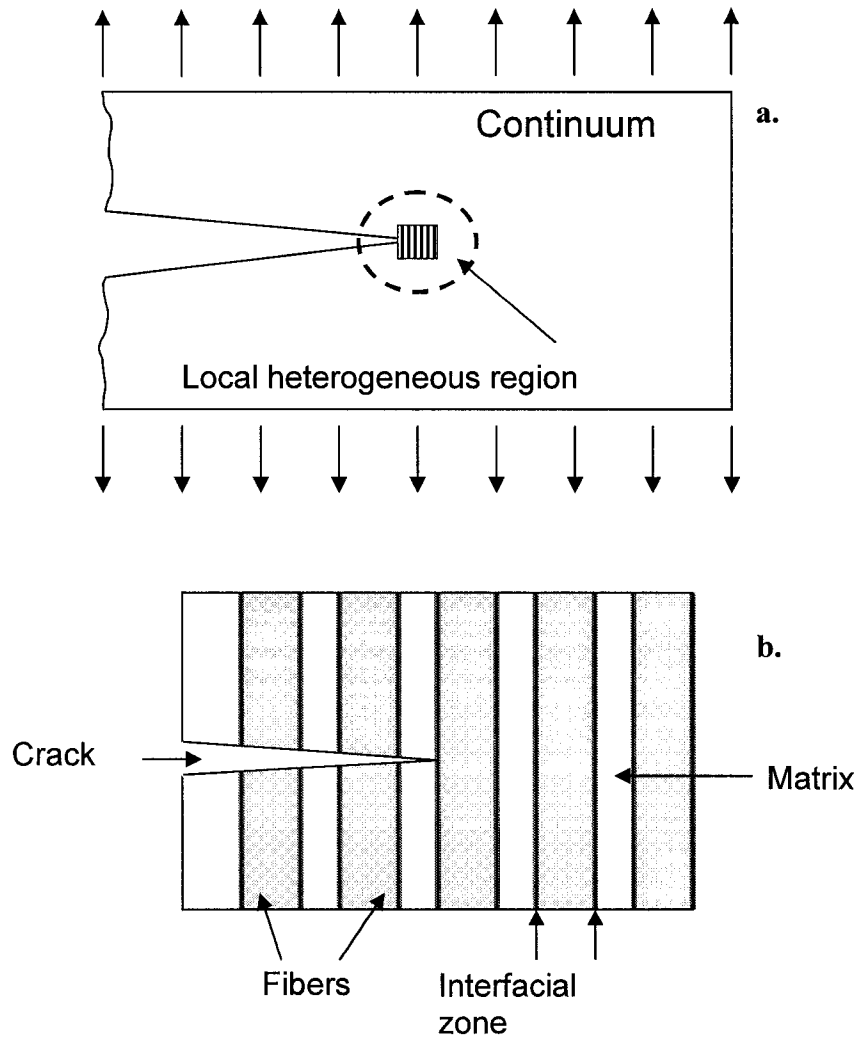

Figure 2.5 Model of crack interaction in a simple composite with strong interface adhesion. (a) Global region loaded in tension. (b) Local heterogeneous region embedded in a linear elastic anisotropic continuum [44].

A weak interface bond is detrimental to some mechanical properties (e.g., tensile and compressive strengths). However, it has the ameliorating effect of allowing other failure mechanisms to take place more readily and extensively with enhanced stability in crack growth. As a result, composite materials exhibit an overall improvement in their energy absorption capability and thus in their fracture toughness. The Cook-Gordon mechanism (Figure 2.6) explains high fracture toughness originating when failure occurs preferentially along the interface (i.e., debonding) before fiber fracture. Many investigators have recognized the occurrence of this failure mechanism in unidirectional fiber composites, and have presented evidence of tensile debonding ahead of the crack tip. Marston, Atkins and Felbeck [45] developed an equation for the work of fracture due to Cook-Gordon debonding, as:

$$R_{CG} \approx V_f \frac{l_c}{d} R_m . \qquad (2.3)$$

Where V_f represents the fiber volume fraction of the composite; R_{CG}, the specific work of fracture due to Cook-Gordon debonding; d, the fiber diameter; l_c, the critical fiber length (i.e., length over which stress

can be transferred along the fiber matrix interface); and, R_m is the work of fracture of the matrix.

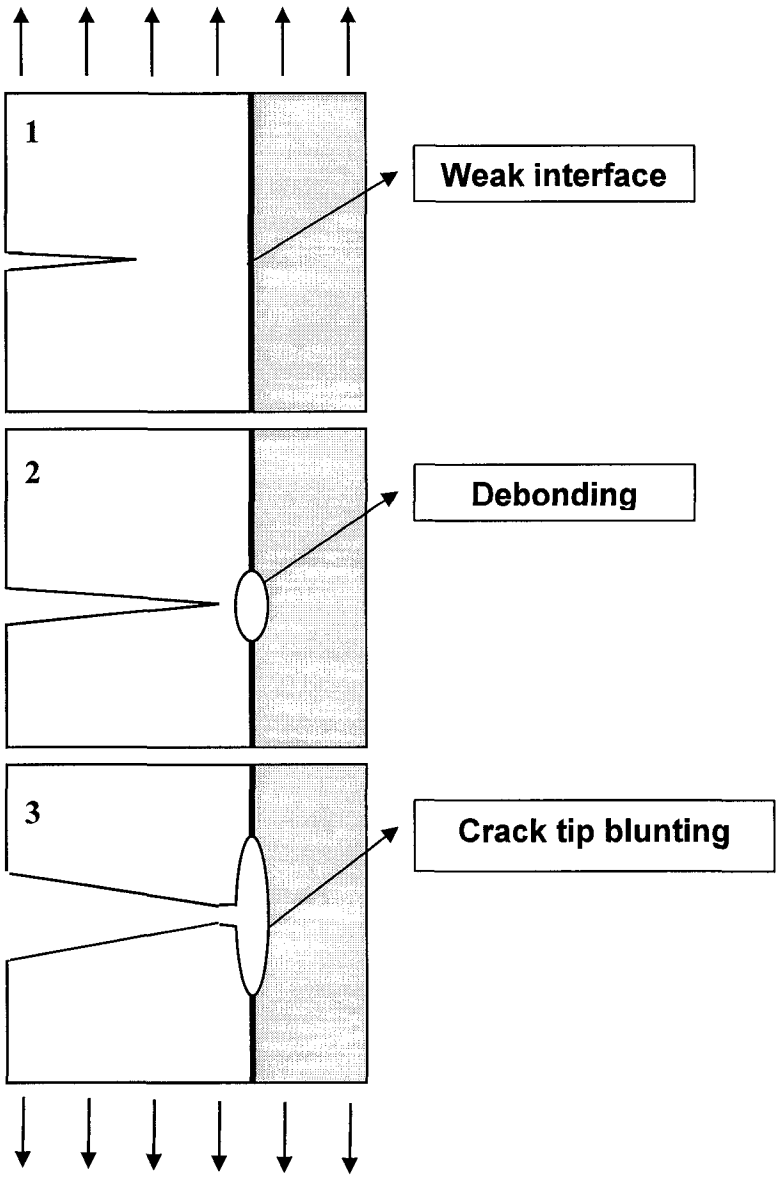

Figure 2.6 Crack progression and arrest in a model composite due to a debonding or Cook-Gordon mechanism. Adapted from [37].

References

1. L.H. Sharpe, in: *The Interfacial Interactions in Polymeric Composites*, G. Akovali (Ed.). Kluwer Academic Publishers, Dordrecth, The Netherlands, pp. 1-20 (1993)
2. J. Israelachvili, in: *Intermolecular & Surface Forces*, Academic Press, New York, pp. 312-337 (1992)
3. W.D. Bascom, in: *The Wetting Behavior of Fibers*, M.E. Schrader and G.I. Loeb (Eds.). Plenum Press, New York, pp. 359-373 (1992)
4. B. Larson and L. Drzal, *Composites* **25**, 711 (1994).
5. J.-I. Yamaki and Y. Katayama, *J. Appl. Polym. Sci.* **19**, 2897 (1975)
6. T. Ogawa and M. Ikeda, *J. Adhes.* **43**, 69 (1993)
7. L. Jenkins and A. Donald, *Langmuir* **15**, 7829 (1999)
8. L. Skartsis, B. Khomami and J.L. Kardos, *SAMPE J.* **28**, 19 (1992)
9. V. Rohatgi, N. Patel and J. Lee, *Polym. Composites* **17**, 161 (1996)
10. H.J. Barraza, Y.K. Hamidi, L. Aktas, E.A. O'Rear and M.C. Altan, J. *Composite Mater*, in press.
11. J. Wilhelmy, *Ann. Physik.* **119**, 177 (1863)
12. B. Miller and R. Young, *Text. Res. J.* (**May**), 359 (1975)
13. J. Seebergh and J. Berg, Cahn *Application Note* **1715**, 1 (1991)

14. A.-C. Lassas, L. Fagerholm, B. Stenlund and J. Näsman, *Polym. Composites* **14**, 1 (1993)

15. H. Fagerholm, C. Lindsjö, J. Rosenholm and K. Rökman, *Colloids Surf.* **69**, 79 (1992)

16. S. Shalaby, D. Clupper and T. Taylor, US Patent 5874509, p6 (1999)

17. H. Fagerholm, C. Lindsjö, J. Rosenholm, *J. Mater. Sci.* **30**, 2420 (1995)

18. H. Fagerholm, C. Lindsjö, J. Rosenholm, K. Rökman, *Colloids. Surf.* **69**, 79 (1992)

19. G. Funkhouser, M. Arevalo, D. Glatzhofer and E.A. O'Rear, *Langmuir* **11**, 1443 (1995)

20. D. Glatzhofer, G. Cho, C. Lai, E.A. O'Rear and B. Fung, *Langmuir* **9**, 2949 (1993)

21. C. Lai, E.A. O'Rear, J. Harwell and M. Hwa, *Langmuir* **13**, 4267 (1997)

22. B. Kitinayan, J. O'Haver, J. Harwell and S. Osuwan, *Langmuir* **12**, 2162 (1996)

23. J. O'Haver, J. Reynolds, J. Harwell, B. Grady, L. Evans and W. Waddell, *Book of Abstracts, 219th ACS National Meeting, San Francisco, 2000*; American Chemical Society: Washington, DC (2000)

24. W.-L. Yuan, E.A. O'Rear, B.P. Grady and D.T. Glatzhofer, *Langmuir* **18**, 3343 (2002)

25. W. Genetti, W.-L. Yuan, B.P. Grady, E.A. O'Rear, C. Lai and D. Glatzhofer, *J. Mater. Sci.* **33**, 3085 (1998)

26. S. Sakhalkar and D. Hirt, *Langmuir* **11**, 3369 (1995)

27. B. Grady, E.A. O'Rear, L. Penn and A. Pedicini, *Polym. Compos.* **19**, 579 (1998)

28. J. O'Haver, B. Grady, J.H. Harwell and E.A. O'Rear, in: *Reaction and Synthesis in Surfactant Systems*, J. Texter (Ed.), pp. 537-545. Marcel Dekker, New York (2001)

29. M. Drach, W. Rudzinski and J. Narkiewics-Michalek, *J. Dispersion Sci. Technol.* **21**, 683 (2000)

30. P. Somasundaran and L. Huang, *Adv. Colloids Interface Sci.* **88**, 179 (2000)

31. K. Esumi, K. Sakai and T. Kanjiro, *J. Colloid Interface Sci.* **224**, 198 (2000)

32. K. Esumi, H. Toyoda, M. Goino, T. Suhara and H. Fukui, *Langmuir* **14**, 199 (1998)

33. C. Lee and H. Tsai, *Separation Sci. Technol.* **30**, 285 (1995)

34. K. Esumi, H. Hayasi, K. Yoshifumi, S. Tsuneo and F. Hiroshi, *Colloids Surf. Sci. A* **144**, 201 (1998)

35. F.J. McGarry, *Annu. Rev. Mater. Sci.* **24**, 63 (1994)

36. K.J. Rao, in: *Structural Chemistry of Glasses*. Elsevier, Amsterdam, pp. 401-427 (2002)

37. J-K. Kim and Y-W. Mai, in: *Engineered Interfaces in Fiber Reinforced Composites*. Elsevier, Amsterdam, pp. 239-327 (1998)

38. V.A. Matonis and N.C. Small, *Polym. Eng. Sci.* **9**, 90 (1969)

39. S.H. Jao and F.J. McGarry, *J. Composite Mater.* **26**, 2632 (1992)

40. S.A. Hayes, R. Lane and F.R. Jones, *Composites Part A* **32**, 379 (2001)

41. R. E. Lavengood and M.J. Michno, Jr., in: *Proc. Div. Tech. Conf., Engrg. Props. And Structure Div.* Society of Plastics Engineers, p. 127-129 (1975)

42. L.D. Tryson and J.L. Kardos, in: *36th Ann. Conf. Reinf. Plast. /Compos. Inst., The Society of the Plastics Industry*, Session 2-E, p. 1 (1981)

43. M. Labronici and H. Ishida, *Compos. Interfaces* **2**, 199 (1994)

44. V. Papaspyropoulos, J. Ahmad and M.F. Kanninen, in: *Effect of Defects in Composite Materials*, ASTM Special Tech. Pub. 836, pp.237-249 (1982)

45. T.U. Marston, A.G. Atkins and D.K. Felbeck, *J. Mater. Sci.* **9**, 447 (1974)

3. Experimental Methods

3.1 Dynamic contact angles on admicellar-coated fibers

The micro-Wilhelmy technique is a well-known method of assessing the surface free energy of monofilaments by indirectly measuring the contact angle of an advancing (or receding) fluid front over a fibrous substrate. As explained in the previous chapter (Figure 2.2), this technique relies on gravimetric measurements of the force exerted by the probe liquid while moving over a constant-geometry solid phase [1]. Several authors have used this technique in the past to evaluate changes in wettability of glass and carbon fibers after physical or chemical modification of their surfaces [2-5]. Herein, we used the automated micro-Wilhelmy system Cahn DCA-322 consisting of a Cahn microbalance, micro-stepping motor and on-line control/data acquisition software (WinDCA 1.02). A thorough description of the components and operational features of this equipment can be found elsewhere [6].

The procedure for measuring the contact angle started by mounting a single fiber onto a thin metallic wire that was subsequently hung from the arm of the microbalance. To do this, a monofilament was taken carefully out of the fiber mat – using tweezers – and then brought in contact with a thermoplastic adhesive (Tempfix®) that fixed it to the wire. To avoid fiber kinking while entering the liquid probe, especially with high viscosity resins, the fibers were trimmed to a length of approximately 5 mm. In addition, the total submersed depth during advancing and receding of the liquid was kept to only 2 mm. More details on common preparation steps for dynamic contact angle analysis on fibers are available in a report by Domingue and Francisco [7].

After ensuring the fiber was positioned perpendicularly to the liquid probe surface, the stage supporting the liquid container was raised at a constant velocity (e.g., 2 μm/s) with the aid of the micro-stepper motor until a zero depth of immersion (ZDOI) was detected. The ZDOI was set in advance to a threshold value between 0.01 and 0.025 mg. Forces above the ZDOI triggered the system to recording the transient force as a function of the liquid front position. Figure 3.1 shows a typical tensiogram including the ZDOI and both the advancing and receding regions of the analysis. Regression analysis of the

transient force coupled with the Wilhelmy equation (i.e., equation 2.2) allowed the calculation of both advancing and receding dynamic contact angles.

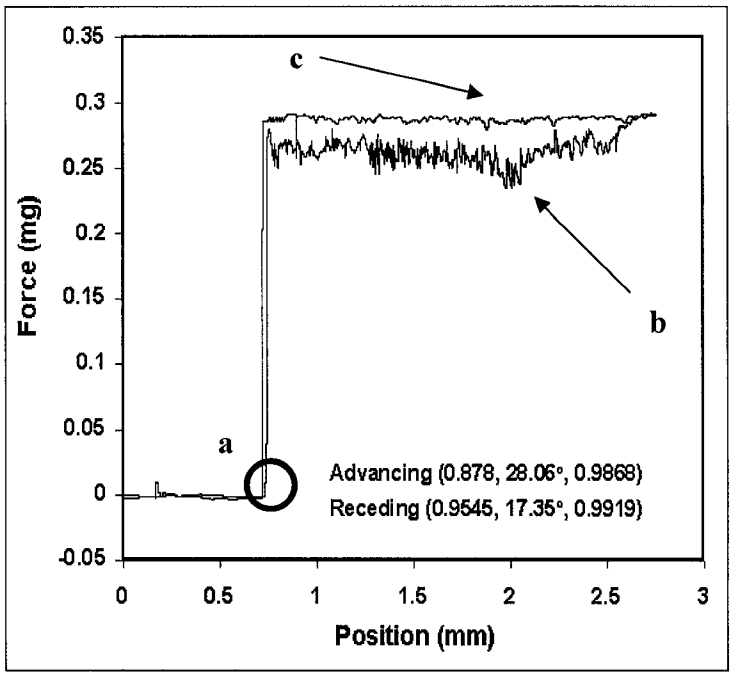

Figure 3.1 Typical tensiogram and its major components: (a) ZDOI; (b) Advancing arm; and (c) Receding arm.

3.2 Procedure for RTM composites fabrication

Resin Transfer Molding (RTM) is an example of the more general family of Liquid Molding (LM) techniques devised to manufacture high-performance composites for aerospace and structural applications. In RTM, an uncured liquid resin is mechanically injected into a mold containing an inorganic porous or fibrous reinforcement. The resin is

expected to displace the air inside the mold, quickly filling up all empty spaces within the preform as was shown schematically in Chapter 1, Figure 1.2. To force the impregnating liquid through the porous-solid reinforcement mechanical energy must be applied. Typically, RTM is conducted either at constant pressure or at constant injection flow rate. In the former procedure, a one-component resin, or a premixed system, contained in a 'pressure-pot' is forced into the mold by applied pressures in the order of 0.1 – 0.9 MPa [8]. The second variant, constant flow RTM, uses positive displacement pumps to ensure a constant liquid flow rate.

Herein, we used a high-speed molding setup consisting of two major components: a hydraulic press and a rectangular aluminum mold containing the preform. The molding press had two hollow cylinders, two plungers and a 40-ton hydraulic (ARCAN, Model CP402) press that provided the force necessary to inject the reacting mixture into a disk-shaped mold cavity. Prior to the injection, EPON 815C epoxy resin (Shell Chemicals Inc.) and Epicure 3282 curing agent were separately loaded into the two hollow stainless-steel cylinders. These cylinders had inner diameters of 55.5 mm for the resin and 25.5 mm for the curing agent, such that a ratio of 4.7 to 1 by volume was achieved with the constant displacement rate of the plungers. During

molding, a linear velocity of 2 x 10^{-3} m/s of the hydraulic ram was maintained through most of the 152.4 mm stroke, which yielded an injection rate of approximately 5.32 cm^3/s. Details of the components in the molding press are sketched in Figures 3.2 to 3.4. The circled area in Figure 3.2 corresponds to the ram-plate connector accessory, sketched in more detail in Figure 3.3. The area in the box beneath the circle comprises the resin and curing agent reservoirs (i.e., cylinders), whose dimensions are given in Figure 3.4.



Figure 3.2 RTM molding setup and data acquisition system. Photo courtesy of the Composites Group, Aerospace and Mechanical Engineering, University of Oklahoma.

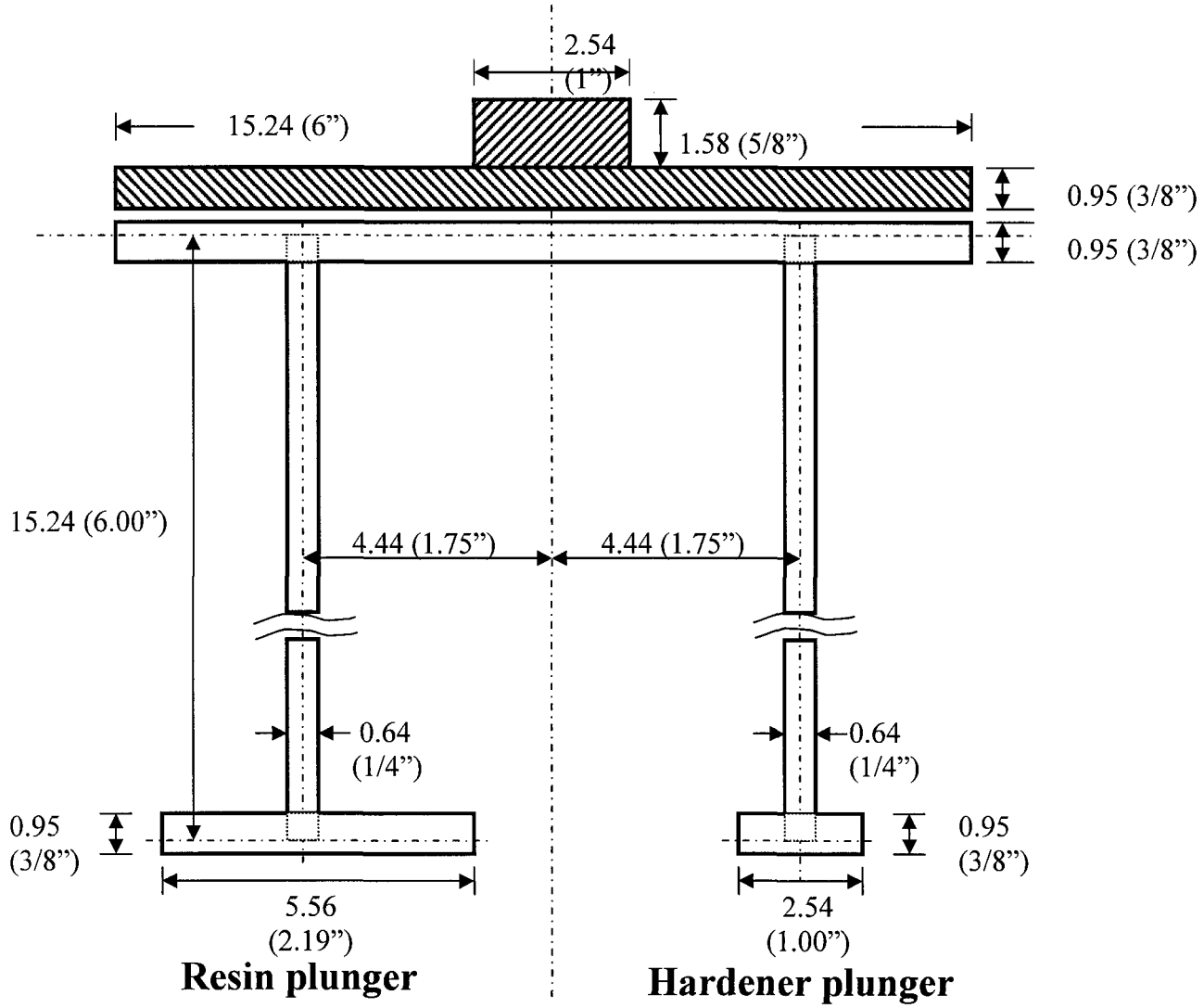

Figure 3.3 Ram-plate connector accessory and plungers of the molding press. Note: all dimensions in centimeters.

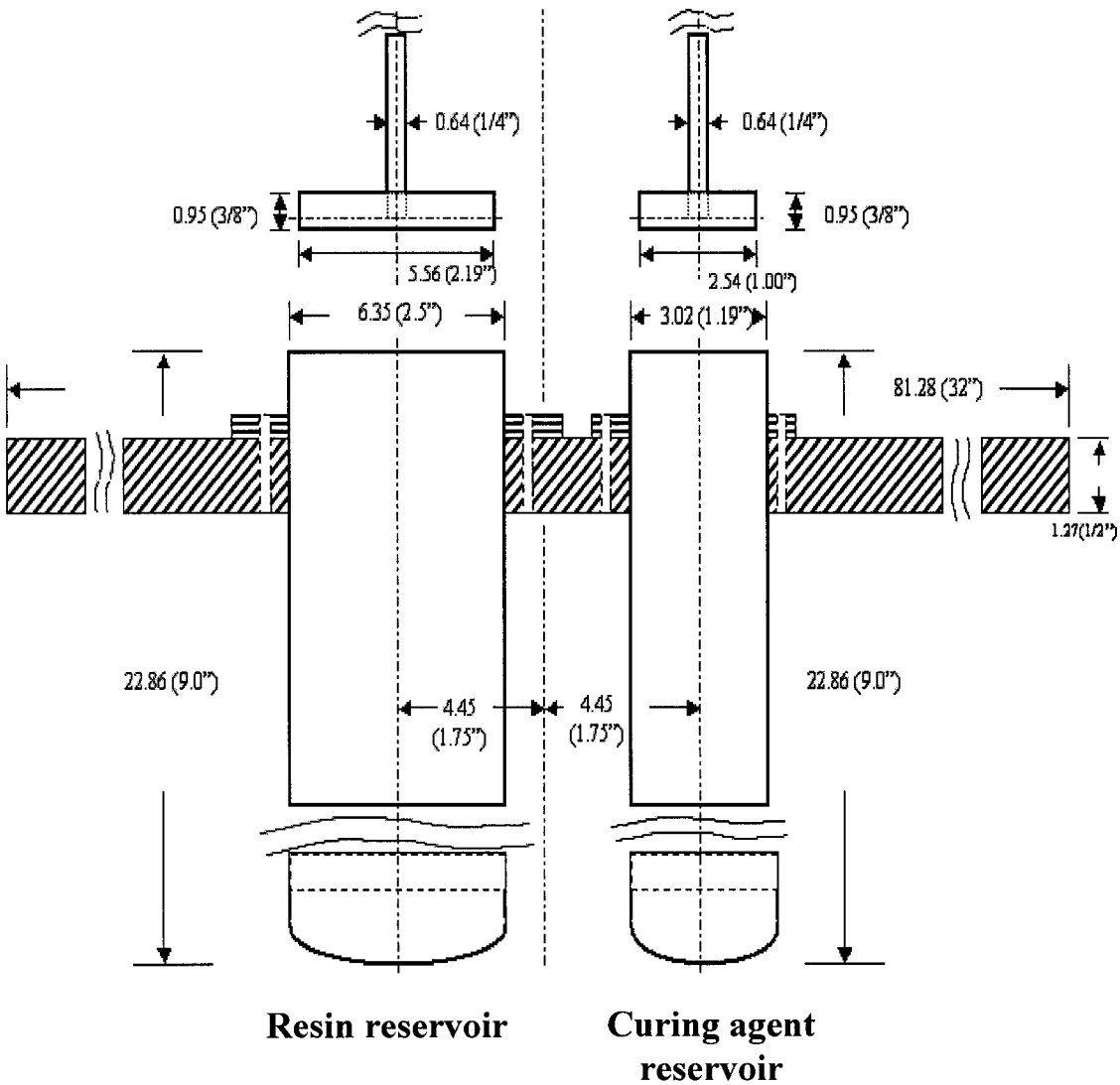

Figure 3.4 Positive displacement system (plunger/cylinder) for liquid prepolymer injection. Note: all dimensions in centimeters.

The resin and curing agent flows merged in a T-connector and thereafter passed through a Statomix® inline mixer (ConProTec, Inc.) comprising 32 alternating helical segments placed inside a 155 mm-long polypropylene tube with 5 mm inner diameter and 8 mm outer diameter. The center-gated disk-shaped aluminum molds were made of two square walls with dimensions: 228.6 mm x 228.6 mm x 6.35 mm, separated by a 3.18 mm-thick aluminum spacer plate. To create the mold cavity, a 152.4 mm diameter disk was cut out of the center of the aluminum spacer plate. Both the top and bottom aluminum parts had a circular groove of 184 mm in diameter and 0.3 mm in depth carved out to accommodate a rubber seal. Inlet gate and exit vents were drilled and tapped on the top mold wall. The inlet was located in the center of the disk and had either plastic or brass barbed fittings connected to the feeding hose (ID=6.2 mm). The four symmetrical vents (ID=1.6 mm) were positioned 90° apart at a radius of 88.9 mm.

The reinforcement was cut and loaded into the mold cavity to obtain the specified fiber volume fractions. Positive displacement of the plungers by the molding press ensured that infusion of the reacting prepolymer through the preform would take place at a constant volumetric flow rate. Due to the circular mold geometry, the resin

front advances through the dry preform and towards the exits; and in most cases, a radial liquid front symmetry could be assumed. Figure 3.5 shows the progression of the impregnating front geometry during the fabrication of random mat composites by RTM.

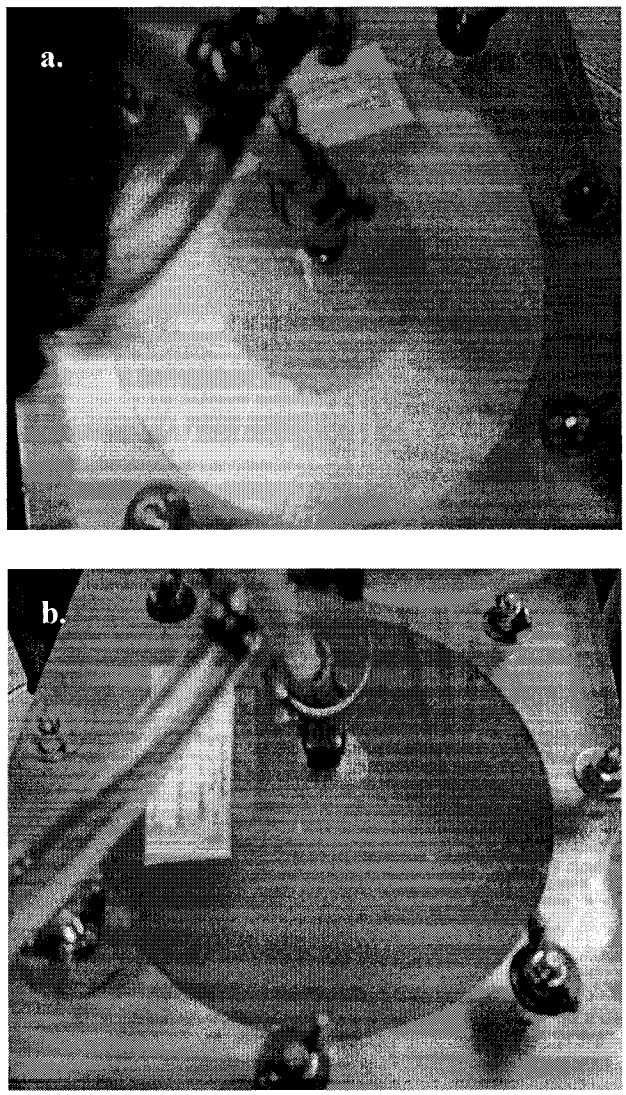

Figure 3.5 Impregnating flow front progression for the RTM fabrication of random-mat composites. (a) Radial liquid front symmetry at early times; (b) Fully impregnated preform. Photos courtesy of the Composites Group, Aerospace and Mechanical Engineering, University of Oklahoma.

Very close to the entrance, the impregnating front moves at high velocities yielding much faster local velocities at the mold cavity mid-plane. Further away from the injection port, the advancing front velocity decreases monotonically at radial positions. The total energy of the liquid is reduced due to the mold geometry, together with the resistance exerted by the dry preform surface. This energy dissipation becomes greater as the dry surface area opposing the flow increases radially, until the fluid impregnates the whole solid and finally reaches the vents (Figure 3.5b).

3.3 Mechanical testing

3.3.1 Interfaciai adhesion in fibrous composites. Among the different specimen geometry and loading configurations available in the literature for measuring in-plane properties of fiber-reinforced composites, the short beam shear test stands out because it ideally provides a region of pure uniform shear stress necessary for assessing the interlaminar shear properties. The short beam shear test method was standardized by ASTM, as ASTM D2344/D2344M-00, and can be applied to all kinds of fiber-reinforced composites. It is worth saying that although an interlaminar shear failure is not always obtained; interlaminar shear strength (ILSS) test data are relatively consistent within batches and between different test sites. This consistency

coupled with low fabrication, preparation and testing costs, supports its popular use to evaluate the effects of fiber finish and surface treatments, as well as fiber-matrix compatibility.

The specimen preparation requirements for the short beam shear test are simple and only a small amount of material is needed. Typically, the specimen thickness is around 2 mm for advanced composites, and even materials with thicknesses other than 2 mm can also be tested provided both the geometric relations (length/thickness) and (width/thickness) are equal to 5. Figure 3.6 shows an experimental setup for the ASTM D2344/D2344M-00 test.

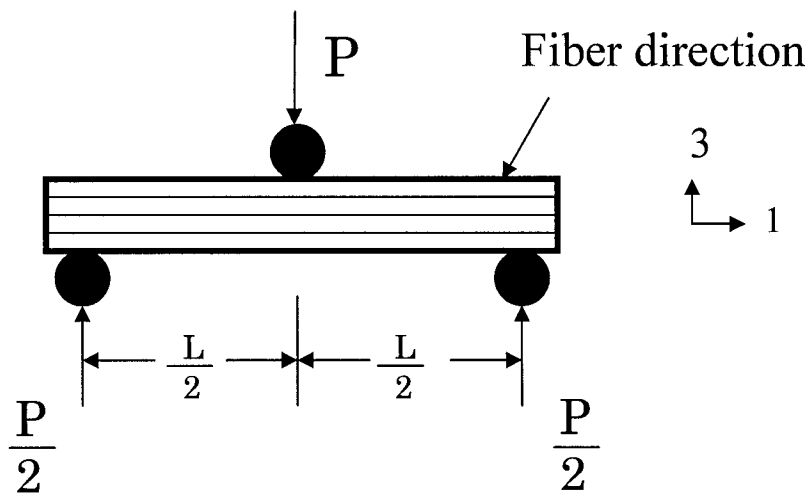

Figure 3.6 Three-point bending configuration for the short beam shear strength test according to ASTM D2344/D2344M-00.

The case portrayed in the figure involves loading a beam from a unidirectional laminate composite in a three-point bending fixture. In interpreting the short beam shear test results, the maximum value τ_{max} (i.e., the ILSS of the shear stress distribution along the thickness direction) is related to the maximum applied load P_{max} (specimen width b, and thickness t), according to the classic short beam relationship:

$$\tau_{\max} = \frac{3P_{\max}}{4bt} \tag{3.1}$$

3.3.2 Tensile testing. The standard ASTM D3039/D3039M-00 was used herein to determine the in-plane tensile properties of all RTM-molded composites. As it is stated by the standard, this test can be performed over continuous or discontinuous fiber-reinforced composites provided that the laminate specimen is balanced and symmetric with respect to the test direction. Tensile specimen geometry requirements for the test are reported in Table 1 of the ASTM D3039/D3039M-00 standard report.

Tensile strength of fiber-reinforced composites is mostly a fiber-dominated property, and it gives little information on the state of the interface. However, it is well known that the beneficial effect resulting

from the introduction of a sizing could definitely be observed on the overall resistance of the composite part. We measured two important parameters using the tensile testing: the ultimate tensile strength (UTS) and the stiffness (E). A typical testing procedure consisted in cutting specimens of dimensions 11.43 cm x 1.27 cm x 0.4 cm and mounting them into the grips of a materials testing system (MTS 810), as depicted in Figure 3.7, and subsequently applying a tensile force ramped linearly from 0 to 8.9 kN over 120 s. Strain measurements were obtained simultaneously during tensile tests by placing a calibrated extensometer over a 2.54 cm span at the center of the specimen.

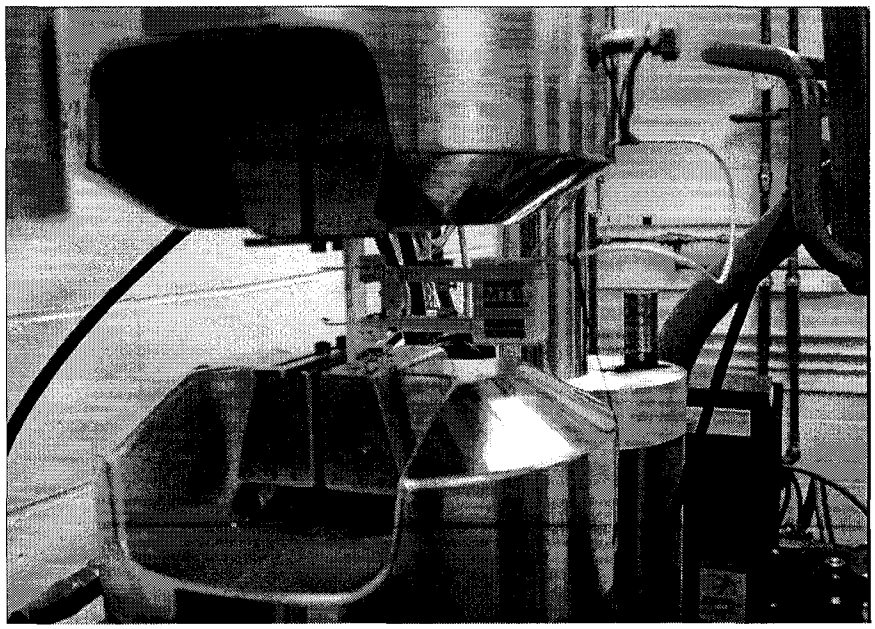

Figure 3.7 Setup used for tensile testing according to ASTM D3039/D3039M-00. Photo courtesy of the Composites Group, Aerospace and Mechanical Engineering, University of Oklahoma.

Typical maximum loads for specimens used in the current study were around 1000 – 1600 lbs. Representative stress-strain curves for two different kinds (with and without sizing) of RTM epoxy/glass composites tested with the procedure described above are shown in Figure 3.8.

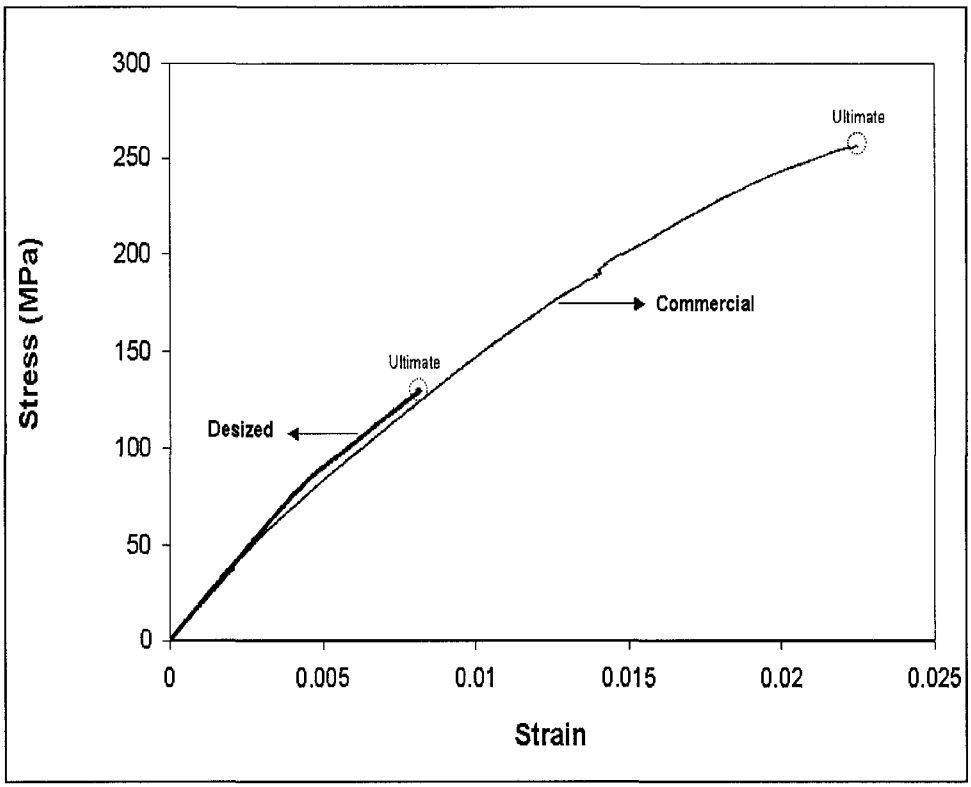

Figure 3.8 Typical tensile stress-strain curves

3.4 Voids characterization

Porosity evaluation in composite materials by means of optical image analysis has been demonstrated to be among the most accurate methods for measuring the true void content [9]. Furthermore, the

image analysis technique has the advantage of providing detailed information of other important parameters such as voids distribution, shape and size that can not be assessed by either physical (e.g., relative density) or chemical (e.g., acid digestion) methods. It is well known that voids with different characteristics are likely to originate from various sources during filling, and will contribute to mechanical properties and failure mechanisms differently. For instance, void size directly affects void mobility, consequently changing the void distribution inside the part. Void shape affects mechanical properties, with irregular voids being more likely to induce early crack formation.

Voidage measurements by optical imaging usually imply the random acquisition of pictures over the area of interest followed by the statistical averaging of the void areas measured in each picture. In the current work, unlike most previous work, we performed image analysis over the entire cross-sections of specimens cut from the center of fully cured disks. These cross-sections, that in most cases had average length and thickness of 76.27 mm and 3.98 mm, respectively, were first embedded in a commercial resin (Embed 812-DER 736) and subsequently machined to have a flat base surface for further polishing. A series of silicon carbide pastes of different grit sizes ranging from 240 to 1200 ensured a smooth finish. Once polished the

cross-sections were analyzed and pictures of individual voids taken at 100x with an optical microscope/image capture system: Nikon OPTIPHOT-2 and CCD camera (Hammatsu C2400). Thereafter, individually captured pictures were processed with the aid of an image analysis software (Optimas v4.1), which had features such as area morphometry that enabled not only the void area measurement, but also the classification of the voids according to their size and shape (i.e., circularity, φ= perimeter^2/area). The void volume fraction at each cross section was assumed to be linearly equivalent to the ratio of the total void area by the entire area of the cross section [10].

To account for the void morphometry, we classified the voids into three categories based on their circularity values: circular, ellipsoidal and irregular. A circularity of 12.58 was used as the defining threshold value for circular voids as the one shown in Figure 3.9a. Circular voids were mostly found in matrix-rich zones. Values in the range $12.58 < \varphi < 20$, were typically assigned to ellipsoidal geometries (Figure 3.9b). Ellipsoidal voids are trapped in the intertow spacing and take this shape by conforming to the channel geometry. Lastly, circularities above 20 represented voids with a completely irregular shape. The irregular voids were, in most cases, found either inside the intratow areas or engulfing a group of fibers from a tow.

They appeared as if they were originated from rounded bubbles that had been pushed into the tows by a high shear force during resin flow (Figure 3.9c).

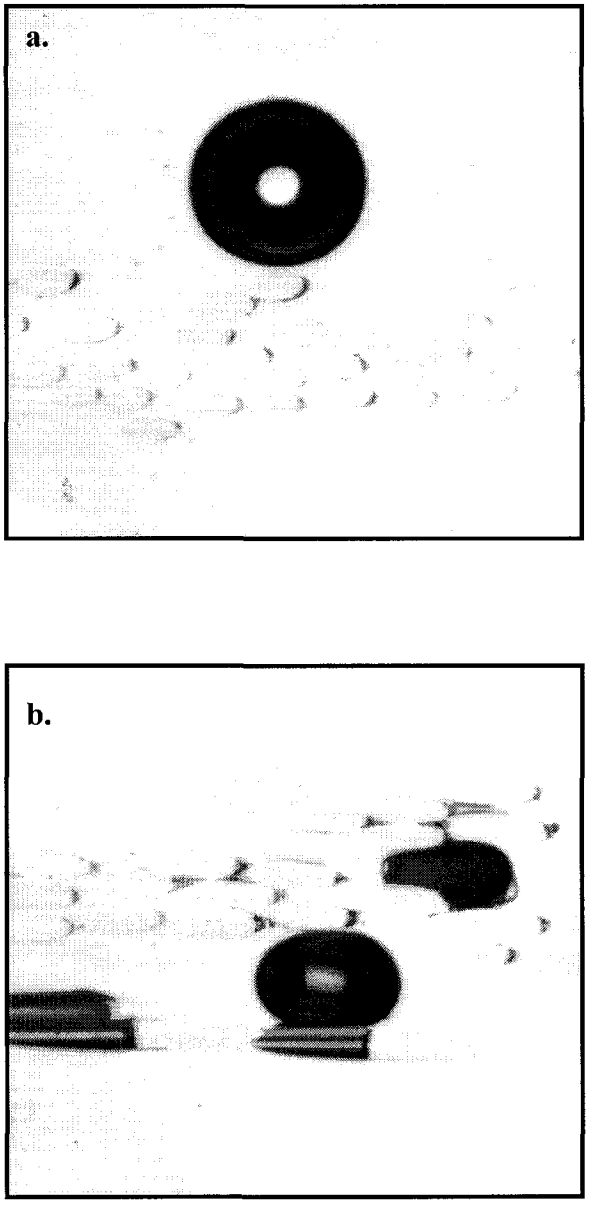

Figure 3.9 Examples of circular (a), Ellipsoidal (b) and Irregular (c) voids found in RTM composites. Pictures taken at 200x.



Figure 3.9 (Continued).

References

1. B. Miller and R. Young, *Text. Res. J.* (**May**), 359 (1975)
2. K. Tsutsumi, S. Ishida and K. Shibata, *Colloid Polym. Sci.* **268**, 31 (1990)
3. J. Schultz, L. Lavielle and C. Martin, *J. Adhes.* **23**, 45 (1987)
4. Y-L. Lee, *Langmuir* **15**, 1796 (1999)
5. A. Bismarck, M. Pfaffernoschke and J. Springer, *J. Appl. Polym. Sci.* **71**, 1175 (1999)
6. J. Domingue, *Cahn Application Note* **1725**, 1 (1991)
7. J. Domingue and E. Francisco, *Cahn Technical Note* **1726**, 1 (1991)

8. R. Gebart and L. Strömbeck, in: *Processing of Composites*, R.S Davé and A.C. Loos (Eds.). Hanser Publishers, Munich, Germany, pp. 358-387 (2000)
9. S.R. Ghiorse, in: *A Comparison of Void Measurement Methods for Carbon/Epoxy Composites*. US Army Materials Technology Report MTLTR 91-13, pp.1-25 (1991)
10. J. Russ, in: Practical Stereology, 1st Edition. Plenum Press, New York (1986)

4. Wetting Behavior of Elastomer-Modified Glass Fibers*

4.1 Introduction

Materials usually referred to as polymer-matrix composites (PMC) combine particulate or fibrous fillers with a polymeric matrix. The purpose of the filler is to impart some unique property to the material, often high stiffness or strength, while the thermoplastic or thermoset polymer binds the reinforcing fibers or particles. In essence, the reinforcement and the matrix retain their original physical and chemical identities, yet together they produce a combination of mechanical properties that cannot be achieved with either of the constituents acting alone.

The interface between the two constituents has such a dramatic effect on the mechanical performance and structural integrity of the

* Material in this chapter was published in *Langmuir* **17**, 5288 (2001).

composite that continued research efforts have been undertaken to tailor the surface of the reinforcement for particular end applications [1-4]. For glass fibers, modification of the surface by means of organosilane coupling agents is the standard commercial approach because these agents have proven to be an effective way to enhance the adhesion of glass fibers to many thermoset polymer matrices, including epoxies. However, these proprietary formulations are often expensive and designed for specific resin systems.

Our research group has recently introduced an alternative surface modification method applicable to glass fibers that uses surfactants and elastomeric monomers. Admicellar polymerization is the term used to describe this procedure and involves the formation of a thin polymeric film on the fiber surface. The elastomeric film present at the interface has been shown to produce test results consistent with good interfacial adhesion for single-filament pullout and three-point bend tests [5].

During composite fabrication the presence of a large number of small diameter fibers generates time-dependent phenomena directly associated to the interfacial properties of the reinforcement (e.g., flow instabilities caused by rapid mold filling processes and large capillary

forces originated inside the fiber tows). Initial wetting of the fiber by the liquid incipient matrix also significantly affects ultimate interfacial adhesion and composite integrity. Many studies have shown that good wetting is particularly important, not only in achieving high interfacial adhesion, but also because wetting quality influences the entrapment of air and whether any resulting voids remain in the interface or are displaced into the matrix [6].

The driving force for the adhesional wetting of a liquid, not originally in contact with a substrate, is the balance between the surface energy of the solid (i.e., reinforcement in composites), γ_{SV}; the surface tension of the liquid (i.e., matrix resin), γ_{LV}; and the interfacial tension between the substrate and the wetting liquid, γ_{SL}. Although the familiar Young-Dupré equation (equation 4.1) does not take into account the adsorption of liquid vapors in equilibrium with the solid and other surface-related variables, like the average surface roughness; this equation is still widely used to describe the reversible 'work of adhesion' (W_a), because only the surface energy of the liquid, γ_{LV}, and the equilibrium contact angle, θ, are required to be measured.

$$W_a = \gamma_{LV}(1+\cos\theta) \tag{4.1}$$

Differences in wetting behavior of sized/unsized and surface treated/untreated carbon fibers immersed in a number of different thermoplastics and epoxy resins [7-12] have demonstrated that a good correlation exists between the contact angle and some important design variables like the composite transverse flexural strength. In contrast to carbon fibers, no simple correlation has been reported between the work of adhesion to various polymer resins determined from the contact angle and the amount of silane coating applied to the glass fibers. This lack of data is apparently because good adhesional wetting is not the primary mechanism to improve adhesion using the silane surface-modifiers. The dissolution and/or chemical reaction of the silane sizing with the liquid matrix are considered to be of much more relevance than simple wetting properties [1]. This result also suggests that correlations between the work of adhesion and composite properties should be limited to non-reactive systems, where no chemical bonds dominate the adhesion at the fiber/matrix interface [13].

Contact angles of inorganic substrates modified by the admicellar polymerization technique have not been well investigated. Therefore, the purpose of this chapter is to complement the analysis of polymer-modified glass fibers by assessing their interfacial characteristics when

probed with different model hydrophilic and hydrophobic liquids. The conclusions drawn herein will later constitute the basis to examine the role of wetting in the improved mechanical properties of composites fabricated with the admicellar-coated reinforcements.

4.2 Experimental section

4.2.1 Characterization of glass fibers. Currently, there are two commercial general-purpose fibers on the market. Both are variants of products within the broad category of E-glass fibers: one is the generic boron-containing glass fiber, and the other is a boron-free or calcium-magnesium-aluminum silicate glass fiber. In this study, we made use of boron-free E-glass fibers produced by two different companies: Clark-Schwebel and FibreGlast. The first five sets of fibers (Fibers C1 to C5) correspond to the Clark-Schwebel's 181 Series cloths. Fibers F1 to F4 came from chopped strand mat fabricated by FibreGlast (Plast # 248). Table 4.1 depicts the specifications for each set of samples. Clark-Schwebel was kind enough to supply one set of fibers with no silane-coupling agent, that is, the only sizing was a proprietary coating to improve handling and processing.

Some fibers received a pretreatment to remove the coating prior to modification. These pretreated fibers also served as control

samples. Desizing of the commercial fibers was achieved by heat treatment at 500 °C during 12 minutes, followed by a short immersion and continuous stirring in a diluted acid wash [14]. The acid was then removed from the fibers by washing them thoroughly with double deionized water (DDI), and after that, fibers were placed in a vacuum-oven overnight at 60 °C prior to their utilization.

Table 4.1 Classification of samples by origin and specifications

Fiber Code	Details	Fiber Diameter (μm)*
Fibers from Clark-Schwebel		
C1	Desized fiber C4 Heat-treated (500 °C)	6.2-7.0
C2	Desized and soaked in SDS (98% purity). Air Dried.	6.2-7.0
C3	Admicellar coating Poly (styrene-co-isoprene)	6.2-7.0
C4	Commercial Sizing	6.2-7.0
C5	Commercial sizing with no silane coupling agent	6.2-7.0
Fibers from FibreGlast		
F1	Desized fiber F4 Heat-treated (500 °C).	12.5-13.0
F2	Desized fiber F. Soaked in SDS (98% purity). Air Dried.	12.5-13.0
F3	Admicellar coating Poly (styrene-co-isoprene)	12.5-13.0
F4	Commercial Sizing	12.5-13.0

*Fiber diameter measured by AFM and corroborated by SEM

Given that contact angle measurements are extremely sensitive to any variation on the solid surface properties, X-ray photoelectron spectroscopy (XPS) was used in order to evaluate the surface chemical composition of the desized fibers. A Physical Electronics PHI 5800 ESCA system with a concentric hemispherical analyzer and a monochromatic Al Kα X-ray source (1486.6 eV) was operated at 100 W, 15 kV, in an evacuated chamber at approximately 2.0 x 10^{-9} Torr. A spot of 800 μm in diameter, 58.7 eV of pass energy, and an electron takeoff angle of 45° with respect to the sample plane were used in all the measurements.

Glass fibers were placed under a molybdenum mask having a central hole and then secured to the sample holder. Inside the cavity, between the mask and the holder, the fibers were oriented parallel to each other, as accurately as possible, to have the maximum number of fibers exposed to the beam. For every specimen, a survey spectrum was recorded over the available energy range in order to determine which elements were present. Peak areas were determined using a multiplex routine with a nonlinear Shirley-type background subtraction, and subsequently converted to surface atomic concentrations using the sensitivity factors provided by the PHI 5800 system software.

From this particular analysis, the surface composition of the desized fibers was assessed and is presented in Table 4.2. It is interesting to note that the surface concentration of carbon is relatively small after the pretreatment, between 5-6%. This result confirms that the organic finish and silane-coupling agents were almost completely removed and the surface obtained is thus comparable to the surface compositions of unsized or water-sized glass fibers used by other authors [15, 16]. On this basis, any effect in the contact angle hysteresis originated from organic coating residues can be ruled-out. The remaining carbon observed in the glass fiber surface has been attributed either to adventitious hydrocarbon adsorption in the laboratory environment [17-19], or to alkali carbonate precipitates formed due to the adsorption of CO_2 from the atmosphere into the water layer present in the hydrophilic glass [20, 21].

Table 4.2 Surface atomic concentration for desized (F1) and commercial (F4, C4) fibers

	% Atomic						
Fiber Code	C_1(s) [0.314]	O_1(s) [0.733]	Al(2p) [0.256]	Si(2p) [0.368]	Ca(2p) [1.927]	Mg(2s) [0.274]	Cl(2p) [0.954]
F1	5.65	66.24	0.88	25.56	1.67	-	-
F4	60.70	30.44	1.15	5.73	1.40	0.29	0.27
C4	70.18	23.88	1.31	3.59	1.04	-	-

Besides the compositional heterogeneity of the surface, the other parameter of considerable importance to contact angle and wettability studies is the average surface roughness. Different authors have tried to theoretically correlate the presence of regular roughness perturbations with the contact angle measurements. In this way, the well-known equation of Wenzel (equation 4.2) predicts the observed value of *cos* θ_{obs} as the product of an intrinsic *cos* θ_i, and a roughness factor, *r*.

$$\cos\theta_{obs} = r \cdot \cos\theta_i \qquad (4.2)$$

The quantity '*r*' is defined as the ratio of the actual surface area to the area projected from the surface into a flat, parallel surface. A major drawback for this approach is that equation (4.2) does not suggest the existence of two experimental contact angles: θ_a and θ_r ($\theta_a > \theta_i > \theta_r$), obtained when the triple line advances and recedes. Moreover, the average surface roughness has been proven recently to exert an appreciable influence on both the advancing, θ_a, and receding contact angles, θ_r, as measured from the Wilhelmy technique, especially in the case of nonplanar substrates [22].

Contact angle hysteresis, which corresponds to the difference between the advancing and receding contact angles, increases with an increase in the surface roughness. Usually, both the advancing contact angle increases and the receding contact angle decreases with an increase in roughness. However, if the roughness is less than about 0.5 μm, the roughness no longer has a significant role in the contact angle hysteresis [16, 23-24]. To evaluate the extent of hysteresis in the contact angle measurements due to roughness, a comparative study of the topographical differences and the average surface roughness between desized glass fibers (F1), and those coated with either a silane coupling agent (F4) or the admicellar-polymerized elastomer (F3) was performed. A commercial AFM scanning probe, Nanoscope IIIa microscope (Digital Instruments Inc., Santa Barbara, CA), was used to scan the top of the fibers, which were previously secured to the sample pucks by a thermoplastic adhesive (TEMPFIX). From those images, both topographic and line profile data were extracted. SEM (ETEC Autoscan) micrographs from several fibers (C1, C4, F1, and F4) confirmed the observations made with AFM.

The experiments were carried out using the TappingMode™ or intermittent contact imaging capability of the AFM because this mode has been recently demonstrated to give more accurate results for

surface roughness than those obtained with contact force scanning [25]. Several researchers [26-28] that have previously employed AFM to measure the roughness of glass fibers make use of the parameter R_a to describe the average roughness, which is defined as the mean value of the roughness curve relative to the centerline and is calculated by:

$$R_a = \frac{1}{L}\int_0^L |f(x)|dx \tag{4.3}$$

Here, L is the length of the roughness curve and *f(x)* is the roughness curve relative to the center line. In this study, we chose the approach of establishing the surface profile from the intersection of a reference plane perpendicular to the fiber axis. To avoid differences all the surfaces were adjusted by using the planefit function of the software, which influences the tilt in the captured image. A total of 20 images of 5μm x 5μm were scanned per kind of fiber in arbitrarily chosen positions along the length of different fibers (usually two or three points per fiber). The processed data was then analyzed by using line profiles over a sampling length of 2.5 μm at five roughly evenly spaced locations in the region located on top of the fibers. 100 data

values were used in the calculation of the average roughness for each kind of fiber.

As presented in Figure 4.1, the average roughness of the three kinds of fibers has a fairly narrow distribution of values, and all data points are well below the 500-nm range. This result indicates that roughness should not significantly influence the contact angle hysteresis measurements. However, the average roughness for the sized fibers is much different from the other types of fibers studied. This difference, as will be explained later, is closely related to the topography characteristics of the commercial sizing treatments.

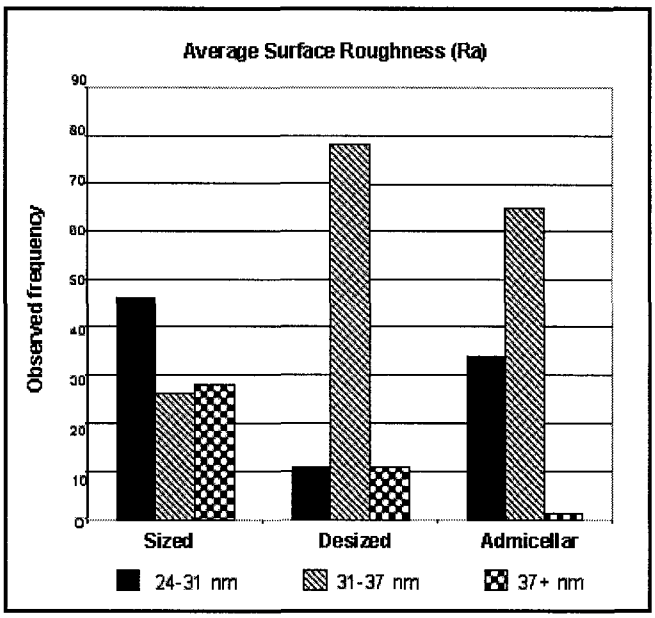

Figure 4.1 Average surface roughness (R_a) of 13.0 μm diameter fibers with various surface treatments.

The surface is mostly homogeneous for the desized fibers, although some areas show increased roughness. We attribute this behavior to the presence of corrosion zones created by the acid-wash treatment where the dissolution of ions can originate local microdepressions. Compared to the admicellar-treated fibers, the desized fibers appear to be rougher. Although this observation could indicate the presence of a smooth film in the former samples, neither the statistical evidence nor the AFM imaging analysis support this hypothesis.

A regular distribution of very minute particles of various dimensions 100-200 nm projected from a relatively smooth surface constituted the main topographical feature (Figure 4.2) observed in almost all of the desized fibers analyzed (C1 and F1). Other authors have also reported these morphological features, and their origin has been related to reversible crystal growth of alkali precipitates as a result of glass fiber aging when exposed to humid air [20]. The same observations made with SEM showed images with a smooth structure and some of the protrusions mentioned before. However, the small granulations of less than 200 nm could not be perceived in the SEM, which requires more extensive variations in heights to better contrast images.

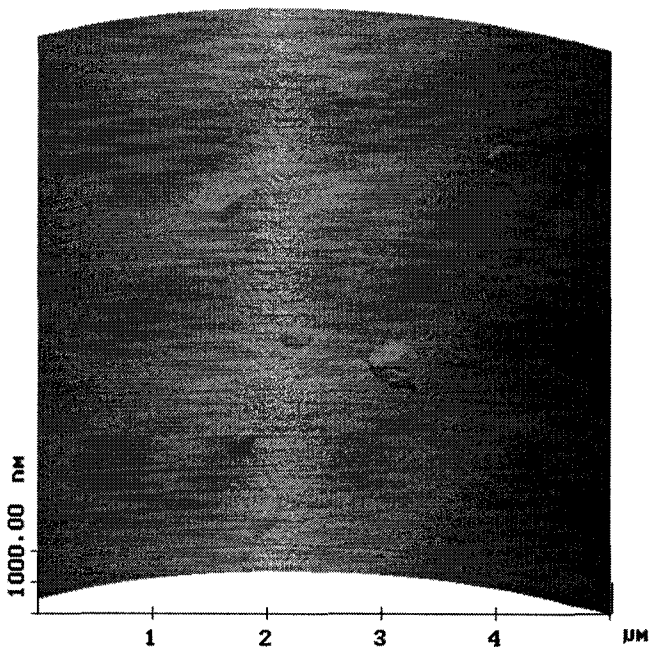

Figure 4.2 Topographical features of desized fibers (F1) by AFM.

In the case of the admicellar-modified fibers, some of the 100-200 nm protrusions were also observed, but mostly the surface was very smooth as shown in Figure 4.3. A completely different situation was encountered with the commercial sized fibers (C4 and F4). The images from these fibers show a repeated distribution of solitary bumps or patches that protrude from the fiber's overall plane. Their size varied: the patches shown in Figure 4.4a, for instance, had dimensions between 0.3 to 0.4 μm. These patches probably correspond to physically linked sizing. In addition to the protrusions,

SEM micrographs (Figures 4.4b and 4.4c) show areas not covered with these patches; which most likely would either be zones with chemically liked sizing or bare glass surface. Some of the roughness values in these particular areas without protrusions were very close to values obtained for the desized glass fibers ($31 < R_a < 37$ nm), suggesting an absence of coating.

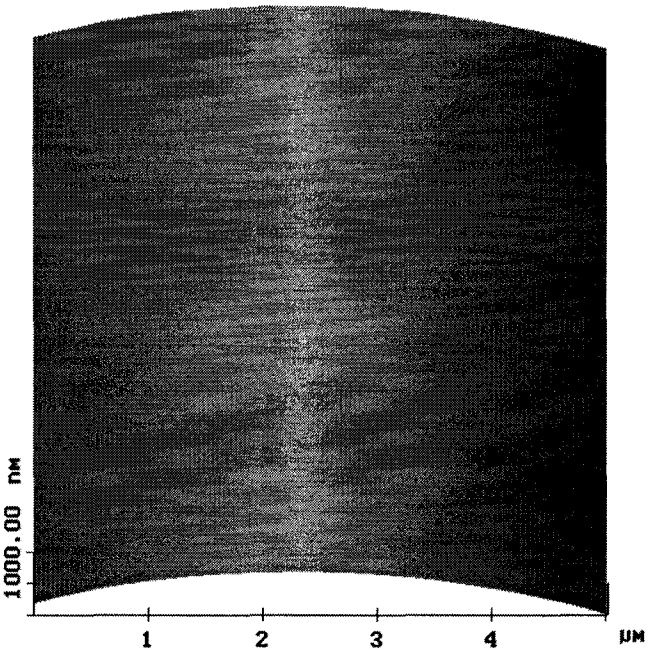

Figure 4.3 Topographical features of admicellar-coated fiber (F3) by AFM.

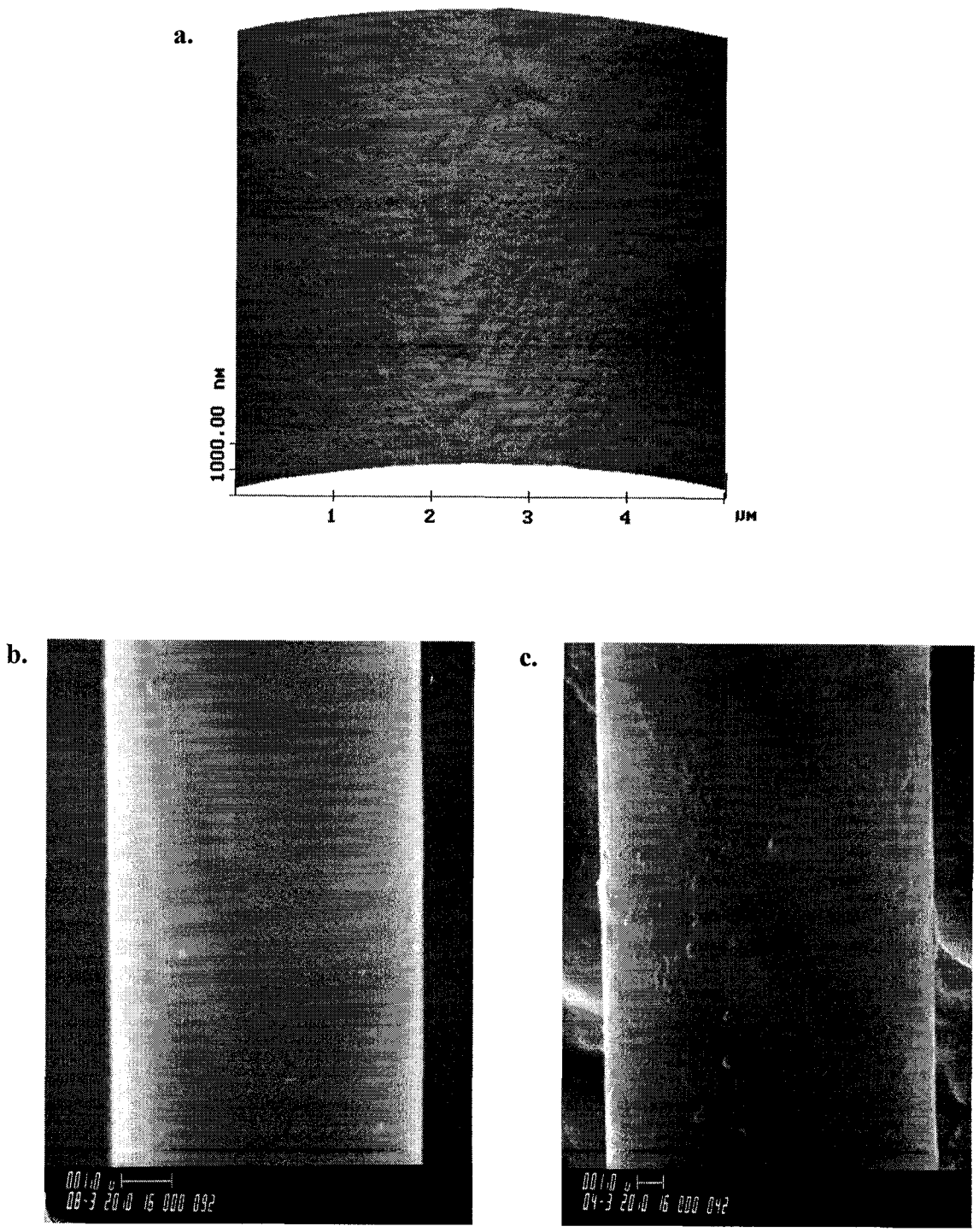

Figure 4.4 Topographical features of commercial sized fibers:
(a) AFM micrograph of fiber F4;
(b) SEM micrograph of fiber C4;
(c) SEM micrograph of fiber F4.

4.2.2 Modification of glass fibers by admicellar polymerization. The development of alternative treatments to modify the interfacial characteristics of glass fibers is a subject of continuous research, and several techniques have been recently devised and patented [14,18,29-31]. Admicellar polymerization stands as a relatively new and versatile technique that has proven successful for the formation of thin films [32-39]. These ultrathin films are formed from different monomers (i.e., styrene and isoprene) over inorganic oxides of low surface area, including glass fibers, using low-cost materials like surfactants and redox and/or AIBN-type initiators [5, 39]. The adsolubilization process is not limited to fairly hydrophobic molecules. Nonionic long-chain alcohols, aromatic alcohols and metal ions have been also shown to partition inside the admicelles [40-43]. A complete overview of the main steps of surface modification by the admicellar polymerization method may be found in Chapter 2.

Herein, the amount of surfactant adsorbed on the glass fiber surface was determined through the construction of adsorption isotherms following the well-known surfactant depletion method. Sodium dodecyl sulfate (SDS) from Sigma-Aldrich, 98% purity, was chosen as the surfactant; and each point of the isotherm was obtained by exposing a measured weight of glass fibers to a surfactant solution

of known initial concentration, and then allowing the mixture to equilibrate for at least 30 hours. The initial pH was set in every experiment to 3.6 with HCl. The equilibrium concentration of surfactant was then measured by high-pressure liquid chromatography (HPLC), and the difference from the known initial concentration gave us the equilibrium-adsorbed amount of SDS. The chromatographic analysis was carried out on a Hewlett-Packard Series 900 HPLC equipped with a Pascal Chemstation and an Alltech 350-conductivity detector interfaced to a HP 35900 analog-to-digital converter. The column was a 100 x 4.6-mm Hypersil ODS 5-micron column using a 57:43 mixture of methanol/water as a carrier solvent at flow rate of 1 ml/min. The conductivity detector and the column were both at room temperature. A typical adsorption isotherm for SDS on desized fibers from FibreGlast (Fiber F1), measured by the procedure described above, is depicted in Figure 2.4 (Chapter 2). The adsorption isotherm for Fiber C1 was presented elsewhere [5]. Both fibers had plateau adsorptions of approximately 20 μmol SDS/gram of fiber, and the plateau occurred at an SDS concentration near the CMC of SDS in water (~8,000 micromolar).

After equilibration with the surfactant solution, two different monomers, styrene and isoprene in a 1:1 mol ratio, were adsolubilized

concurrently into the admicelles formed by the adsorbed surfactant (SDS) on the aluminosilicate-rich surface of the glass fibers. A 2:1 monomer to surfactant ratio and 10:1 monomer to initiator ratio was used in all experiments. The solution containing the surfactant and the monomer was left to equilibrate with the glass fibers (0.5g) at room temperature in small neoprene-capped vials (40 ml) for 14 to 24 hours. A typical preparation using fibers from FibreGlast (F1) and the procedure described above reached an equilibrium surfactant solution concentration of 5800 μM after the adsorption step, at a constant pH of 3.6. This point corresponds to about 70% of the maximum surface coverage, considering the shift in CMC and the amount of surfactant at the interface caused by adding a strong nonpolar adsolubilizate to the system [44]. Maximum coverage of surfactant may be interpreted as desirable to produce a more uniform coating. However, low surfactant coverage might as well be beneficial for improving mechanical properties as demonstrated recently by O'Haver in the case of rubber composites reinforced with admicellar-coated silica [36].

Sodium persulfate was added to the reaction medium and the vial vigorously shaken for a period of one hour at room temperature to allow dissolution of the free radical initiator. The temperature was then raised above 80 °C to thermally initiate polymerization. Finally, post-

reaction washing was carried out four times with double de-ionized water at room temperature, followed by drying overnight in a vacuum oven at 60 °C.

4.2.3 Contact angle measurements. Measuring the contact angle with probe liquids can be used to assess the changes in wettability of fibrous materials resulting from surface modifications carried out by either physical or chemical procedures. Visual techniques [11, 45] and the Wilhelmy balance [46-49] methods are currently employed for this purpose. The latter approach is based on the continuous recording of the force exerted by a test liquid when advancing or receding over a solid probe at a constant front displacement velocity. This technique is often preferred because it is suitable for measuring contact angles smaller than 15°, where most optical methods fail [50]. A schematic drawing and the mathematical expression accounting for the force balance to derive the contact angle from a Wilhelmy experiment were presented in Chapter 2 (Figure 2.2 and equation 2.2).

Herein, three different test liquids (double deionized water, pure glycerol, and a commercial epoxy resin: EPON 815C) were used to test the surface treatment variations (desized, commercial sized, SDS soaked, processing lubricants, and elastomer modified) of the two

types of fibers (Clark-Schwebel's 181 Series, and FibreGlast Plast # 248). A dynamic contact angle analyzer (Cahn Instruments, Inc., DCA-322) was used in all cases, following a special protocol for fibrous materials described by Domingue [51]. The fibers were relatively small in diameter (6.5 and 13.0 μm), and hence bending of the fibers can be a problem when the fibers are submerged into test liquids. To minimize this situation each fiber was cut to a length of 5 mm and hung from the arm of a highly sensitive microbalance (0.1 μg), taking care to load the fiber perpendicular to the liquid surface. Once the experiment started, 2 mm along the fiber axis was immersed into the liquid at a very slow stage velocity (2 μm/s). This particularly slow velocity was selected in order to minimize bending, and also to avoid disturbances in the recorded force coming from viscous friction, especially in the measurements with glycerol and the epoxy resin. Reported results correspond to an average of 8 to 10 individual measurements.

The surface tensions of the probe liquids were measured using substrates of different surface energy and geometry (i.e., glass plates, platinum slide, platinum ring, and plexiglas), in order to have a broad range of values to reference the experiments with the fibers. Values for the surface tensions, assuming a zero contact angle, are presented

in Table 4.3. As can be observed, all the measured surface tensions are the same within experimental error, with the exception of EPON 815C. This result is consistent with the finding that the EPON resin does not wet glass well (i.e., contact angle greater than 40°).

Table 4.3 Surface tension (dyne/cm) for different substrates at 25 °C

Test Liquid	Du Noüy Ring (n=4)	Glass Slide (n=7)	Platinum Plate (n=5)
EPON 815 C	39.8 ± 0.4	36.7 ± 1.3	40.0 ± 1.0
Water	71.5 ± 0.4	72.6 ± 0.9	72.6 ± 0.9
Glycerol	-	64.0 ± 1.0	64.3 ± 1.1

4.3 Results and discussion

As the fiber moves into or from the liquid during the analysis stage of a contact angle measurement, the three phase contact line also moves. In that case, the heterogeneity of the fiber surface will result in various local contact angles, which are translated as an irregular variation of the acting force. In this section, the results of the experiments will be interpreted not only in terms of the actual values for the macroscopic advancing and receding contact angles, but also by considering the contact line behavior and the hysteresis level. Contact angles for all the fiber samples appear in Tables 4.4 to 4.6.

Table 4.4 Contact angles in water measured at 25 °C for different fiber treatments and reference substrates

Fiber Treatment	Advancing Contact Angle (θ_a)	Receding Contact Angle (θ_r)	Hysteresis ($\Delta\theta$)
C1	0 ± 0	0 ± 0	0
C2	33 ± 2	0 ± 0	33
C3	58 ± 10	11 ± 9	47
C4	77 ± 6	56 ± 7	21
C5	49 ± 9	0 ± 0	49
F1	0 ± 0	0 ± 0	0
F2	39 ± 5	36 ± 5	3
F3	72 ± 8	62±5	10
F4	59 ± 3	54 ± 4	5
Glass slide	17 ± 4	0 ± 0	17
Plexiglas slide	83 ± 3	38 ± 3	45

Table 4.5 Contact angles in glycerol measured at 25 °C for different fiber treatments and reference substrates

Fiber Treatment	Advancing Contact Angle (θ_a)	Receding Contact Angle (θ_r)	Hysteresis ($\Delta\theta$)
C1	3 ± 1	0 ± 0	3
C2	52 ± 2	0 ± 0	52
C3	51 ± 10	18 ± 3	33
C4	72 ± 1	63 ± 4	9
C5	52 ± 8	0 ± 0	52
F1	30 ± 2	28 ± 2	2
F2	49 ± 7	39 ± 6	10
F3	55 ± 4	47±2	8
F4	68 ± 2	42 ± 5	26
Glass slide	21 ± 1	0 ± 0	21
Plexiglas slide	72 ± 1	71 ± 1	1

Table 4.6 Contact angles in EPON 815C measured at 25 °C for different fiber treatments and reference substrates

Fiber Treatment	Advancing Contact Angle (θ_a)	Receding Contact Angle (θ_r)	Hysteresis ($\Delta\theta$)
C1	42 ± 2	34 ± 5	8
C2	30 ± 5	8 ± 5	22
C3	27 ± 7	7 ± 7	20
C4	31 ± 4	21 ± 5	10
C5	41 ± 5	0 ± 0	41
F1	43 ± 3	32 ± 5	11
F2	42 ± 2	35 ± 6	13
F3	38 ± 2	12 ± 5	26
F4	34 ± 5	24 ± 4	10
Glass slide	39 ± 1	0 ± 0	39

Figure 4.5a shows a typical tensiogram obtained for the desized fiber (F1) using water as the test liquid. A very smooth contact line both in the advancing and receding modes, as well as a zero hysteresis value, are indicative of a chemically homogeneous surface being completely wetted (i.e., zero contact angle) by the test liquid. This smooth baseline was obtained when the desized fibers were taken from the oven and immediately put into a desiccator containing silica gel. However, when the fibers were exposed to the atmosphere for different periods of times and then immersed in water, the advancing contact line became jagged, which indicates a process of pinning and de-pinning caused by contamination of the fiber surface with other

chemical constituents (Figures 4.5b and 4.5c). Thus, after a combined exposure to ambient air and water the contact angle of the desized glass fibers changed from zero to an average advancing contact angle of 20 to 25°, which must be taken as the reference value for the other measurements. The hysteresis value also increased by 4 to 7°.

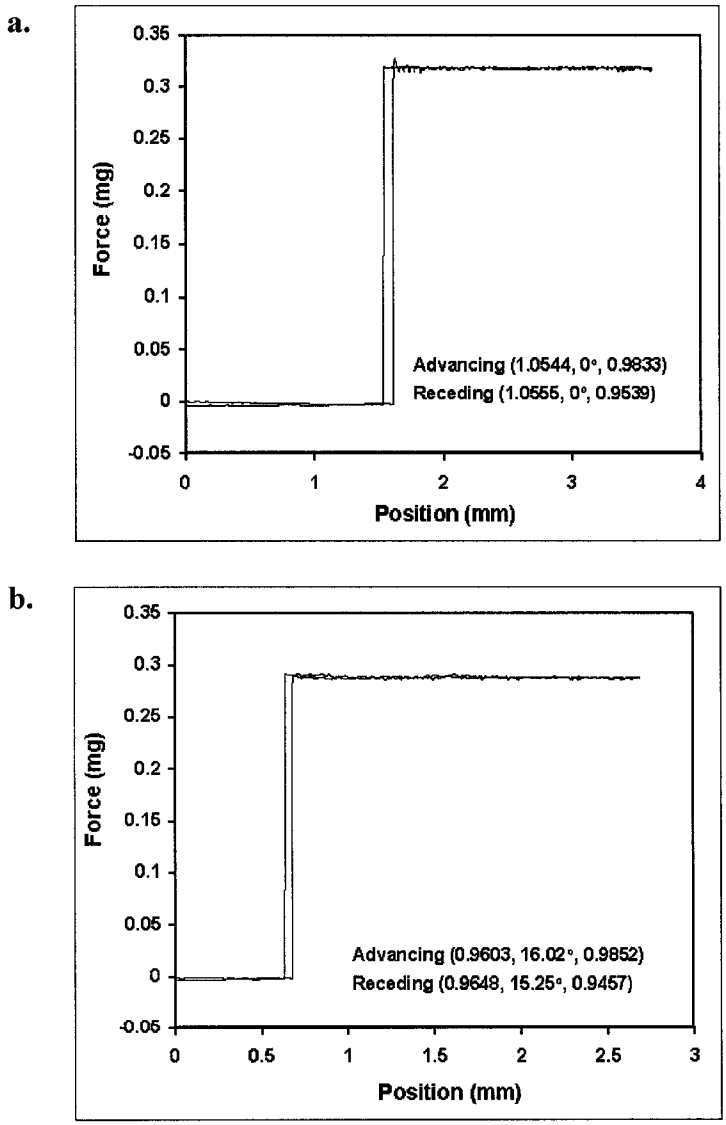

Figure 4.5 Tensiogram of desized fiber (F1) in water: (a) No previous exposure; (b) 1 h exposure; and (c) 12 h exposure.

c.

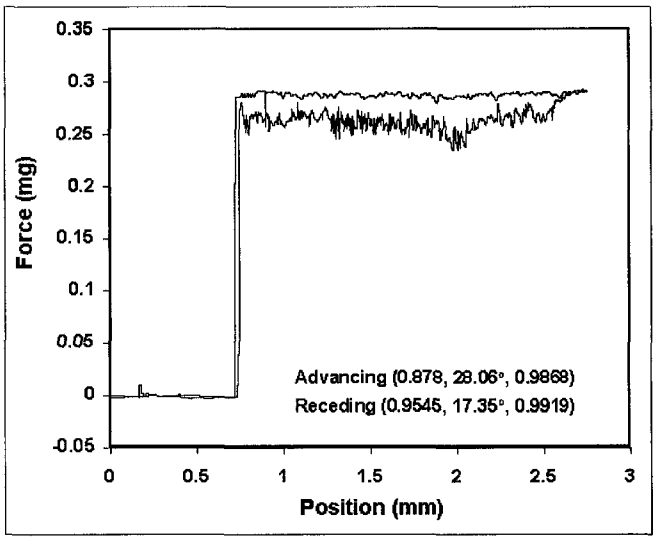

Figure 4.5 (Continued).

From Tables 4.4 to 4.6, contact angles in a highly polar medium (water) for both silane-treated (C4 and F4) and admicellar polymerized poly (styrene-co-isoprene) (C3 and F3) fibers are fairly large, suggesting difficulty in wetting due to an increased hydrophobicity. Statistical analysis using *t* tests on the cos (θ_a) and cos (θ_r) revealed that the contact angles for fibers C4 and C3 were significantly different ($p < 0.05$) from desized fiber C1, and contact angles for fibers F4 and F3 were different from desized fiber F1. When compared as groups, commercial (C4, F4) versus admicellar treated (C3, F3), the contact angle measurements do not give a definite trend to differentiate a higher or lesser hydrophobic characteristic of each type of treatment.

Contact line behavior also shows that water does not wet the coated fibers well (C4, F4, C3, and F3). As can be seen in Figure 4.6a, 4.6b and 4.7, the contact line jumps abruptly in different positions along the fiber length forming a saw-toothed line which is characteristic of a surface having sites of different surface energy, or better said, hydrophobic/hydrophilic behavior. The hysteresis values for the admicellar-modified fibers (C3 and F3) are much more pronounced than the ones for commercial sizings (C4 and F4). This result suggests that the discontinuous commercial sizings are more homogeneous compared to the elastomeric films formed by admicellar polymerization. Further, the receding contact angles for the admicellar-modified fibers of small diameter were in all cases lower than those for commercial sizings when probed with a test liquid like water (i.e., highly polar and low molecule size). According to Bismark [49], the advancing contact angles are characteristic for the low energy sites of the fiber surface, while the receding contact angles are related to the high-energy part. Thus, excluding the effect of fiber diameter [52], the lower contact angles in the elastomeric-coated fiber are suggestive of more high surface energy sites (i.e., bare glass) that tend to resist the dewetting of the front. A poorer coating coverage may explain the statistically similar receding contact angles observed

between fibers F3 and F4, as inferred from the C/Si and O/Si atomic ratios shown in Table 4.2.

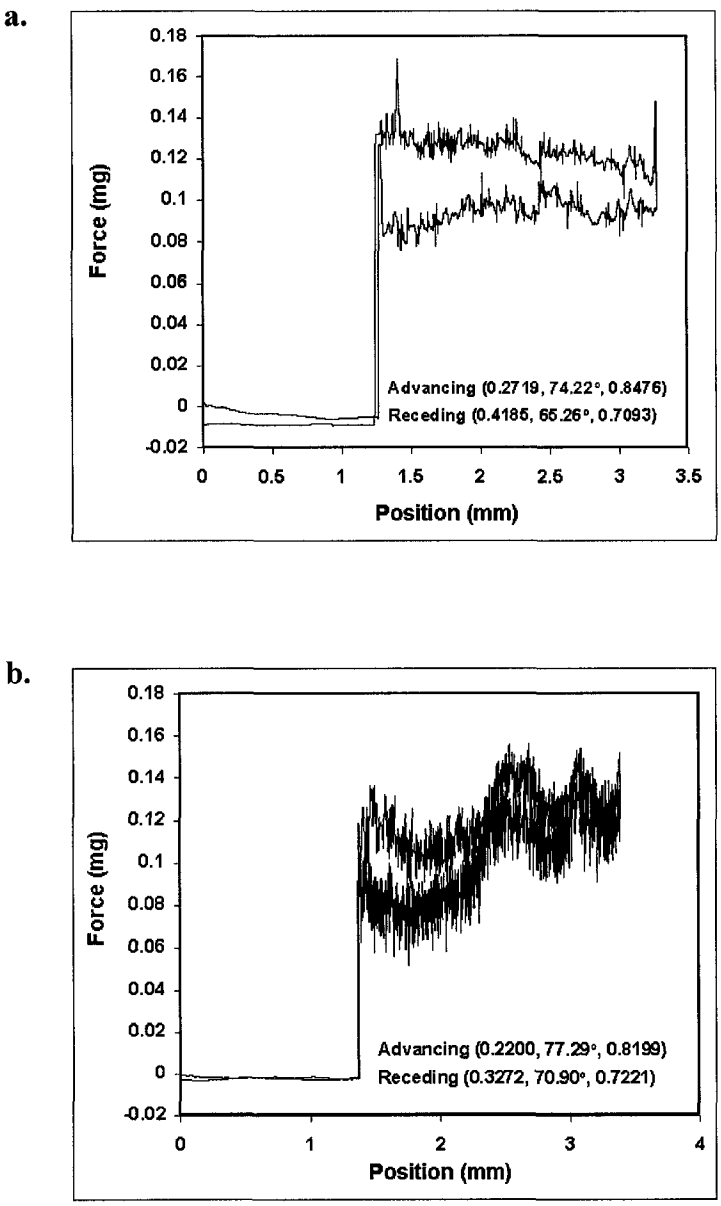

Figure 4.6 Tensiograms of an elastomer-coated fiber (F3) in water: (a) Regular patch coverage; and (b) Zone of two different surface energies.

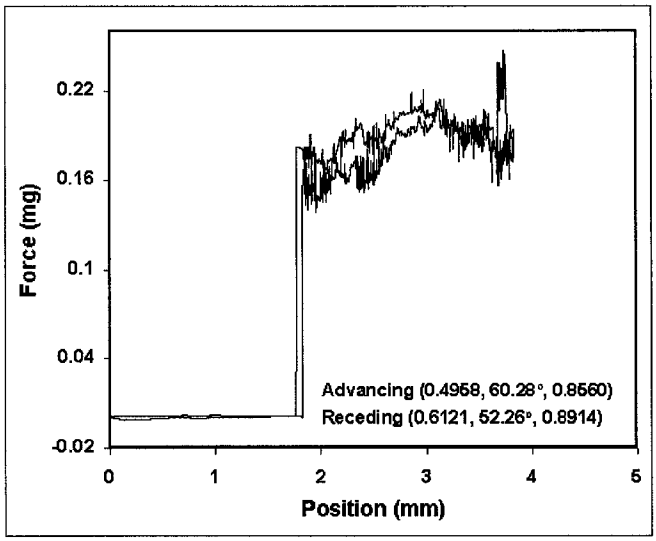

Figure 4.7 Tensiogram of a commercial sized fiber (F4) in water.

In glycerol the fibers showed large contact angles, indicating a high level of incompatibility with the silane and admicellar modified fibers. The average contact angles for the elastomer-modified fibers C3 and F3 showed a small degree of improved wetting with this relatively less polar liquid (vs. water), presumably because of the stronger nonpolar interactions between the dispersive component of the glycerol and the elastomeric film. A curious situation was observed with the wettability of the commercial sizing of fiber F4. This fiber showed better compatibility with water than with glycerol, unlike commercially sized fiber C4. Sizings for fibers C4 and F4 were reported by the manufacturers as being epoxy-compatible; however, the chemical functionality and coverage of these sizings were not disclosed. Perhaps the sizing for fiber F4 contained more polar

moieties that rendered a reduced interaction with the nondispersive component of glycerol. An argument supporting this speculation is the more hydrophilic behavior displayed by fiber F4 (θ_a = 59 ± 3) compared to that of fiber C4 (θ_a = 77 ± 6) when probed with water.

Fibers treated with SDS (C2 and F2) showed similar or less wettability for both water and glycerol when compared to the baseline values of the desized fibers. Lower wettability suggests that the most highly polar sites are covered by surfactant, and that the surfactant is less wettable than the bare glass. The contact angle value clearly indicates that adsorption does not result in stable monolayer coverage (e.g., hemimicelles) because in such case the contact angles with water would have been much higher than the ones obtained, as the hydrocarbon tails would be in contact with water. Therefore, it is reasonable to conclude that a morphology where the head groups contact the water was formed. Further, the high hysteresis values indicate the presence of a large amount of bare fiber.

For the thermoset resin EPON 815C, surface tension and contact angle results show nonzero contact angles with both the glass slide and furnace treated fibers. Fibers with silane coupling agent, C4 and F4, had average contact angles statistically smaller ($p < 0.05$) than

those of bare fibers (C1 and F1) when probed with the resin EPON 815 C. These results are in good agreement with expectations, because the organic sizing should be more compatible with the resin than the more polar clean fibers. Fibers with an admicellar coating (C3 and F3) also showed a significant improved compatibility with the epoxy resin and the advancing contact angle (θ_a) was statistically equivalent to that obtained with silane coupling agent treated fibers. Tensiograms presented in Figures 4.8 and 4.9 are examples of the contact line behavior for an elastomer-coated fiber and a commercial silane sized fiber with the epoxy resin. The horizontal advancing and receding arms suggest a unique dependence of the measured force on the interfacial energetics with no undesirable contributions from fiber/resin shear stresses [53].

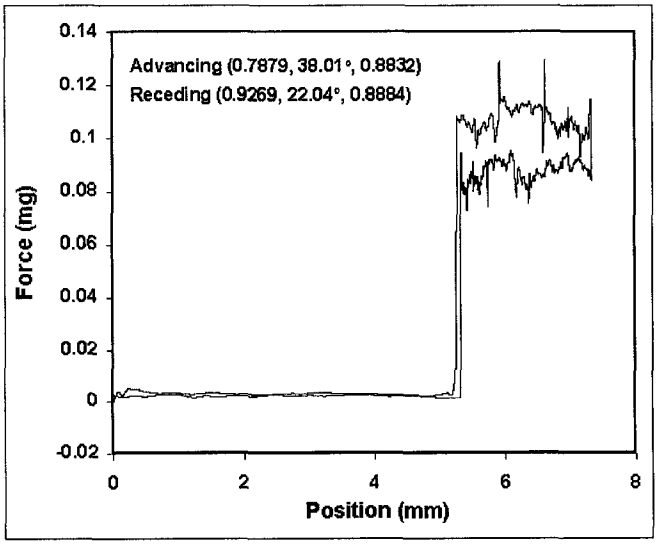

Figure 4.8 Tensiogram of an elastomer-coated fiber (F3) in Epon 815C.

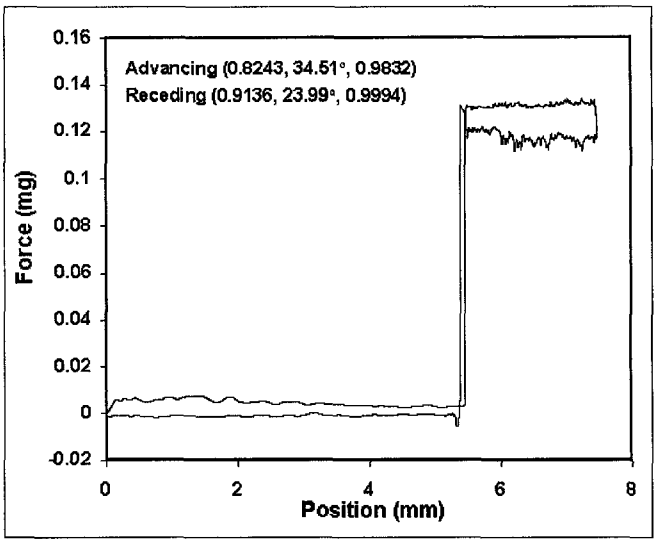

Figure 4.9 Tensiogram of a commercial sized fiber (F4) in Epon 815C.

The ultrathin poly (styrene-co-isoprene) film was not uniform throughout the glass on a macroscopic length scale. Several fibers had contact angles similar to the unsized fibers, suggesting a total absence of polymer. This absence of polymer indicates that one or more of the ingredients (surfactant, monomer, or initiator) were unable to reach parts of the cloth. Unfortunately, there was no systematic way of finding a particular area where fibers were bare, however presumably the ingredients had trouble reaching more concealed fibers in the cloth. The reader should note that the system was unagitated, perhaps with agitation a globally more uniform coating would result. Finally, the fibers coated with only processing lubricants (i.e., non-covalently bonded material) were found to have slightly better wetting than bare fibers. In all cases these samples showed a relatively heterogeneous

surface when advancing, but a more homogeneous surface when receding. This behavior suggests that some of the lubricant from fiber C5 dissolved into the resin during the course of the experiment.

4.4 Conclusions

Fibers with different surface treatments were found to have distinctly different contact angles with EPON 815C, a thermoset resin. Fibers treated in a high temperature furnace to remove the organic sizing, leaving only oxidized glass, have the largest contact angle (worst wetting) with EPON 815C. As expected, commercially sized fibers have lower contact angles compared to fibers without surface treatment. Treatment by admicellar polymerization, a technique less expensive relative to coupling agents, leads to fibers with statistically identical wettability as the fibers that have been modified with a proprietary sizing that included silane-coupling agents. Fibers treated only with SDS gave observable, but limited, enhancement in resin wettability. These findings are consistent with results of mechanical tests previously reported.

The dynamic contact angle method, used to determine the contact angles of the various fibers with the probe liquids, also gave valuable information about the chemical nature of the fiber surface.

Bare-glass fibers have a chemically homogeneous surface according to these measurements. However, sized fibers, especially those with coupling agents and admicellar-polymerized poly (styrene-co-isoprene), are chemically heterogeneous at the surface.

References

1. B. Larson and L. Drzal, *Composites* **25**, 711 (1994).
2. A. Straub, M. Slivka and P. Schwartz, *Composites Sci. Technol.* **57**, 991 (1997)
3. A. Sjogren, R. Joffe, L. Berglund and E. Mäder, *Composites Part A* **30**,1009, (1999)
4. S. Keus and R. Haessler, *Composites Part A* **30**, 997 (1999)
5. B. Grady, E. O'Rear, L. Penna and A. Pedicini, *Polym. Composites* **19**, 579 (1998)
6. J. L. Thomason, *Composites* **26**, 467 (1995)
7. B. Jang, *Composites. Sci. Technol.* **44**, 333 (1992)
8. H. Wu, G. Biresaw and J. Laemmle, *Polym. Composites* **12**, 281 (1991)
9. L. Tang and J. Kardos, *Polym. Composites* **18**, 100 (1997)
10. K. Tsutsumi, S. Ishida and K. Shibata, *Colloid Polym. Sci.* **268**, 31 (1990)
11. T. Ogawa and M. Ikeda, *J. Adhes.* **43**, 69 (1993)

12. M. Tagawa, N. Ohmae, M. Umeno, K. Gotoh, A. Yasukawa and M. Tagawa, *Colloid Polym. Sci.* **267**, 702 (1989)
13. J-K Kim and Y-W Mai, In: *Engineered Interfaces in Fiber Reinforced Composites*, 1st ed.; Elsevier: Amsterdam, Chapter 2 (1998)
14. A-C. Lassas, L. Fagerholm, B. Stenlund and J. Näsman, *Polym. Composites* **14**, 1 (1993)
15. J. L. Thomason, *Composites* **26**, 487 (**1995)**
16. P. Gao, K. Su, Y. Ward and L. Weng, *Polym. Composites* **21**, 312 (2000)
17. A. Provatas, J. Matisons and R. Smart, *Langmuir* **14**, 1656 (1998)
18. H. Fagerholm, C. Lindsjö, J. Rosenholm and K. Rökman, *Colloids Surf.* **69**, 79 (1992)
19. T. Horr, J. Ralston and R. Smart, *Colloids Surf. A* **97**, 183 (1995)
20. M. Carter, N. McIntyre, H. King and A. Pratt, *J. Noncryst. Solids.* **220**, 127 (1997)
21. G. Rudd, S. Garofalini and D. Hensley, *J. Am. Ceram. Soc.* **76**, 2555 (1993)
22. T. Chow, *J. Phys. Cond. Matter.* **10**, L445 (1998)
23. J. Domingue, *Cahn Application Note.* **1716**, 1 (1991)
24. V. Wolff, A. Perwuelz, E. Achari, C. Caze and E. Carlier, *J. Mat. Sci.* **34**, 3821 (1999)

25. G. Simpson, D. Sedin, K. Rowlen, *Langmuir* **15**, 1429 (1999)

26. A. Achari, A. Ghenaim, V. Wolff, C. Caze and E. Carlier, *Text. Res. J.* **66**, 483 (1996)

27. N. Behary, A. Ghenaim, A. Achari and C. Caze, *J. Appl. Polym. Sci.* **75**, 1013 (2000)

28. S. Maughdal, G. Sims, J. Jhonestone and N. Jennett, *Natl. Physical Lab. Meas. Note*. **CMMT(MN)024**, 1 (1998)

29. S. Shalaby, D. Clupper and T. Taylor, *US 5874509*, 6p (1999)

30. H. Fagerholm, C. Lindsjö and J. Rosenholm, *J. Mat. Sci.* **30**, 2420 (1995)

31. H. Fagerholm, J. Rosenholm, T. Horr and R. Smart, *Colloids Surf. A* **110**, 11 (1996)

32. G. Funkhouser, M. Arevalo, D. Glatzhofer and E. O'Rear, *Langmuir* **11**, 1443 (1995)

33. D. Glatzhofer, G. Cho, C. Lai, E. O'Rear and B. Fung, *Langmuir* **9**, 2949 (1993)

34. C. Lai, E. O'Rear, J. Harwell and M. Hwa, *Langmuir* **13**, 4267 (1997)

35. B. Kitiyanan, J. O'Haver, J. Harwell and S. Osuwan, *Langmuir* **12**, 2162 (1996)

36. J. O'Haver, J. Reynolds, J. Harwell, B. Grady, L. Evans, and W. Waddell, *Book of Abstracts, 219th ACS National Meeting*; San Francisco (2000)

37. W-L. Yuan, E. O'Rear, G. Cho, G. Funkhouser and D. Glatzhofer, *Thin Solid Films* **385**, 96 (2001)

38. W. Genetti, W-L. Yuan, B. Grady, E. O'Rear, C. Lai and D. Glatzhofer, *J. Mat. Sci.* **33**, 3085 (1998)

39. S. Sakhalkar and D. Hirt, *Langmuir* **11**, 3369 (1995)

40. K. Esumi, K. Sakai and T. Kanjiro, *J. Colloid Interface Sci.* **224**, 198 (2000)

41. K. Esumi, H. Toyoda, M. Goino, T. Suhara and H. Fukui, *Langmuir* **14**, 199 (1998)

42. C. Lee and H. Tsai, *Separation. Sci. Technol.* **30**, 285 (1995)

43. K. Esumi, H. Hayashi, K. Yoshifumi, S. Tsuneo and F. Hiroshi, *Colloids Surf. Sci. A* **144**, 201 (1998)

44. J. Wu, J. Harwell and E. O'Rear, *Langmuir* **3**, 531 (1987)

45. L. Jenkins and A. Donald, *Langmuir* **15**, 7829 (1999)

46. K. Tsutsumi, S. Ishida and K. Shibata, *Colloid Polym. Sci.* **268**, 31 (1990)

47. J. Schultz, L. Lavielle and C. Martin, *J. Adhes.* **23**, 45 (1987)

48. Y-L. Lee, *Langmuir* **15**, 1796 (1999)

49. A. Bismarck, M. Pfaffernoschke and J. Springer, *J. Appl. Polym. Sci.* **71**, 1175 (1999)

50. B. Miller and R. Young, *Text. Res. J.* **May**, 359 (1975)

51. J. Domingue and E. Francisco, *Cahn Technical Note*. **1726**, 1 (1991)

52. K. Van de Velde and P. Kiekens, *Angw. Makrom. Chem.* **272**, 87 (1999)

53. E. Mäder, *Compos. Sci. Technol.* **57**, 1077 (1997)

5. Elastomeric Sizings for Glass Fibers and their Role in Fiber Wetting and Adhesion in Resin Transfer Molded Composites[†]

5.1 Introduction

The utilization of glass fiber reinforced polymeric composites in space-related applications, as well as in other industries such as transportation and infrastructure, has been driven by the potential of achieving improved performance, longer lifetimes, weight reduction and lower cost. Although a rapid integration of fiber-reinforced composite materials into key technological areas has been observed in recent years, there are still several unresolved issues concerning our ability to accurately predict their mechanical performance and reliability throughout their lifetime. For instance, in certain structural

[†] Material in this chapter was published in *Composite Interfaces* **9**, 477 (2002).

applications that require large-scale parts to withstand aggressive environments (e.g., offshore petroleum platforms), the reduction of mechanical properties due to exogenous factors cannot be easily modeled due to the concurrent effect of different degradation pathways. Further, most of the problems faced by fiber-reinforced composites during their final applications are not only attributed to external factors, but also to defects induced during the fabrication process.

Relatively high operational costs and low production rates of current autoclave-processed composites have led manufacturers to search for alternative processing concepts aimed at higher production rate, and lower cost applications. Among them, Resin Transfer Molding (RTM), Vacuum Assisted Resin Transfer Molding (VARTM) and Resin Infusion (RI) are thought to be the mainstream fabrication processes for high-performance composites for the next decade [1, 2]. However, it is usually agreed that future research efforts need to be directed towards controlling the imbalance between viscous and surface forces, as well as non-isothermal effects, that significantly affect the resin flow in these high-speed liquid molding schemes. Transient phenomena at the fiber tows scale may decrease impregnation quality and ease of spreading of the resin through the fibrous preform, thus leading to

macroflow- and microflow-driven defects like dry spots and voids. A reduction between 2-10 MPa in the interlaminar shear strength (ILSS) can take place within a composite part even with as low as a 1% increase in void content [3].

Glass fibers are typically coated with proprietary formulations containing up to 10% of active silane coupling agents, while the remaining 90% is a mixture of low molecular weight epoxies, lubricants, surfactants, anti-stats, and other polymeric film formers [4, 5]. The thickness of the sizings that have dominated the commercial markets lies in the range between 0.1 μm to 0.5 μm. These coatings, besides minimizing the interfacial free energy for better wetting, are designed to react with the polymeric matrix as a mechanism to enhance bond strength and stability for superior adhesion [6]. However, recent investigations have demonstrated that excessive non-reactive components (e.g., binding agent) present in the commercial sizings tend to remain in high concentrations within the interphase, weakening the resin network crosslink density [7], reducing the fiber/matrix interface adhesion [8] and increasing the potential for water ingress [9].

Thinner sizings containing less inactive 'building' agents are expected to create an almost one-dimensional interphase region,

sufficiently thin, such that no drastic changes in the matrix network structure could probably take place. Among the studies relating fiber coating thickness to composite stiffness and toughness, the theoretical work by Matonis and Small [10] is the first one indicating that the interlayer thickness is very critical. Their major finding was that in order to obtain an adequate stress transfer and maintain a higher modulus than that of the matrix, only a very thin layer of rubber is admissible: $R_0/R_1 \approx 0.999$; where the ratio $R_0/R_1 = 1$ represents the limiting case when the rubbery interlayer thickness diminishes to zero. The use of slightly thicker layers of rubber ($R_0/R_1 \approx 0.96$) was shown to lower the modulus considerably, leading to an overall improved toughness but reduced strength. Hayes et al. [11] also presented theoretical results suggesting that the presence of an interphase region between fibers and matrix in a composite can significantly affect the load transfer characteristics, even when the interphase is very thin.

Experimental evidence to the influence of sizing thickness on composite performance, although hard to obtain, has corroborated some of the previous theoretical results. Pioneering work by Lavengood and Michno [12], and later by Tryson and Kardos [13], showed that solution-cast thick ductile innerlayers are effective in

preventing filament abrasion as well as in enhancing crack-arrest mechanisms during composite fracture. However, more recently, Mäder et al. [14] found that rather thick layers of film formers applied as sizing in glass fiber reinforced polypropylene tend to initiate plastic yielding in the sublayer followed by a localized sublayer failure. Novel approaches based on the self-assembled technology also suggest that only a monolayer or close to monolayer of silane coupling agent may be enough to obtain good chemical adhesion [15] and good flexural properties for glass-fiber reinforced composites [16].

In addition to sizing thickness, a great deal of attention has been given recently to the concept of 'flexible interphase' in composites fabrication [17-19]. The application of a low-modulus coating on an inorganic reinforcement to create what is known as a 'soft' interphase has been largely experimented with different elastomeric compositions and thickness ranges. It is generally accepted [20-22] that a soft interphase is advantageous because it changes the stress distribution and decreases stress concentration, consequently increasing the fracture toughness properties of the composite. Many researchers have worked on toughening composites by weakening the interfacial strength, which they basically attained by coating the fibers with silicone rubber, silicone oil, SBS rubber or other elastomers or

thermoplastics. A comprehensive review [21] of the methods used by various investigators in this field showed a general trend of fracture toughness increases by 0 to 100%, while the strength and modulus values decreased by 0 to 50 % with the use of rubbery coatings.

Based on the previous studies, it would seem like the simultaneous improvement of stiffness and toughness is seldom achieved with composites exhibiting a soft interphase. However, some theoretical modeling [22] and experimental work [4, 23-27], including chemically modified and unmodified elastomeric sizings, have demonstrated the potential utilization of a flexible interphase in obtaining a good balance between composite modulus and impact strength. For instance, Ahlstrom and Gérard [24] and Daoust et al. [25], using the single-filament fragmentation technique, showed that an elastomer coating applied over glass fibers led to a superior interfacial strength of an epoxy/glass fiber composite. The enhanced adhesion in this case was interpreted as the soft interphase being able to reduce the shear stress concentrations at the fragment ends. Further evidence is presented by the work of Tillie et al. [26]. They considered an application system where hydroxylated polydimethylsiloxane (PDMS) oligomers were deposited on-line over glass fibers as an alternative to create a controlled low-modulus and

low-thickness (ca. 130 nm) interphase in unidirectional filament-winding composites. Off-axis tensile tests and three-point bend results for composites fabricated with the low glass transition temperature interphase did not show significant difference from the mechanical performance of those parts reinforced with commercially sized glass fibers. However, Charpy tests did confirm an increase of the impact toughness as a result of the introduction of the soft interphase.

Most current solvent-based methods used to incorporate commercial and model sizings to glass fibers have inherent limitations on the film thicknesses they can produce. The physisorbed and chemisorbed components of the commercial finishes usually have a combined thickness greater than 100 nm, and the smallest thickness that the authors are aware of for model elastomeric coatings is around 100 nm to 130 nm [26, 27]. All these indicate that the systematic utilization of polymeric coatings with thicknesses well below 100 nm as sizings for glass fibers may still be considered as an unexplored alternative. Ultrathin hydrophobic coatings of various polymeric entities can be formed on the surface of inorganic reinforcements like glass fibers [28-30], as well as in other types of substrate [31, 32], by using the surfactant-enhanced technique known as admicellar polymerization. Characterization studies of these thin polymeric

coatings through contact angle measurements [29] have suggested the establishment of an adequate level of surface energy interactions between admicellar-modified glass fibers and a DGEBA-type epoxy resin (e.g., EPON 815C), leading to a wetting behavior comparable to that attained by commercial sizings. Furthermore, a very thin elastomeric film present at the interface has been shown to produce test results consistent with good interfacial adhesion for single-filament pullout and three-point bend tests [30].

Our current investigation involves the fabrication and mechanical testing of RTM parts to measure the degree of structural integrity enhancement achieved by the use of admicellar-polymerized thin flexible coatings as sizings for random glass fiber preforms. A preliminary study was conducted to compare the mechanical properties and processing-induced defects of composites reinforced by commercial glass-fiber random-mats, molded at two different constant speeds: a high-speed molding setup, which allowed mold-filling in an average of 20 seconds; and a low-speed molding fixture [33], with an average fill time of 15 minutes. These fill times are consistent with current industrial molding cycles for small to medium sized RTM-parts fabrication. After selecting the molding setup, the main thrust of the paper is dedicated to correlate the effect of sizing type, architecture

and void content to strength, stiffness, and ILSS results obtained for RTM-parts molded at high-speed.

5.2 Experimental

5.2.1 Matrix characterization. The relatively low viscosities of epoxy-amine systems are usually preferred for liquid molding processes like RTM because the injection pressure requirements are substantially reduced. The polymeric matrix used in this study was a two-part system: a low-toxicity epoxy resin manufactured by Shell Chemicals, EPON 815C, with a room-temperature viscosity of 500-700 cP, as reported by the manufacturer; and a modified aliphatic amine adduct with an amine value of 761-809, EPICURE 3282. A 5:1 weight-ratio mixture of this particular epoxy-amine system had a gel time of about 20 minutes, which helped us ensure that the mold-filling step would not be affected by sharp viscosity changes resulting from cross-linking reactions. The curing agent had a reported average room-temperature viscosity of 4000 cP, while the average viscosity measured for the liquid prepolymer mixture was 980 cP.

Thermosetting polymer systems often exhibit a direct relationship between the degree of chemical conversion and both the molecular network structure and the final mechanical properties. The

development of an ideal regular three-dimensional polymeric network is not always attained in practice, as the epoxy resin curing reactions are known to be complex multistep processes with highly nonlinear relationships to time and temperature [34]. Further, poor physical mixing of reactants causes variations in the resin to curing agent ratio, which ultimately lead to structural inhomogeneity characterized by regions of higher and lower cross-linking density. In this way, Van Landingham [35] recently demonstrated that the room-temperature fracture toughness of epoxy-amine systems increases whenever they are cured with an amine curing agent content higher than the stoichiometric ratio.

Resin infiltration does not seem to have all the nonlinearities generally attributed to the chemical reactions involved in the composite matrix curing. However, in certain liquid molding techniques like RTM where long distances and high shear forces are present, phase segregation phenomena, preferential partitioning of components and changes in local transport properties (e.g., viscosity) can occur prior to the development of the expected composite mechanical properties. These flow-induced anomalies may affect the matrix uniformity, and it has been suggested previously that parts molded by

RTM are prone to have resin-rich areas preferentially localized towards the edges [2].

Matrix uniformity in our high-speed molding experiments was identified as an important variable of study because poor mixing effects could obscure the impact of sizing types in the mechanical properties of the composites fabricated. To evaluate the degree of matrix uniformity and the optimal curing schedule of our composite parts, we molded disks with and without reinforcement, and subsequently tested them with a Rheometric Scientific RSAII Dynamic Mechanical Analyzer (DMA) operated at a fixed frequency of 1 Hz, strain rate of 0.04%, in the three-point bend configuration spanning 48 mm. The temperature inside the chamber was changed within the –5 °C to 170 °C range at incremental steps of 4 °C; maintaining a minimum of 10 s soaking time to account for the temperature transients inside the sample. Specimen selection and other experimental procedures were carried out according to the ASTM D 4065-94 standard.

5.2.2 Preform characteristics and sizing types. Commercial general-purpose E-glass fibers have two variants: one is the generic boron-containing glass fiber, and the other is a boron-free or calcium-magnesium-aluminum silicate glass fiber. In all cases, 13-μm diameter

boron-free E-glass fibers produced by FibreGlast was the starting material for the inorganic reinforcement phase, which were subjected to different pretreatments and postreatments depending on the type of sizing that was going to be applied. Table 5.1 depicts the specifications for the different preform architectures and sizing types utilized herein.

Sizing types considered for study in this paper include: (a) Commercial epoxy-compatible coating applied to the chopped strand mat Plast # 248 fabricated by FibreGlast; (b) Admicellar-coated poly (styrene-co-isoprene); and (c) Admicellar-coated polystyrene. Desized fibers used as control samples were prepared by burning off the sizing from the chopped strand mats in a furnace at 500 °C during 15 min. Similar heat cleaning procedures for E-glass fibers have been described previously [16, 36–37], and it is expected that no significant crystallization of the amorphous phase governing the fibers tensile strength properties would take place at the furnace temperatures utilized herein [40].

The same heat treatment applied to the control samples was also used as a pretreatment for those fibers modified with the ultrathin coating obtained by the admicellar polymerization method. Individual batches of 200 grams of desized fibers were put into a 6-liter glass reactor containing 7.000 μM solution of sodium dodecyl sulfate (SDS)

surfactant equilibrated at a pH close to 3.6. After 4 to 6 hours of surfactant adsorption, enhanced by moderate agitation, a 1:1 molar ratio of monomer (e.g., styrene or styrene/isoprene) to surfactant was injected into the reactor and strong mixing was kept up for an additional four hours. At the end of the adsorption-adsolubilization period, a fairly lipophilic organic azo-initiator (AIBN) was dissolved in absolute ethanol and added to the reacting mixture. Approximately 30 minutes after the addition of AIBN, the reactor was brought to a temperature between 80 to 90 °C and the surface polymerization reaction on the bilayers adsorbed on the glass fibers was initiated. To expose the polymeric thin film, excess surfactant was removed by rinsing the fibers liberally two to three times with distilled water. Finally, overnight vacuum drying at 60 °C was used to drive-off any unreacted monomer and moisture from the fiber surface. Further details on the fundamentals of the admicellar polymerization technique are available in other recent publications [28-31].

5.2.3 Molding setup and filling procedure. Two different molding setups were constructed to fabricate resin transfer molded disks. The constant flow rate press, utilized in the current study to mold parts at low-speed (ca. 0.067 cm^3/s), consisted of two stainless-steel hollow cylinders serving as reservoirs for the resin and curing

agent. Both cylinders were held in place with an aluminum fixture. The top part of the fixture had a moving plate with plungers that displaced the resin and curing agent in the cylinders by equal distances when the top plate was pushed downward. The force acting on the moving plate came from a computer-controlled materials testing system (MTS 810) that provided a controllable constant linear velocity, resulting in a constant volume flow rate. A detailed sketch of this particular molding setup has been recently described elsewhere [33].

In the case of the short-fill time experiments, a similar molding press was designed in such way that the two-component epoxy resin system would be injected at a constant rate around 5.32 cm^3/s. Figure 5.1 depicts the components of the high-speed filling fixture. The moving plate and the plungers were secured to the ram of a 40-ton hydraulic press (ARCAN, Model CP402). The stainless-steel cylinders were welded to a steel plate placed perpendicular to the plungers, which was held in place on the press body with c-clamps. The internal diameters of the two cylinders containing the resin and curing agent were the same as the ones used in the low-speed fill press: 55.47 mm and 25.53 mm in order to achieve the appropriate mix ratio, 4.7 to 1 by volume, of resin to curing agent.

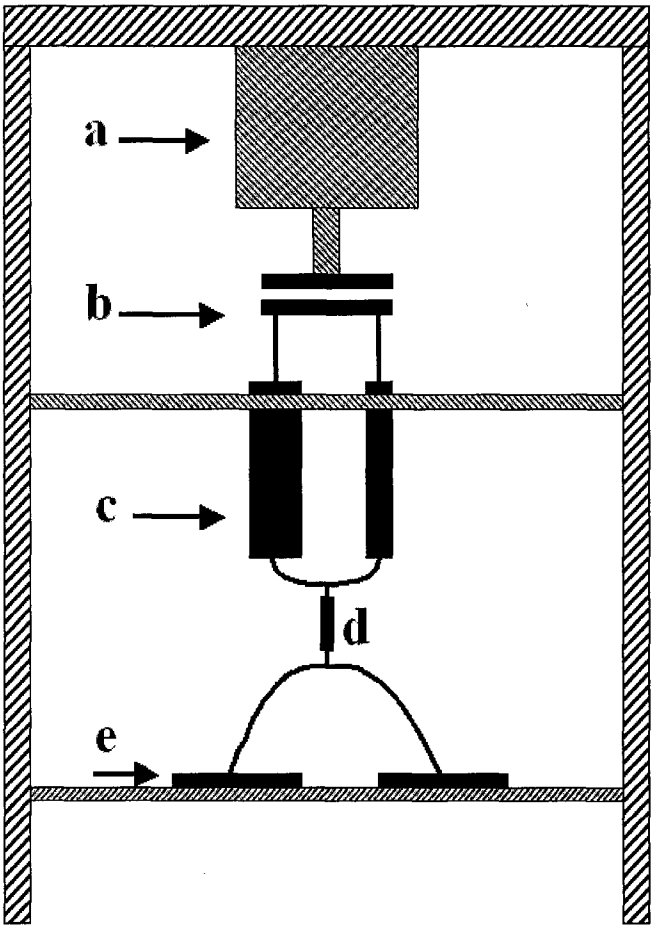

Figure 5.1 High-speed filling RTM fixture (**a.** Hydraulic press motor-ram ensemble; **b.** Piston plugs; **c.** Resin and curing agent cylindrical containers; **d.** In-line mixer; **e.** Molds).

The flow coming from both cylinders was thoroughly mixed by passing it through an 18.6 cm-long polypropylene in-line Statomix® (Technical Resin Packaging Inc.) and subsequently injected into a sealed center-gated, disk-shaped aluminum mold. The mold cavity with a volume capacity of approximately 58 cm^3 was constructed by inserting a flat aluminum spacer plate with a thickness of 3.18 mm

between two 6.35 mm thick aluminum mold wall. A 15.24-cm diameter circle cut from the center of the spacer plate formed the disk-shaped cavity. Four ports located 90° apart, vented air during filling. Prior to the injection, a total of 30 g of fibers were set inside the mold cavity, which represents a fiber volume fraction of approximately 21 % for all composite parts fabricated. Preform placement operations depended on the specific fiber architecture. For fibers types S, I and II (Table 5.1), circular layers of the same diameter as the mold cavity were cut from the fiber rolls, and subsequently 4 layers were stacked as random mats one on top of the other. The nonlayered structure of fiber types Im, IIm, III and IV, also described in Table 5.1, required a slightly different placement procedure: the fiber tows were manually pulled apart, and then meticulously positioned inside the mold cavity so that fiber orientations would be distributed as randomly as possible.

After filling, the four vents were closed to allow the application of an extra post-fill packing pressure on the molds, which has been found to be beneficial for the mechanical performance of liquid-molded parts [8]. As the final step, the inlet hose is clamped to maintain the pressure, and the part left for 24 hours inside the mold until it reached the so-called 'green' state when it could be taken out of the mold without difficulty. Typically, two molds containing the same type of

fibers were impregnated concurrently by dividing the outflow from the mixer with a plastic tee. The average fill time for both molds was 20 seconds. With the resin and curing agent contained in the cylinders it was possible to impregnate three pairs of disks of different sizing types. A total of 10 to 12 disks for each sizing type were fabricated under the same experimental conditions.

Table 5.1 Preform architectures and sizing types

Sample Code	Molding scheme	Sizing Type	Preform architecture	Fiber surface pretreatment/postreatment
N	High-speed	None	Neat resin	None
S	Low-speed	Commercial epoxy-compatible	Random mats. 4 layers stacked	None
I	High-speed	Commercial epoxy-compatible	Random mats. 4 layers stacked	None
II	High-speed	None	Random mats. 4 layers stacked	500 °C for 15 min.
Im	High-speed	Commercial epoxy-compatible	Fiber tows pulled-apart	None
IIm	High-speed	None	Fiber tows pulled-apart	500 °C for 15 min.
III	High-speed	Polystyrene	Fiber tows pulled-apart	500 °C for 15 min + admicellar polymerization
IV	High-speed	Poly (styrene-co-isoprene)	Fiber tows pulled-apart	500 °C for 15 min + admicellar polymerization

5.2.4 Specimen preparation and mechanical testing. Each molded disk was sectioned using a vertical milling machine into five rectangular specimens with dimensions: 11.43 cm x 1.27 cm x 0.4 cm; and thereafter polished on the sides with a 320 grit sand paper to even out the asperities left by the cutting bit. Thickness variation for each specimen was assessed by recording thickness data with a digital micrometer at five random points along the length of every specimen. Specimen widths were also averaged from five random measurements, while the length was calculated from a three-point average.

The relative spatial position of the five specimens within each molded disk is presented in Figure 5.2. Specimens marked 1 and 2 from all molded disks were tested under tension according to ASTM D3039/D3039M-00 standard. Tensile forces applied were ramped linearly from 0 to 8.90 kN over 120 seconds. Strain measurements were obtained simultaneously with the tensile strength tests by placing a calibrated extensometer over a 2.54 cm span at the center of the specimen. Specimen 3, which is located at the center of the disk, did not comply with the requirements for mechanical testing because of the presence of surface defects at the inlet gate caused during the demolding process. As such, they were used later for void content and morphometry analysis. Specimen 4 demanded further sectioning to fit

into the special three-point bend fixture (MTS 642.001) spanning of 25.4 mm that was used to measure the interlaminar shear strength (ILSS). With the aid of a band saw three identical coupons 3.8 cm-long were cut out from specimen 4, and only the coupon located in the central position was used for testing.

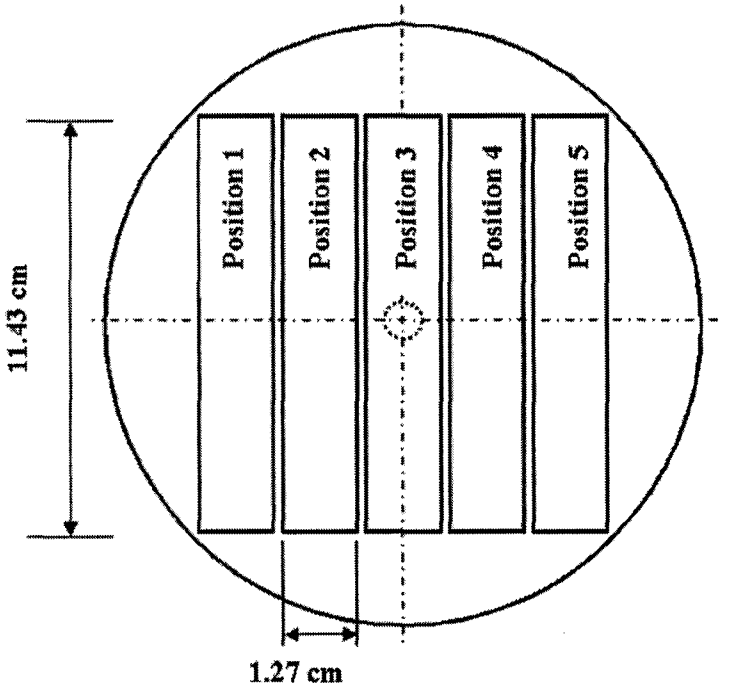

Figure 5.2 Relative spatial positions of test specimens in a molded disk.

The MTS 810 machine moving at a crosshead speed of 1.0 mm/min provided the force applied to the specimens during the three-point bend test, and the experimental parameters like the maximum force and maximum displacement were read and recorded automatically by the system. Interlaminar strength and other relevant

calculations were performed in accordance with the ASTM D2344/D2344M-00 standard. Finally, specimen 5 has been reserved for future studies on the hydrothermal resistance of admicellar-coated interfaces.

5.2.5 Void content quantification by microscopic image analysis. The void volume fractions, as well as other important parameters such as void size, shape and roundness were assessed by microscopic analysis performed on at least three different samples taken from specimen 3 of disk-shaped parts molded with fibers of distinct sizing types. Voids with different characteristics are likely to originate from different sources during filling, and will contribute to mechanical properties and failure mechanisms differently. For example, void size directly affects void mobility and thus, voids distribution. Void shape affects mechanical properties, with irregular voids being more likely to induce early crack formation [38]. Cross sections of every specimen selected for the void analysis were embedded in a commercial resin (Embed 812-DER 736), and then machined on a lathe to have a flat base surface for further polishing. A series of diamond lapping films (Alliedtech) of different grit sizes ranging from 30 μm to 1 μm ensured a smooth finish for adequate optical reflection. Once polished, the cross sections were analyzed and

digital pictures of individual voids taken at 100x with an opticai microscope (Nikon Optiphot-2) – CCD camera (Hammatsu C2400) system. Individually captured pictures were subsequently processed with the aid of an image analysis software (Optimas 4.1), which has features such as area morphometry that enable not only void area measurements, but also the classification of the voids according to their size and shape (e.g., circularity, ϕ = perimeter^2/area). Finally, assuming a linear equivalence, the volumetric void content of a particular sample was simply calculated as the percentage ratio of the total cross sectional void area divided by the geometric cross sectional area of the sample.

5.3 Results and discussion

5.3.1 Matrix uniformity. The DMA analysis is based on the principle that whenever an oscillatory force (e.g., sinusoidal stress) is applied to a solid sample, a sinusoidal strain will be generated in response if the test is performed in the linear viscoelastic region. By measuring both the amplitude of the deformation at the peak of the sine wave and the lag between the stress and strain waves, quantities such as the storage and loss moduli can be calculated [39]. In the current study, only two DMA parameters were of special interest: the glass transition temperature (T_g) and the elastic modulus (E′). The

glass transition is the point where the polymer transforms from a glassy to a rubbery state upon heating [40-41]. In this particular region the modulus (E') usually drops several orders of magnitude.

Figure 5.3 shows the elastic modulus (E') response of the neat resin and a control fiber composite at two different curing conditions: room temperature cured (RT), and heat post-cured (HC) in an oven at 110 °C for 1 h. Control fiber samples consisted of desized fibers that were prepared by burning off the sizing from the chopped strand mats in a furnace at 500 °C for 15 min. The reinforcing effect of the glass fibers is clearly evidenced from the higher elasticity modulus of the desized composites at all temperatures. Another important fact observed herein is that physical and/or chemical interaction of the fiber surface with the resin reduces the chain mobility, leading to a rise in the glass transition temperature from around 60 °C up to 75 °C. The mechanical relaxation processes described above are also influenced by the application of a heat post-curing treatment. For instance, whenever the neat resin cured at room temperature was heated to temperatures higher than the glass transition temperature, a slight increase in the elasticity modulus took place during the test, reaching a value comparable to that of the HC-cured neat resin specimens. In the desized fiber composites, the difference in elasticity modulus

between RT-cured and HC-cured was not as dramatic; notwithstanding, a higher crosslinking density was always observed for the annealed samples.

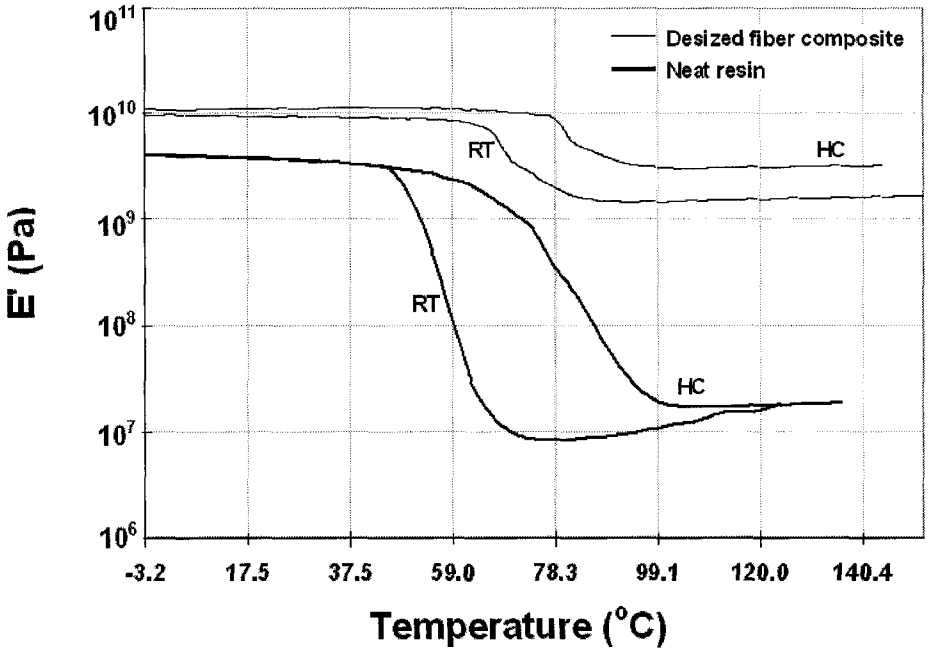

Figure 5.3 Elastic modulus (E′) response of neat resin and desized fiber composite at two different curing conditions: room temperature (RT) and heat post-cured (HC) at 110 °C.

After comparing T_g and E′ values for several RT-cured neat resin and composite specimens, we did not find significant variations suggesting deficient mixing or matrix inhomogeneity caused by component segregation. The next step was then to find the optimal point between curing conditions, structural integrity and processing cycle time for all composite parts. Table 5.2 presents glass transition

temperatures, elasticity modulus and other important thermo-mechanical parameters evaluated at RT and HC conditions as a function of curing time. According to these results, the HC-post treatment generally yielded the maximum modulus values for both the neat resin and desized fiber composite. However, we believe that additional sources of error could be introduced by inhomogeneous distribution of heat whenever the samples are set in the oven. For this reason, the 7 days RT curing program was chosen as the optimal between mechanical properties development and total testing schedule time. It is worth noting that at the end of the 7 days period the elasticity modulus of the neat resin reached almost 90% of the $E'_{@\ E''\ max}$ value for the same sample cured at RT for 30 days.

Table 5.2 Important thermo-mechanical parameters measured by DMA

Description	**E' (at E" max) x 10^9 (dyn/cm^2)**	**E' (at Tan δ max) x 10^8 (dyn/cm^2)**	**T_g (°C)**
Neat resin, RT, 4 days	8.11 ± 0.54	1.84 ± 0.36	59.7 ± 0.04
Neat resin, RT, 7 days	13.70 ± 3.82	2.69 ± 0.21	63.3 ± 0.08
Neat resin, RT, 30 days	16.52 ± 2.45	3.61 ± 1.26	65.2 ± 2.6
Neat resin, HC (1 h at 110 °C)	11.2 ± 0.098	5.66 ± 2.18	90.3 ± 3.9
Neat resin, HC (18 h at 110 °C)*	10.9	6.65	100.6
Desized fiber composite, RT*	34.1	256	75.1
Desized fiber composite, HC (1 h at 110 °C)*	49	360	86.3

Note: Confidence interval of 95 % shown for all measurements, except for single-experiment data shown with asterisk (*) for comparison.

5.3.2 Effect of molding speed. One of the advantages of RTM over similar composites fabrication techniques is its short cycle time. Therefore, a critical step during RTM molding is to impregnate the preform as quickly as possible while minimizing undesirable features such as a race-tracking, high void content or incomplete wet-out that may result in premature failure or poor overall performance [42, 43]. Basically, two types of flow are believed to occur at different mold fill velocities in liquid composite molding [44, 45]. At low filling velocity, the flow inside the fiber tows or intratow flow is dominant. High capillary pressures cause the microflow within the narrow channels formed by two parallel fibers inside a tow to move ahead of the macroflow, which takes place in the inter-tow spacing. At high flow velocity the situation is reversed: the macroflow moves ahead of the microflow. In this latter case, the capillary effect is very small compared to the applied pressure, and therefore the viscous forces dominate the filling pattern.

An optimum condition of uniform front between the micro- and macro-flows seems imperative for minimizing void formation during a given mold filling process. Recent theoretical models [46] suggest that the capillary number (*Ca*) can be used as the sole parameter to predict the onset of the voidage phenomena, as it describes the hydrodynamic

balance between the effects of resin velocity and capillary pressure. Experiments with different fiber architectures and model fluids also favor the existence of a critical range of capillary numbers wherein small void contents can be achieved [47-49]. Notwithstanding the physical barriers imposed by the surface and viscous forces, there have been successful attempts to overcome void formation at high-speed molding. Among such strategies, the change of the inlet location [50, 51] and the utilization of higher injection pressures [3, 52] have demonstrated a significant reduction both in mold filling times and void inclusions. More economical alternatives like preheating the preform to remove volatiles from the sizing system prior to resin injection [6]; and also applying a 'post-fill' cure pressure or 'packing pressure' after the mold fill operation, have been shown to supersede surface influences which otherwise would have led to void formation [6, 33].

In the current work, we introduced an extra packing pressure following the normal mold fill operation as a way to control the quality of our composite parts. The packing pressure in both the low-speed and high-speed molding schemes was estimated to be always greater than 230 kPa, which we previously determined as the minimum packing pressure required to obtain appreciable improvement in the mechanical properties [33]. Void volume fractions were analyzed in

the disk-shaped composites produced with both processing cycles according to the procedure described in section 5.2.5. Exceptionally low void contents for these fill rates and processing conditions were obtained, which is indicative of a good matrix infiltration. However, the high-speed molded parts (I) did show slightly higher void content compared to the low-speed parts (S) as depicted in Table 5.3.

Table 5.3 *Void volume fraction for composites fabricated with different fiber treatments and molding velocities.*

Sample Code	Void Content (%)	Number of samples (n)
S	0.08 ± 0.05	3
I	0.18 ± 0.2	3
II	0.006 ± 0.002	3
Im	<0.005	2
IIm	<0.005	1
III	<0.005	3
IV	<0.005	3

Representative images from the microscopic analysis of samples S and I are depicted in Figures 5.4a-c. Figure 5.4a shows a void-free area where the fibers perpendicular to the cross-section are seen as small and white circular dots, while the white elliptical objects correspond to fibers nearly parallel to the cross section. The fiber tows appear in the figure as a collection of similarly oriented fibers bundled together within the layered random mats. In Figure 5.4b, a small ellipsoidal void of approximately 90 μm is located in a resin-dominated

area, which suggests a higher mobility of this kind of void during the infiltration. Small voids as the one presented in Figure 5.4b were typically found in the samples molded at low velocities. At higher velocities the voids were more irregularly shaped and preferentially located closer to the intratow spacing as depicted in Figure 5.4c.

a.

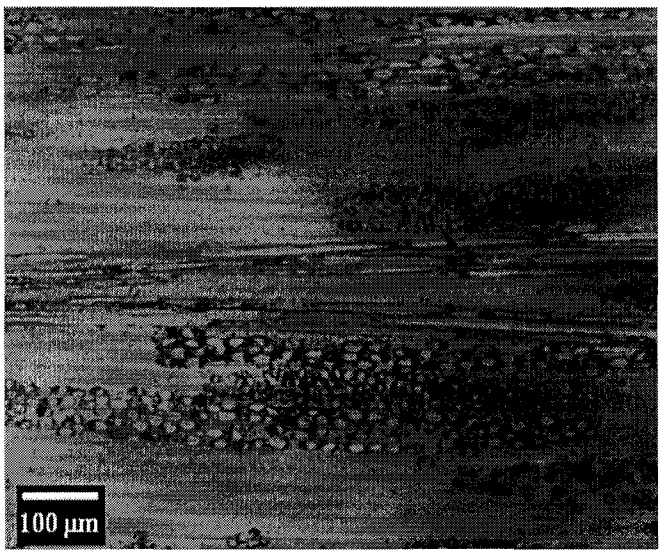

b.

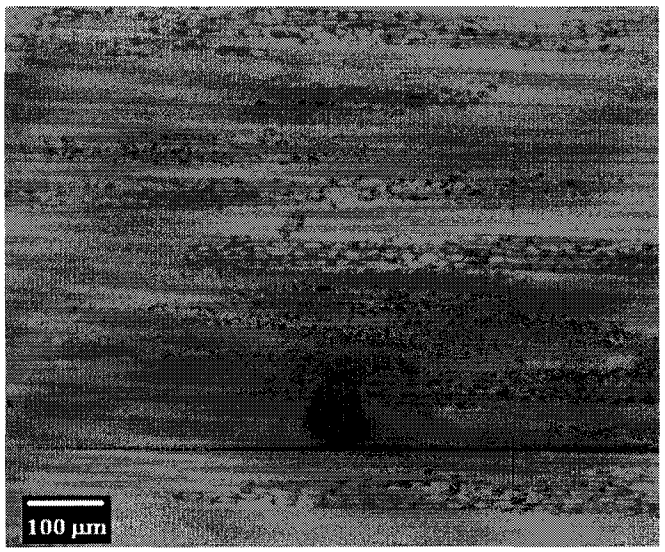

Figure 5.4 Cross-section micrographs of composites molded at different velocities: (a) Void free area; (b) Ellipsoidal void in a low-velocity molded part; and (c) Irregular shape voids in a high-velocity molded part.

c.

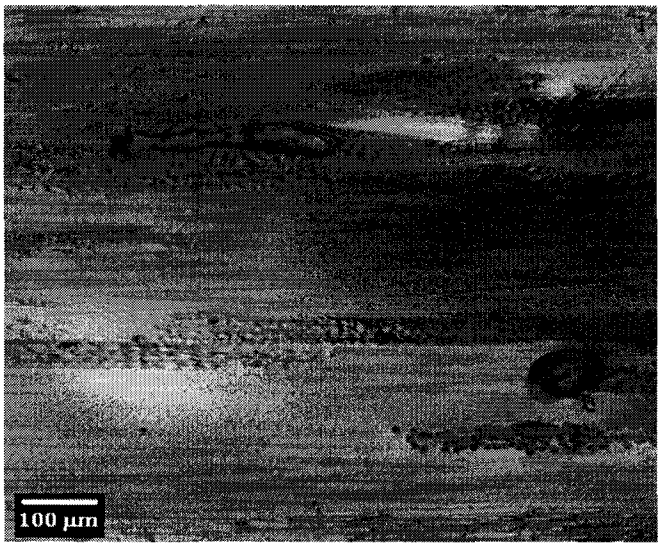

Figure 5.4 (Continued).

Average ultimate tensile strength (UTS) and stiffness data from positions 1 and 2 in the composites molded at two different flow rates: 0.067 cm^3/s and 2.66 cm^3/s are reported in Table 5.4. A moderate increase in the tensile strength by at least 10%, from 85 MPa to 94 MPa, is observed for the high-speed molded composites compared to the parts molded at a slower velocity. Stiffness values follow a similar trend, with a smaller increase of nearly 7% between the stiffness level at low speed (ca. 8000 MPa) and that at high speed (ca. 8500 MPa). At first, these observations seem to contradict the expectation of a sharp decrease in the tensile strength and stiffness properties at higher molding velocities, as faster fluid fronts originate more air entrapped in the intra- and inter-bundle spaces. However, at this low void concentration, a plausible explanation for the results found herein would be related to the particular crack growth mechanisms operating

in each sample. Varna et al. [53] reported that low void content specimens can achieve high strength levels when tested under uniaxial tension, but also the formation of large transverse cracks make them brittle with low strain to failure. Meanwhile, for laminates with slightly more voids the fracture mechanism is initiated with the formation of many small cracks connecting large spherical voids, and some of them connecting small cylindrical voids only. Often times, says the author, a small crack is arrested at a weft bundle, and the crack tip is somewhat displaced with respect to the first crack. This irregularity in the crack growth mechanism results in a lower stress concentration and stress level at the fiber bundles, which in turn explains the slightly higher transverse strain to failure of specimens containing slightly more voids.

Table 5.4 Mechanical properties of layered composites

Sample Code	UTS (MPa)	Stiffness (GPa)	Interlaminar Shear Strength (MPa)
S	85.136 ± 2.544	7.998 ± 0.310	15.371 ± 0.654
I	94.159 ± 2.654	8.478 ± 0.289	14.138 ± 0.607
II	72.910 ± 2.394	7.486 ± 0.545	11.277 ± 0.731

Note: Confidence interval of 95 % shown for all measurements

Interlaminar shear strength (ILSS) is another important criterion for rapidly evaluating differences in composites performance related to either the quality of the materials involved or to variations in the fabrication schemes. Average values for the interlaminar adhesion evaluated at position 4 for the same set of composites molded at high and low velocities appear in Table 5.4. In contrast to the data for UTS and stiffness, the interlaminar adhesion for the long-fill time composites is 9% greater (15.4 MPa), than that of the short-fill time parts (14 MPa). The possibility that this behavior originated from random variations in the data was ruled out since the statistical analysis showed strong evidence rejecting the hypothesis of identical populations ($p = 0.007$). A substantial decrease of the interlaminar adhesion properties with increasing levels of voidage has been long recognized in literature, and empirical correlations of exponential type have been put forward to represent the void-property relation [33, 54]. Very few works in the literature have addressed the topic of interlaminar shear strength reduction by discrete voids, or the influence of void shapes in the failure initiation mechanisms. A general trend observed recently by Wisnom et al. [55] in glass-fiber specimens with discrete inclusions suggests that longer voids can cause premature failure to initiate from the defect, not only by a stress concentration mechanism but also from the reduction in cross-

sectional area. Howe et al. [56] present similar arguments favoring the fact that, at the same void volume fraction, voids with lower radius of curvature section lead to higher stress concentration. It appears then, that the poorer performance attained by the high-speed molded composite parts in the three-point bend test can be attributed to the more frequent occurrence of longer irregular voids as opposed to the smaller and round-shaped voids found in the low-speed molded samples.

The presence of any type of sizing changes the interfacial thermodynamics between the glass fiber surface and the prepolymer matrix used in composite fabrication. Many studies have shown that good wetting is particularly important in achieving high interfacial adhesion. Furthermore, wetting quality influences the entrapment of air and whether any resulting voids remain in the interface or are displaced into the matrix [3]. Particularly in molding operations involving short infiltration times, a favorable interaction of the penetrating liquid and the reinforcing solid may help prevent some of the imperfections caused by a rapidly moving front. With the objective of testing the capabilities of our high-speed molding setup to effectively reproduce the influence of sizing in the mechanical properties of composites, we decided to mold parts with glass fibers

organized in the same random mat architecture, but having the commercial silane coating removed. Special precaution was necessary during the placement operation of the heat-cleaned preform so the fiber architecture would remain as intact as possible.

Figure 5.5 is a micrograph showing that the impregnation quality for the composites having desized fibers is considerably good, which in part may be anticipated from the somewhat low contact angles measured for this particular epoxy resin system in single desized-fibers experiments [29]. On the unexpected side, we found that all type II samples analyzed had void contents consistently lower than those parts molded with the original sized reinforcement irrespective of the molding velocity (Table 5.3). It is worth mentioning that according to the information provided by the manufacturer the random mats used in these experiments had an epoxy compatible sizing formulation. Apparently, the introduction of an organic surface treatment in the fiber bundles promotes the entrapment of air during the impregnation. Similar evidence of superior impregnation properties, as well as reduced porosity, in composites fabricated with either heat cleaned [36, 38] or 'water-sized' glass fibers [3, 6] confirm the validity of our results. Although we believe that the oven treatment may cause subtle changes in the preform architecture making it easy for the fibers to

spread out while impregnated by the resin front, no further efforts were dedicated to investigate this phenomenon.

Heat cleaned fibers are extremely hydrophilic and usually exhibit a molecularly adsorbed layer of water; even if they are sufficiently dried and placed in a desiccator before use as was done in the current study. This water monolayer is known to interfere with the formation of chemical bonds needed for an adequate adhesion between the fiber surface and the polymeric matrix [6]. As a consequence, it is expected that desized fibers would not show comparable levels of strength, stiffness or interlaminar adhesion as those normally attained by surface-coated fibers.

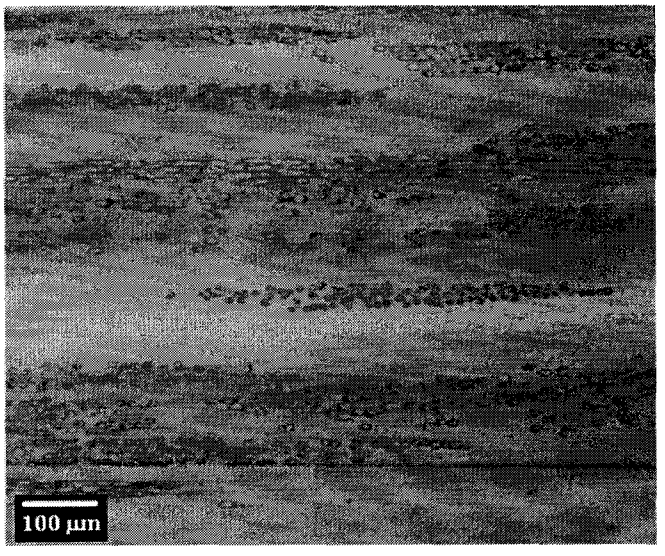

Figure 5.5 Impregnation qualities of composites with desized reinforcement (Type II).

Results from the mechanical performance of composites fabricated with desized fibers in comparison to those containing the untreated reinforcement are summarized in Table 5.4. The sharp drop in tensile properties from 94.1 MPa for composites with sized fibers, down to 72.9 MPa for those parts with desized fibers is indicative of the lack of chemical interactions between the bare glass surface and the matrix. A less dramatic, but consistent decrease in the stiffness and interlaminar shear strength levels corroborate the previous finding.

Mechanical interlocking between the polymeric matrix and the solid asperities are also believed to contribute to composite adhesion. Damljanovic and Sottos [57] showed how in fiber push-out tests rougher fibers introduce higher stresses at the interface increasing the level of energy needed for crack propagation. Meanwhile, for smoother fibers, like the glass fibers used in the current study, the debonding initiation energy is so high that catastrophic debonding occurs. In all, these results give us a point of reference to conclude that it is possible to adequately study the influence of fiber/matrix interactions at the operational levels of high-speed molding and high post-fill cure pressure.

5.3.3 Effect of fiber architecture. Within the admicellar polymerization treatment, heat-cleaned fibers were contacted with a surfactant solution containing the reacting monomers under moderate mixing conditions. Such treatment unavoidably caused a complete disruption of the original planar random-mat architecture that the desized fibers initially had. Hence, a separate set of experiments was planned to test the viability of detecting the contribution of sizing presence on the overall performance of composites molded at high velocity and high packing pressure. Figure 5.6a is a representative micrograph of the microstructure of composites Im, IIm, III, and IV. In all these cases the fibers were pulled apart from the original mat and subsequently distributed inside the mold, maintaining a random pattern but not necessarily a two-dimensional layered structure. The effect of the preform placement by hand is evidenced by comparing the compact and layered organization of the fiber tows in Figure 5.4a and Figure 5.5, with the looser and apparently more uniformly distributed reinforcement over the cross section of Figure 5.6a. A wider pore space in the nonlayered reinforcement originates an even more favorable resin impregnation, which in part explains the negligible void content values listed for these samples on Table 5.3. Typically, the scattered voids found during the microscopic analysis had a circular to ellipsoidal shape with diameters under 60 μm (Figure

5.6b). Given that the intrabundle space was nonexistent, the voids were all located in the resin-rich areas with a tendency to concentrate towards the outer edge of the disk. Porosity migration is known to be significant, especially in the case of small diameter bubbles that travel with the resin flow [38, 58]. Isolated voids of bigger diameter, as the one depicted in Figure 5.6c, were very infrequent and all had circular shapes.

a.

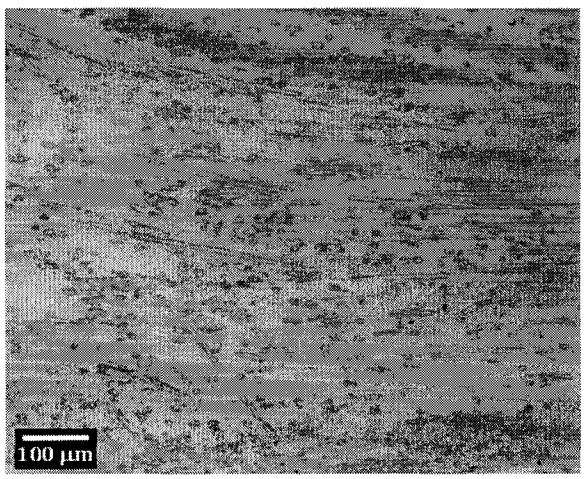

b.

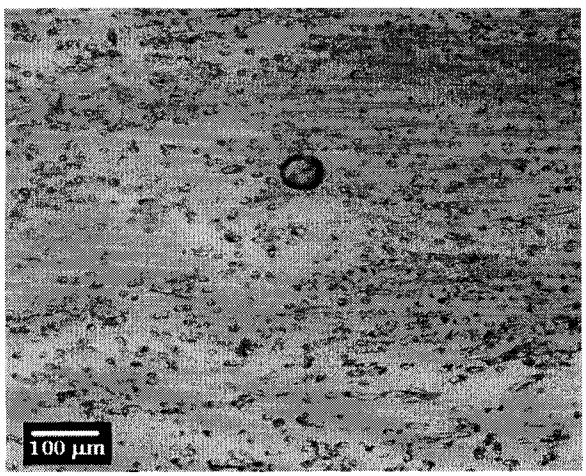

Figure 5.6 Cross-section micrographs of composites having a random nonlayered structure: (a) Typical fiber orientation distribution; (b) Mobile circular void; and (c) Large inclusion.

c.

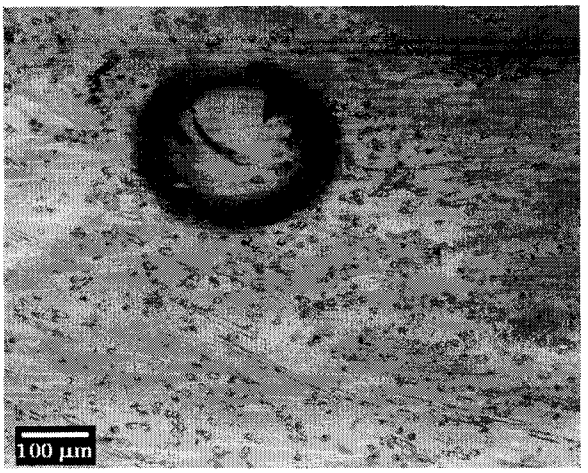

Figure 5.6 (Continued)

This new reinforcement arrangement brought about significant changes in the mechanical properties of the composites exhibiting a higher interfiber distance. Confronting the values plotted in Figures 5.7a to 5.7c for composites type IIm and Im with those values reported in Table 5.4 for composites type II and I, there is a manifest reduction in all the mechanical parameters measured for the nonlayered composites. An average decrease of 15.2% in the ultimate tensile strength, as well as a 6% decrease in stiffness and 9.8% in the interlaminar shear strength, took place within the sized samples. For the desized composites the average UTS and stiffness is reduced by similar percentages: 11% and 10.5% respectively. No statistical difference was found for the interlaminar shear strength of desized samples (II vs. IIm); although the test did show a noticeable decrease

(ca. 11.4%) in the interlaminar adhesion attributed to the desizing process (IIm vs. Im).

The results presented so far are suggestive of more catastrophic failure mechanisms acting on composites with nonlayered structure. Seemingly, crack-tip blunting or crack arrest can be performed more effectively by a layered bundle of fibers [53]. Otherwise, the crack will have no trouble in dissipating through the entire brittle matrix. At these marginal void volume fractions, we believe it is safe to presume that any differences in the mechanical performance between sized composites (Im) and the desized ones (IIm) are most likely originated from interfacial interactions. Admittedly, minimal changes in the fiber orientation distribution can also dim the response coming from the interfacial tests. However, increasing the number of specimens tested, and consistently using the same procedure for the preform placement, averages out any discrete variations in fiber orientation.

An interesting point that arises from testing random, nonlayered reinforced composites is the effect of material nonlinearities in the mechanical properties. Glass reinforced polymers with the fibers arranged in a random pattern, especially if having a wide range in the fiber orientation distribution, are known to display a highly nonlinear

stress-strain relationship in tension due to matrix cracking [59]. This anisotropy confers an intrinsic statistical dependence to the strength properties of composite materials [60].

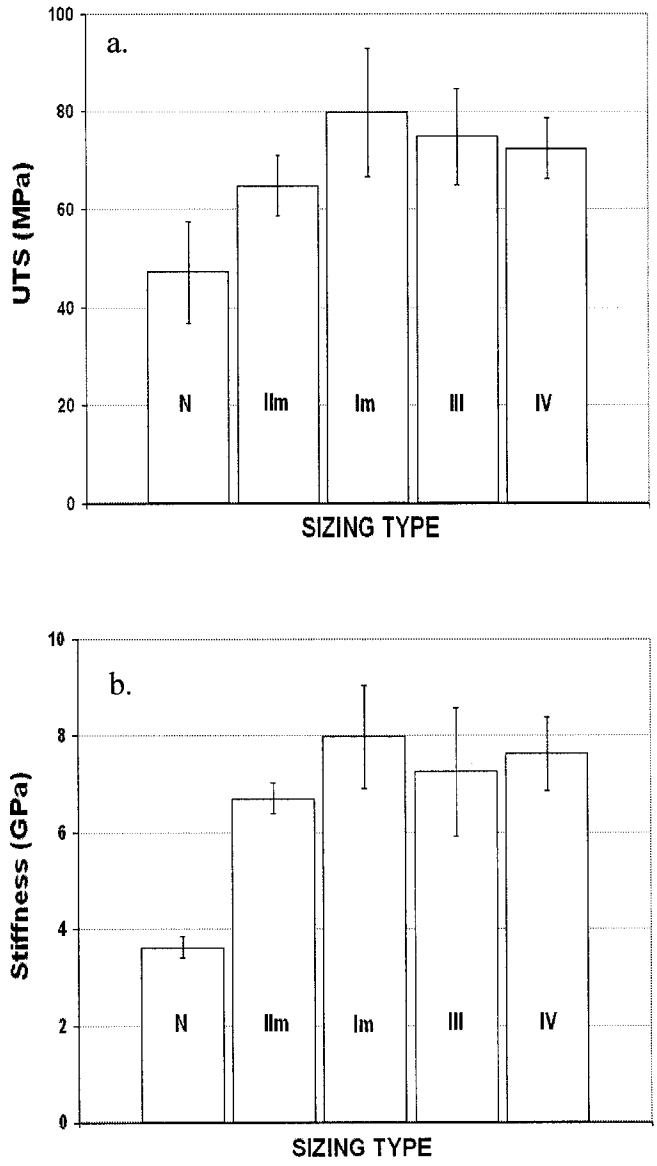

Figure 5.7 Mechanical properties of composites with random nonlayered structure: (a) UTS (MPa); (B) Stiffness (GPa); and (c) Interlaminar shear strength (MPa).

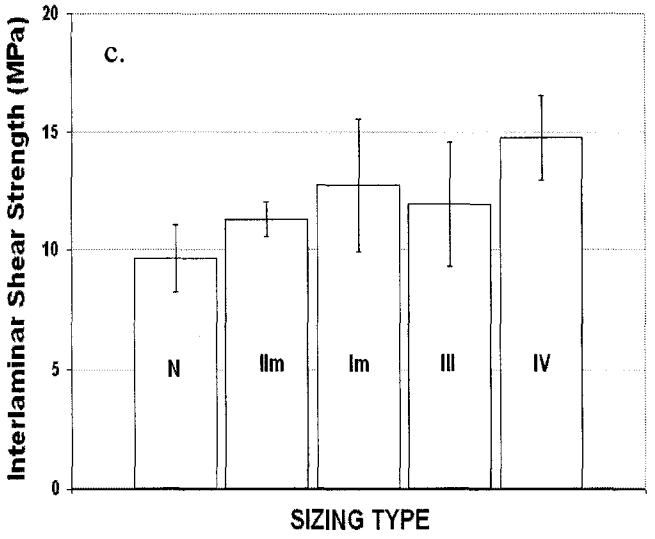

Figure 5.7 (Continued).

In our tensile tests with commercial layered composites, the statistical coefficient of variation (CV) for the UTS and stiffness data typically remained within 5 to 12%. Meanwhile, when the preform was changed to a nonlayered structure (Im), the signal-to-noise ratio in both UTS and stiffness decreased substantially, and the CV values were predominantly in the 15 to 25% range. Flexural tests, like the three-point bending, do not seem to be perturbed as much as the tensile tests by the material inhomogeneity. However, other disturbances such as friction forces and large deflections may be expected to cause significant variations in measured data, particularly for fiber patterns other than unidirectional [59]. Indeed, we observed much more data scatter in the interlaminar shear strength results for nonlayered composites with a statistical variation of 20-25%, as

compared to the layered composites, which had variations only in the 7% to 11% range.

5.3.4 Effect of sizing type. As the reacting liquid matrix flows over the glass fiber surface it encounters zones of varying degrees of surface energy and heterogeneous chemical characteristics. From the information presented in previous paragraphs, it can be inferred that the establishment of a strong adhesive-bond between the inorganic solid and the polymeric matrix will be dictated not only by the surface energy relations (thermodynamic work of adhesion or wetting quality) but also from specific chemical interactions. The probability of inducing primary chemical bonds is expected to be maximized by using tailored commercial sizings. Abundant evidence on the reactivity of organosilane coupling agents with both inorganic solids and polymeric matrices has been well established and documented [61]. In line with previous findings, our experiments showed a marked influence of the commercial sizing on the final mechanical properties of the composite parts regardless of any changes in the operational variables. That is, either at different levels of molding velocity or with distinct fiber architectures, the commercially sized composites always performed significantly better than the composites fabricated with control fibers in both tensile and flexural tests. In the specific case of nonlayered

reinforcement with commercial sizing, the results as depicted on Figure 5.7a to Figure 5.7c show appreciably high increases in UTS and stiffness values, 23% and 19% respectively, when compared to the control samples (IIm). Only a moderate increase (ca. 13%) resulted in the interlaminar shear strength for the same type of sizing.

By covering the glass fiber surface with thin films of polymers exhibiting electron-rich aromatic rings and unsaturated π-bonds we anticipate increased acid/base pairs and other physical (e.g., dispersion forces) interactions with the epoxy prepolymeric mixture, prior to the final curing step. An admicellar-polymerized coating of styrene-isoprene similar to the one used in a previous study [29], was introduced herein to fabricate the composites type IV. A comparison of the average values obtained for UTS and stiffness of type IV composites, as depicted in Figure 5.7a and 5.7b, indicate moderate to very high increases in the mechanical properties due to the presence of the elastomeric coating. The ultimate tensile strength for the composites with the poly (styrene-co-isoprene) coated preform turned out to be 11.7% higher than the desized control sample, whereas the stiffness showed a higher increase up to 13.7%. A statistical analysis using the t-test revealed that although significantly high data variability may exist, particularly in the tensile mode (CV = 17%),

there is suggestive evidence ($p < 0.075$) that the elastomeric-coated fibers behave differently from the control samples in the aforementioned tests. The statistical difference supporting the better performance of samples IV against the control sample (IIm) is even stronger after analyzing the results for the three-point bend tests ($p < 0.002$). From Figure 5.7c it appears that simply by introducing a thin film of elastomeric nature the interlaminar shear strength of the composite may be improved by almost 31% as compared to a completely bare fiber.

The other sizing tried during the current study was polystyrene (PS), a non-elastomeric polymer in the bulk. In contrast to the poly (styrene-co-isoprene) copolymer, no previous evidence about polystyrene sizing compatibility with the epoxy resin was available. Therefore the primary reason behind using this specific coating was to test the hypothesis that by increasing the amount of sites available on the glass fiber surface for chemical/physical interactions, substantially higher adhesive force at the interfacial level could take place; thus leading to increased mechanical properties. Average values for the three mechanical parameters measured on composites fabricated with polystyrene-coated reinforcement are also presented in Figure 5.7a to 5.7c. The ultimate tensile strength for the composites type III reached

a value 15.5% higher, on average, than the one attained by the control sample. Considerably lower increases in stiffness, 8.1%, and interlaminar adhesion, 5.6%, were observed for this kind of sizing with respect to the desized composites. Although it would be tempting to conclude that these results support the underlying hypothesis mentioned above, the coefficient of variation for this particular data set was so high that, in general, the values reported as the 'average' for each specific property are not very representative of the sample dispersion. CV's in the order of 25% to 35% were detected, and this in fact obscures any slight differences in mechanical behavior between composites type III and the control samples (IIm). P-values found during the statistical analysis were: 0.105, for the UTS; 0.300, for the stiffness; and 0.334 for the interlaminar shear strength. Based on these statistical probabilities the t-test showed little or no real evidence to conclude that a difference in mechanical performance operates as a result of introducing the polystyrene thin film as a sizing.

At this point we do not have a complete explanation as to why the polystyrene film failed to exert a positive influence in the mechanical properties of type III composites. Single-fiber contact angle experiments with water yielded advancing angles that were close to 70 degrees. A typical tensiogram is presented in Figure 5.8. The

contact line jumps abruptly in different positions along the fiber length, forming a saw-toothed line that is characteristic of a surface having sites of different surface energy, or in other words, hydrophobic/hydrophilic behavior. This result unequivocally demonstrates that the polystyrene thin film has a patchy distribution over the fiber surface. A similar discontinuous organization was observed for the poly (styrene-co-isoprene) thin films on glass fibers obtained by an identical polymerization method [29]. Therefore, we believe that simple discrepancies in film coverage or number of basic sites may not fully account for the appreciable difference in adhesion levels attained by composites IV with respect to composites III, when compared to the control samples.

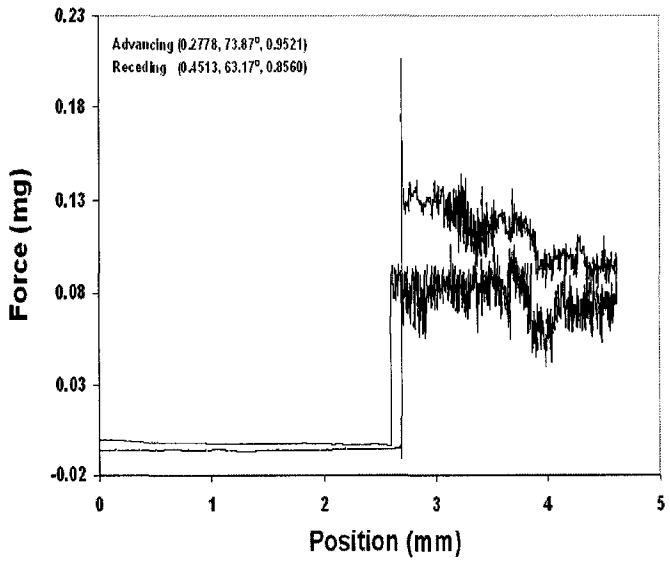

Figure 5.8 Tensiogram for water advancing over polystyrene coated fiber.

The molecular weight numbers of the admicellar polystyrene and the poly (styrene-co-isoprene) thin films used in the current study have not been yet measured, and surely this will be a focus of future research efforts. Tetrahydrofuran (THF) extractions performed by O'Haver et al. [62] suggest the molecular weight number (M_n) of admicellar polystyrene over silica to be in the order of 3000. In general, the amount of reactive monomer adsolubilized depends on the surfactant adsorption plateau values, which ultimately are a function of the available oxide surface area and adsorption conditions (e.g., pH and ionic strength). For this reason, we expect the average M_n for the polymer obtained on the glass fiber surface to be smaller than reported values for the much higher surface area silica substrate. Thin films of low molecular weight have distinct features in their thermal and mechanical properties intimately related to the molecular motions in the polymeric system. Small-amplitude motions such as vibrations and rotations of the elementary groups of the polymer chains as well as cooperative large-amplitude motions of chain segments are enhanced in films with low degree of polymerization. Consequently, physical properties exhibited by the thin films like the glass transition temperature (T_g) and surface elastic modulus (E') are notoriously affected, showing values completely different from those of the bulk polymer. For instance, Li et al. [63] used nanoindentation

measurements to evaluate the elastic modulus and work of adhesion of polystyrene films of different molecular weights supported on glass substrates. Their results indicate that all polystyrene thin films had similar elastic modulus values regardless of the molecular weights, although the low molecular weight polystyrene was rubbery while the medium and high molecular weight polystyrene samples were glassy at room temperature. Takahara et al. [64] also deposited monodispersed polystyrene thin films of different molecular weights over silica plates and measured individual elastic modulus with the aid of a scanning viscoelasticity microscope (SVM). They concluded that thermal molecular motions at the film surface are activated to a greater extent in comparison with the bulk polymers, especially in the case of molecular weight numbers (M_n) smaller than ca. 30000. Below this particular M_n value, the authors suggest that surface T_g would be lower than 293 K (20 °C), so the film can be expected to be in a glass transition state even at room temperature.

A great deal of controversy still exists on the measurement of glass transition in supported thin films. However, in the case of polystyrene films Forrest et al. [65] consider that consensus has been reached in the observation of T_g being reduced below the bulk value, with this effect becoming more pronounced for films of smaller

thicknesses. In the case of block copolymers T_g is predominantly a function of the microphase separation, weight percentage of the blocks in the system, as well as other structural parameters such as molecular weight and segmental motion. In fact, it has been shown that for anionic polymerized poly (styrene-co-isoprene) block copolymers an abnormal decrease in T_g for the hard styrene phase is evidenced, which is not only related to the molecular weight of the polystyrene block, but to a greater extent on the mobility of the polyisoprene chains in the soft microphase [66]. Low molecular weight poly (styrene-co-isoprene) copolymer are usually pictured as having an unentangled and disordered structure that contributes to depressing its glass transition temperature relative to the same copolymers of higher molecular weight with lamellar structure [67]. T_g estimates based on dynamic scanning calorimetry (DSC) for poly (styrene-co-isoprene) copolymer with low polymerization degree (M_n = 2700), and 50% weight of polystyrene, are in the range of –46 °C to –23 °C [66].

We expect both the admicellar polystyrene and poly (styrene-co-isoprene) coatings to be in a rubbery state at room temperature due to their low molecular weight and predominantly disordered microstructure. Particularly for polymers in a rubbery state, it has

been demonstrated that large molecular probes can diffuse thanks to a coupled effect from the probe average rotational motions and the cooperative segmental mobility of the polymer. This segmental mobility can in turn be affected by external factors such as thickness in ultrathin supported films and polymer-substrate affinity [68]. Therefore, it would be reasonable to consider that a great deal of the interactions between the admicellar thin films, used as sizings in the current study, and large segments of the epoxy chains may be in part modeled as a diffusion process involving a sufficiently large probe into an ultrathin supported polymer film. In a study about the mechanical effects of diblock copolymers at interfaces, Brown and Reichert [69] showed that increased compatibilization and interface toughness could be achieved by introducing an 8 nm layer of a diblock elastomer between two immiscible homopolymers. An interdiffusion-entanglement mechanism based on the extension of the diblock chains into the homopolymer was proposed, which resulted to be more favorable at smaller film thicknesses.

Diffusion of organic probes into polystyrene thin films supported over silicon oxide is known to drastically decrease with film thicknesses less than 150 nm. Several authors have explained such behavior as the result of a 'pinning' mechanism acting between the polystyrene

chains and the inorganic substrate [68, 70], entrapping chain entanglements near the surface. Hall and Torkelson [71] recently suggested that interactions between polystyrene and a silicon oxide substrate are negligible because of the weak affinity of these two components. In order to prove this hypothesis they prepared thin films with more polar character (e.g., polyisobutylmethacrylate, polyvinyl pyridine) and higher affinity for the silicon oxide substrate, and showed that no drop in probe diffusivity was observed for these polymers with decreasing thickness, even at films thicknesses as small as 50 nm. These facts constitute proof that other mechanisms linked to the local chain architecture (e.g., flexibility, number of available conformations) may be responsible for a reduced local cooperative segmental motion hindering the diffusion into polystyrene ultrathin films, not necessarily related to the polymer-substrate interaction.

Extending the observations reported previously in the literature to our admicellar system, it appears that the differences in sizing performance for composites type III and type IV may be related to a higher segmental motion, and consequently more effective interdiffusion occurring between the poly (styrene-co-isoprene) chains and the long epoxy segments present in the matrix before gelation. Admittedly, other factors like chain structure (e.g., linear for

polystyrene, and branched for poly (styrene-co-isoprene)), as well as the presence of unsaturated moieties in the isoprene block branches, may also contribute to augment the interactions between poly (styrene-co-isoprene) and the epoxy functional groups. However, at this point we are convinced that a combined effect of reduced sizing thickness and glass transition temperatures well below the room temperature is responsible for the noticeably increased flexural properties of composites type IV. Recent examples in the literature confirm our hypothesis that a thin elastomeric sizing of significantly low T_g would originate positive changes in the mechanical performance of composite materials. For instance, Tillie [26] showed that it is possible to promote better impact strength properties of unidirectional composites, without any detriment to the stiffness, by introducing a hybrid elastomeric interphase composed of hydroxylated polydimethylsiloxane (PDMS) with a glass transition temperature of -115 °C. Commercial sizings often include in their formulations elastomeric agents that are miscible but non-reactive with the polymeric matrix [4]. These elastomers have T_g values in the same order of magnitude than the glass transition temperature of the poly (styrene-co-isoprene) thin films used herein. However, once the elastomer is mixed with organosilanes and other additives (e.g., film formers) it is very likely that the glass transition temperature of the

composite film acting as the sizing would rise to much higher values than that for the original rubber. Although the sizing present in composites type I and Im were only known to be epoxy-compatible, no details about the exact composition or the introduction of rubbery agents were available to us. A higher glass transition temperature and a thicker film, resulting from a greater number of components, may explain in part the poorer flexural properties observed for composites fabricated with commercial sizings (Figure 5.7c) as opposed to those composites with reinforcements sized with a polymeric film only several nanometers thick. These results have implications for composite manufacture applications because they show the possibility of creating tailored interfaces from pure polymers with relatively low market prices.

5.4 Conclusions

The insertion of an elastomeric interphase into glass-fiber epoxy composites has long been recognized to provide greater impact properties to the reinforced parts. Along with an increased toughness, a softer interphase usually caused a reduction in the overall strength performance mainly due to the noncontrolled sizing thickness obtained with current solvent-deposition methods. In this chapter we have demonstrated that it is possible to utilize the admicellar polymerization

technique to create an elastomeric sizing of finite thickness over glass fiber reinforcements. Resin transfer molded parts fabricated with random, nonlayered glass-fiber preforms coated with a very thin poly (styrene-co-isoprene) sizing showed a moderate increase in strength and stiffness with respect to the control samples. Furthermore, flexural properties measured by the three-point bend test were improved in more than 30% from the control level and statistically comparable to the interlaminar shear strength level attained by the proprietary commercial sizings.

It appears that positive effects coming from the introduction of a nanometer-thick elastomeric interlayer can be noticed only if extensive cooperative segmental motions are present, that is, when the glass transition temperature of the admicellar-polymerized thin films is far below the room temperature. This fact was particularly seen in the case of polystyrene thin films used as sizing in composites type III, where no beneficial effects could be detected. Work in progress will attempt to perfect the admicellar-film coverage to create more available sites for chemical/physical interaction, as well as to extend the use of this polymerization technique to obtain new sizings from elastomers with a much lower glass transition temperature than the poly (styrene-co-isoprene).

References

1. N. J. Jhonston, *Book of Abstracts, Composites 2000: An International Symposium on Composite Materials.* University of Delaware (2000)
2. L. Fong and S. Advani, *Resin Transfer Molding - Technical Report CCM 95-09.* University of Delaware Center for Composite Materials, Newark (1995)
3. J.L. Thomason, *Composites* **26**, 467 (1995)
4. K. Bezarti, L. Cangemi and F. Dal Maso, *Composites Part A* **32**, 197 (2001)
5. J.L. Thomason and L.J. Adzima, *Composites Part A* **32**, 313 (2001)
6. B. Larson and L. Drzal, *Composites* **25**, 711 (1994)
7. J.K. Kim, M.L. Sham and J. Wu, *Composites Part A* **32**, 607 (2001)
8. A. Nakai, T. Osada, H. Hamada and N. Takeda, *Composites Part A* **32**, 487 (2001)
9. R.J. Gorowara, W.E. Kosik, S.H. McKnight and R.L. McCullough, *Composites Part A* **32**, 323 (2001)
10. V.A. Matonis and N.C. Small, *Polym. Eng. Sci.* **9**, 90 (1969)
11. S.A. Hayes, R. Lane and F.R. Jones, *Composites Part A* **32**, 379 (2001)

12. R.E. Lavengood and M.J. Michno, Jr., *Proc. Div. Tech. Conf., Engr. Props. And Structure Div.*, Society of Plastics Engineers, 127 (1975)
13. L.D. Tryson and J.L. Kardos, *36th Ann. Conf. Reinf. Plast. /Compos. Inst., The Society of the Plastics Industry*, Session 2-E, 1 (1981)
14. E. Mäder, E. Moos and J. Karger-Kocsis, *Composites Part A* **32**, 631 (2001)
15. G.A. Holmes, E.B. Feresenbet and D. Raghavan, *Amer. Chem. Soc. Polym. Preprints* **42**, 296 (2001)
16. H. Ishida and T. Chaisuwan, *Proc. Amer. Chem. Soc., PMSE Div.* **85**, 534 (2001).
17. R.T. Graf, J.L. Koening and H. Ishida, *J. Adhesion* **16**, 97 (1983)
18. A. Nakai, A. Ohtani, T. Ohki, T. Osada, M. Iwamoto, H. Hamada and N. Takeda, *Compos. Interfaces* **7**, 399 (2001)
19. H. Hamada, Y. Fujii, M. Ochi, K. Kitagawa, K. Nishiyabu, T. Nishiwaki, Y. Uetsuji, M. Kotaki, M. Mizoguchi, A. Nakai, N. Oya, T. Osada, M. Yamanouchi and N. Kajioka, *Proc. SPE Ann. Tech. Conf., ANTEC* **2**, 2157 (2001)
20. L.J. Broutman and B.D. Agarwal, *Polym. Eng. Sci.* **15**, 757 (1974)
21. M. Labronici and H. Ishida, *Compos. Interfaces* **2**, 199 (1994)
22. G. Vörös and B. Pukánszky, *Composites Part A* **32**, 343 (2001)

23. S.D. Gardner, C.U. Pittman and R.M. Hackett, *Compos. Sci. Technol.* **46**, 307 (1993)

24. C. Alhstrom and J.F. Gérard, *Polym. Compos.* **16**, 305 (1995)

25. J. Daoust, T. Vu-Khanh, C. Ahlstrom and J.F. Gérard, *Compos. Sci. Technol.* **48**, 143 (1993)

26. M.N. Tillie, T.M. Lam and J.F. Gérard, *Compos. Sci. Technol.* **58**, 659 (1998)

27. D. G. Peiffer, *J. Appl. Polym. Sci.* **24**, 1451 (1979)

28. S. Sakhalkar and D. Hirt, *Langmuir* **11**, 3369 (1995)

29. H. J. Barraza, M. Hwa, K. Blakley, E. O'Rear and B.P. Grady, *Langmuir* **17**, 5288 (2001)

30. B.P. Grady, E. O'Rear, L. Penn and A. Pedicini, *Polym. Compos.* **19**, 579 (1998)

31. W-L. Yuan, E. O'Rear, G. Cho, G. Funkhouser and D. Glatzhofer, *Thin Solid Films* **385**, 96 (2001)

32. W. Genetti, W.L Yuan, B. Grady, E. O'Rear, C. Lai and D. Glatzhofer, *J. Mater. Sci.* **33**, 3085 (1998)

33. K.A. Olivero, H.J. Barraza, E. O'Rear and M.C. Altan. *J. Compos. Mater.* **36**, 2011 (2002).

34. B. Bilyeu and W. Brostow, *Proc. SPE Ann. Tech. Conf., ANTEC* **2**, 2095 (2001)

35. M. R. Van Landingham, R.R. Dagastine, R.F. Eduljee, R.L. McCullough and J.W. Gillespie, *Composites Part A* **30**, 75 (1999)
36. H. Hamada, Z. Maekawa and N. Ikegawa, *J. Mat. Sci. Japan* **43**, 229 (1994)
37. T. Ootsuka, K. Hamano, M. Kurano and K. Sonobe, *J. Ceram. Soc. Japan* **105**, 175 (1997)
38. T.S. Lundström and B.R. Gebart, *Polym. Compos.* **15**, 25 (1994)
39. Menard, K.P., *Dynamic Mechanical Analysis: A Practical Introduction.* CRC Press, New York (1999)
40. H.S. Chu and J.C. Seferis, *Polym. Compos.* **5**, 124 (1984)
41. U. Schröder, T. Marzi, M. Heβ and R. Kosfeld, *Mat. Res. Soc. Symp. Proc.* **170**, 129 (1990)
42. A.W. Chan, D.E. Larive and R.J. Morgan, *J. Compos. Mater.* **27**, 996 (1993)
43. G.R. Palmese and V.M. Karbhari, *Polym. Compos.* **16**, 313 (1995)
44. N. Patel, V. Rohatgi and L.J. Lee, *Polym Compos.* **14**, 161 (1993)
45. W.B. Young, *J. Compos. Mater.* **30**, 1191 (1996)
46. M.K. Kang, W.I. Lee and H. T. Hahn, Comp. Sci. Technol. **60**, 2427 (2000)
47. T. Nowak and J.H. Chun, *Mat. Res. Soc. Symp. Proc.* **305**, 241 (1993)

48. Y.T. Chen, H.T. Davis and C.W. Macosko, *AICHE J.* **41**, 2274 (1995)

49. V. Rohatgi, N. Patel and L.J. Lee, *Polym. Compos.* **17**, 161 (1996)

50. A. Strömbeck, *Proc. Int. Conf. Compos. Mater.* **3**, 497 (1993)

51. C.L. Lee and K. H. Wei, *J. Appl. Polym. Sci.* **77**, 2149 (2000)

52. C.H. Lee and K.H. Wei, *Polym. Eng. Sci.* **40**, 935 (2000)

53. J. Varna, R. Joffe, L.A. Berglund and T.S. Lundström, *Compos. Sci. Technol.* **53**, 241 (1995)

54. S.R. Ghiorse, *Sampe Q.* **24**, 54 (1993)

55. M.R. Wisnom, T. Reynolds and N. Gwilliam, *Compos. Sci. Technol.* **56**, 93 (1996)

56. C.A. Howe, R.J. Paton and A.A. Goodwin, *Proc. ICCM-11* **4**, 46 (1997)

57. V. Damljanovic and N.R. Sottos, *Proc. ICCM-12* **5**, 126 (1999)

58. W.K. Chui, J. Glimm, F.M. Tangerman, A.P. Jardine, J.S. Madsen, T.M. Donnellan and R. Leek, *Proc. 9th Intl. Conf. Num. Meth. In Thermal Prob.,* Atlanta, 1323 (1995)

59. J.A. Holmberg, *J. Reinf. Plast. Compos.* **11**, 1302 (1992)

60. E. Barbero, J. Fernández-Sáez and C. Navarro, *Composites: Part B* **31**, 375 (2000)

61. C.L. Schutte, *Mater. Sci. Eng. Reports* **R13**, 265 (1994)

62. J. O'Haver, B. Grady, J.H. Harwell and E. A. O'Rear, in: *Reaction and Synthesis in Surfactant Systems*, J. Texter (Ed.). Marcel Dekker Inc., New York, p. 537-545 (2001)

63. M. Li, C.B. Carter and W.W. Gerberich, *Mat. Res. Soc. Symp.* **649**, Q721-1 (2001)

64. A. Takahara, X. Jiang, N. Satomi, K. Tanaka and T. Kajiyama, in: *Interfacial Aspects of Multicomponent Polymer Materials*, D. Lohse, T.P. Russell and L.H. Sperling (Eds.), Plenum Press, New York, p. 63 (1997)

65. J.A. Forrest and K. Danolki-Veress, *Adv. Coll. Interface Sci.* **94**, 167 (2001)

66. B. Morèse-Séguéla, M. St-Jacques, J.M. Renaud and J. Prud'homme, *Macromolecules* **13**, 100 (1980)

67. M.W. Hamersky, M. Tirrell and T.P. Lodge, *Langmuir* **14**, 6974 (1998)

68. B. Frank, A.P. Gast, T.P. Russell, H.R. Brown and C. Hawker, *Macromolecules* **29**, 6531 (1996)

69. H.R. Brown and W. F. Reichert, *Macrom. Rep.* **A29(Suppl. 2)**, 201 (1992)

70. X. Zheng, B. B. Sauer, J.G. Van Alsten, S.A. Schwartz, M.H. Rafailovich, J. Sokolov and M. Rubinstein, *Phys. Rev. Lett.* **74**, 407 (1995)

71. D.B. Hall and J. M. Torkelson, *Macromolecules* **31**, 8817 (1998)

6. Moisture Absorption and Wet-adhesion Properties of Resin Transfer Molded Composites Containing Elastomer-Coated Glass Fibers[‡]

6.1 Introduction

The structural integrity and lifetime performance of fiber-reinforced composites are highly dependent on the stability of the interfacial region between the matrix and fiber surfaces. For glass fibers, modification of the surface by means of organosilane coupling agents is the standard commercial approach. These agents have proven to be an effective way to enhance the adhesion of glass fibers to a number of thermoset polymer matrixes, including epoxies. However, proprietary formulations are often expensive and are

[‡] Material in this chapter was published in *Journal of Adhesion Science and Technology* **17**, 217 (2003).

designed for specific resin systems. The sizings that have dominated the glass-reinforcement market are usually in the range between 0.1 μm and 0.5 μm thick, and contain only a small percentage of active coupling agents (ca. 10%) [1]. The remaining 90% is a mixture of low molecular weight epoxies, lubricants, surfactants, anti-stats, and other polymeric film formers [1-2].

Dissolution and/or chemical reaction of the sizing components prior to the gelling of the matrix has been commonly regarded as a necessary step to increase both the adhesion and resistance to environmental degradation of the composite parts [3]. There is ample evidence suggesting that the diffusion of the loosely bound material contained in the sizing occurs quickly and long before the matrix starts gelling, although this may not necessarily lead to a better interface. Tanoglu [4], for example, found that the portion of sizing material that remained either chemically bonded to or physically adsorbed onto the fiber surface affected to a large extent the interfacial region formation and final mechanical properties. This insoluble sizing material, claims the author, will create an interphase with different network structure and lower stiffness than the bulk matrix. Other recent investigations have also demonstrated that excessive nonreactive components (e.g., binding agent) present in the commercial sizings tend to remain in

high concentrations within the interphase, thus weakening the resin network crosslink density [5], reducing the fiber/matrix interface adhesion [6], and increasing the potential for water ingress [7].

Both reversible and irreversible changes in the mechanical properties of thermoset polymers are known to occur as a result of water absorption. The transport of water into polymeric matrixes originates from the chemical potential imbalance between the water content of the surrounding medium and the water concentration in the polymer, which can be very low but not zero [8]. This water concentration gradient creates a material flux towards the bulk of the material, which is controlled by the strength of polymer-water hydrogen bonds and the rate of jump of water molecules from one active site to the other [8, 9]. Plasticization and swelling are among the adverse consequences of water absorption in both thermoplastics and thermosets. Plasticization is a strong function of the equilibrium moisture content in the polymer, and in addition to lowering the T_g, it is known to induce plastic deformation. Swelling, on the other hand, is especially prominent during the transient part of the diffusion. In general, it is believed that swelling is related to the differential strain, or induced stress, created by the expansion force exerted by the liquid while stretching the polymeric chains. These two damage mechanisms

are augmented in polymeric composites by the contributions of capillarity and the hydrophilic nature of the inorganic reinforcement and its interface. For instance, the combination of highly hygroscopic materials such as glass fibers and polymers containing hydrophilic sites (e.g., epoxies) make glass fibers/epoxy composites especially susceptible to water ingress. Aging studies of composites subjected to wet environments have demonstrated that water accumulates at unprotected glass fibers over a period of time causing both loss of adhesion and a reduction of fiber strength. Piggott et al. [10] found that plasticization and depression of T_g in a glass fiber/polyester composite could be reversed after desorption if the composite had not been subjected to mechanical loads or thermal degradation. They implied that the main reason for permanent mechanical performance loss was the damage and debonding of the fiber/resin interface. Therefore, covering the hydrophilic glass surface with polymers with good water-repellency properties is expected to prevent the water accumulation phenomenon and consequently the adhesion bond rupture.

Wet-strength adhesion studies have shown the importance of sizing composition and network structure on the property retention characteristics of composites. Chaudhury et al. [11] suggested that a

coupling agent with a lower crosslink density might exhibit higher hydrophilicity and consequently could be more susceptible to attack by moisture. With regard to the sizing composition, Schrader and Block [12] observed a lower wet-adhesion in an epoxy/glass composite system whenever there was an excessive amount of the loose-bound component present in the silane coating applied to Pyrex glass. Also, they found less debonding as the proportion of chemisorbed and 'monolayer' components became larger. Similar results have been reported by Graf et al. [13], who used tetrahydrofuran (THF) to remove the physisorbed fraction of a γ-methacryloxypropyltriethoxysilane (MPS) coating applied to E-glass fibers and then tested glass fiber/polyester composites under dry and wet conditions. The dry composite samples containing fibers previously washed with THF had flexural strengths that were slightly higher than those with unwashed fibers for surface coverages above 0.4 weight percent. The 'washed-samples' that were treated in water at 80 °C for 48 h had, unexpectedly, a wet strength greater than that for dry samples.

These deficiencies in the composites performance related to excessive nonreactive components (e.g., binding agent) have led researchers to focus their attention to creating monomolecular,

reactive surface layers which may strongly interact with both the organic and inorganic constituents present at the interphase [14]. Monolayer and submonolayer coatings [15], polysulfone [16], as well as polystyrene [17] tethered chains on the surface of E-glass fibers are some of the examples found in the literature showing that only a thin reactive interphase is required to provide optimum interfacial bond strength.

Our research group has recently introduced an alternative surface modification method applicable to glass fibers that uses surfactants and elastomeric monomers. This procedure, called admicellar polymerization, involves the formation of a polymeric film on the fiber surface with thicknesses well below 100 nm. Characterization studies of these thin polymeric coatings through contact angle measurements [18] confirmed the hydrophobic nature of the modified surface, as well as a favorable wetting of the admicellar-modified glass fibers by a DGEBA-type epoxy resin (e.g., EPON 815C). Recent work using glass fiber reinforcements modified with thin elastomeric films via admicellar polymerization showed an increase in the interlaminar shear strength over 30% with respect to those composites containing desized fibers. Also, the dry-adhesion levels obtained with these admicellar sizings were statistically comparable to

that exhibited by commercially sized reinforcements [19]. Hydrothermal effects on the adhesion strength of composites containing fibers coated with elastomeric sizings have not been investigated in detail. Therefore, the purpose of this study was to assess the effectiveness of admicellar-coated elastomeric sizings in preventing adverse consequences of moisture absorption to the strength, stiffness, and interlaminar shear strength of resin transfer molded glass fiber/epoxy resin parts.

6.2 Experimental studies

6.2.1 Modification of glass fibers by admicellar polymerization. The high surface energy characteristic of inorganic reinforcements hinders their compatibilization with low surface energy materials such as polymeric matrices. As mentioned in previous chapters, alternative treatments [20-24], including admicellar polymerization [25-31], have been the object of continuous research to modify the interfacial characteristics of technologically important reinforcements (i.e., glass fibers).

Herein, 200 g of heat cleaned (500 °C, 15 min) boron-free E-glass fibers (Plast # 248 from FibreGlast, Brookville, OH) were equilibrated in a sealed 6-liter glass reactor with a 7000-μM solution of

sodium dodecyl sulfate surfactant (SDS). The surfactant solution was adjusted to pH 3.6 with hydrochloric acid (HCl) prior to contact with the fibers. Subsequently, pure styrene or styrene/isoprene monomers in a 1:1 (monomer : surfactant) weight ratio were added depending on the type of polymeric film desired.

Monomers injected into the reactor are expected to partition towards the hydrophobic core of the surface aggregates created by the surfactant moieties. As soon as free radicals produced by the thermal decomposition (80 to 90 °C) of oil-soluble azo-initiator (AIBN) reach the monomers in the admicelle, polymerization takes place, forming an admicellar-coated polystyrene or poly (styrene-co-isoprene) glass surface. The polymerization reaction was assumed to be complete after 14 hours. To expose the polymeric thin film, excess surfactant was removed by rinsing the fibers thoroughly two or three times with distilled water. Finally, the fibers were vacuum dried overnight at 60 °C to drive-off any unreacted monomer and moisture from the fibers surface.

6.2.2 Molding setup and fabrication procedure for composites. A molding press was designed so mixing of the two-component system: DGEBA-type epoxy resin (EPON 815C, Shell

Chemicals) and the aliphatic amine catalyst (EPICURE 3282, Shell Chemicals) would take place at a weight ratio of 5:1. The molding apparatus consisted of a steel plate and plungers secured to the ram of a 40-ton hydraulic press (ARCAN, Model CP 402). A detailed sketch of the molding fixture is presented in Figure 5.1 (Chapter 5). The molding procedure included resin and curing agent displacement by the plungers to yield a volumetric rate of 5.32 cm^3/s. Further details on the specifications of the high-speed molding system may be found in Chapter 5, section 5.2.3.

Prior to the injection, a total of 30 g fibers were placed inside the mold cavity, which represented a fiber volume fraction of approximately 21% for all composite parts fabricated. The admicellar treatment unavoidably caused a complete disruption of the original planar, random-mat architecture of the commercial silane-coated fibers. Hence, the experiments aimed to test the different sizings were performed with fibers that were manually pulled apart from the original mat and meticulously positioned inside the 58-cm^3 disk-shaped mold cavity, maintaining randomly distributed fiber orientations within a non-layered structure. For comparison purposes, parts containing the same fiber volume fraction but with heat cleaned reinforcement were also molded at the same resin infiltration velocity.

The complete set of experiments and conditions are summarized in Table 6.1.

Table 6.1 Experimental conditions for RTM-composites fabrication and related properties.

Sample Code	Sizing Type	Fiber surface pretreatment/postreatment	Preform architecture	Void Content (%)
N	None	None	Neat resin	0
Im	Commercial epoxy-compatible	None	Fiber tows pulled-apart	<0.005
IIm	None	500 °C for 15 min.	Fiber tows pulled-apart	<0.005
III	Polystyrene	500 °C for 15 min + admicellar polymerization	Fiber tows pulled-apart	<0.005
IV	Poly (styrene-co-isoprene)	500 °C for 15 min + admicellar polymerization	Fiber tows pulled-apart	<0.005

6.2.3 Specimen preparation, mechanical testing and moisture diffusion studies. Disk-shaped molded composites were sectioned using a milling machine into five rectangular specimens with dimensions: 11.43 cm x 1.27 cm x 0.4 cm; and thereafter polished on the sides with a 320 grit sand paper to even out the asperities left by the cutting bit. The relative spatial positions of the five specimens within each molded disk are the same as the ones depicted in Figure 5.2 (Chapter 5). Dry-tensile strength was measured according to the

ASTM D3039/D3039M-00 standard with a materials testing system (MTS 810) by applying a tensile force ramped linearly from 0 to 8.90 kN over 120 s. Strain measurements were obtained simultaneously during tensile tests by placing a calibrated extensometer over a 2.54 cm span at the center of the specimen. Results from the tensile strengths for specimens taken from position 1 and 2 have already been reported elsewhere [19] and will serve as reference for data obtained in the wet-adhesion measurements. Samples from position 5 were also tested under tension, using the same procedure as described above, but after being immersed in water for over 2800 h during the moisture absorption studies.

Specimen 4 from each disk was further sectioned into three identical 3.8 cm-long coupons, using a band saw. These smaller coupons easily fit into the three-point bend fixture (MTS 642.001) used to measure both dry and wet interlaminar shear strengths (ILSS). The coupon located in the center of specimen 4 was used to assess the dry ILSS, whereas the other two were selected for water diffusion and short-beam shear tests. The MTS 810 machine was programmed to move at a crosshead speed of 1.0 mm/min, applying the required force to the specimens during the three-point bend test. Experimental parameters such as the maximum force and maximum

displacement were recorded automatically. Interlaminar strength and other relevant calculations were performed in accordance with the ASTM D 2344/D2344M-00 standard.

As mentioned before, moisture absorption studies were conducted independently on large (specimen 5) and small (cut from location 4) coupons. The first step was to dry the test samples in a vacuum oven at 65 °C for 1 week until it was presumed that all the initial moisture contained in the composites was removed. The vacuum-dried coupons were then weighed in order to determine their initial dry mass. Thereafter, the large specimens were placed in labeled-plastic racks and immersed in a constant-temperature water bath (Fisher Scientific Isotemp Immersion Circulator Model 70) set at 45 °C. Similarly, the small samples (3 to 4 for each surface treatment) were placed in tightly capped glass-bottles filled with distilled water. These bottles were subsequently stacked and immersed in another constant temperature reservoir, the Brookfield TC200 (accuracy of 0.03 °C). Individual coupons were taken periodically out of the water, dried with a lint-free cloth and weighed on an electronic balance (accuracy of 0.1 mg). Transient sorption values were recorded and thereafter fitted to a mathematical model based on a simple

differential mass balance scheme, also called Fick's law of single free-phase diffusion, to describe the moisture absorption kinetics.

Physically, the Fickian model assumes a homogeneous isotropic material and explains diffusion only as the collaborative movement of a probe molecule into a fixed-volume reference solid without explicit consideration of molecule-molecule interactions. In the particular case of unidirectional transport, this formalism predicts a linear increase of adsorbed water content in the composite with the square root of time. Eventually, as the interior of the material approaches equilibrium, moisture absorption rates gradually slow down until a plateau or saturation value is reached. Classical analytical solutions to the diffusion equation, such as the one presented by Crank [32], express the mass gain, M_t, resulting from moisture absorption at time t, in terms of a constant diffusion coefficient or effective diffusivity, D_{eff}, and the equilibrium moisture content, M_m as,

$$\frac{M_t}{M_m} = 1 - \frac{8}{\pi^2} \sum_{n=0}^{\infty} \frac{1}{(2n+1)^2} e^{-\left[\left(\frac{D_{eff}\, t}{h^2}\right)\pi^2 (2n+1)^2\right]}, \qquad (6.1)$$

where *h* is the thickness of the specimen; and *n* is the summation integer. A total of 7 – 12 big samples for each surface treatment outlined in Table 6.1 were used during sorption tests to obtain the average transient weights and equilibrium moisture, whereas only 3 – 4 of the small samples were chosen for the same purpose. The parameter, M_m, was estimated by following the definition of effective moisture equilibrium, that is, the state at which the average moisture content of the material changes by less than 0.01% within the span of the reference period. With these values, we fitted equation 6.1 to the measured average transient weights and obtained the series-solution diffusivity constants. For comparison, diffusivities calculated by the series-solution method were contrasted to the average values obtained with the simplified solution recommended by the ASTM D 5229/D 5229M. In the latter case, average diffusivity values are calculated from the initial gradient of the sorption curve when plotted against the square root of time. The simplified solution:

$$\frac{M_t}{M_m} = \frac{4}{\pi^{\frac{1}{2}}}\left(\frac{D_{eff}\,t}{h^2}\right)^{\frac{1}{2}} \tag{6.2}$$

Specimen size and shape are critical for moisture diffusivity measurement using the ASTM approximation. For instance, on

coupons without sealed edges, correction factors accounting for moisture ingress through the edges call for 100:1 aspect ratio. That is, in a nominally square plate or curved panel, the specimen ratio of the nominal length of one side to the nominal thickness should be higher than 100 so that diffusivity determination would be within acceptable engineering accuracy levels (ca. 4.1% error). Although our samples were not within the recommended ASTM specimen geometry guidelines, it seemed worth to at least check the order of magnitudes of the two estimations. It must be noted that Crank's solution, given as equation 6.1, is the primary method used in our assessment, and it is not as restrictive as the simplified solution in terms of the specimen geometry.

From equation 6.1, it seems obvious that one way to accelerate aging and shorten the equilibration time is to decrease the sample thickness. This holds true whenever the focus of the study is only on through-the-thickness moisture absorption. However, as it is often the case, in-plane moisture absorption will locally dominate near edges and may even control the overall absorption process. Such special situation is most likely to occur in those composite parts where the edge area is a substantial portion of the total area exposed to moisture. In the current study, sample thickness was kept much

smaller than the two other planar dimensions. Thus, by immersing surface and edge areas of both big and small samples, our major objective was to observe whether the presence of any multidimensional diffusion effect could override the influence of different fiber sizing types. Average surface area and edge area ratios between big and small samples were 4.5 and 3.5, respectively.

6.2.4 Fractography studies. Plasticization/swelling caused by water absorption governs the stress transfer mechanisms and fracture modes of composites tested under hydrothermal conditions. In general, fractography analysis performed on failed composite samples allows a visual evaluation of the interfacial region stability to water attack. For the current study, failure modes of fractured tensile and short beam shear samples were examined by optical and scanning electron microscopies. Once a sample was tested, the broken pieces were viewed with a Bausch & Lomb Stereozoom 7 (10 – 70X) that permitted image capture by a digital video/frame grabber system attached to it. Using this optical system, we classified the fractured surfaces from different samples, and those with particularly flat regions or interesting features were selected for further sectioning so they could fit in the electron microscope (ETEC Autoscan) holder. In order to avoid electrical charging during examinations under the

electron beam, the samples required preliminary trimming, mounting and sputter coating with a conducting Au-Pd layer. Scanning electron microscopy (SEM) photomicrographs were taken at 20 kV acceleration voltages at various magnifications.

6.3 Results and discussion

6.3.1 Moisture saturation levels and diffusion rate behavior. During admicellar polymerization, heat-cleaned glass fibers were equilibrated in a surfactant solution containing the reacting monomers under moderate mixing conditions. After such treatment, the original planar random-mat architecture of the desized fibers was completely disrupted as can be inferred by comparing the fiber orientations and tow arrangement shown in the micrographs of Figure 6.1a and Figure 6.1b. Figure 6.1a corresponds to an RTM-part molded with a commercial sizing treated reinforcement having a layered structure. Here, the fibers are randomly oriented in planar layers, and thus the intertow and intratow (small fiber-to-fiber distance) regions are clearly visible.

Figure 6.1b depicts how the intratow space of samples molded with admicellar-treated reinforcement disappears, and the fiber-to-fiber distance increases. We refer to this particular configuration as a

random nonlayered arrangement. Average void contents of random nonlayered samples from location 3 were previously calculated using optical analysis over cross sections and reported elsewhere [19]. This wider pore space in the nonlayered reinforcement brought about a more favorable resin impregnation, which, in part, explains the negligible void content values listed for these samples in Table 6.1.

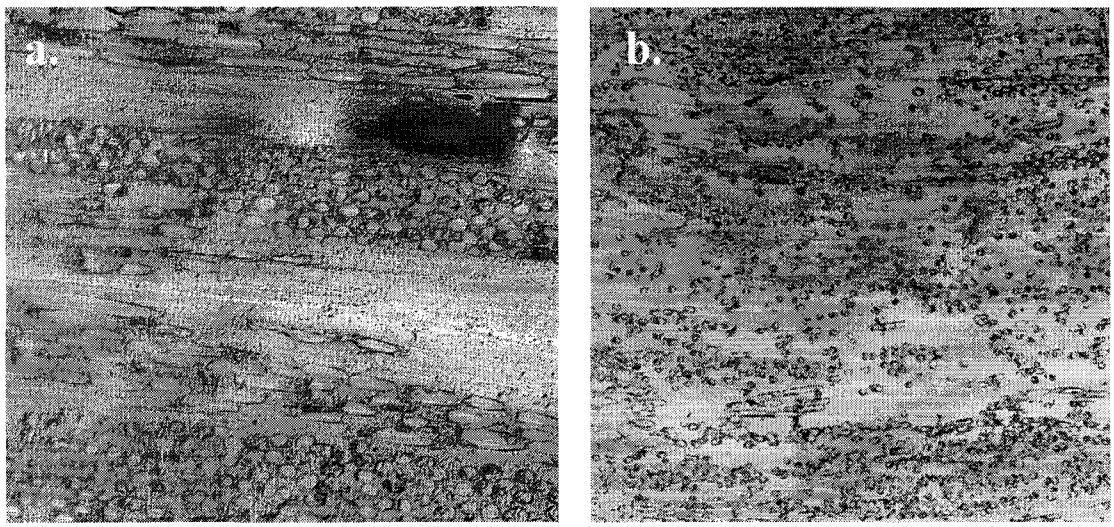

Figure 6.1 Representative micrographs of two different reinforcement architectures: (a) Random layered fibers commonly used in conventional RTM processes (100X); and (b) Random nonlayered fibers (50X).

Very few studies have dealt directly with equilibrium moisture values and sorption rates for fiber-reinforced composites as a function of fiber surface treatments; and even some of the data presented in the literature seem contradictory. For instance, Avena and Bunsell [33]

subjected epoxy/glass composite samples – with and without organosilane sizing – to hydrothermal treatments at different hydrostatic pressures. They concluded that the rate of water uptake was mostly influenced by the quality of the interface, with unsized samples having more susceptibility to microdefects at the interface and poor bonding between fiber and matrix. Thomason [34], on the other hand, suggested that void content overrides the influence of the coating and the fiber-matrix interface adhesion in the water absorption behavior of composites. A prove of this, claims the author, is that the removal of the fiber surface coating had no apparent effect on the kinetics of water absorption, despite the large detrimental effect on the interfacial strength. Hoppel et al. [35] studied a high-performance graphite fiber-reinforced epoxy composite with void volume fractions in the order of 0.4 – 1.5 % and found that diffusion rates changed by a factor of six with only small percent increases in the void content. In addition, these authors demonstrated that equilibrium moisture content for this material was only a function of the exposed relative humidity and independent of void volume fraction and temperature. Other authors [36, 37] have rationalized non-Fickian diffusion as well as unexpectedly high water uptakes in composites as the result of additional moisture residing in surface porosity and internal void spaces.

In the current work, both the appreciably low void content and the almost nonexistent intrabundle space found in the composites molded with different reinforcement sizings may be considered as advantageous for separating individual effects from the overall hydrothermal damage mechanism. Fewer voids mean less variation in the diffusion coefficient from the theoretical framework of the Fickian formalism. And, due to the absence of fiber tows, the capillarity effects may be deemed negligible. Therefore, we presume that the dominant features would be the pure diffusional transport of water through the matrix, followed by water attack and bond rupture at the interface. Figures 6.2 – 6.6 show the transient moisture gain and moisture saturation levels for neat resin, desized fibers and the different sizing types investigated.

In all cases, the results correspond to specimens taken from location 5 in the molded disks. Focusing on the maximum moisture content, it is evident that amine cross-linked epoxy polymers such as the EPON/EPICURE system used herein have the ability of absorbing relatively high amounts of water at the specific temperature set for the hydrothermal experiments (45 °C). The neat resin sample (N) accumulated a maximum of nearly 2.8% of water by weight, which was the largest increase registered for all samples studied.

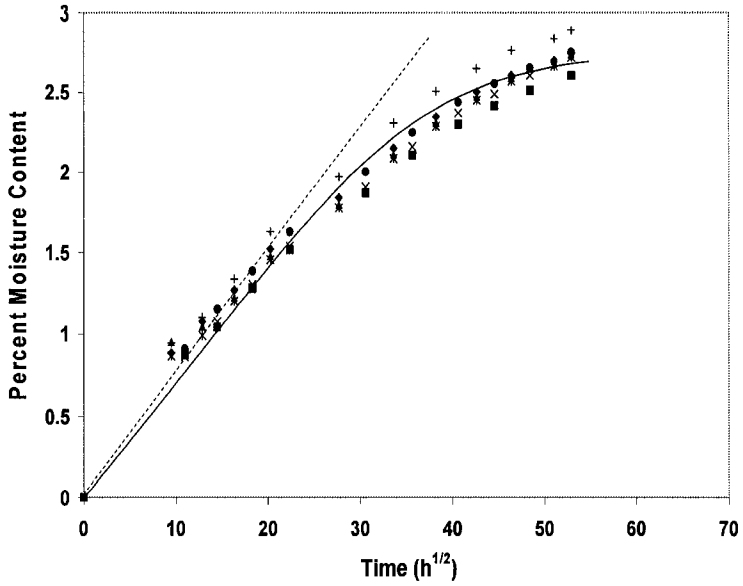

Figure 6.2 Percent moisture gain with time for big samples of neat resin parts (N). Each marker type in the figure corresponds to a different sample. Solid line: series-solution fit. Dotted line: ASTM-simplified approach.

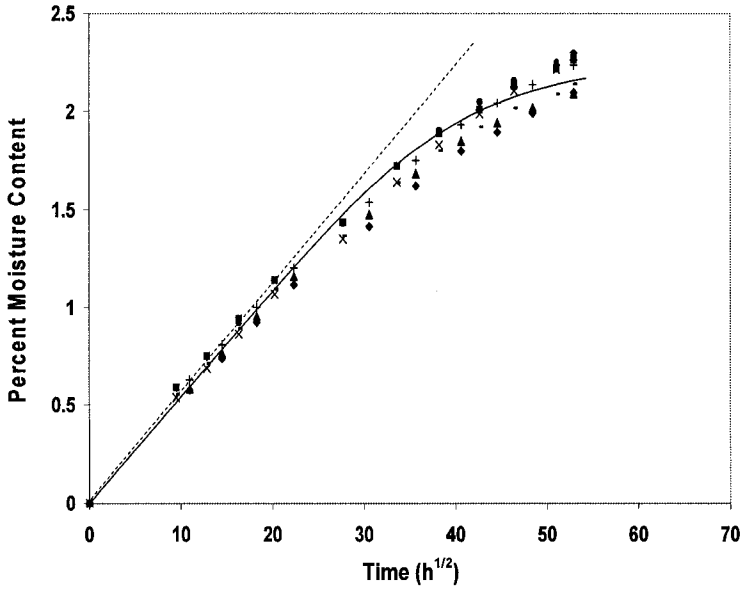

Figure 6.3 Percent moisture gain with time for big samples of commercial sized composites (Im). Each marker type in the figure corresponds to a different sample. Solid line: series-solution fit. Dotted line: ASTM-simplified approach.

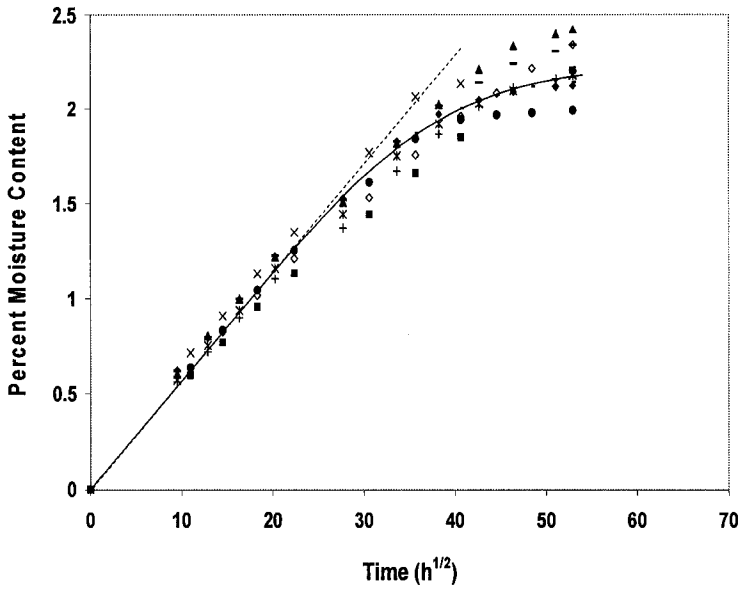

Figure 6.4 Percent moisture gain with time for big samples of desized (control) composites (IIm). Each marker type in the figure corresponds to a different sample. Solid line: series-solution fit. Dotted line: ASTM-simplified approach.

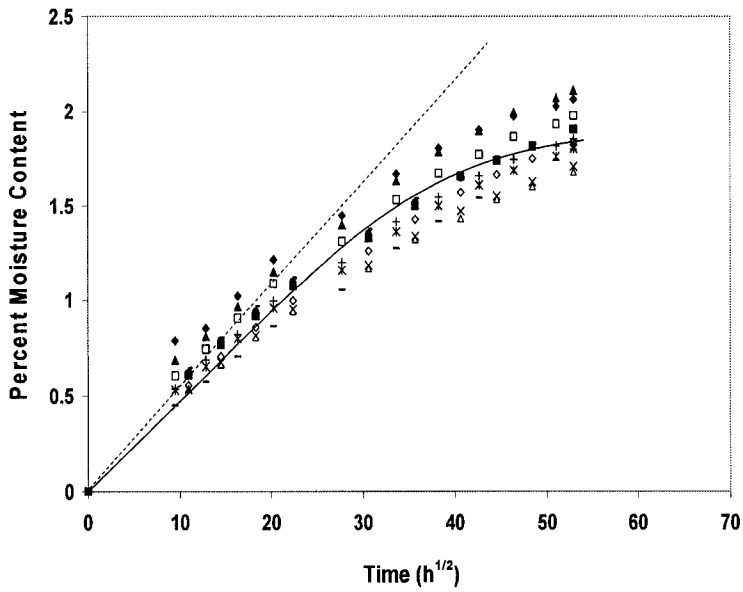

Figure 6.5 Percent moisture gain with time for big samples of polystyrene-coated composites (III). Each marker type in the figure corresponds to a different sample. Solid line: series-solution fit. Dotted line: ASTM-simplified approach.

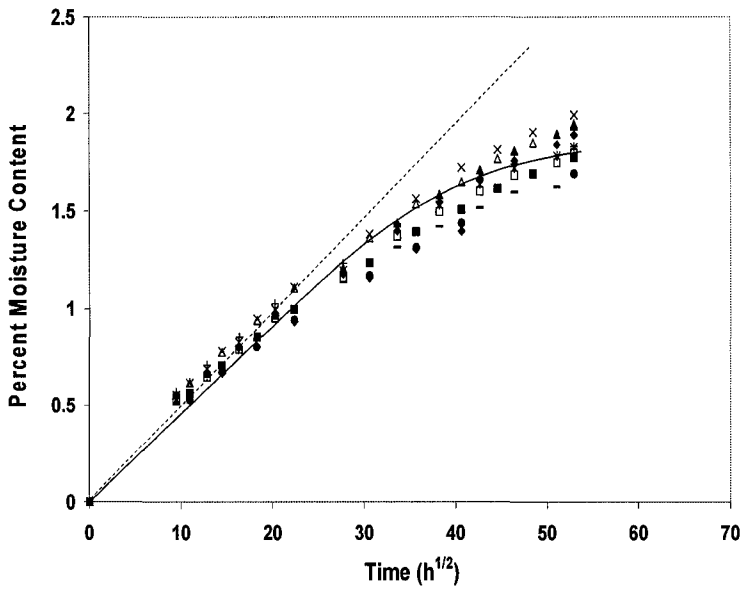

Figure 6.6 Percent moisture gain with time for big samples of poly (styrene-co-isoprene) coated composites (IV). Each marker type in the figure corresponds to a different sample. Solid line: series-solution fit. Dotted line: ASTM-simplified approach.

In Dynamic Mechanical Analysis (DMA) tests with dry samples the neat resin exhibited a glass transition temperature of 60 °C [19]. Physical and/or chemical interaction of the glass-fiber surface with the epoxy matrix was shown to reduce the chain mobility, leading to a rise in the glass transition temperature (T_g) from 60 °C to around 75 °C. Thus, given the lower T_g of the neat resin it is reasonable to anticipate an increased free volume in the chain packing of the polymer at the temperature conditions set for the hydrothermal experiments, facilitating the water absorption process. Utilizing the average resin mass fraction (0.85) for all molded parts, a maximum moisture

saturation value between 2.3 and 2.4% is expected to be present in the composites according to theoretical calculations [38].

The desized fiber composites (IIm) preformed as well as the parts reinforced with fibers coated with the commercial sizing (Im), and both had average moisture saturation values well in agreement with the theoretical estimate. Percent differences with the theoretical values did not exceed 10%. This particular behavior suggests that under the present experimental conditions, diffusion is the major mechanism of moisture penetration in these composites. Otherwise, had the other two additional mechanisms of moisture penetration (e.g., capillarity and transport by microcracks) been operating, the composites would have absorbed much more water than theoretically predicted [38].

In composites with admicellar-coated fibers the equilibrium moisture contents were substantially lower than the theoretical predictions (25% less than theoretical level). Interestingly, samples III and IV that had a more hydrophobic sizing showed maximum water absorption values ca. 15% smaller than the commercial samples; although in the case of specimens III the data scatter was more pronounced than sample IV. Statistically similar results with respect to

moisture saturation levels were obtained with the coupons cut from position 4 as depicted in Figures 6.7 – 6.9. Considering all the results from Figures 6.2 – 6.9, it seems reasonable to infer that reduction in moisture transport to the interfacial region in admicellar-coated composites may be due to a modified glass surface, exhibiting higher contact angles with respect to water.

In addition to moisture saturation levels, the other parameter controlling, in part, the final performance of composites under wet conditions is the magnitude of the diffusion rate. As observed in Figures 6.2 – 6.9 all molded parts, including the neat resin, followed the Fickian diffusion approximation for water absorption and exhibited initial linear regions that in all cases extended to moisture levels close to 60% of the saturation limit. The solid line in these figures represents the theoretical series-solution fit given by equation 6.1, which constitutes the basis for our assessment; whereas the dotted line corresponds to the approach described by ASTM D 5229/D 5229M (equation 6.2). Calculated values for D_{eff}, with both approaches, are listed in Table 6.2.

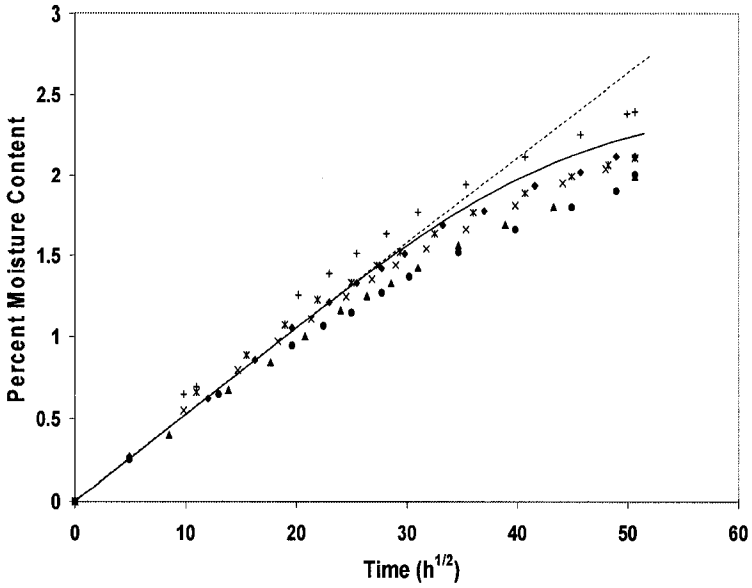

Figure 6.7 Percent moisture gain with time for small samples of commercial sized composites (Im). Each marker type in the figure corresponds to a different sample. Solid line: series-solution fit. Dotted line: ASTM-simplified approach.

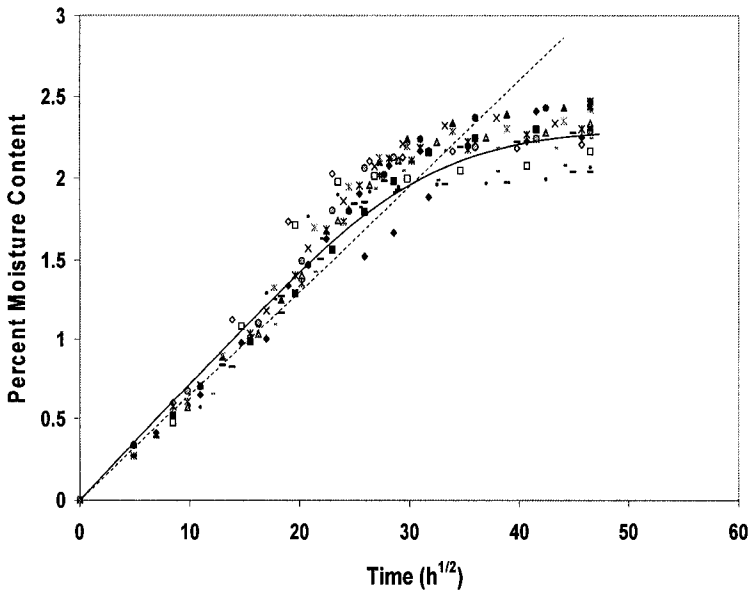

Figure 6.8 Percent moisture gain with time for small samples of desized (control) composites (IIm). Each marker type in the figure corresponds to a different sample. Solid line: series-solution fit. Dotted line: ASTM-simplified approach.

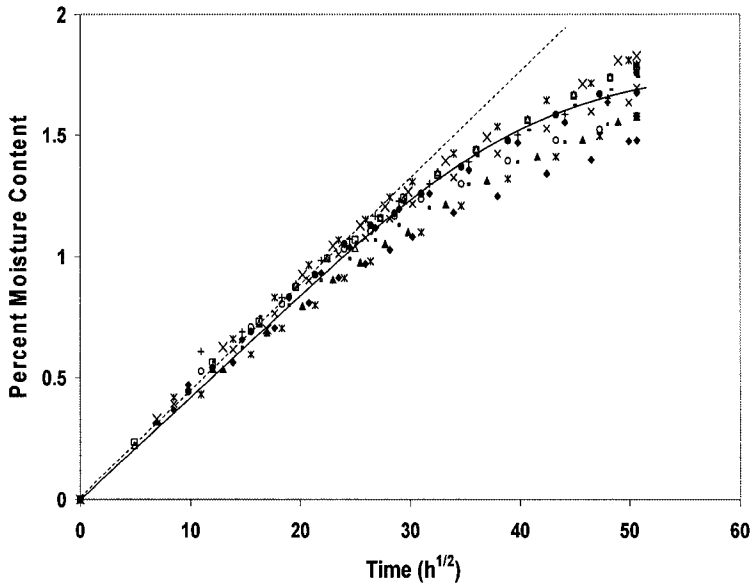

Figure 6.9 Percent moisture gain with time for small samples of poly (styrene-co-isoprene) coated composites (IV). Each marker type in the figure corresponds to a different sample. Solid line: series-solution fit. Dotted line: ASTM-simplified approach.

It can be easily deduced from these data that diffusivity values obtained for each sizing type lie within the same order of magnitude and do not vary much with respect to the calculation method. This, to a certain extent, may be considered as an expected result whenever the single-phase diffusion model holds true. Nevertheless, it should be noted that calculations based on the initial sorption rate (ASTM-method) tend to overpredict the average diffusivities in percentages that range between 10 and 30%. The reason for these disparities seem to reside in the mathematical simplification ($Dt/h^2<0.05$) over

which the ASTM solution is based; and to a lesser extent, in the width-to-thickness aspect ratio of the samples.

Table 6.2 Effective diffusivity constants for different molded parts evaluated by the ASTM D2344 standard (ASTM) and the Crank's [32] complete series-solution (SERIES).

BIG SAMPLES, D_{eff} (x 10^9 m^2/h)					
	Im	IIm	III	IV	N
ASTM	2.52	3.01	3.12	3.21	2.28
SERIES	2.22	2.70	2.20	2.35	1.63
SMALL SAMPLES, D_{eff} (x 10^9 m^2/h)					
ASTM	2.11	3.35	2.1	2.87	1.97
SERIES	1.82	4.24	1.56	2.31	2.32

(Probe: Water at 45 °C)

From the same data set it is clear that geometry, and more precisely the surface area to edge area ratio, has a greater impact on the diffusion coefficients. With the exception of the desized composites (IIm) and neat resin (N), the diffusivity of water in the big samples was proportionally higher than that in the small samples. Admittedly, diffusivity is a directional property. However, we observe that the diffusion rate behavior of the control samples (desized fibers) was significantly different from the other treatments regardless of the geometry. This reaffirms the preliminary conclusions drawn from the maximum saturation levels in showing the importance of sizings in the reduction of water ingress levels. The influential role of the bare glass

interface in the water diffusion was also manifest in that, although the neat resin reached an expected higher moisture saturation value due to its lower T_g, the rate at which the water penetrated to the desized composite (IIm) was faster than for the neat resin (N) despite its much higher T_g. For composites with sized reinforcements Im, III and IV, the introduction of a coating resulted in a slight reduction in the values of D_{eff}. It appears that higher interfacial interactions constitute further hindrance on both moisture equilibrium and absorption rates. Such behavior has already been described by other authors in the case of injection molded thermoplastic composites containing short glass fibers [36, 37]. Finally, the fact that diffusion coefficients for the admicellar-treated fiber composites were significantly lower than the control samples, as well as statistically identical to the parts with commercial reinforcement, may be interpreted as a positive sign of the resistance of the nanoscale sizing to long-term exposure in humid environments.

6.3.2 Effect of sizing type on wet-adhesion. The degradation of the structural integrity of composites upon moisture sorption is associated, to a great extent, with the mechanical response near the fiber/matrix interface. After penetration through the bulk matrix, water begins to accumulate at the interfacial region creating a

zone of high tensile stress concentration. The intensity of such stress has been shown to be dependent on moisture content, fiber spacing and applied load [39]. Other factors related to the composites wet-adhesion strength are: the hydrolytic stability of the chemical bonds formed between sizing and organic matrix, and the stress transfer effectiveness of the fiber surface treatment. In hydrothermal studies with single-fiber composites Drzal et al. [40] showed that the average interfacial shear strength (IFSS) of untreated fiber composites was reduced by 50 % and 80% after hydrothermal exposure at 20 °C and 125 °C, respectively; whereas, at the highest temperature, IFSS for the coated fiber composite decreased only by 40%. For reinforced composites a similar trend is observed. Generally, matrix-dominated mechanical properties (e.g., interlaminar shear strength and compressive force resistance) decrease with increases in moisture content and temperature. This degradation is a highly nonlinear function of the environmental conditions of the test. For those structural properties dominated by the inorganic reinforcement (e.g., unidirectional tension), the reduction in mechanical properties after hydrothermal treatment may not occur, or be minimal over moderate temperature ranges [41]. Figures 6.10 – 6.12 summarize the mechanical properties measured for RTM-composites with different sizing types (Table 6.1) after more than 2800 h of hydrothermal

treatment. Results for the dry state properties of the same composites were presented and discussed elsewhere [19].

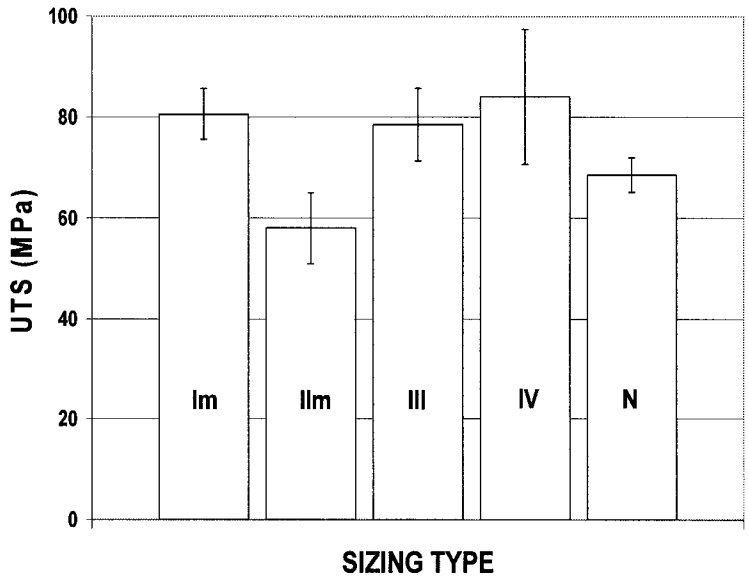

Figure 6.10 Ultimate tensile strength of RTM-parts after moisture saturation.

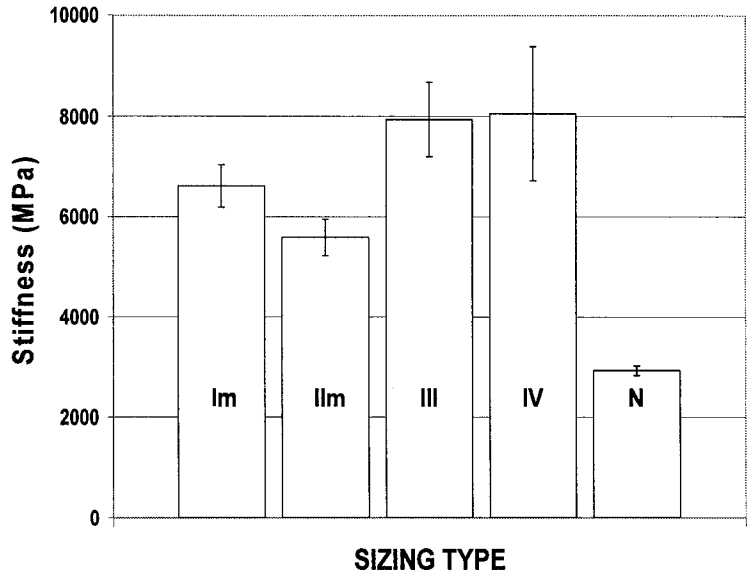

Figure 6.11 Stiffness of RTM-parts after moisture saturation.

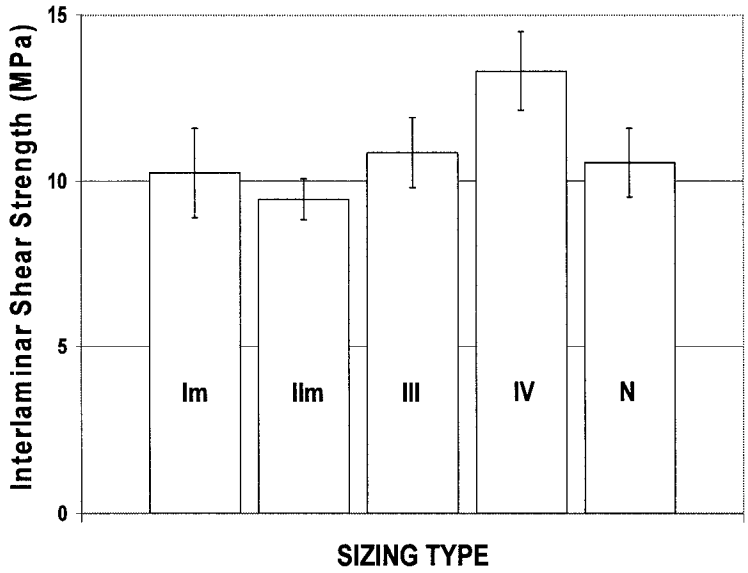

Figure 6.12 Interlaminar shear strength (ILSS) of RTM-parts after moisture saturation.

A first observation that could be drawn from comparing individual data for properties before and after water immersion is that plasticization of the matrix and heat-related perturbations modify the composites mechanical properties in a highly nonlinear fashion. For instance, the ultimate tensile strength, a fiber-dominated property, suffers significant degradation (IIm), no change (Im), or even increases (III and IV) after the water attack. This same sort of inconsistency occurred with the stiffness and interlaminar shear strength (ILSS) data. We suspect post-curing of the epoxy network could have taken place during the preconditioning step (vacuum oven at 65 °C for 7 days) chosen to remove the surface moisture from the samples before submersion in water. It is worth noting that the dry-

state properties were evaluated in samples without heat postcuring [19]. Hence, a comparison of dry- and wet-state property variations due to moisture effects did not yield conclusive results, as the differences in sample preconditioning may have introduced structural changes that could obscure, or even prevent, a direct comparison. Under these particular circumstances, a more suitable approach would be to compare only wet samples among themselves, and specifically the performance of composites with coated reinforcement against the wet-control samples (IIm). In the following paragraph we present this latter analysis together with a property normalization approach that explains property retention as a result of differences in sizing performance, with respect to the unsized reference value, both in the wet and dry states.

Figure 6.10 depicts the ultimate tensile strength for all wet samples tested. Three major conclusions were derived from these tensile data: first, without exception composites with coated fibers (Im, III and IV) resisted water attack more efficiently than those parts with uncoated reinforcement (IIm). This may be interpreted as primarily driven by changes in the surface energy characteristics of the glass surface as well as to propitious sizing/matrix interactions. Second, no single sizing type proved superior over the others under

the same hydrothermal conditions. Therefore, it could be inferred that nanoscale sizings compare favorably to commercial sizings in wet-adhesion levels under tension. And third, equilibrium moisture content does not correlate directly with the ultimate tensile properties. Despite exhibiting almost a 15% higher water uptake level than the admicellar-coated samples, the commercial sizing (Im) had the same tensile strength levels as samples III and IV. Furthermore, although Im and IIm reached equivalent moisture saturation levels, they had completely different tensile properties. Conversely, the diffusion coefficient does seem to correlate with mechanical properties: samples with the highest D_{eff} had the poorest overall performance. With regard to the stiffness results presented in Figure 6.11, the most salient feature is the severe plasticization effect undergone in the neat resin parts. It is clear that regardless of the apparently high UTS (i.e., even higher than that for IIm), water creates residual stresses from swelling that change the fracture characteristics of the material. Lower stiffness, as shown in Figure 6.11, is always indicative of increased propensity to brittle failure. Concerning the stress transfer capabilities (ILSS) of the fiber coatings measured after hydrothermal exposure; there is good resemblance with the results obtained when the same coatings were tested in the dry-state. As depicted in Figure 6.12, composites type IV showed far better resistance to delamination under

shear than those composites with commercial coatings (Im). Furthermore, the poly (styrene-co-isoprene) sizing (IV) effectiveness in the wet state was even higher than that obtained with reinforcements modified with the same admicellar treatment but with different polymer (III). In a previous publication [19], the beneficial effects of the nanometer thick elastomeric interlayer present on the reinforcement (IV) were explained as resulting from both extensive cooperative segmental motions of the copolymer and its lower T_g. It appears that the strong sizing/matrix interactions shown by composites type IV in the dry state are maintained even under hydrolytic attack.

The effectiveness of fiber surface treatments is definitely a function of moisture concentration. Doxsee et al. [42] measured the interlaminar shear strengths of aramid/epoxy composites and demonstrated that the fiber surface treatment was less effective for higher moisture concentrations. They indicated that their treated specimens were approximately 44% stronger than the untreated specimens in the dry state. Then, at 1% moisture concentration, the treated specimens were approximately 40% stronger than the untreated specimens; and finally, at 2% moisture concentration they were only 30% stronger.

With this in mind, we decided to evaluate the sizing effectiveness of our composites by measuring their relative mechanical performance with respect to the uncoated parts in both wet and dry states. Using an analogy with the definition of thermodynamic state properties, the effectiveness in property retention was expressed as the percent difference between the deviation of that particular property from the IIm value in the wet state minus that in the dry state. Percent property values for coated composites (Im, III and IV), in both wet and dry states, were measured as the relative performance increase achieved by introducing the sizing, with respect to the uncoated reference states: uncoated-wet $(IIm)_w$ and uncoated-dry $(IIm)_d$.

Figure 6.13 depicts the effectiveness in property retention for three types of sizings. Clearly, these results suggest that simply coating the reinforcement surface with any type of sizing does not guarantee equal levels of adhesion in completely different environmental conditions. The commercial sizing, for example, performs adequately in composites tested in the dry state with property increases ranging from 13% to 23%. However, when saturated with moisture, the percent difference between commercial-coated and uncoated samples is largely reduced.

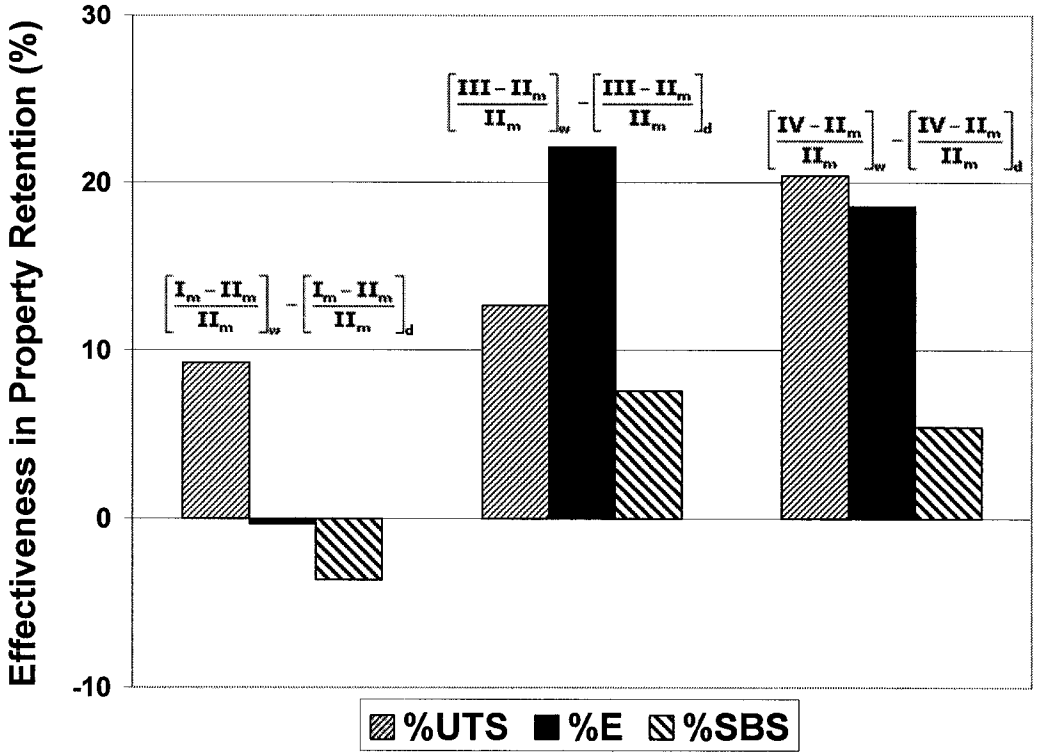

Figure 6.13 Effectiveness in mechanical properties retention (UTS: Ultimate Tensile Strength; E: Stiffness; and SBS: Short Beam Shear Strength) of investigated sizings.

Such reductions in the protection level offered by the coating in the wet-state explain the poor results obtained for mechanical parameters such as stiffness and ILSS in composites type Im. In a sense, this lower effectiveness in property retention observed for the commercial sizing was not completely unexpected. Plenty of evidence presented in the literature indicates that lower mechanical property retention is attained with increasing levels of 'inert' material in these sizings, especially while immersed and equilibrated in water [7]. Nanoscale sizings of very hydrophobic nature (types III and IV),

prepared by admicellar polymerization, do not contain any binder or inactive material. In the dry state, composites modified with elastomeric coatings exhibited comparable adhesion levels to the commercial sizings, and even much greater interlaminar shear strength (ILSS) values were achieved with the poly (styrene-co-isoprene) interlayer [19]. When exposed to water, the admicellar coating/matrix interactions appear to hinder further moisture penetration and matrix swelling, perhaps due to the establishment of a more distinctly hydrophobic interface. Therefore, less bond disruption and less permanent damage at the interface may explain the positive increments in relative protection levels generated by this particular class of sizings when compared to the reference dry state performance. In all, the better effectiveness in property retention observed for type III and IV reinforcements correlate positively with the lower equilibrium moisture contents and diffusion rates found for their molded parts.

6.3.3 Microscopic analysis of failed surfaces. Figures 6.14a to Figure 6.14d are low- and high-magnification SEM micrographs of representative fractured surfaces from different sizing type composites after hydrothermal exposure. For clarity purposes, individual micrographs will be referred in the text by the figure number followed

by the letter L or H which relate to the low and high magnification cases, respectively.

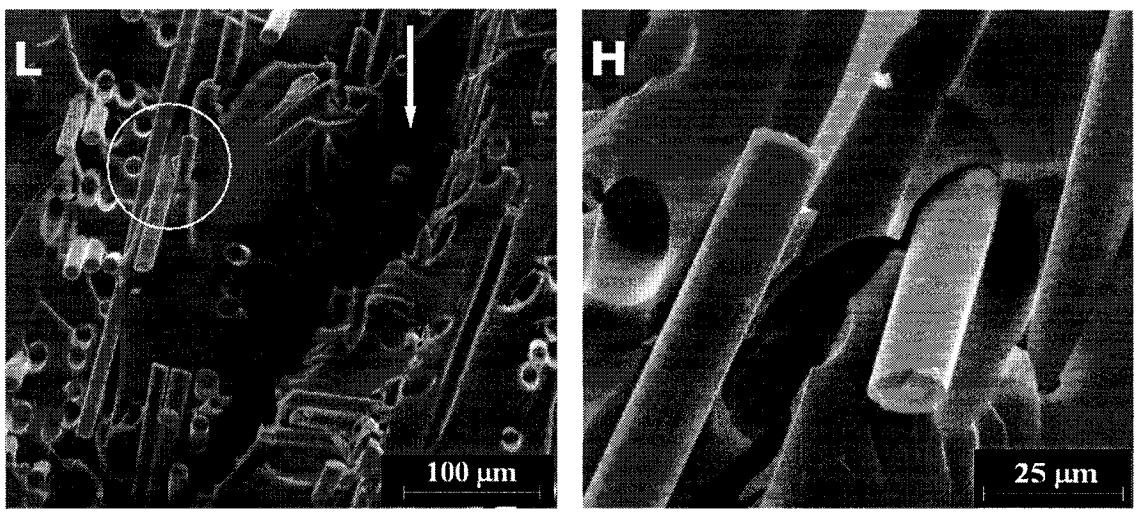

(a)

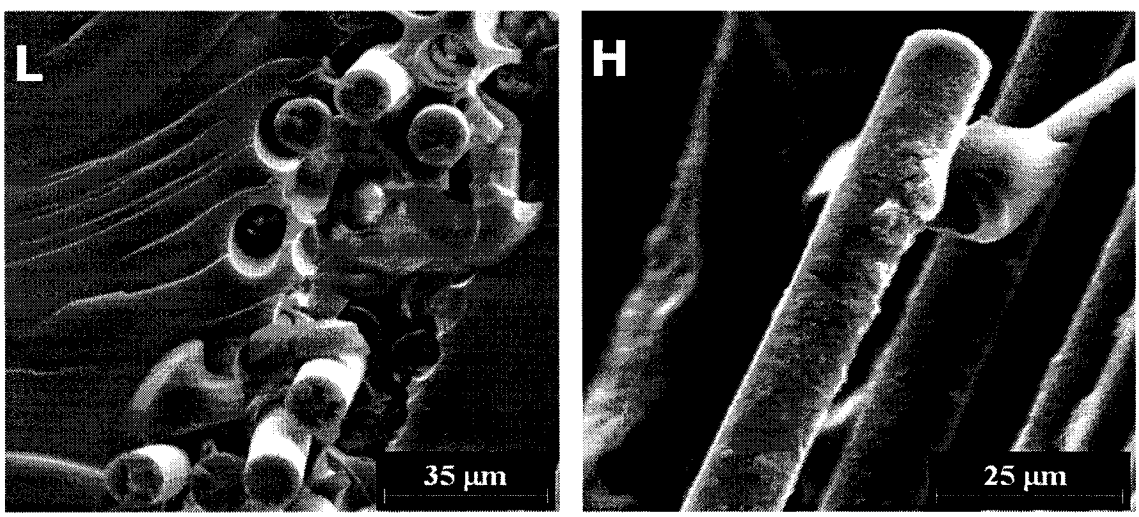

(b)

Figure 6.14 SEM micrographs at low (L) and high (H) magnifications of failed surfaces from: (a) Uncoated fiber composites (IIm); (b) Commercial sizing (Im); (c) Admicellar-coated polystyrene (III); and (d) Admicellar-coated poly (styrene-co-isoprene), (IV).

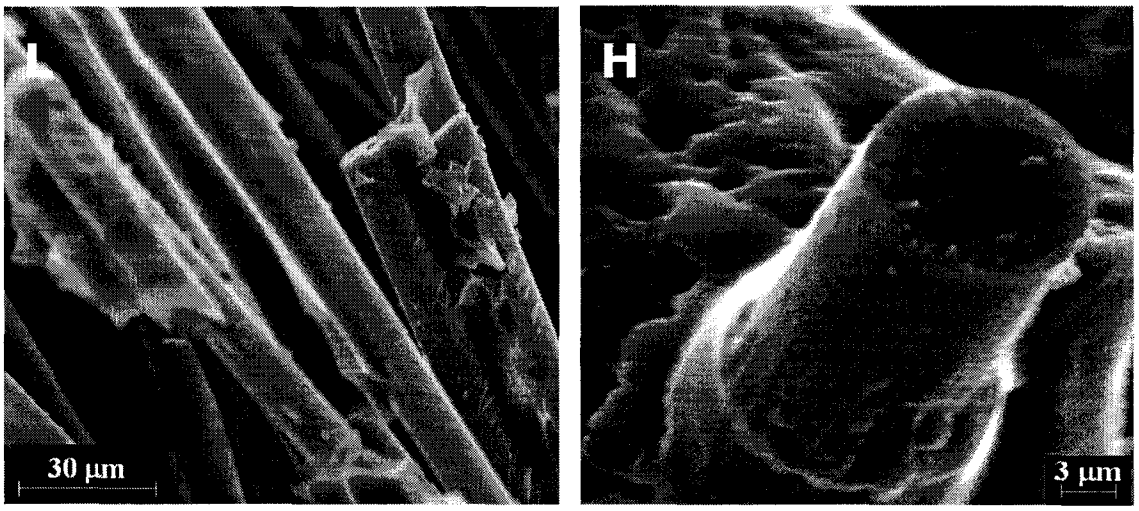

(c)

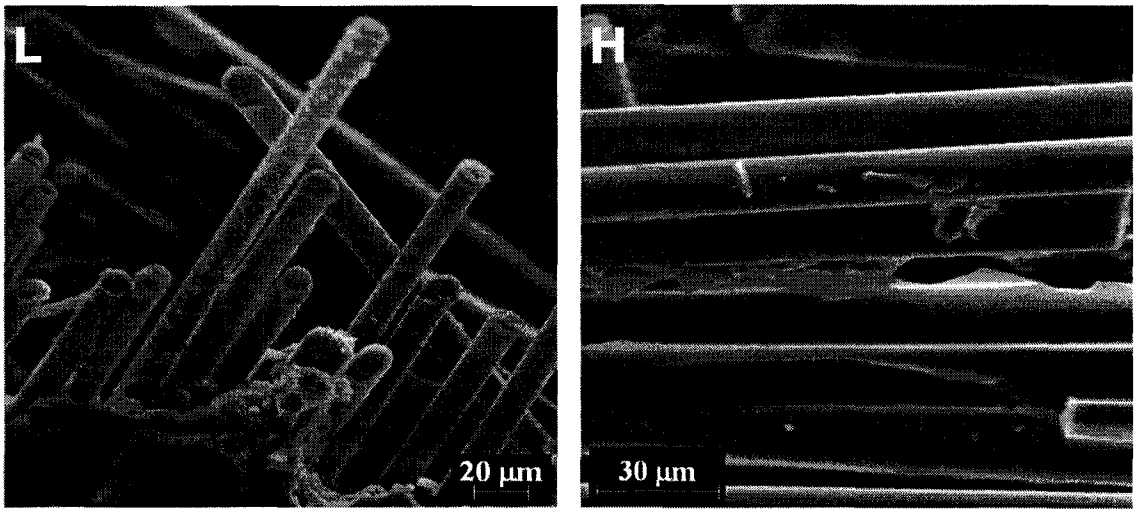

(d)

Figure 6.14 (Continued).

Figure 6.14a corresponds to failed surfaces of uncoated fiber composites (IIm). In Figure 6.14aL there is evidence of craze remnants on the fractured surface, as well as a big crack (marked with an arrow) that runs along the pathway of areas suffering from

extensive fiber pullout. Crazing is an unequivocal sign of matrix embrittlement, whereas the fiber pullout is more associated with a weakened interface prone to chemical/physical debonding. Figure 6.14aH was taken from the circled area shown in Figure 6.14aL. This picture specifically highlights the presence of multiple craze lines occurring in the matrix surrounding the fiber surface, and the way cracks circumvent the fiber surface. Another feature from this micrograph signaling fiber/matrix debonding, as a major component of the overall failure mechanism of IIm composites is the fact that pulled-out fibers look completely smooth and clean.

At various locations, images of the fractured surfaces of composites with fibers coated with commercial sizing (Im) appeared very similar to those in uncoated fiber composites (Figure 6.14bL). Matrix crazing and fiber pullout were also present, but contrary to the uncoated fibers, pulled-out fibers from Im had a rougher surface due to sizing/resin residues adhering to the surface (Figure 6.14bH). Often, a group of fibers remained bound together by residual matrix that may undoubtedly be attributed to a combination of good impregnation and high interfacial strength. Failed surfaces in the admicellar-coated fiber composites are presented in Figures 6.14c and 6.14d. Although there was no significant difference between these samples with respect to

the crazing mechanism acting on the matrix-rich areas observed in the control samples (IIm), failure paths near the fibers looked much more tortuous implying more shear resistance at the interface. Figure 6.14cL shows some hackles (triangular regions of matrix resulting from the shear failure path), as well as matrix residues on a group of fibers from type III composites. The hackles are believed to be the result of the failure path varying from predominantly fiber/matrix interfacial failure to a combination of cohesive matrix failure and fiber/matrix interfacial failure. The larger and more numerous the hackles, the higher the degree of fiber-matrix adhesion [3]. A close-up region (Figure 6.14cH) for a fiber coated with the polystyrene sizing (III) shows tightly bound resin, without any signs of interfacial debonding.

Figure 6.14dL corresponds to a pulled-out area from type IV composites. It is interesting to note that although pullout has occurred, the fibers look rougher and still connected to other fibers by some matrix residue. Finally, in Figure 6.14dH hackles and other polymer remnants are clearly seen, thus confirming the good wet-adhesion and shear transfer capabilities of composites with type IV interfaces.

6.4 Conclusions

The structural integrity or durability of fiber-reinforced composites depends largely on the hydrolytic stability of their interfaces. In this investigation, we have conducted moisture absorption studies and subsequently measured various mechanical properties (UTS, stiffness, ILSS) to assess the wet-adhesion resistance of RTM-composites containing reinforcements with different surface treatments. All molded parts closely followed the predictions of Fick's second law. This fact allowed us to fit a series-solution of the free-phase absorption model to the experimental data and calculate the apparent diffusion coefficient – which was found to inversely correlate with the overall mechanical performance of the composites. The presence of a sizing definitely changes the moisture absorption characteristics, and specially the diffusivity values. For instance, admicellar-coated samples (III and IV) had the lowest moisture equilibrium absorption values as well as significantly lower diffusion constants; whereas, the uncoated composites had much higher water uptakes and diffusivities. The same was true for the commercial samples (Im).

Mechanical properties of uncoated fiber composites suffered from more dramatic failure mechanism, and consequently, showed the most

significant reduction in adhesion levels after the hydrothermal treatment. The sized fiber composites (Im, III and IV) exhibited somewhat lower reductions, especially in properties such as the interlaminar shear strength (a matrix dominated property). Using the effectiveness in property retention parameter, we found that samples with admicellar-treated reinforcements (III and IV) behaved satisfactorily against water attack and their property retention values were always superior compared to commercial sizings. Commercial sizing composites (Im), although showing considerable improvements in all mechanical parameters in the dry state, had poorer effectiveness in stress transfer when saturated with water. All wet-composites, with fibers coated or not, suffered from matrix craze and fiber pullout as evidenced by fractography studies with SEM. However, the introduction of sizing brought about distinctive features related to improved adhesion such as rougher fiber surface, fiber-to-fiber sticking by residual matrix, and more importantly hackles (in composites III and IV) left by a tortuous failure path. These results have implications in the field of composite interfaces and show that nanoscale sizings formed from pure polymers can improve the resistance of fiber-reinforced composites to hydrolytic attack at the same level, or perhaps better, than commercial sizings based on organosilanes.

References

1. J.L. Thomason and L.J. Adzima, *Composites: Part A* **32**, 313 (2001)
2. K. Bezarti, L. Cangemi and F. Dal Maso, *Composites: Part A* **32**, 197 (2001)
3. B.K. Larson and L. Drzal, *Composites* **25**, 711 (1994)
4. M. Tanoglu, PhD Dissertation, University of Delaware, (2000).
5. J.K. Kim, M.L. Sham and J. Wu, *Composites Part A* **32**, 607 (2001)
6. A. Nakai, T. Osada, H. Hamada and N. Takeda, *Composites Part A* **32**, 487 (2001)
7. R.J. Gorowara, W.E. Kosik, S.H. McKnight and R.L. McCullough, *Composites Part A* **32**, 323 (2001)
8. J-P. Pascault, H. Sauterau, J. Verdu and R.J.J. Williams, Thermosetting Polymers. Marcel Dekker, New York (2002)
9. I. Merdas, F. Thominette, A. Tcharkhtchi and J. Verdu, *Composites Sci. Technol.* **62**, 487 (2002)
10. M.R. Piggott, A. Sanadi, P.S. Chua and D. Adison in: Composite Interfaces, H. Ishida and J.L Koenig (Eds.). Elsevier, New York (1986)
11. M.K. Chaudhury, T.M. Gentle and E.P. Plueddemann, *J. Adhesion Sci. Technol.* **1**, 29 (1987)
12. M.E. Schrader and A. Block, *J. Polym. Sci. C* **34**, 281 (1971)

13. R.T. Graf, J.L. Koenig and H. Ishida, *J. Adhesion.* **16**, 97 (1983)
14. H. Ishida and T. Chaisuwan, *Polym. Mater. Sci. Eng.* **85**, 534 (2001)
15. A.T. DiBenedetto, *Mater. Sci. Eng.* **A302**, 74 (2001)
16. A.T. DiBenedetto, S.J. Huang, D. Birch, J. Gomez and W.C. Lee, *Composite Structures* **27**, 73 (1994)
17. R. Lin, R.P. Quirk, J. Kuang and L.S. Penn, *J. Adhesion Sci. Technol.* **10**, 341 (1996)
18. H.J. Barraza, M.J. Hwa, K. Blakely, E.A. O'Rear and B.P. Grady, Langmuir **17**, 5288 (2001)
19. H.J. Barraza, K. Olivero, Y. Hamidi, E.A. O'Rear and M.C. Altan, *Composite Interfaces* **9**, 477 (2002)
20. A.-C. Lassas, L. Fagerholm, B. Stenlund and J. Näsman, *Polym. Composites* **14**, 1 (1993)
21. H. Fagerholm, C. Lindsjö, J. Rosenholm and K. Rökman, *Colloids Surf.* **69**, 79 (1992)
22. S. Shalaby, D. Clupper and T. Taylor, Patent US 5874509, (1999)
23. H. Fagerholm, C. Lindsjö and J. Rosenholm, *J. Mater. Sci.* **30**, 2420 (1995)
24. H. Fagerholm, J. Rosenholm, T. Horr and R. Smart, *Colloids Surf. A* **110**, 11 (1996)

25. G. Funkhouser, M. Arevalo, D. Glatzhofer and E. O'Rear, *Langmuir* **11**, 1443 (1995)
26. D. Glatzhofer, G. Cho, C. Lai, E. O'Rear and B. Fung, *Langmuir* **9**, 2949 (1993)
27. C. Lai, E. O'Rear, J. Harwell and M. Hwa, *Langmuir* **13**, 4267 (1997)
28. B. Kitiyanan, J. O'Haver, J. Harwell and S. Osuwan, *Langmuir* **12**, 2162 (1996)
29. J. O'Haver, J. Reynolds, J. Harwell, B. Grady, L. Evans and W. Waddell, Paper presented at the 219th American Chemical Society Meeting, San Francisco (2000)
30. B. Grady, E. O'Rear, L. Penn and A. Pedicini, *Polym. Composites* **19**, 579 (1998)
31. S. Sakhalkar and D. Hirt, *Langmuir* **11**, 3369-3373 (1995)
32. J. Crank, The Mathematics of Diffusion. Oxford University Press, London (1956)
33. A. Avena and A.R. Bunsell, *Composites* **19**, 355 (1988)
34. J.L. Thomason, *Composites* **26**, 477 (1995)
35. C. Hoppel, T. Bogetti and J.F. Newill in: Proceedings of the American Society for Composites 15th Technical Conference, O. Ochoa, O'Brien, D. Lagoudas and H.J.Sue (Eds.), pp. 1094-1102. Technomics, Lancaster, PA, (2000)

36. T.A. Bullions, J.M. Jungk and A.C. Loos, *J. Thermoplast. Composite Mater.* **13**, 460 (2000)

37. F.U. Buehler and J.C. Seferis, *Composites Part A* **31**, 741 (2000)

38. Z.A. Mohd Ishak, A. Ariffin and R. Senawi, *Eur. Polym. J.* **37**, 1635 (2001)

39. X.S. Bian, L. Ambrosio, J.M. Kenn, L. Nicolais and A.T. DiBenedetto, *Polym. Composites* **12**, 333 (1991)

40. L. Drzal, M.J. Rich and M.F. Koenig, Proc. 38th Annual Conf. Reinf Plast. Composites. Inst., SPI, 4-F (1983)

41. Department of Defense (DOD) Handbook, Polymer Matrix Composites MIL-HDBK-17-3E, vol. 3, p. 2-25 (1997)

42. L.E. Doxsee, W. Janssens, I. Verpoest and P. de Meester, *J. Reinf. Plast. Composites.* **10**, 645 (1991)

7. Performance of Glass Woven Fabric Composites with Admicellar-Coated Thin Elastomeric Interphase[§]

7.1 Introduction

Structural integrity and extended lifetime performance are two of the most important engineering design criteria for fiber-reinforced composites. In practical circumstances, both the structural integrity and reliability of composite parts are dictated not only by the relative strength of their individual components while subjected to tensile loads (i.e., simple rule of mixture of individual properties), but by their capacity to absorb potential energy coming from other mechanical stress conditions, namely, bending, torsion, compression as well as concentrated loads. Thus, a necessary element for the structural

[§] Material in preparation for submission to *Journal of Composite Materials.*

composites design is to obtain the maximum efficiency in stress transfer between the fiber and matrix across the interface.

To control the interface and/or interlaminar properties in composites, a viable alternative is to coat the fibers with appropriate polymers so that a new interphase/interlayer region will be formed. Studies relating fiber coating to composite stiffness and toughness are abundant, and the long-standing consensus is that high strength and high toughness appear to be mutually exclusive in composites involving the combination of brittle fiber/brittle matrix [1]. A strong interfacial bond between fiber and matrix ensures high tensile and interlaminar strength. However, these types of strong interfaces often result in very high crack propagation rates and thus lead to brittle fracture of both matrix and fibers (i.e., fracture toughness of the composite is low).

An alternative to avoid poor impact properties in composites has been, literally, to 'weaken' the interface by applying low-modulus coatings to the reinforcement in order to create a soft interphase. It is generally accepted [2-7] that a soft interphase is advantageous because it changes the stress distribution and decreases stress concentration, consequently increasing toughness properties of the

composite. In a review paper about the use of rubbery interlayers (e.g., silicone rubber, SBS rubber) in composites, Labronici and Ishida [6] indicated that the general trend observed was typical toughness increments of 0 to 100%, together with consistent reductions in strength and modulus values between 0 and 50 %.

Although previous studies have suggested that simultaneous improvement of stiffness and toughness is seldom achieved with composites exhibiting a soft interphase, some theoretical modeling and recent experimental work are increasingly in favor of the potential utilization of a flexible interphase in obtaining good balance between composite modulus and impact strength. For instance, the theoretical work by Matonis and Small [8] is the first one indicating the introduction of a soft interlayer of finite thickness. Their major finding was that in order to obtain adequate stress transfer, only a very thin layer of rubber is admissible: $R_0/R_1 \approx 0.999$; where $R_0/R_1 = 1$ represents the limiting case when the rubber interlayer thickness diminishes to zero. Jao and McGarry [4] later found that local stress concentrations occur in fiber-reinforced polymer composites, and showed that the incorporation of a thin rubber coating, in the order of a 1% of the fiber diameter, significantly mitigates the stress intensity, especially at the fiber-end corner. Other theoretical works have

reached similar conclusions in that the interphase region between fibers and matrix in a composite can significantly affect the load transfer characteristics, even when the interphase is very thin [9].

Experimental evidence of the benefits of soft interlayers began with the pioneering work of Lavengood and Michno [10], followed by the work of Tryson and Kardos [11]. These authors concurred in explaining that solution-cast thick ductile innerlayers are effective in preventing filament abrasion as well as in enhancing crack-arrest mechanisms during composite fracture. Ahlstrom and Gérard [12] and Daoust et al. [13], using the single-filament fragmentation technique, showed that, in both cases, an elastomer coating (e.g., a copolymer of CTBN, carboxyl-terminated acrylonitrile-butadiene; and an epoxy prepolymer, DGEBA) applied over glass fibers led to a superior interfacial strength when embedded in a two-component matrix (e.g., epoxy/cyclic amine system). The enhanced adhesion in this case was interpreted as the soft interphase being able to reduce the shear stress concentrations at the fragment ends. Further evidence is presented by the work of Tillie et al. [14]. They considered a system where hydroxylated polydimethylsiloxane (PDMS) oligomers were deposited on-line over glass fibers as an alternative to create a controlled low-modulus and low-thickness (ca. 130 nm) interphase in unidirectional

filament-winding composites. Off-axis tensile tests and three-point bend results for composites fabricated with the low glass transition temperature interphase did not show significant difference from the mechanical performance of those parts reinforced with commercially sized glass fibers. However, Charpy tests did confirm an increase of the impact toughness as a result of the introduction of the soft interphase.

Most current solvent-based methods used to incorporate commercial and model sizings to glass fibers have inherent limitations on the film thicknesses they can produce. The physisorbed and chemisorbed components of the commercial finishes usually have a combined thickness greater than 100 nm, and the smallest thickness that the authors are aware of for model elastomeric coatings is around 100 nm to 130 nm [14, 15]. All these indicate that the systematic utilization of polymeric coatings with thicknesses well below 100 nm as sizings for glass fibers may still be considered as an alternative worth exploring. Ultrathin hydrophobic coatings for glass fibers obtained by admicellar polymerization [16-20] were shown to provide an adequate level of interaction with a DGEBA (dyglicidyl ether of bisphenol A)-type epoxy resin (e.g., EPON 815C), leading to a wetting behavior comparable to that attained by commercial sizings [18]. Furthermore,

when a very thin elastomeric coating was used as sizing in resin transfer molded (RTM) glass/epoxy composites an increase in the interlaminar shear strength over 30% with respect to those composites containing desized fibers was observed. All mechanical properties measured in dry conditions for composites with admicellar sizings were statistically equivalent to those of commercially sized reinforcements [19]. When equilibrated with water at 45 °C, admicellar-coated composite samples had both significantly low moisture saturation values and diffusion constants. Perhaps due to a higher stability of the interface against hydrolytic attack, composites with admicellar sizings ranked consistently higher, in terms of the effectiveness in property retention, than those composites with either bare fibers or commercial sizings [20].

The surfactant-mediated polymerization used in previous studies (i.e., admicellar polymerization) has a number of process variables that can be tuned to provide optimal interface properties in composites. For instance, by manipulating the type of surfactant (e.g., anionic, cationic, non-ionic) as well as other solution parameters, such as concentration, pH and ionic strength, different levels of surfactant adsorption or surfactant coverage on the solid surface may be obtained [21-23]. Incrementing surfactant coverage over the solid

substrate translates in more available sites for monomer partitioning (i.e., adsolubilization); which in theory, should lead to higher polymerization rates and larger surface areas of the substrate coated with the thin admicellar sizing. Besides surfactant coverage, admicellar polymerization is also amenable to changes in the amount of feed monomer. By setting the surfactant/monomer ratios prior to carrying out the polymerization reaction, a relatively good control in the dimensional properties of the polymer coatings, especially film thickness, has been reported to occur while using various monomers as well as flat, low-surface area substrates such as silica, mica and graphite [24-26].

Herein, cetyltrimethylammonium bromide (CTAB) surfactant aggregates adsorbed over woven glass textiles were used as in situ reactors for forming admicellar poly (styrene-co-isoprene) thin coatings that later served as elastomeric interlayers in RTM glass/epoxy composites. The mechanical performance of these woven composites in the dry state was correlated to the sizing characteristics (e.g., amount of deposited polymer, sizing coverage, film microstructure/heterogeneity and average thickness); which, at the same time, were tailored by specific changes in the feed monomer concentrations before the surface modification reaction. Such

procedure of controlling the initial reactant load during admicellar polymerization to vary the extent of sizing coverage and/or film thickness was not examined in the previously reported experiments [19, 20]. Thus, the conclusions drawn herein complement the ongoing analysis carried out by our research group on the role of thin elastomeric interphases formed by admicellar polymerization in improving the structural integrity of glass/epoxy composites.

7.2 Experimental studies

7.2.1 Preform characteristics and laminae configuration.

Commercial general-purpose E-glass fibers have two variants: one is the generic boron-containing glass fiber, and the other is a boron-free or calcium-magnesium-aluminum silicate glass fiber. Both types of fibers are used in the composites industry as reinforcements for polymer matrixes. Fibers in textile forms are known to produce composites with high intra- and interlaminar strength and damage resistance. In addition, textile structures have better dimensional stability, subtle conformability, and deep draw moldability/shapeability [27]. Herein, boron-free E-glass fibers produced by FibreGlast (Plast # 245 Fiberglass Fabric, style 7500) were the starting material for the inorganic reinforcement phase. Composites made with this commercially sized fibers are designated as type C. Fibers used as

control samples (i.e., type B) were prepared by burning off the sizing from the woven fabric in a furnace at 500 °C during 15 min. Similar heat cleaning procedures for E-glass fibers have been described previously [28-31], and it is expected that no significant crystallization of the amorphous phase governing the fibers tensile strength properties would take place at the furnace temperatures used herein [30]. Finally, the same heat treatment applied to the control samples was also used as a pretreatment for those fibers modified with the ultrathin coating by the admicellar polymerization method (i.e., SI1, SI5 and SI10).

As seen in the picture (Figure 7.1a), the fiber yarns are woven in a plain weave structure (WF) with interlacing warp (0°) and fill (90°) yarns in a regular pattern (i.e., each warp yarn passes alternately under and over each fill yarn). Note that for this particular fabric the number of fibers in the warp and fill directions is not the same, as deduced from the difference in yarn thickness. For fabric #245 the manufacturer reports a count of 16 x 14. Also disclosed in the product data sheet are the presence of an epoxy and vinyl ester compatible finish, as well as other fabric specifications such as an areal density of 0.034 g/cm2 (OSY, 9.64) and a fabric layer thickness of 0.356 mm (0.0154").

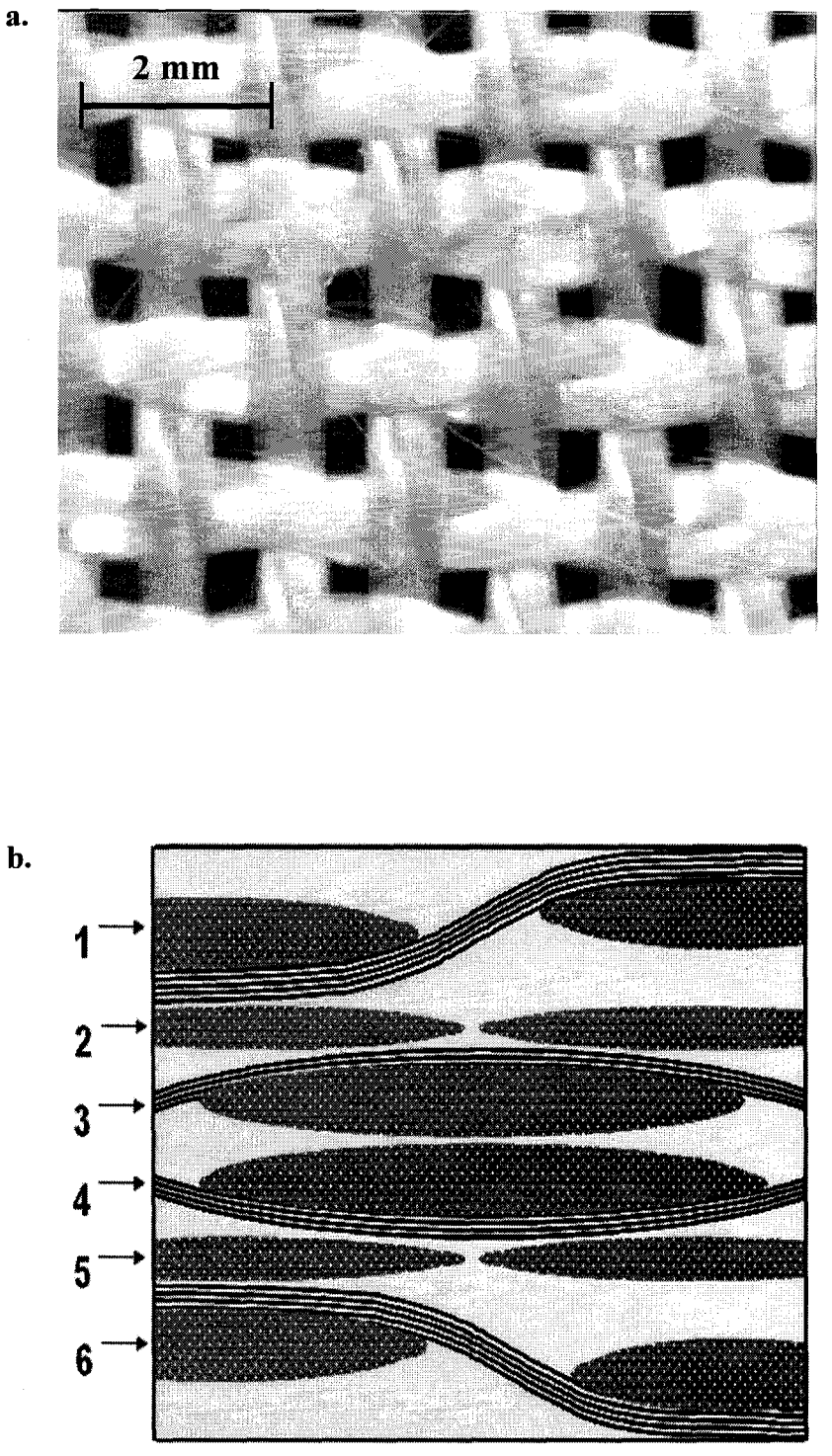

Figure 7.1 (a) Micrograph of FibreGlast Plast # 245 plain weave fabric; and (b) Laminae configuration in RTM composites.

Each RTM part was built with a total of 6 layers of fabric cut from the roll and set tightly into a 15.24 cm (6")-diameter sewing loop. To obtain a symmetric and balanced configuration, the laminae stacking followed a sequence that began with a first layer at 0° orientation, that is, taking the warp yarns as the reference axis. A second layer was laid on top, but this time, with the warps oriented orthogonally with respect to the warps of the previous layer. Subsequently, the interior 3rd and 4th laminae were both again oriented at 0°. Finally, the 5th and 6th layers were a mirror image of the 1st and 2nd layers. The resulting symmetric balanced configuration (Figure 1b) resembled one of the theoretical plain-weave fabric laminates configuration studied by Naik [27]. After all layers were carefully stacked, sewing of the edges with a common thread helped prevent any lamina displacement or change in the orientation configuration. The 6-layer stack was then taken out of the sewing loop and shaped into a 15.24 cm-diameter circle to fit the internal cavity of the aluminum RTM molds.

7.2.2 Modification of glass fibers by admicellar polymerization. Many of the deleterious phenomena compromising the structural integrity of fiber-reinforced composites takes place at, or is intensified by, the interfacial region between glass fibers and polymeric matrix. By way of example, it has been reported [32] that

the diffusion rate of water along the interphase in glass-reinforced polymers is about 450 times greater than that through the resin layers. Wicking at the interphase appears to be the dominant mechanism for such preferential diffusion path as evidenced with autoradiographic tests using tritiated water [33]. For this reason, as well as for the many other advantages derived from having a strong adhesive bond, alternative treatments to modify the interfacial properties of glass fibers are still a subject of current research efforts [34-39].

The admicellar polymerization method was originally conceived and tested for highly porous materials (e.g., alumina and silica) [40-44], although it has been also proven successful in forming thin films from different monomers (e.g., styrene and styrene/isoprene) over inorganic oxides of low surface area, including glass fibers [16-20]. A sketch and detailed explanations on the major steps of the admicellar polymerization technique were presented earlier in Chapter 2. Herein, 150 g of heat cleaned (500 °C, 15 min) boron-free E-glass fibers (Plast # 245 from FibreGlast, Brookville, OH) were equilibrated in a sealed 6-liter glass reactor with a 750-μM solution of cetyltrimethylammonium bromide surfactant (CTAB). After contact with the glass fibers, the almost neutral (pH = 6.5 – 7.0) surfactant solution turned into a

moderately basic pH range of 8.5 – 8.8 without further addition of electrolytes. Glass fibers typically bear negative surface charges in aqueous solutions at pH values over 3.6 – 4.0. Thus, we expect that at the equilibration pH numerous sites for adsorption of the cationic part of the surfactant (CTA^+) will be available on the fibers surface. In all polymerizations carried out herein, the surfactant solution was maintained at the same initial concentration (750 μM) regardless of the amount of monomer fed into the reactor.

An equimolar mixture of pure styrene/isoprene was used as the 'monomer' in every reaction, and only the surfactant/monomer (S/M) weight ratios were varied from experiment to experiment in order to form sizings with distinctive properties. Three different (S/M) ratios were studied, namely, 1:1, 1:5 and 1:10. Once the monomers are injected into the reactor, they readily partition inside the hydrophobic core of the surface aggregates created by the surfactant aggregates. As soon as free radicals produced by the thermal decomposition (80 to 90 °C) of oil-soluble azo-initiator (AIBN) combine with monomers in the admicelle, polymerization begins, forming an admicellar-coated poly (styrene-co-isoprene) glass surface. The polymerization reaction was assumed to be complete after 14 hours. To expose the polymeric thin film, excess surfactant was removed by rinsing the fibers

thoroughly two or three times with distilled water. Finally, the fibers were vacuum dried overnight at 60 °C to drive-off any unreacted monomer and moisture from the fibers surface.

7.2.3 Molding setup and fabrication procedure for composites. The high-speed molding setup used to fabricate woven fabric glass/epoxy RTM composites was similar to the one described previously in Chapter 5, and in a recent publication [45], and includes a hydraulic press and a rectangular aluminum mold containing the textile preform. A thorough description of the molding press and typical procedures followed for RTM composites fabrication were provided in Chapter 3 (section 3.2).

The six circular layers (152.4 mm diameter) of the preform – described in section 7.2.1 – were stacked into the mold cavity, which represented an average fiber volume fraction of 37% in all composite parts fabricated. To impregnate the preform, the resin and curing agent mixture was injected into the mold cavity by a constant displacement of the plungers as described above. On average, filling the mold cavity took less than 10 s, after which the exit gates were securely clamped and no resin bleeding was allowed to occur. Thereafter, the hydraulic press was run for a few additional seconds to

apply a post-fill pressure level approximately higher than 300 kPa. This packing pressure was found to be beneficial in reducing the overall void content in RTM composites [45, 46]. Molded disks cured inside the molds at room temperature for 48 hours until they reached their "green state", and then were taken out of the molds. Finally, to ensure complete cross-linking of the resin, the disks were post-cured at 50 °C in an oven for 24 h. Mechanical testing was preceded by cutting and polishing procedures that were performed at least one week after the disks were post-cured.

7.2.4 Specimen preparation and mechanical testing. Each molded disk was sectioned using a vertical milling machine into five rectangular specimens with dimensions: 11.43 cm x 1.27 cm x 0.2 cm; and thereafter polished on the sides with a 320 grit sand paper to even out the asperities left by the cutting bit. The relative spatial positions of the five specimens within each molded disk coincided with those depicted in Chapter 5 (Figure 5.2).

Composite parts for each sizing type were tested under tension, according to ASTM D3039/D3039M-00, using 8 specimens selected from positions 1, 2, 4 and 5. Tensile forces applied were ramped linearly from 0 to 8.90 kN over 120 seconds. Strain measurements

were obtained simultaneously with the tensile strength tests by placing a calibrated extensometer over a 2.54 cm span at the center of the specimen. Specimens from position 3, located at the center of the disk, did not comply with the requirements for mechanical testing because of the presence of surface defects at the inlet gate caused during the demolding process.

For the three-point bending experiments a total of six specimens per sizing type were tested. These specimens were also taken from positions 1, 2, 4 and 5; but this time, further sectioning was required to fit them into the special three-point bend fixture (MTS 642.001) spanning of 25.4 mm that was used to measure the interlaminar shear strength (ILSS). With the aid of a band saw three identical coupons 3.8 cm-long were cut out, making sure they remained symmetrical with respect to the radial axis. The MTS 810 machine moving at a crosshead speed of 1.0 mm/min provided the force applied to the specimens during the three-point bend test, and the experimental parameters like the maximum force and maximum displacement were read and recorded automatically by the system. Interlaminar strength and other relevant calculations were performed in accordance with the ASTM D2344/D2344M-00 standard.

7.2.5 Chemical and surface analysis of coated fibers. The relative amount of elastomeric polymer formed on the glass fibers through the admicellar polymerization reaction was estimated by two different analytical techniques: Ultraviolet-visible absorption spectroscopy (UV/Vis) and X-ray photoelectron spectroscopy (XPS). UV/Vis is a powerful technique for polymers characterization, especially for those macromolecules containing pendant aromatic ring groups. In general, both polymers and copolymers derived from styrene monomer have been well characterized by UV/Vis and their absorption bands are readily available in the literature [47, 48]. Herein, UV/Vis spectra were recorded with a Shimadzu double-beam spectrometer (UV-2101) that allowed scanning in the wavelength range of 200 to 800 nm. The analysis consisted in extracting the poly (styrene-co-isoprene) coating formed on the glass fibers with tetrahydrofuran (THF, Fisher Class 1B); and subsequently comparing the UV/Vis absorption peaks intensities for the three different admicellar sizing types (i.e., SI1, SI5 and SI10). To carry out the polymer extraction, 1 gram of modified fiber was soaked in 25 ml of TFH solvent; from which, samples of the supernatant were taken out and analyzed – at the third and fifth day – in order to ensure the extraction was complete. This protocol was adapted from the work of Sakhalkar and Hirt [16], although recent experiments have proven

these solvent-extractions to be inefficient as only small percentages, ca. 15 – 30 %, of the admicellar polymer initially bound to the inorganic surfaces (e.g., alumina and titania) is removed [49].

Although UV/Vis is able to provide a qualitative picture of the amount of polymer bound to the glass surface after polymerization at various monomer/surfactant ratios, it cannot be used to determine how the polymeric coating is distributed over the solid substrate. One alternative to obtain such an estimate is by taking advantage of the XPS ability to quantify the atomic concentrations present on a given sample surface. In this way, some authors have been able to perform a complete analysis of coverage and composition of commercial coatings on glass fibers [50, 51] as well as to propose models for the sizing and interphase characteristics in glass fiber reinforcements [52]. XPS data presented in the current study were collected with a Physical Electronics PHI 5800 ESCA system equipped with a concentric hemispherical analyzer and a monochromatic Al-Kα X-ray source operated at 400 W. A spot of approximately 800 μm in diameter, 187.85 eV of pass energy, and an electron takeoff angle of 45° with respect to the sample surface were used in all measurements. For every specimen, a survey spectrum was recorded over the available energy range in order to determine which elements were present.

Peak areas were determined using a multiplex routine with a nonlinear Shirley-type background subtraction, and subsequently converted to surface atomic concentrations using the sensitivity factors provided in the PHI Multipack 6.1A software.

7.2.6 Atomic Force Microscopy (AFM) analysis. A commercial AFM scanning probe: Nanoscope IIIa microscope (Digital Instruments Inc., Santa Barbara, CA) was used to scan the top of the fibers, which were previously secured to the sample pucks by a thermoplastic adhesive (TEMPFIX). All images were acquired in the TappingMode™ or intermittent contact imaging capability of the AFM because it considerably reduces the interaction between the tip and the substrate (i.e., no deformations induced on the polymer thin film). Typically, areas of 5 μm x 5 μm were scanned in arbitrarily chosen positions along the length of different fibers (usually two or three points per fiber). These images were adjusted by using a planefit function that influences the tilt in the captured images. Finally, to investigate the topology of the admicellar coatings on fibers we recurred to performing individual line profile analysis from cross-sections, as well as referring to the complete distribution of surface elevations recorded by the AFM. The latter parameter is automatically generated by the Nanoscope v5.12B control/analysis software, and is

displayed as a cumulative distribution that reveals what percentage of a surface lies above and below any arbitrarily chosen height. The latter measurement is commonly known as the 'bearing ratio'. Rough surfaces will show comparatively wider heights distribution in the bearing analysis than a smooth surface [53].

7.3 Results and discussion

7.3.1 Performance of WF composites with elastomeric coatings. The introduction of woven fabric E-glass reinforcements in engineering composite structures has been driven by various attractive aspects such as ease of handling, high adaptability, damage tolerance, and, if compared to unidirectional laminates, for their better out-of-plane stiffness properties [27]. Although some of these advantages reside on the particular geometry and configuration of textile reinforcements, there is still the necessity of maintaining good interfacial properties. Similar to UD composites, fibers in commercial woven fabrics are also coated with organosilane coupling agents that are designed to create primary chemical bonds that maximize their adhesive bonding to the polymeric matrix. Abundant evidence on the reactivity of organosilane coupling agents with both inorganic solids and polymeric matrices has been established and documented [54]. Figure 7.2 depicts typical stress-strain curves of composites with

various fiber surface treatments: B (desized fibers), C (commercially sized) and SI10 (admicellar coated, 1:10 monomer/surfactant ratio). As observed, for all specimens stress levels increased linearly in the early stages of testing, and then nonlinearly until the ultimate stress in reached at the fracture point.

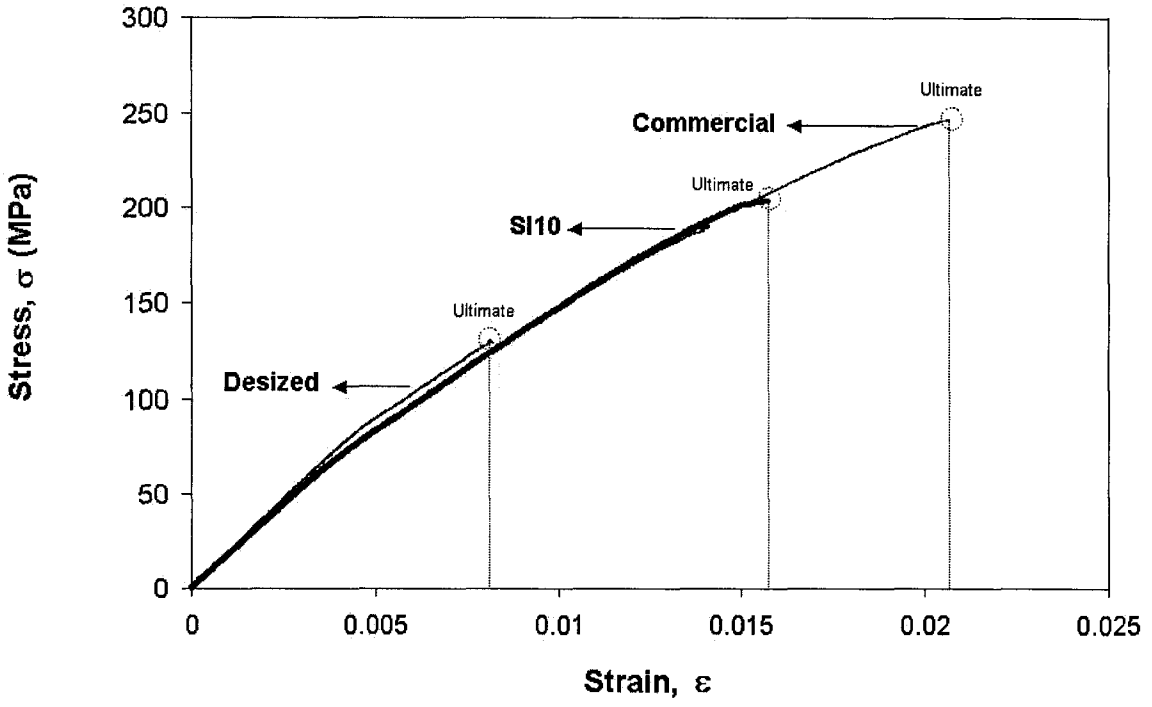

Figure 7.2 Stress-strain behaviors of composites with different surface treatments.

Rather than focusing on the elasto-plastic behavior described by the curves per se, it is much more instructive at this point to note how the presence of an interphase appreciably changes the ultimate mechanical resistance of fiber-reinforced parts. Specimens with desized fibers are the weakest, failing at ultimate tensile stresses in

the range of 125 – 130 MPa. Such behavior is not uncommon for composites with bare glass fibers. Heat cleaned fibers are extremely hydrophilic and usually exhibit a molecularly adsorbed layer of water, even if they are sufficiently dry. This water monolayer is known to interfere with the formation of chemical bonds needed for an adequate adhesion between fiber surface and polymeric matrix [55]. As a consequence, desized fibers would not show comparable levels of strength, stiffness or interlaminar adhesion as those normally attained by surface-coated fibers. Another factor contributing to the poor tensile strength properties of desized composites (B) is perhaps related to the fact that bare glass fibers suffer from extensive abrasion while put in contact with other fibers. This mechanical friction originates surface flaws that induce different crack initiation mechanisms and propagation rates when the material is loaded or strained [56].

As the fibers are covered with a sizing, noticeably different behaviors in the stress-strain relationship take place. For instance, those composites containing an elastomeric thin sizing (e.g., SI10) fail at ultimate stresses between 195 – 205 MPa, which represents a performance improvement of 50 – 55 % over the control samples. Comparable improvements in tensile properties were attained using

the other two types of elastomeric sizings, SI1 and SI5, as appears listed in Table 7.1. Overall, tensile properties of composites with admicellar coatings were appreciably higher than desized composites irrespective of the sizing characteristics attained during the three different admicellar polymerization reactions.

Table 7.1 Sizing types and tensile properties of RTM-parts.

	COMPOSITE TYPE	UTS (MPa)	E (GPa)
B	Desized (500 °C, 15 min)	129.67 ± 5.84	17.85 ± 0.67
SI1	*Desized *Admicellar polymerization (1:1 surfactant /monomer)	195.98 ± 12.47	17.73 ± 0.48
SI5	*Desized *Admicellar polymerization (1:5 surfactant /monomer)	203.32 ± 3.78	17.90 ± 0.76
SI10	*Desized *Admicellar polymerization (1:10 surfactant /monomer)	201.64 ± 5.93	17.78 ± 0.61
C	*Epoxy and vinyl resin compatible coating	247.05 ± 9.59	17.12 ± 0.82

*Note: confidence interval of 95% shown for all measurements.

From the tabulated results it is clearly inferred that a thin elastomeric interphase is beneficial in terms of enhancing the interfacial properties of the fibers. A combined effect of reduced sizing thickness and glass transition temperatures well below room temperature may be regarded as plausible reasons for this enhancement, as was suggested elsewhere [19]. Notwithstanding, such mechanisms alone would not be sufficient to explain why there seemed to be no statistical difference among admicellar treatments with respect to their composites tensile properties. At this point we do not have a complete interpretation for these results. However, one thing to consider is that beneficial effects coming from the use of admicellar coatings may be less dependent on the type and strength of the adhesive bonds formed at the interface. And therefore, the improvement could be more closely linked to increased acid/base pair and other physical interactions (e.g., dispersion forces) with the epoxy prepolymeric mixture. Moreover, concurrent filament abrasion reduction and enhanced crack-arrest mechanisms, absent in composites with desized fibers, could also be active.

Commercial coatings, besides providing coverage to prevent mechanical friction among fibers, impart higher tensile strength to the composites possibly due to a stronger adhesive bond at the interface

(i.e., sizing with more chemically reactive moieties). The average ultimate tensile strength for these parts was approximately 247 MPa, which represents a major mechanical improvement with respect to the control samples (e.g., total increase of 89 %). This, of course, is in line with previous findings, and shows a marked influence of organosilane coupling sizings on the final mechanical properties of the composite parts. When compared to commercial sizings, admicellar treatments exhibited ultimate tensile strength values about 17 to 20 % lower. This again is consistent with similar comparisons performed in the past between admicellar and commercial coatings [19], and most likely implies a greater affinity of organosilanes for the epoxy matrix.

The modulus of elasticity in tension calculated for composites with different fiber surface treatments appear in Table 1. Statistical t-test analysis of these data populations indicates, with great certainty ($p < 0.05$), that they all have identical means. Although minimal changes in stiffness were observed in a previous study for random-mat glass/epoxy composites containing admicellar coatings [19], much lower coefficients of variation, CV, for the data obtained here (e.g., CV = 3 – 7%), as well as the fact of working with higher fiber volume fractions, gives us confidence in validating the current observation of stiffness properties being insensitive to the composites interfacial

characteristics. Additionally, there is plenty of evidence suggesting that elasticity modulus in fiber-reinforced composites is basically a matrix-dominated property [57].

In contrast to the previous two mechanical parameters evaluated in tension, the interlaminar shear strength (ILSS) properties measured through the three-point bending test proved more sensitive to both the presence of an interiayer and the type of interphase formed by the admicellar and commercial sizings. Referring to the data depicted in Figure 7.3, the weakest interphase, once again, corresponds to those composites fabricated with desized fibers. ILSS values for type B composites were in the 8.5 – 9.5 MPa range. Such low dry-adhesion strength level between desized fibers and epoxy was well anticipated, as the ubiquitous water monolayer present in the hydrophilic fibers of the control composites would disrupt the establishment of either chemical or physical interactions between reinforcement and organic matrix [55]. For the sake of comparison, three-point bending results for neat resin parts (e.g., type N), which are in the order of 3.01 – 3.5 MPa, are also presented in this figure. It is worth noting that the ILSS of composites has a definite lower bound limit represented by the shear strength of the matrix [58].

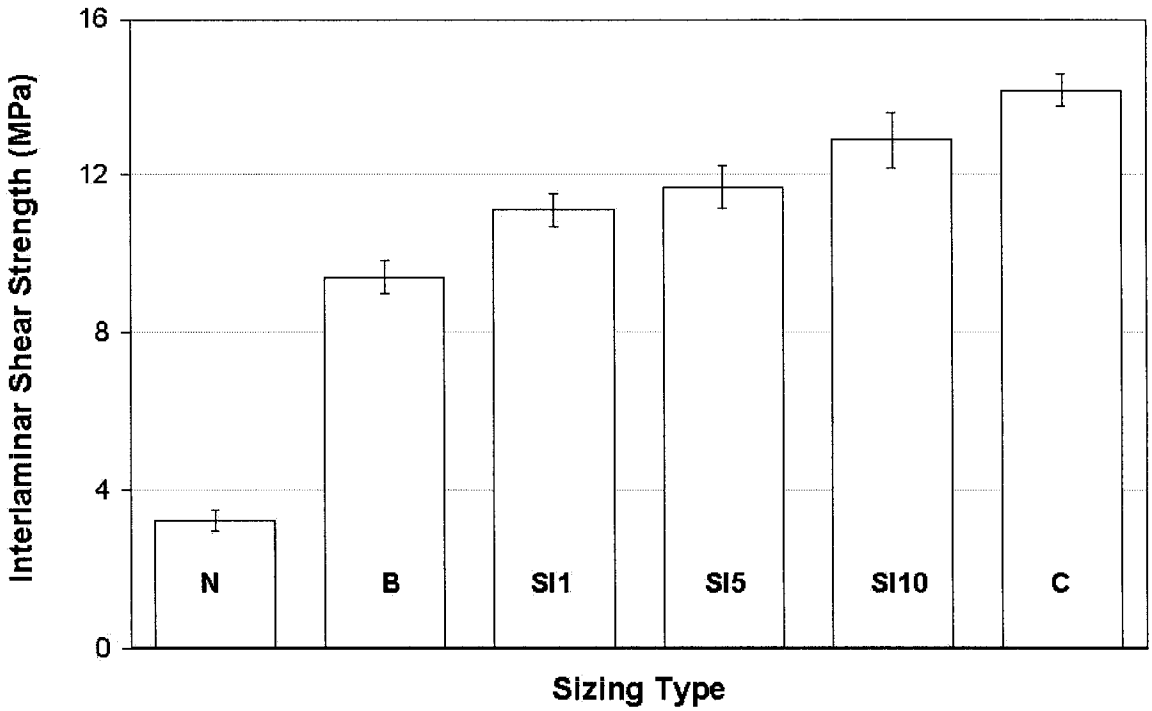

Figure 7.3 Interlaminar Shear Strength (ILSS) properties of RTM-parts.

Surface treatment of fibers with admicellar coatings had an overall positive influence on the composites interlaminar properties as inferred from the average ILSS values shown in Figure 7.3. Interestingly, the level of improvement was not the same for each admicellar treatment. SI1 type composites, which were treated in a reaction with 1:1 surfactant/monomer ratio, recorded interlaminar shear strengths in the range of 10.40 MPa up to 11.90 MPa. This represents an average ILSS improvement of 18.2% with respect to the control specimens. Moderately higher improvements were recorded for admicellar-coated parts type SI5 (i.e., 1:5 surfactant/monomer ratio). Interlaminar shear stress values for these composites fell within the

interval 10.6 – 12.45 MPa, which totals an average property increment of ca. 25% over the controls. Augmenting the amount of monomer employed within the admicellar reaction up to a 1:10 surfactant/monomer ratio (e.g., composites SI10) causes the flexural properties to go up dramatically. Shear strength data for these particular composites ranged between 12.03 MPa and 14.13 MPa, which in average constitute about 38% increase over the ILSS for type B composites and twice the improvement attained with SI1 composites. Undoubtedly, such strong correlation between admicellar polymerization conditions and composites interfacial strength must come from the particular characteristics of each sizing. Further explanation to this behavior will be presented in the coming sections, which will be dealing with admicellar sizings coverage and morphological structure.

Finally, commercial coatings also provided a much stronger interphase than the control samples with interlaminar shear strength values between 14.0 and 15.4 MPa. This 51.3 % average ILSS improvement over the desized composites interlaminar strength may be also traced back to both a facile interpenetration capacity and good bond strength between organosilanes and the epoxy matrix (e.g., especially with the amine pendant groups in the curing agent). In

comparison to admicellar coatings, commercial sizings had performances in the three-point bending test ranking from moderately higher to negligibly different. For instance, admicellar-treated composites with highest average ILSS (i.e., SI10) had flexural properties only 9% lower than type C composites.

In the past, flexural properties of composites with admicellar coatings have been often contrasted to those of composites containing commercially sized reinforcements. This practice has, until now, produced mixed results. For example, three-point bending experiments performed by Grady et al. [17] showed average flexural strengths for admicellar-treated glass/epoxy laminates to be 14.3% lower than laminates with Clark-Schwebel commercial glass cloths (e.g., Series 181, silane-coated). In a more recent study [19], a similar admicellar treatment gave average interlaminar strengths 13.7% higher than another commercial sizing (FibreGlast, Plast # 248 chopped strand mat). Usually, sizings for commercial applications vary in the number and type of chemical components of their formulations as they are intentionally designed to interact, and be effective, with a multitude of organic matrices bearing dissimilar properties. The great difficulty in assessing such a variety of existing commercial sizings available in the market has already been addressed by J.L Thomason and others [50-

52]. Consequently, we resorted to using comparable microstructural features and/or compositional parameters as a basis for contrasting both admicellar and commercial sizings performances. As will be presented later in the chemical characterization section, a good parameter for establishing such comparison is the C/Si ratio of the coating obtained by XPS. A C/Si ratio below 10 is indicative of XPS data dominated by both the glass fiber surface and its silane coating (i.e., chemically bound), whereas ratios above this value represent data dominated by a physisorbed organic sizing containing organosilanes mixed within [51].

7.3.2 Chemical characterization and surface distribution of admicellar coatings on woven fabrics. Admicellar polymerization is a highly versatile technique as it is amenable to introducing monomers of different hydrophobicity, using a wide range of surfactants or even setting optimum surfactant/monomer ratios. This latter parameter is perhaps the easiest to control during admicellar polymerization to obtain various levels of thin film coverage. It is well known that film coverage over a glass fiber surface is of primary importance to fiber strength (e.g., to avoid abrasion and environmental attack). Figure 7.4 depicts UV/Vis spectra of poly (styrene-co-isoprene) THF-extracts from admicellar coated woven

fabrics; namely, reinforcements from composites SI1, SI5 and SI10. Spectra from desized composites, type B, were not included in the plot, as they remained completely flat over the scanned wavelengths (i.e., no chromophore present).

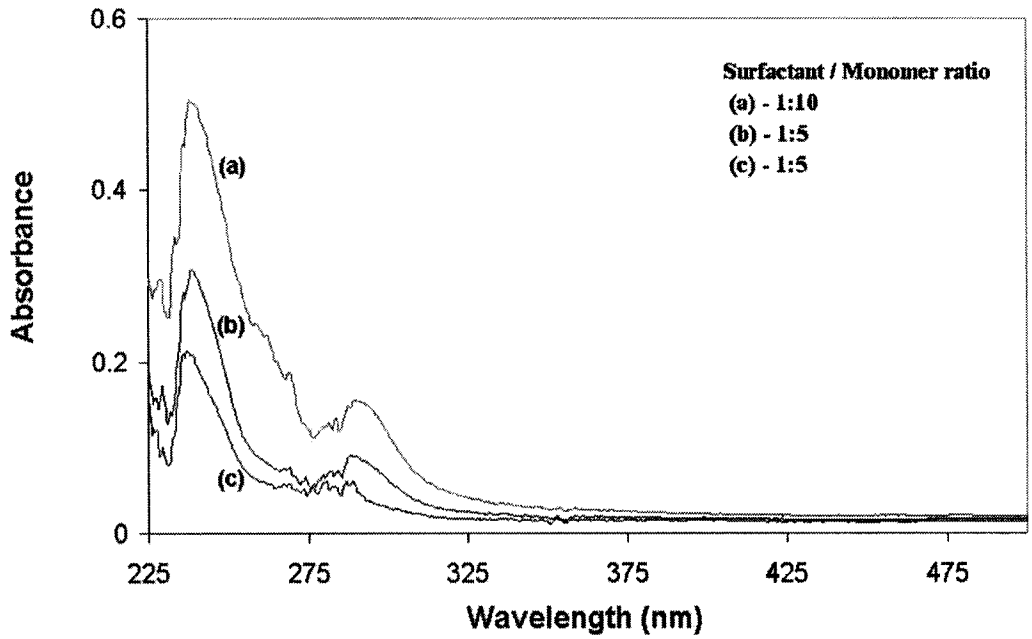

Figure 7.4 UV/Vis analysis of THF-extracts from admicellar-coated fibers at three different surfactant/monomer ratios.

Evidently, phenyl groups coming from the styrene monomer are responsible for much of the response of this macromolecule to the UV/Vis excitation. The absorbance peak at approximately 290 nm is attributable to interactions between adjacent phenyl groups. Such interactions reportedly occur when polystyrene chains are dissolved in a good solvent [47]. Another absorbance band typical of polystyrene is

centered at 260 nm and corresponds to the $\pi \rightarrow \pi^*$ electronic transition of isolated phenyl groups. This strong band in poly (styrene-co-isoprene) seems to suffer from a bathochromic shift and it now appears at 240 nm. In principle, the shift of an absorption band is believed to occur when there is an increase of the interactions of atomic groups and/or solvents with the chromophore units [48]. Therefore, it is reasonable to believe that the random introduction of phenyl groups from the styrene among isoprene segments, containing double bonds, lowers the excited electron level of the polymer (i.e., $\pi \rightarrow \pi^*$ transition) in relation to the ground state, with the attendant bathochromic effect. It is worth noting that blank samples prepared by dissolving equimolar amounts of commercial (Polysciences Inc., Warrington, PA) low-molecular-weight polystyrene (Mw 3550) and polyisoprene (Mw 3000) in THF did not exhibit the same bathochromic effect. No further efforts were dedicated to investigate this phenomenon.

The absorbance intensity of the 240 nm peak served as a reference to compare the amount of polymer formed over the fibers by changing the admicellar polymerization conditions. Spectrum (a) has the highest intensity, and as such indicates that this extract contains the maximum amount of chromophore (i.e., polymer containing phenyl

group). The analogy also works for spectrum (b), as well as for spectrum (c), suggesting that the amount of polymer present in the extract is directly proportional to the mass of admicellar coating formed on the fiber surface. Hence, it may be stated that composites type SI1, SI5 and SI10 had, indeed, elastomeric interphases varying in their polymer contents. Although these results are particularly important for interpreting the mechanical behaviors described in section 7.3.1 for composites with admicellar-polymerized coatings, a more thorough description on surface coverage will be presented below.

Figures 7.5a to 7.5c show typical XPS survey spectra recorded over the binding energy range 100 – 1200 eV for reinforcements type B, SI10 and C1. Individual peaks are identified with their corresponding elements, and atomic compositions are shown in the upper right-hand side table. Desized glass fibers (Figure 7.5a) have a spectrum featuring a very strong oxygen peak, accompanied by much smaller silicon, calcium and carbon peaks. Remaining carbon on these glass surfaces (ca. 10%, atomic percent) may be attributed to either adventitious adsorbed hydrocarbons or calcium carbonates formed by surrounding air humidity [18].

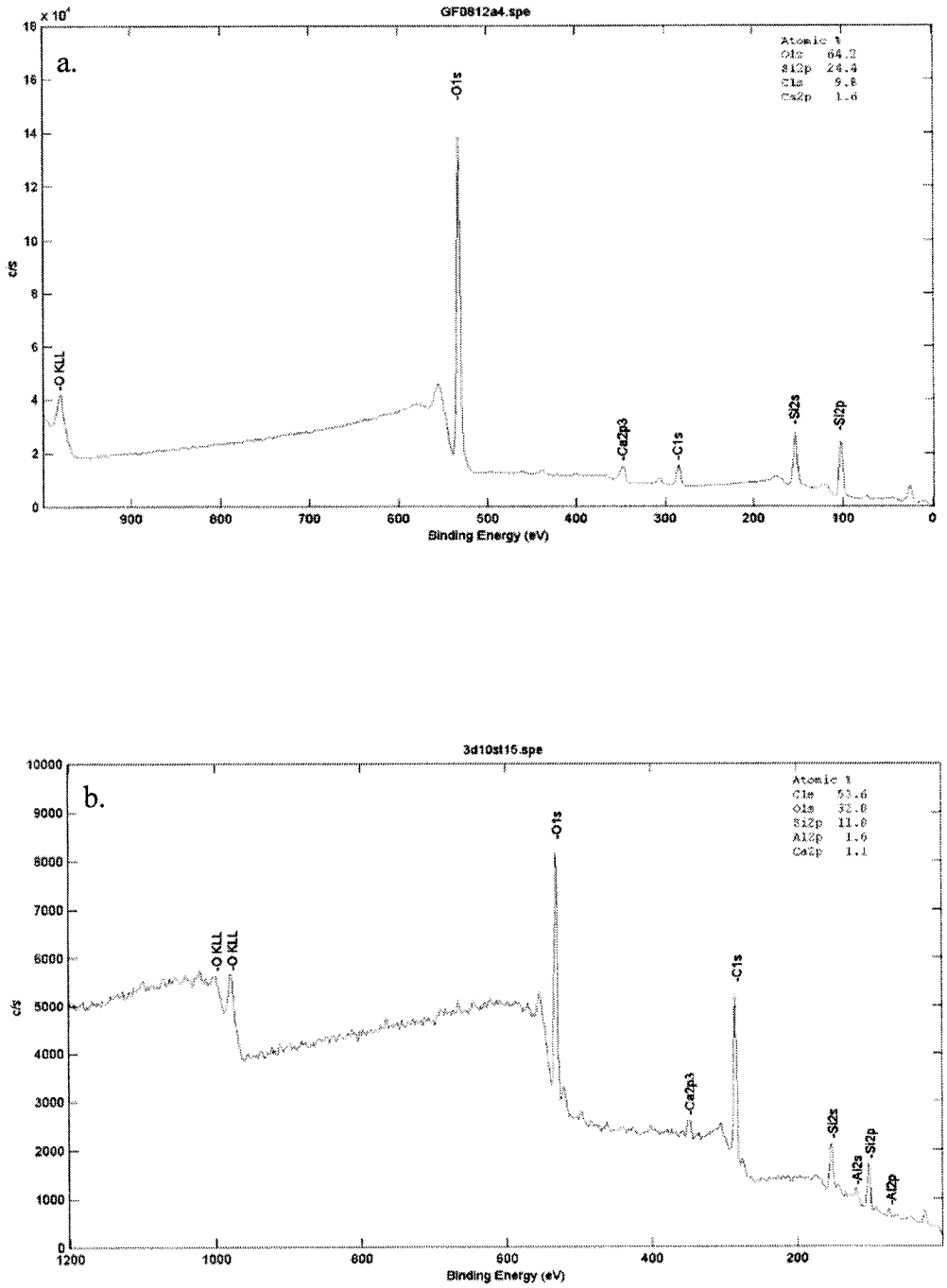

Figure 7.5 XPS survey spectra and atomic compositions of glass fibers with three different surface treatments: (a) Desized; (b) Admicellar SI10; and (c) Commercial.

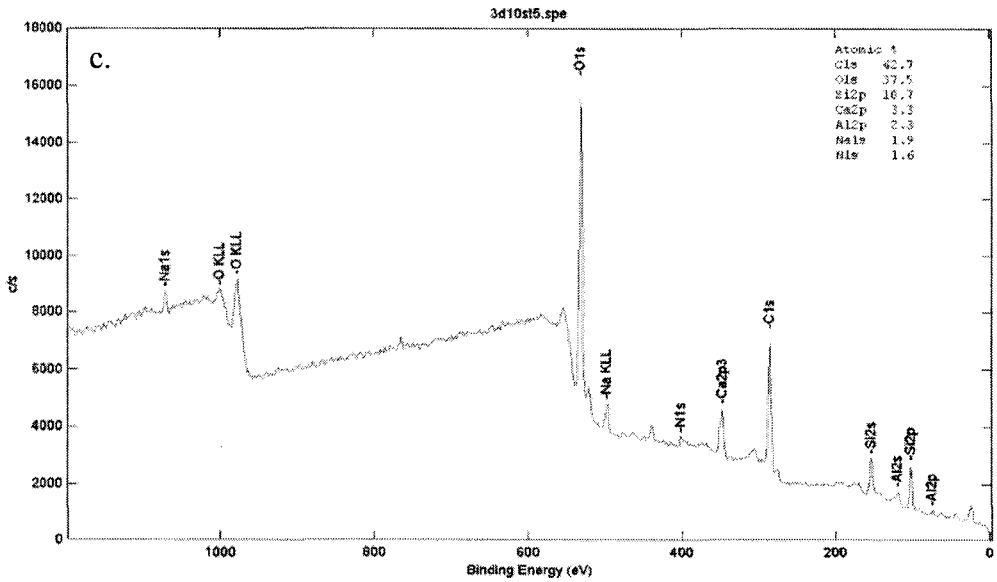

Figure 7.5 (Continued)

Covering the glass fiber surface with admicellar poly (styrene-co-isoprene) brings about a concomitant jump in the carbon peak height (Figure 7.5b). Furthermore, a simultaneous reduction in both oxygen and silicon peak intensities also takes place. Such behavior is indicative not only of the presence of adsorbed elastomer on the fiber surface, but also that the newly formed polymer extends over zones wherein silicon and oxygen were originally present. The increase in the carbon peak followed the order SI10 > SI5 > SI1, with atomic carbon concentrations of 53.6 %, 42.8% and 41.4%, respectively. In all, these results proved to be consistent with the UV/Vis data in demonstrating that the amount of polymer formed on the glass fiber

surfaces is dependent on the initial surfactant/monomer ratios used in the admicellar polymerization.

For commercial coatings (Figure 7.5c) the increase in carbon content is also evident, implying the presence of adsorbed macromolecules bearing hydrocarbon chains. Besides, two new distinct elements appear in the commercial sizings: sodium (Na) and nitrogen (N). Sodium in the coating may not be accurately traced back to a single source; however, it is most probably being incorporated as counterion of the surfactants normally employed to emulsify the coating (i.e., prior to application on the fibers). Nitrogen, on the other hand, is undoubtedly a signal from amine moieties added to the commercial sizing to serve as crosslinking agent for epoxies.

To further characterize the admicellar coatings, both oxygen/silicon and carbon/silicon atomic concentration ratios for each sizing type are plotted in Figure 7.6. Herein, XPS C/Si atomic ratio served as a measure of film coverage, and at the same time, as an indirect way of assessing chemical heterogeneity of the glass fibers surface. In this respect, Thomason and Dwight [52] previously reported that in commercial sizings (i.e., epoxy-compatible and polypropylene-compatible) the C/Si atomic ratio is directly correlated

to a well-known parameter called LOI, or weight loss on ignition. LOI relates the weight of sizing per unit weight of glass and it is often assumed that by varying the LOI a subsequent variation in sizing coverage may be obtained. Therefore, for all purposes a higher C/Si ratio means the surface is better coated.

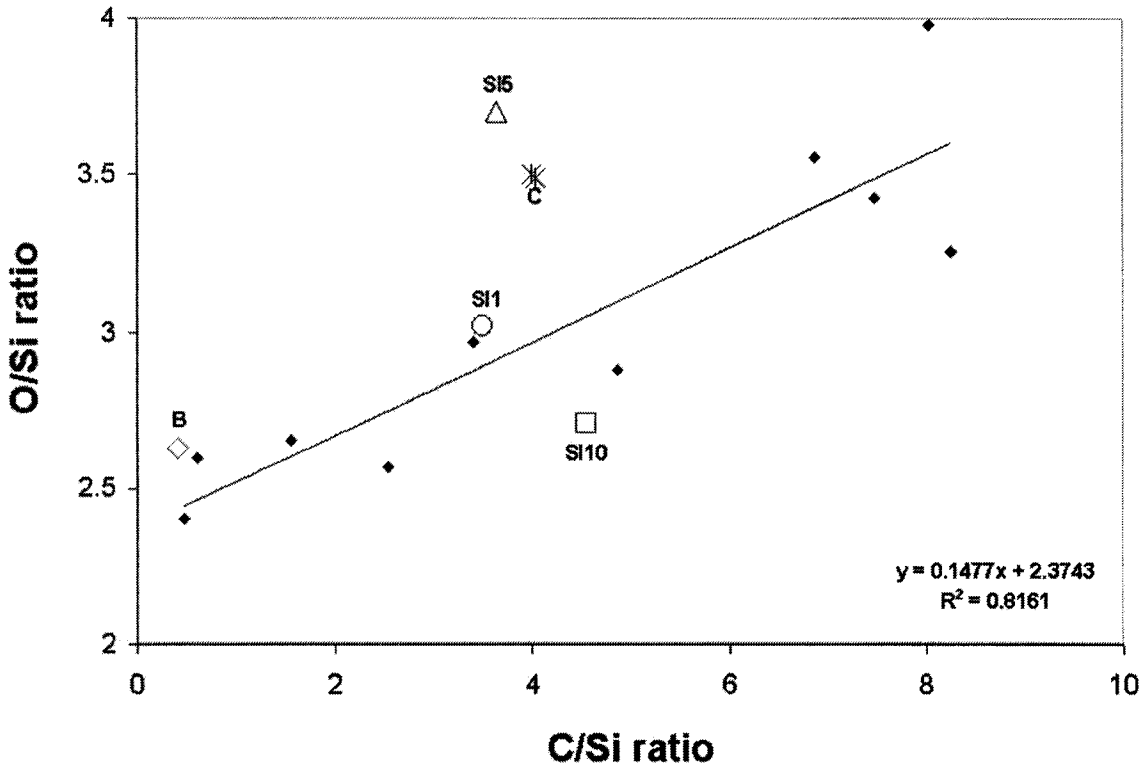

Figure 7.6 XPS oxygen/silicon versus carbon/silicon ratios for different fiber surface treatments. Filled diamonds correspond to data for 'acetone-washed' epoxy-compatible sizings with carbon/silicon<10 from ref [51].

Point B, which represents the desized reinforcement, is located in the abscissa very close to zero suggesting the absence of coating. As the initial surfactant/monomer proportion in the admicellar

polymerization departs from 1:1, increasingly higher C/Si ratios are attained. For example, fibers from composites SI1 have a C/Si ratio of 3.5 (i.e., 8.8 times higher than the control). At 1:5 surfactant/monomer ratio the admicellar sizing coverage is barely different from the SI1 case, with a C/Si of 3.64, that is, 9.1 times higher than in the desized fibers. Finally, when more monomer is loaded prior to the polymerization reaction, the thin elastomeric film will cover the fibers to a greater extent. For the SI10-type reinforcement the C/Si ratio topped at 4.5, which represents an 11.4 times increase over the control data. Furthermore, the C/Si ratio for this latter admicellar sizing (SI10) was even higher than the C/Si ratio for the commercial sizing (C/Si = 4.0).

Also included in Figure 7.6 are data from XPS analysis of acetone-extracted epoxy-compatible commercial coatings – from different sources – compiled recently by Thomason and Dwight [52]. These data points, depicted in the plot with filled diamonds, correspond to sizings whose photoelectron response is dominated by both the glass surface and the organosilane coupling agents chemically bound to the glass surface (i.e., physisorbed coating materials were stripped-off with solvents). The objective behind collapsing C/Si results from the current study with those from commercial 'epoxy-compatible'

sizings is two-fold: firstly, to establish an appropriate reference for comparison. This means, admicellar sizings are assessed by a single analysis parameter, (C/Si), which not only permits a rapid characterization among them; but also, helps in categorizing those commercial sizings with similar coverage levels to the admicellar that may be used as suitable interphase performance benchmarks. Secondly, to provide a clearer picture of how admicellar sizings rank within the broad range of tailored organosilane sizings available for enhancing the interaction with epoxy matrices. It is worth noting that a linear fit for the reference data gives an intercept value of 2.37 (at C/Si=0), which compares closely to the theoretical oxygen/silicon concentration at a bare fiber surface [52]. The O/Si value for the desized fibers used herein, point B, is very close to the theoretical value and is evidence of a predominantly homogeneous, silica-rich surface. In addition, all data for admicellar sizings fits adequately to the same theoretical correlation as the reference data for commercial epoxy-compatible coatings.

Another issue to consider regarding the XPS study of sizing coverage is that there may be some uncertainty with respect to using the silicon peak as exclusively originating from the glass fiber surface, especially when examining organosilane sizings in the low-coverage

range (C/Sl < 10). In such cases, calclum has been proposed as a better choice for a baseline atom to identify the glass surface [51]. XPS atomic concentration ratios of carbon/calcium and carbon/oxygen for all fiber surface treatments are presented in Table 7.2. A basic observation is that as the sizing coverage level increases on the glass fiber surface fewer characteristic photoelectrons from the glass will be detected. Thus, as expected, the C/Ca ratio rapidly shifts from a value of 6.08 for the bare glass fibers up to 48.72 for the admicellar coating with maximum coverage (i.e., SI10). Interestingly, the increasing coverage trend observed by using the C/Ca ratio (SI10 >SI5 >SI1) is consistent with the C/Si ratio results in proving that admicellar sizings coverage could be adequately manipulated through the reaction parameters to have a range of interphases with distinct characteristics.

Table 7.2 XPS atomic concentration ratios for various glass surface treatments.

SIZING TYPE	C/Ca RATIO	C/O RATIO
Desized (B)	6.02	0.15
Admicellar 1:1 (SI1)	18.0	1.16
Admicellar 1:5 (SI5)	20.1	0.98
Admicellar 1:10 (SI10)	48.72	1.68
Commercial (C)	12.94	1.14

7.3.3 Admicellar films wetting and topological properties.

Initial wetting of the fibers by the liquid incipient matrix during composite fabrication significantly affects ultimate interfacial adhesion and composite integrity. Many studies have shown that good wetting is particularly important, not only in achieving high interfacial adhesion but also because wetting quality influences the entrapment of air and whether any resulting voids remain in the interface or are displaced into the matrix [59]. In general, wetting of hydrophilic glass fibers by liquid polymers tends to be incomplete unless a surface treatment with organic materials is performed. For instance, the admicellar polymerization treatment of glass fibers is known to produce a comparatively good hydrophobic surface that facilitates wetting by epoxies [18]. Herein, the hydrophobic character of admicellar poly (styrene-co-isoprene)-treated woven glass fabrics was assessed by a simple water-drop test similar to that employed by Pongprayoon et al. [60] in the case of admicellar-treated cotton fabrics. As seen in Figure 7.7a, a 30-μl drop of deionized water was carefully placed (i.e., no impact force) over the fabric specimen, and the time each drop took to disappear from the surface – by capillary action – subsequently recorded. Fabrics with desized, hydrophilic fibers absorbed the water drop instantaneously regardless of the position wherein the drop was

placed. An advancing liquid front with approximately radial symmetry always formed around the water drop source (Figure 7.7b).

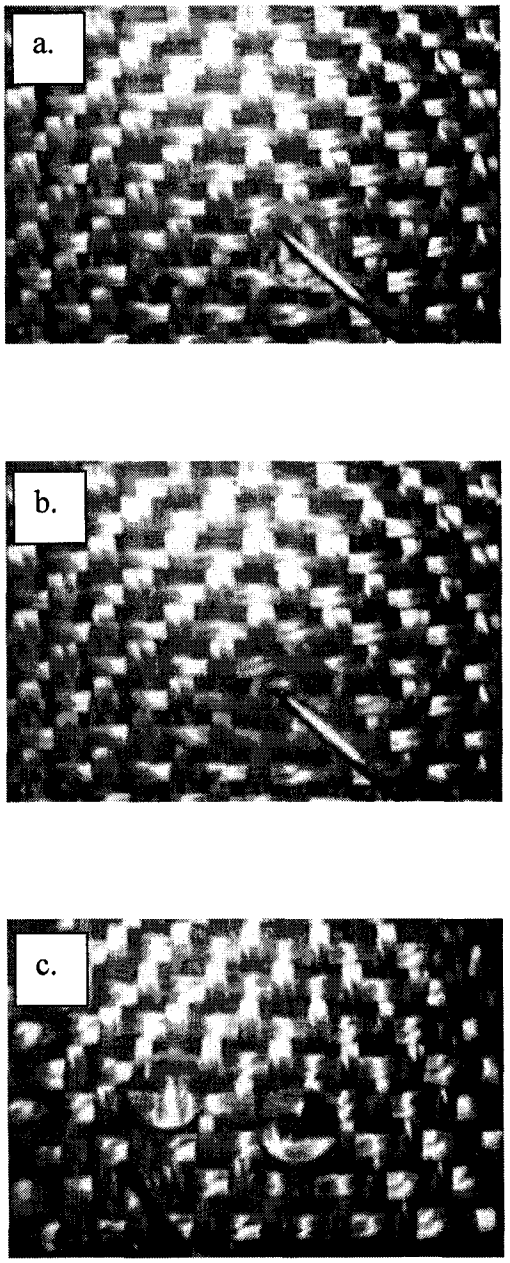

Figure 7.7 Hydrophobicity assessment by the drop test: (a) Drop positioning; (b) Capillary suction effect on hydrophilic fabric, and (c) Admicellar-treated fabric exhibiting good hydrophobicity.

When the drop was positioned over elastomer-modified woven fabrics (i.e., SI1, SI5 or SI10) no immediate tendency to detach from the injection needle was observed. Contrarily, some shear force was necessary to leave the drop on the surface. Once detached, the drop maintained a seemingly spherical shape for more than 20 min suggesting a strong nonwetting interaction with the solid as evidenced in Figure 7.7c. Furthermore, placing a second drop at random locations over the test zone gave the same hydrophobic response; which is a good indication that the polymeric thin film is appreciably well distributed at the whole fabric scale. To further test this hypothesis, hydrophobicity experiments on single yarns were carried out. The test drops used in this case were much smaller (ca. 10 μl), and the yarns were taken at random from both the warp and fill directions. In Figure 7.8a (bottom), two drops are seen sitting on an admicellar-modified yarn. Notice the almost spherical shape resembles that of nonwetting drops at the fabric scale. For these sessile water drops on modified yarns contact angles in the order of 100 – 110° were estimated using image analysis and the approximate θ/2-method [60]. The top part of Figure 7.8a shows the initial time when a water drop is placed on a control (i.e., desized) hydrophilic yarn. The strong capillary pressures within the interfiber space helps the water drop to detach easily from the needle. Thereafter, the water penetrates the yarn by capillary

transport until it practically disappears from the surface as depicted in the top portions of Figures 7.8b and 7.8c. In conclusion, hydrophobicity tests showed that admicellar-treated woven fabrics have wetting properties comparatively similar to those of the pure polymeric coating. Additionally, the thin elastomeric films formed on the fibers surface appear to be very well distributed at both the fabric and yarn scales; preventing typical surface phenomena that otherwise would occur such as water spreading and capillary transport.

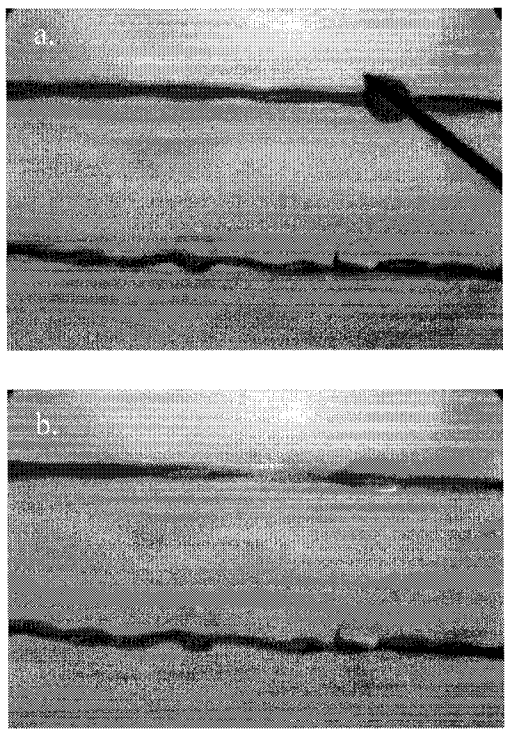

Figure 7.8 Hydrophobicity test sequence at the yarn scale: (a) (Top) Initial drop placement on hydrophilic yarn, (Bottom) sessile drops on admicellar-treated yarn; (b) (Top) Capillary transport of water; and (c) (Top) Complete penetration of water into interfiber yarn space

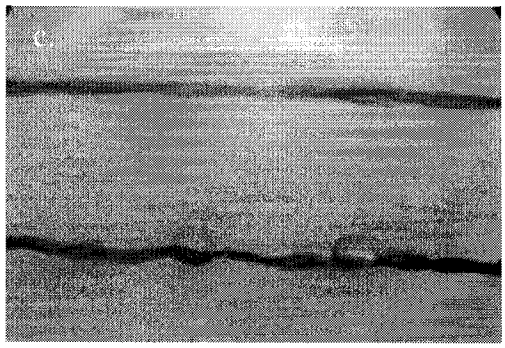

Figure 7.8 (Continued)

Wetting behavior, as well as interfacial adhesion of surface treated fibers, depends on coating parameters such as coverage distribution and film topology. So far, the analysis of admicellar coatings has been devoted to properties in the macroscale: fabric and yarn. Using AFM, images at the single-fiber scale helped assess the elastomeric coatings topology as a function of the monomer/surfactant ratio of the admicellar polymerization reaction. Figure 7.9 corresponds to a three-dimensional portrait of the desized fibers uppermost region, which shows a very smooth surface with the occasional presence of small bumps with heights in the order of 5 – 30 nm. Minute particles of the same type, but with a much steeper height distribution (e.g., 100 – 200 nm) were reported to form on desized glass fibers. These particular features are attributed to reversible crystal growth of alkali precipitates resulting from glass fiber aging [18].

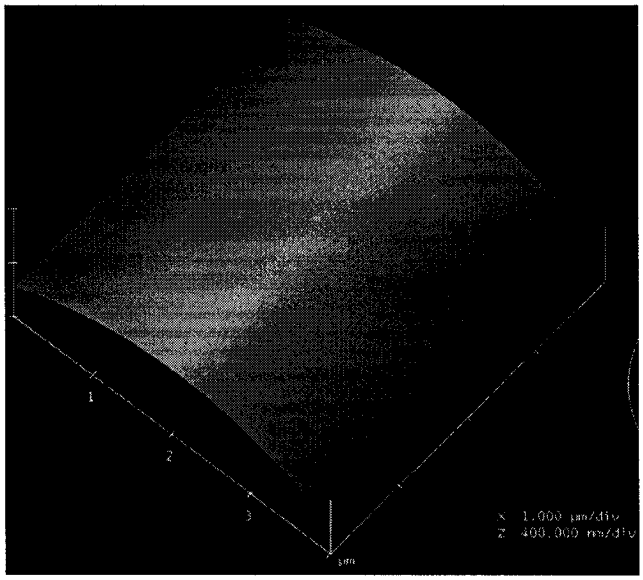

Figure 7.9 Topmost surface morphology of desized fibers by AFM: three-dimensional view.

Relative to the featureless bare glass surface, the admicellar-treated fibers surface appears dominated by polymeric aggregates with distinct morphological features. For the sake of clarity only results from the topological characterization of fibers type SI1 and SI10 will be presented, as these two groups exemplify the maximum contrast in the initial polymerization conditions used herein. Figure 7.10a is a three-dimensional image of a representative SI1-type fiber surface. The coating in this case is primarily formed by polymer patches that seem evenly distributed over the entire glass surface. Interestingly, there is a predominant flat, oblong structure for all these aggregates with height/diameter ratios of 1/20 up to 1/10. This restricted growth in the vertical direction is perhaps a consequence of the surfactant

template, or admicelle, wherein the polymerization takes place. A cross-section analysis (Figure 10b) shows that the more abundant small polymer patches, with heights in the order of 20 – 30 nm, are frequently found surrounding fewer patches of much greater size (e.g., 60 – 80 nm).

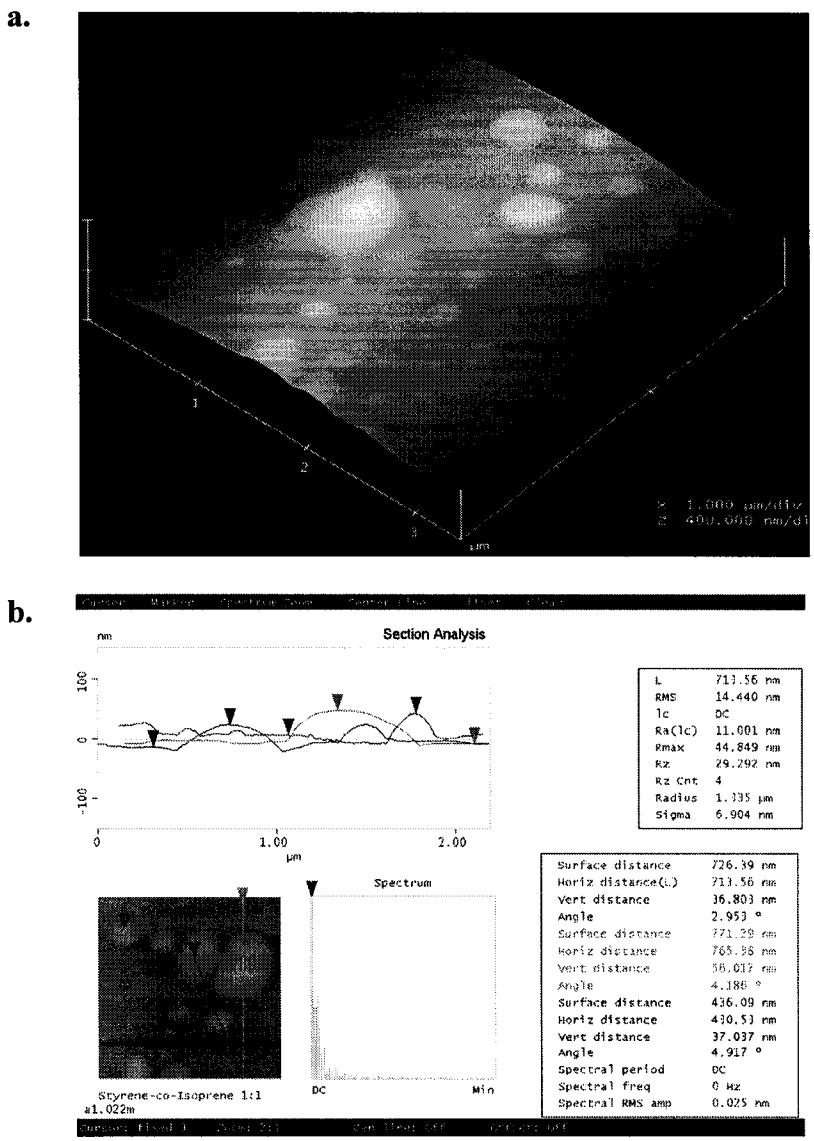

Figure 7.10 Dimensional and topographical features of admicellar-treated fibers type SI1 by AFM: (a) Topmost surface morphology; (b) Cross-sectional analysis; and (c) Aggregates coalescing.

c.

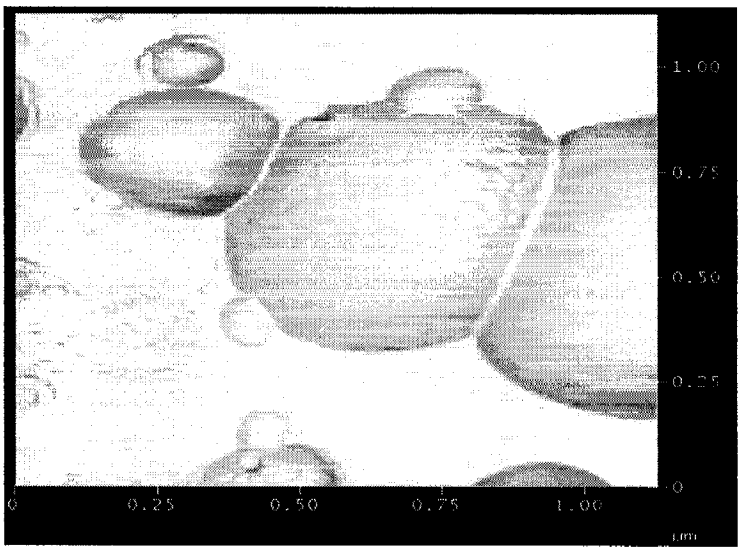

Figure 7.10 (Continued)

Two mechanisms are believed to be responsible for this particular coating morphology. First of all, CTAB adsorption over the silica-rich glass surface may be rationalized as forming patchy bilayers or strongly flattened micelle-like adsorbed aggregates. Some extraneous factors such as a heterogeneous surface charge density and a rough solid surface may be deemed responsible as they can substantially decrease the level of surfactant adsorption and/or coverage [23]. These deformed aggregates have vertical dimensions much greater than what is expected for surfactant bilayers alone, increasing the chances for more monomer adsolubilization with the attendant formation of thicker films.

The other mechanism is related to instabilities created on supported ultrathin (thickness below 100 nm) polymeric films as a result of the imbalance between long-range Van der Waals forces (i.e., disjoining pressure) across the film, and the opposing Laplace pressure. This imbalance drives the initial stage of the process leading to the rupture of the films, and it is especially augmented when the films are brought to temperatures above their glass transition (T_g). Green and Limary [62] recently demonstrated that annealed block copolymer thin films (e.g., PS-b-PMMA) over silica become unstable if their thickness fell below a certain threshold value. For instance, initially smooth films in the thickness range of 19 – 35 nm spontaneously ruptured as holes appeared randomly throughout the surface of the film. The final state of this morphology change process was characterized by the formation of droplets of copolymer on the underlying substrate.

A similar mechanism may be envisioned to operate in the formation of 'patchy' admicellar poly (styrene-co-isoprene) coatings as found in SI1-type fabrics. Once the admicellar film created with the aid of the surfactant template (e.g., thickness between 6 to 10 nm) is brought into contact with a poor solvent – such as air – for drying, it becomes unstable and forms polymer aggregates that rapidly dewet

from the glass surface. Some of these small aggregates encounter one another and they begin to coalesce, generating polymer particles with relatively broad height and surface area distributions. Figure 7.10c exemplifies how this clustering and coalescence phenomena occurs, with small poly (styrene-co-isoprene) aggregates being engulfed by other larger copolymer particles.

See and O'Haver [24] also reported destabilization of admicellar polystyrene thin films formed over smooth silica disks, particularly when using a constant CTAB concentration and low monomer loadings. They attributed the appearance of droplet-like aggregates to either the uneven adsolubilization of the styrene monomer within the admicelle or the dewetting effect during washing and drying.

A key element supporting the latter analogy is the fact that, independent of the initial surfactant/monomer loading, the glass transition temperature (T_g) of the copolymer formed during the admicellar treatment is expected to be always below room temperature. In all polymerizations carried out herein, an equimolar ratio of monomers was used, that is, $[M_{styrene}]/[M_{isoprene}] = 1$. Based on the relative reactivity (r_i) values reported by Wiley and Davis [63] for these monomers in a radical-initiated emulsion copolymerization at 80

°C ($r_{styrene}$ =0.54 and $r_{isoprene}$ = 1.92), it is evident that isoprene radicals have a strong tendency to self-propagate. Using these monomer reactivity data, a good approximation to the relative presence of each monomer in the resulting copolymer can be calculated by means of the well-known copolymer equation [64]:

$$R_p = R_m\,(r_{styrene} \times R_m)/(r_{isoprene} + R_m), \qquad (7.1)$$

where R_m is equal to $[M_{styrene}]/[M_{isoprene}]$ in the monomer mixture and R_p is equal to $[M_{styrene}]/[M_{isoprene}]$ in the polymer formed. Hence, replacing the known values in equation 7.1 an estimated composition of the admicellar poly (styrene-co-isoprene) would be: R_p = 0.527. This means, $[M_{styrene}]$ = 0.527 x $[M_{isoprene}]$; and thus, the T_g of the copolymer would be approximately in the order of - 20 °C (i.e., weighted average of T_g of bulk polymers: polystyrene, T_g = 100 °C; and polyisoprene, T_g = -70 °C).

Finally, notice in Figure 7.10c that although the cross-sectional analysis indicates the larger particles have a diameter of ca. 600 nm, the maximum particle height measured was in the order of 80 nm. More details on the coating thickness distribution will be presented later on in the bearing analysis section.

The admicellar coatings formed at higher surfactant/monomer ratios (i.e., SI10-type) shared some common topographical features with the SI1-type coating such as the presence of small oblong aggregates, as well as groups of coalescing particies (Figure 7.11a, arrow). Notwithstanding these similarities, SI10-type coatings exhibited appreciably higher surface coverage and a wider variety of morphological structures not seen in the other admicellar coating studied. Given that increasing amounts of monomer are available during the reaction, it is reasonable to think more monomer would continuously adsolubilize from solution as the one previously located inside the admicelle polymerizes. This undoubtedly leads to the production of thicker polymer films, especially if a surfactant with long hydrocarbon tails like CTAB is employed [26]. Irrespective of the film thickness, the disjoining pressure, which is the driving force for supported nonwetting film destabilization, continues to create an imbalance to locally decrease the film thickness. The Laplace pressure counters this force by attempting to flatten the film. In the case the disjoining pressure is comparatively larger, then the pattern proceeds to the final stage of droplets [65]. Conversely, if the Laplace pressure remains appreciable, the destabilization kinetics becomes much slower. With a lower disjoining pressure driving the destabilization 'octopus-like' morphology, with bridges between islands of polymers,

is more likely to constitute the equilibrium copolymer film pattern. This sort of ruptured, but still connected, film was readily found in all SI10-type surfaces analyzed. An exemplary case of such topography is presented in Figure 7.11b.

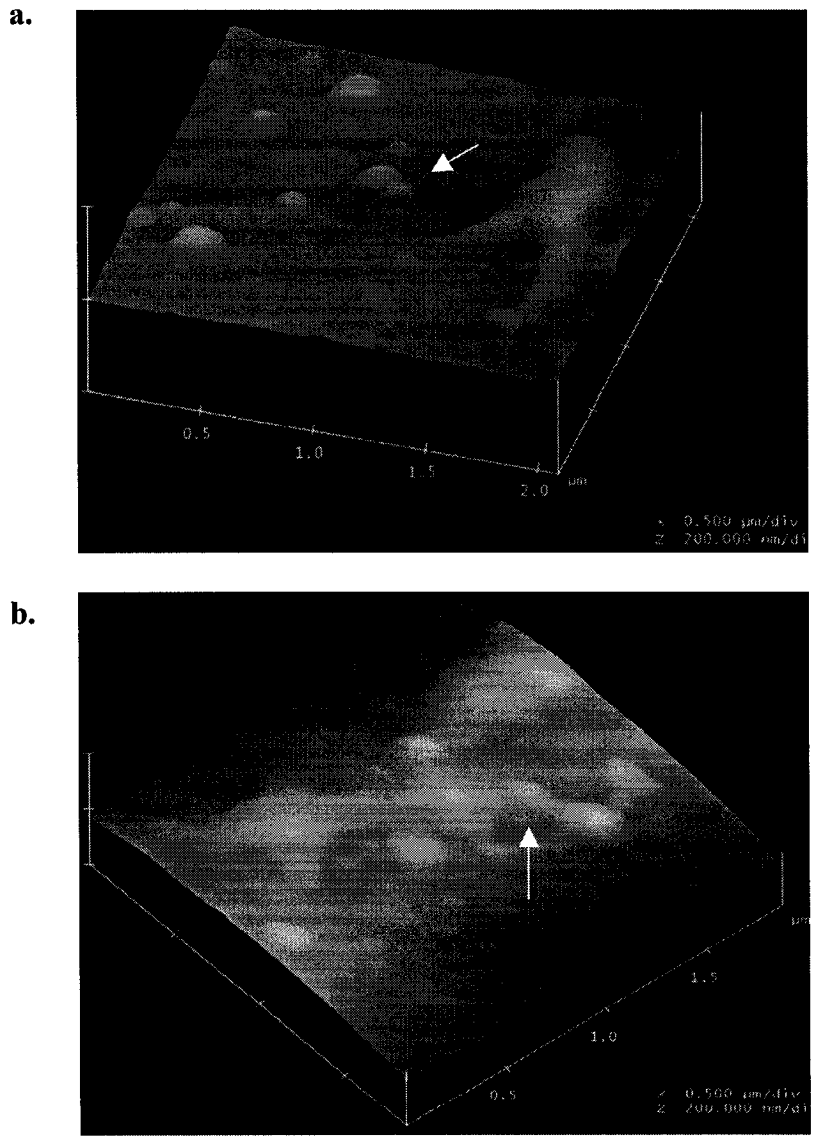

Figure 7.11 Dimensional and topographical features of admicellar-treated fibers type SI10 by AFM: (a) Topmost surface morphology (arrow: coalescing aggregates); (b) Connected island morphology (arrow: film hole); and (c) Section analysis of large aggregate.

c.

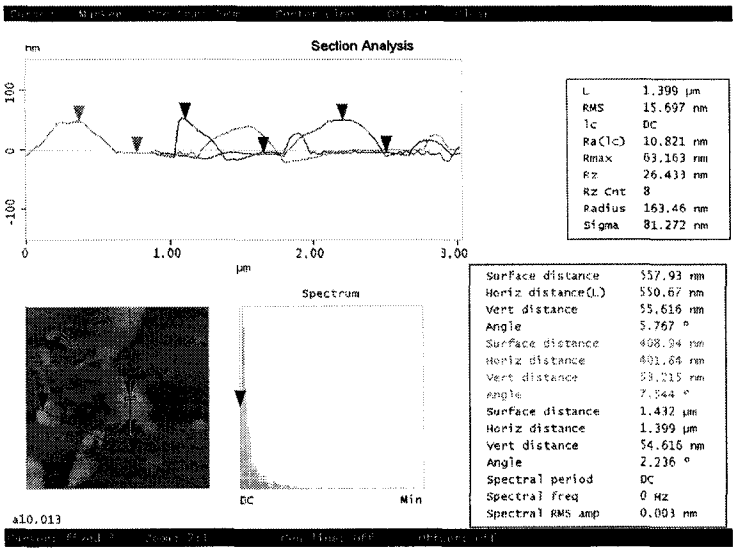

Figure 7.11 (Continued)

Lastly, Figure 7.11c depicts a section analysis of a considerably large polymer aggregate surrounded by isolated particles that seem to have dislodged from the former aggregate. It is worth noting that while the large aggregate had an average height of 40 – 50 nm, some of the surrounding disconnected particles were even higher (e.g., 80 – 85 nm). This supports the idea of particle coalescing to be an essential part of the film thickening mechanism observed for both types of admicellar coatings analyzed.

7.3.4 Thickness distribution of admicellar sizings. Bearing analysis was used as a tool to complement the topological study of admicellar films. In the past, roughness analysis of admicellar poly (styrene-co-isoprene) was carried out by comparison of simple

parameters such as average roughness, R_a, and root-mean-square surface roughness, RMS [18]. Although useful, some of these parameters may lead to erroneous characterization of surfaces containing a variety of feature types [66].

Figure 12a shows a surface height histogram from the bearing analysis of a control glass fiber. There is a main peak with a very narrow distribution centered at 6.3 nm, and some other height data points extending up to 30 nm. Features above 6.3 nm are very infrequent as the bearing area percentage is only close to 7%; which means that features below this cut-off length make up for 93% of the total surface area. Furthermore, the bearing volume (*V*), defined as the volume above the peak depth in the histogram, is very low: 2.55 x 10^{-3} μm^3. Therefore, the bearing analysis confirms the control glass surface is completely smooth with the exception of infrequent elevations related to alkali precipitates caused by fiber aging.

For admicellar-treated fibers type SI1 the bearing histogram displays a very broad distribution ranging from 5 – 60 nm, signaling a rough surface (Figure 12b). Notice the height peak is centered at 41.4 nm, which corresponds to the most frequently encountered elevation. However, aggregates with heights over 41.4 nm are still abundant as

the bearing area percentage is 43.7 %. The bearing volume is an order of magnitude greater than that for control samples, V_{SI1} = 2.31 x 10^{-2} μm^3, which again suggests this surface is much rougher.

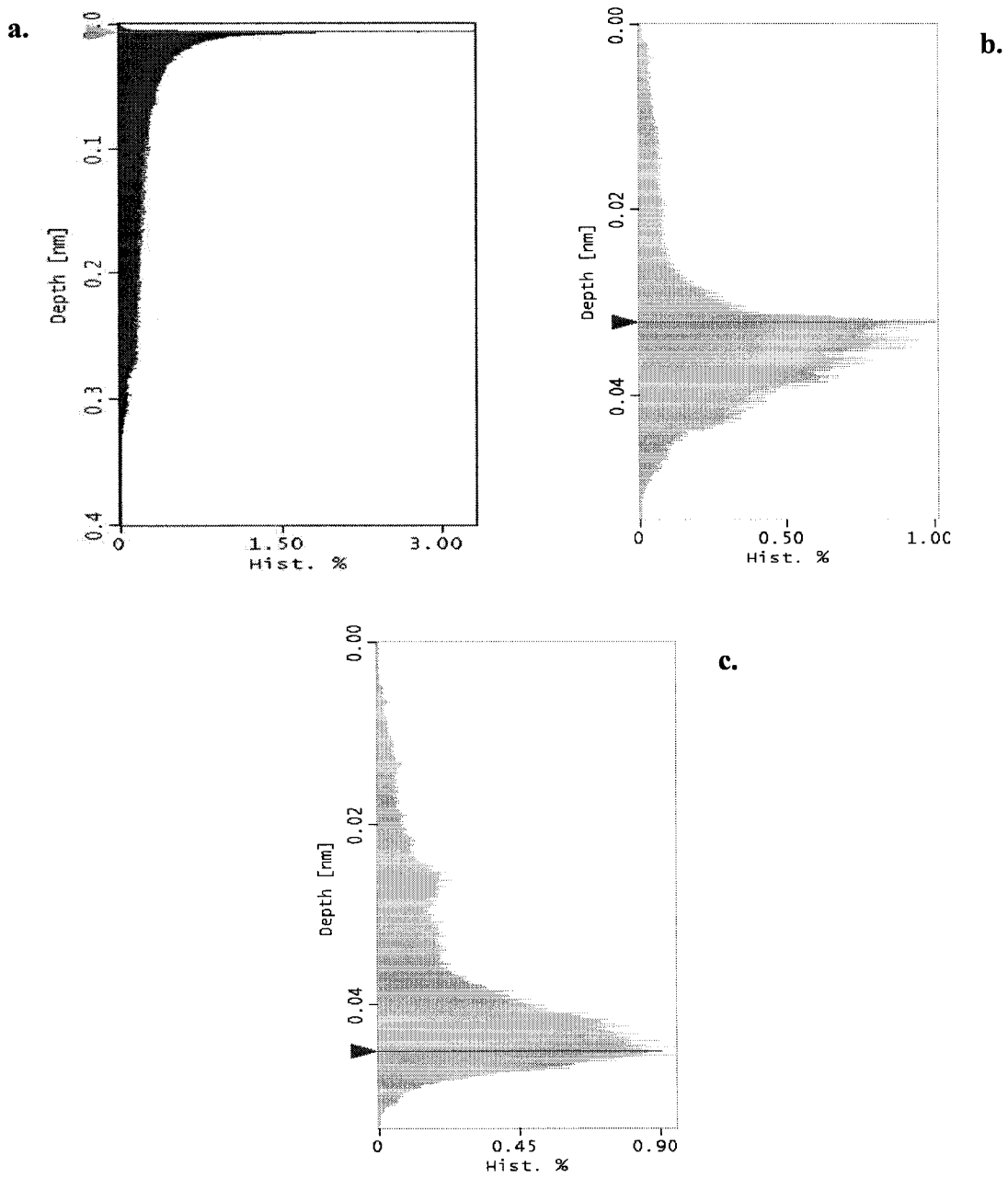

Figure 7.12 Surface height histograms from bearing analysis of fibers with different surface treatments: (a) Desized (type B); (b) Admicellar-treated (type SI1); and (c) Admicellar-treated (type SI10).

Lastly, the bearing histogram for fibers type SI10 (Figure 12c) shows a bimodal distribution of surface elevations, with the most frequently observed heights being 25 nm (smallest peak) and 45 nm (highest peak). Equally important is the fact that 80% of the features are under the cut-off thickness of 45 nm, indicating the SI10 coating has smaller peak-to-valley distances than the SI1 coating. This is consistent with the fact that the bearing volume for SI10 coatings at the main histogram depth is almost twice the value for the SI1 coating, that is, $V_{SI10} = 4.09 \times 10^{-2}\ \mu m^3$. In all, bearing analysis results satisfactorily agree with the topographical information obtained by the AFM.

7.4 Conclusions

Previous attempts to create an elastomeric interphase within epoxy/glass composites have been marked by appreciable increases in toughness properties with a concomitant, but undesirable, reduction in overall strength performance. A great deal of this behavior has been related to the sizing film thickness, which is especially difficult to control with current solvent-deposition methods. Herein, admicellar polymerization was used to create elastomeric sizings with thicknesses well below 100 nm over textile glass reinforcements. These thin coatings, besides rendering the glass surface fairly hydrophobic at

both the fabric and yarn scales, produced consistent changes in the interfacial properties of their composites that translated in an overall mechanical improvement. For instance, ultimate tensile strength of RTM parts containing admicellar-coated textile reinforcements was 50 – 55% higher than the control samples. Furthermore, flexural properties measured for composites with admicellar coatings that had the maximum poly (styrene-co-isoprene) thin film coverage were improved in more than 38% from the control level. Interestingly, the positive effect in flexural properties obtained with the admicellar coatings seem to depend on both sizing surface coverage and film topology. Admicellar-polymerized elastomeric coatings created with a low surfactant/monomer ratio had the lowest coverage and were mainly constituted by unconnected oblong aggregates, possibly formed by extensive dewetting and coalescence of initially flat polymer patches. These low-coverage sizings provided the smallest increase in interlaminar shear strength (ILSS), whereas the coatings formed at surfactant/monomer conditions favoring monomer availability during the reaction (i.e., higher coverage) gave the highest ILSS. In these latter films the dewetting seemed to be slower, leading to a strongly interconnected morphology – with bridges connecting islands of polymer. Work in progress will attempt to perfect the admicellar sizings by introducing new elastomers bearing different functional

groups that may enhance their chemical reactivity and compatibility to epoxy matrices.

References

1. A.G. Atkins, *J Mater. Sci.* **10**, 819 (1975)
2. G. Marom and R.G.C. Arridge, *Mater. Sci. Eng.* **23**, 23 (1976)
3. L.J. Broutman and B.D. Agarwal, *Polym. Eng. Sci.* **15**, 757 (1974)
4. S.H. Jao and F.J. McGarry, *J. Reinf. Plast. Compos.* **11**, 811 (1992)
5. F.J. McGarry, *Annu. Rev. Mater. Sci.* **24**, 63 (1994)
6. M. Labronici and H. Ishida, *Compos. Interfaces* **2**, 199 (1994)
7. G. Vörös and B. Pukánszky, *Composites Part A* **32**, 343 (2001)
8. V.A. Matonis and N.C. Small, *Polym. Eng. Sci.* **9**, 90 (1969)
9. S.A. Hayes, R. Lane and F.R. Jones, *Composites Part A* **32**, 379 (2001)
10. R.E. Lavengood and M.J. Michno, Jr., in: *Proc. Div. Tech. Conf. Engrg. Props. And Structure Div.* Society of Plastics Engineers, p. 127 (1975)
11. L.D. Tryson and J.L. Kardos, in: *36th Ann. Conf. Reinf. Plast. /Compos. Inst., The Society of the Plastics Industry,* Session 2-E, p. 1 (1981)
12. C. Alhstrom and J.F. Gérard, *Polym. Compos.* **16**, 305 (1995)

13. J. Daoust, T. Vu-Khan, C. Ahlstrom and J.F. Gérard, *Compos. Sci. Technol.* **48**, 143 (1993)
14. M.N. Tillie, T.M. Lam and J.F. Gérard, *Compos. Sci. Technol.* **58**, 659 (1998)
15. D.G. Peiffer, *J. Appl. Polym. Sci.* 24, 1451 (1979)
16. S. Sakhalkar and D. Hirt, *Langmuir* **11**, 3369 (1995)
17. B.P. Grady, E. O'Rear, L. Penn and A. Pedicini, *Polym. Compos.* **19**, 579 (1998)
18. H.J. Barraza, M. Hwa, K. Blakley, E.A. O'Rear and B.P. Grady, *Langmuir* **17**, 5288 (2001)
19. H.J. Barraza, K. Olivero, Y. Hamidi, E.A. O'Rear and M.C. Altan, *Compos. Interfaces* 9, 477 (2002)
20. H.J. Barraza, L. Aktas, Y.K. Hamidi, J. Long, Jr., E.A. O'Rear and M.C. Altan, *J. Adhesion Sci. Technol.* **17**, 217 (2003)
21. M. Drach, W. Rudzinski and J. Narjiewics-Michaelek, *J. Dispersion Sci. Technol.* **21**, 683 (2000)
22. P. Somasundaran and L. Huang, *Adv. Colloids Interface Sci.* **88**, 179 (2000)
23. R. Atkin, V.S.J. Craig, E.J. Wanless and S. Biggs, *Adv. Colloids Interface Sci.* **103**, 219 (2003)
24. C.H. See and J. O'Haver, *J. Appl. Polym. Sci.* **89**, 36 (2003)

25. W-.L. Yuan, E. A. O'Rear, B.P. Grady and D.T. Glatzhofer, *Langmuir* **18**, 3343 (2002)

26. W-L. Yuan, E.A. O'Rear, G. Cho, G.P. Funkhouser and D.T. Glatzhofer, *Thin Solid Films* **385**, 96 (2001)

27. N. K. Naik, in: *Woven Fabric Composites.* Technomic Publishing Co. Inc., Lancaster, p.p. 1-72 (1994)

28. H. Ishida and T. Chaisuwan, *Proc. Amer. Chem. Soc., PMSE Div.* **85**, 534 (2001)

29. H. Hamada, Z. Maekawa and N. Ikegawa, *J. Mater. Sci. Japan* **43**, 229 (1994)

30. T. Ootsuka, K. Hamano, M. Kurano and K. Sonobe, *J. Ceram. Soc. Japan* **105**, 175 (1997)

31. A. Milutinović-Nikolić, V. Presburger-Ulniković and S.V. Radoslav-Aleksić, *J. Mater. Sci.: Mater. Electronics* **14**, 75 (2003)

32. R. Yosomiya, in: *Adhesion and Bonding in Composites*. Marcel Dekker Inc., New York, p.p. 133-152 (1990)

33. M.S. Woo and M.R. Piggott, *J. Compos. Technol. Research* **9**, 162 (1987)

34. A.-C. Lassas, L. Fagerholm, B. Stenlund and J. Näsman, *Polym. Composites* **14**, 1 (1993)

35. H. Fagerholm, J. Rosenholm, T. Horr and R. Smart, *Colloids Surf. A* **110**, 11 (1996)

36. J.F. Gérard and B. Chabert, *Macromol. Symp.* **108**, 137 (1996)

37. G.W. Lee, N.J. Lee, J.Jang, K.J. Lee and J.D. Nam, *Compos. Sci. Technol.* **62**, 9 (2002)

38. V. Cech, R. Prikryl, R. Balkova, A. Grycova and J. Vanek, *Composites Part A* **33**, 1367 (2002)

39. D.J. Marks and F.R. Jones, *Composites Part A* **33**, 1293 (2002)

40. G. Funkhouser, M. Arevalo, D. Glatzhofer and E. O'Rear, *Langmuir* **11**, 1443 (1995)

41. D. Glatzhofer, G. Cho, C. Lai, E. O'Rear and B. Fung, *Langmuir* **9**, 2949 (1993)

42. C. Lai, E. O'Rear, J. Harwell and M. Hwa, *Langmuir* **13**, 4267 (1997)

43. B. Kitiyanan, J. O'Haver, J. Harwell and S. Osuwan, *Langmuir* **12**, 2162 (1996)

44. J. O'Haver, J. Reynolds, J. Harwell, B. Grady, L. Evans and W. Waddell, Paper presented at the 219th American Chemical Society Meeting, San Francisco (2000)

45. H.J. Barraza, Y.K. Hamidi, L. Aktas, E.A. O'Rear and M.C. Altan, *J. Compos. Mater*, in press

46. K.A. Olivero, H.J. Barraza, E.A. O'Rear and M.C. Altan, *J. Compos. Mater.* **36**, 2011 (2002)

47. T. Li, Ch. Zhou and M. Jiang, *Polym Bull.* **25**, 211 (1991)

48. B. Gantchev and M. Mihailov, *Polym. Bull.* **41**, 207 (1998)

49. X. Wei, A.D.W. Carswell, W. Alvarez and B.P. Grady, *J. Colloid and Interface Sci.*, 2003, in press.

50. J.L. Thomason and G.E. Schoolenberg, *Composites* **25**, 197 (1994)

51. J.L. Thomason and D.W. Dwight, *Composites Part A* **30**, 1401 (1999)

52. J.L. Thomason and D.W. Dwight, *J. Adhesion. Sci. Technol.* **14**, 745 (2000)

53. M. Higo, X. Lu, U. Mazur and K.W. Hipps, *Thin Solid Films* **384**, 90 (2001)

54. C.L. Schutte, *Mater. Sci. Eng. Reports* **R13**, 265 (1994)

55. B. Larson and L. Drzal, *Composites* **25**, 711 (1994)

56. K.J. Rao, in: *Structural Chemistry of Glasses*. Elsevier, Amsterdam, pp. 401-427 (2002)

57. Department of Defense (DOD) Handbook, Polymer Matrix Composites MIL-HDBK-17-3E, Vol. 3, p. 2-25 (1997)

58. J.K. Kim and Y.W. Mai, in: *Engineered Interfaces in Fiber Reinforced Composites*. Elsevier, Amsterdam, pp. 1- 63 (1998)

59. J.L. Thomason, *Composites* **26**, 467 (1995)

60. T. Pongprayoon, E.A. O'Rear, N. Yanumet and W-L. Yuan, *Langmuir* **19**, 3770 (2003)

61. M.W. Yang and S.Y. Lin, *Colloids and Surfaces A: Physicochem. Eng. Aspects* **220**, 199 (2003)

62. P.F. Green and R. Limary, *Adv. Colloid Interface Sci.* **94**, 53 (2001)

63. R.H. Wiley and B. Davis, *J. Polym. Sci. A* **1**, 2819 (1963)

64. A.D. Jenkins and J. Jenkins, *Macromol. Symp.* **174**, 187 (2001)

65. J.L. Masson and P.F. Green, *J. Chemical Phys.* **112**, 349 (2000)

66. W. Yoshida and Y. Cohen, *J. Membrane Sci.* 215, 249 (2003)

OVERALL CONCLUSIONS AND FUTURE WORK

Market demands are continuously seeking the utilization of fiber-reinforced composites in a wide variety of technological applications. In many of these end applications, good structural integrity and a relatively stable interfacial region against aggressive environments are essential requisites. Herein, admicellar polymerization was introduced as an alternative to existing commercial sizings to create engineered interfaces for enhanced composite performance. Controlled-thickness coatings of either polystyrene or poly (styrene-co-isoprene) were formed over fiberglass reinforcements with different fiber arrangements: layered random mats and woven fabrics. These reinforcements were tested for changes in their surface energy characteristics (i.e., wettability), and subsequently used to prepare disk-shaped specimens by the liquid molding process known as resin transfer molding (RTM). Mold fill times for all experiments were consistent with current industrial molding cycles for small to medium

sized RTM-parts fabrication. This fact provides more significance to these results when extrapolated to scale-up operations or in final commercial applications.

The major conclusion drawn from the current work was that thin elastomeric coatings obtained by admicellar polymerization are effective in increasing the level of structural strength of composites by the simultaneous action of several mechanisms acting along the interfacial region. Firstly, admicellar-coated areas within the fibrous reinforcement can be regarded as zones of higher interfacial adhesion due to their ability to blunt running cracks and dissipate microstresses along the fibers. These mechanisms were particularly evinced as composite parts with elastomeric sizings had average interlaminar shear strength (ILSS) levels higher than the control desized groups. Furthermore, it was found that as the admicellar sizing coverage increased so did the stress-transfer capabilities at the fiber matrix interface (i.e., higher ILSS). Increases in flexural properties with sizing coverage have been known to take place [1] with other sizings of comparatively low modulus (e.g., polystyrene-grafted, polymethyl methacrylate-grafted and polyglycidyl methacrylate-grafted glass fibers); which again confirms the dominant effect of the sizing elastic

properties and thickness on the establishment of adequate stress-transfer properties at the interface.

The second mechanism through which admicellar coatings are able to confer enhanced structural properties to fiber-reinforced composites is by turning the fiber/matrix interface completely hydrophobic. Wettability studies at the fiber, yarn and fabric scales demonstrated that the thin admicellar coatings are able to prevent surface phenomena, such as water spreading and capillary transport, that typically occur in bare glass fibers, and to a certain extent, in commercially sized fibers. When equilibrated with water at 45 °C, admicellar-coated composite samples had both significantly low moisture and saturation values. In all, these results signal a higher stability of the admicellar-coated fibers/epoxy-resin interface against hydrolytic attack. For this reason, admicellar sizings were found to rank consistently higher – in terms of the effectiveness in property retention – than those composites with either bare fibers or commercial sizings.

Another related phenomenon that perhaps favors the stability of admicellar-coated reinforcements in humid environments is their capacity to block the diffusion of mobile sodium ions from the

inorganic fiber surface to the interfacial region. Numerous studies have shown that sodium ions finely dispersed at the interphase become particularly active in the presence of water, thus increasing the rate of degradation of the interface properties [2]. XPS atomic concentration data on admicellar-coated woven fabrics consistently showed lower peak intensities coming from cations such as calcium and sodium. However, the contribution of such mechanism to the interfacial stability of admicellar sizings still needs to be studied in more detail.

Tailoring the interface of glass/epoxy composites with admicellar coatings also helped in the acquisition of general knowledge about the quality of the interface, topographical features of the thin elastomeric sizings, and the interactions of the sizing with the surrounding matrix. Some of the new facts learned through the experimentation described in this work, and that may be considered as a starting point for investigations in the future, are:

- Fibers treated with only surfactant (e.g., SDS) showed similar or less wettability for both water and glycerol when compared to the baseline values of desized fibers. Notwithstanding, when probed with an epoxy resin (e.g., EPON 815C) observable, but limited, enhancement in wettability occurred. This brings up the issue: could

adsorbed surfactant monolayers be effective as sizings in glass-reinforced composites? In the literature, this issue has not been yet addressed thoroughly, and the existing data are still controversial. On one hand, recent experiments by Blakley [3] suggest that performance improvements (e.g., flexural strength) of composites with SDS-treated control fibers compare favorably to those attained with both commercially sized and admicellar-coated reinforcements. Beneficial effects of the addition of surfactants to the bulk resin used in RTM-processing of composites have been also reported by Ilias et al. [4] and Chen et al. [5]. These authors attributed such levels of mechanical enhancement to the attainment of better wetting conditions and less voidage. In contrast to the previous observations, other studies show deleterious effects originated from the presence of surfactants both in the bulk resin and at the fiber/resin interface. Jensen et al. [6, 7] claim that surfactants dissolved in epoxies always act as plasticizers (i.e., lowering the glass transition temperature, T_g); and when present at the epoxy/glass interface, they lead to reductions on the mechanical properties due to higher moisture uptake rates. Clearly, one area for future investigation would be to assess the intensity of mechanical property enhancement – or degradation – when using adsorbed-surfactants over glass fibers. Some of the variables worth studying are related to the surfactant type (anionic, cationic or nonionic), surfactant

chain length, surfactant chemistry (e.g., fluorine-based versus hydrocarbon-based), and the presence of functional groups in the surfactant chains (e.g., ethoxylates).

- Positive effects coming from the introduction of a nanometer-thick elastomeric interlayer can be noticed only if extensive cooperative segmental motions are present, that is, when the glass transition temperature of the admicellar-polymerized coatings is well below room temperature. This specific result opens another research front worth pursuing, which comprises the utilization of monomers amenable to polymerize under the typical reaction conditions of admicellar polymerization. The idea is to produce coatings from polymers with glass transition temperatures close to, or below, that of the poly (styrene-co-isoprene) copolymer used herein. Some examples of polymers with low T_g include the vinyl-type, such as polybutadiene (T_g = - 85 °C) and poly (vinylidene), T_g = - 17 °C; or acrylate copolymers, such as butyl acrylate, T_g = -35 °C.

- Flexural properties proved sensitive to the type of interphase formed at various admicellar polymerization conditions. It seems that higher surface coverage and film connectedness in admicellar sizings promotes better stress transfer at the interfacial region. Therefore,

another issue for future investigations is to find a suitable procedure to inhibit the dewetting kinetics observed for the thin admicellar coatings on the glass surface. Mackay et al. [8] recently presented a listing of the usual approaches to stabilize thin polymeric films on nonwetting substrates, which included: grafting polymer chains onto the surface, sulfonation and metal complexation of the polymer, the introduction of specialized end groups onto the polymer with a high affinity for the inorganic substrate, modification of substrate roughness, or the novel use of nanoparticles, such as fullerenes (C_{60}) and dendrimer additives. Evidently, some of these current stabilization mechanisms are not easily adaptable to the admicellar thin films. However, an idea that might be worth exploring is the simultaneous adsolubilization of metal ions and monomers, followed by a radical polymerization reaction, to form an ion-filled admicellar polymer coating. Esumi et al. [9, 10] have given plenty of evidence on the simultaneous adsorption of Cu^{+2} and aromatic compounds (e.g., 2-naphtol) from aqueous solutions by adsorbed surfactant aggregates. Hence, a polymeric thin film containing ions could be expected to exhibit completely different local dewetting kinetics, as new charge interactions would set in if some of the metal ions segregate to the polymer/substrate interface [11].

- In the realm of micromechanics, the strength of an interface can be defined by two distinct approaches: the shear-strength criterion and the fracture energetics approach. In the current work, only the former criterion was used to characterize the beneficial effects of introducing admicellar coatings on the mechanical properties of composites. Moreover, this sole approach served to benchmark the admicellar coatings performance against that of commercial sizings. In the future, more efforts need to be dedicated to evaluate the fracture toughness of the admicellar-treated composites. One reason for this is that in practical circumstances the interfacial fracture energy, rather than the maximum interfacial stress, is the parameter determining the strength of most structural parts. Suffice it to say that similar shear strength (τ_b) does not necessarily mean similar fracture toughness [12].

References

1. K. Hashimoto, T. Fujisawa, M. Kobayashi and R. Yosomiya, *J. Appl. Polym. Sci.* **27**, 4529 (1982)
2. D. Pawson and F.R. Jones, *J. Adhes.* **52**, 187 (1995)
3. K. Blakley, MS Thesis, University of Oklahoma, 2003
4. S. Ilia, M.C. Siegel, R.L. Sadler and V.S. Avva, *Intl. SAMPE Tech. Conf.* **27**, 457 (1995)

5. Y-T. Chen, H.T. Davis and C.W. Macosko, *AICHE J.* **41**, 2261 (1995)

6. R.E. Jensen, E. O'Brien, J. Wang, J. Briant, T.C. Ward, L.T. James and D.A. Lewis, *J. Polym Sci. B* **36**, 2781 (1998)

7. R.E. Jensen, C.E. Johnson and T.C. Ward, *J. Polym. Sci. B* **38**, 2351 (2000)

8. M.E. Mackay, Y. Hong, M. Jeong, S. Hong, T.P. Russell, C.J. Hawker, R. Vestberg and J.F. Douglas, *Langmuir* **18**, 1877 (2002)

9. K. Esumi, H. Hayashi, Y. Koide, T. Suhara and H. Fukui, *Colloids Surf. A* **144**, 201 (1998)

10. K. Esumi, K. Yoshida, K. Torigoe and Y. Koide, *Colloids Surf. A* **160**, 247 (1999)

11. L.T. Lee, M.V. da Silva and F. Galembeck, *Langmuir* **19**, 6717 (2003)

12. J.K. Kim and Y.W. Mai, in: *Engineered Interfaces in Fiber Reinforced Composites*. Elsevier, Amsterdam, pp. 1-63 (1998)